Molecular Determinants of Phenotype of Orbital Fibroblasts in Thyroid Eye Disease

I-Hui Yang

This Thesis is submitted to University College London for the Degree of Doctor of Philosophy in Cell Biology

2019

Supervisor – Dr Maryse Bailly

UCL Institute of Ophthalmology

11-43 Bath Street, London, EC1V 9EL

Declaration

I, I-Hui Yang, confirm that the work presented in this thesis is my own. Where information has been derived from other sources, I confirm that this has been indicated in the thesis.

Abstract

Thyroid eye disease (TED) is an autoimmune disease originating from the thyroid gland and affecting orbital contents. The orbital fibroblasts are a key component in the pathogenesis of TED, which includes immune reaction/inflammation, adipogenesis, hyaluronic acid (HA) secretion, and fibrosis. Previous work in our lab has shown that TED adipogenic and fibrotic phenotypes could be modelled in a 3D environment *in vitro*. Spontaneous lipid droplet (LD) formation was observed exclusively in 3D soft matrix, more prominent in TED orbital fibroblasts, and enhanced under pressure load simulating elevated intraorbital pressure, suggesting the involvement of mechanical factors in TED pathogenesis. We used this 3D model to further investigate three aspects of the TED phenotype, which includes LD formation, HA secretion, and fibrosis (cell contractility).

We found that myocardin-related transcription factor (MRTF), an important transcriptional cofactor for mechanotransduction, regulated the fibrotic phenotype rather than LD formation in orbital fibroblasts. Spontaneous LD accumulation in orbital fibroblasts was found to involve fatty acid uptake, but none of the classical chemical adipogenesis associated components. Rather, we found that it was linked to the expression of perilipin 2 (PLIN2), a protein surrounding LDs. The presence of stimulated macrophages significantly increased HA production and contractility in orbital fibroblasts, but did not promote LD accumulation. This work suggested that the overall TED phenotype may be regulated by inflammation: LD accumulation mediated by cytokine via upregulating the level of PLIN2, HA secretion induced by macrophages, and fibrosis (cell contractility) stimulated by macrophage through changes in actin dynamics and downstream MRTF/serum response factor (SRF) signalling.

Impact Statement

TED affects about 400,000 people in the UK. TED patients experience eye discomfort, disfigured appearance, visual morbidity, and even blindness. The detailed pathogenesis of the disease is poorly understood and consequently current treatments are limited, with appearance and visual functions often only restored after invasive interventions. This work aimed to use an *in vitro* model of the disease to characterise the phenotype of orbital fibroblasts in TED in order to clarify disease mechanism and identify possible new treatment targets.

We found that lipid droplet accumulation in orbital fibroblasts is associated with the expression of perilipin 2 (PLIN2), a protein that is involved in the make-up of the lipid droplets, and which has never been reported in TED. Our data suggest that PLIN2 could be a new marker for TED progression, as well as a potential treatment target as reducing PLIN2 level decreases lipid droplet formation in orbital fibroblasts and thus may prevent fat expansion in TED development. In addition, macrophages contribute to TED by stimulating HA production via TGF-β and PI3K pathways and promoting fibrosis by PI3K pathway. Fibrosis is also mediated by mechanotransduction transcriptional coactivator – MRTF. Therefore, interfering macrophage, TGF-β, PI3K, and MRTF may impede TED pathogenesis. This work reveals novel molecular determinants in TED, which brings inspiring new directions for future research to develop tracking markers and regimen.

Acknowledgements

First, I would like to thank my supervisor Dr. Maryse Bailly for accepting me as her student in her lab, and for all her guidance and mentoring throughout my PhD. I have learned a lot in science research here. I also thank my secondary supervisor Dr. Daniel Ezra for his support and help in clinical sample and data collection. This work would not have been possible without their mentoring.

I am grateful to Professor Sir Peng Tee Khaw and Lady Peggy Khaw for their help and thoughtfulness. It is really touching that they always know what I need the most.

I thank all the people who work around the lab for their help in many ways. Thank you to previous and current MB lab members: Jenny, He, Garima, Cynthia, Bruna, Dom, Viesturs, Max, Leslie, and Chiyun; in neighbouring group: Karen, Erika, Rachel, and Will. I particularly thank Diana for teaching me microscopy techniques in imaging and analysis, and our collaborator in Oxford, Dr. Katharine Pinnick, for lipid analysis and explaining her knowledge and experience about lipids to me.

I thank my hospital in Taiwan, Chang Gung Memorial Hospital, for funding my PhD studies.

Last but not least, I thank my parents for all their love, encouragement, support, and prayers for me.

Table of Contents

List of Tables

List of Figures

Abbreviations

Ab	Antibody
ABHD5	Alpha beta hydrolase domain protein 5, a.k.a. CGI-58
ACC	Acetyl-CoA carboxylase
ADRP	Adipose differentiation related protein, a.k.a. adipophilin or perilipin2
AMPK	AMP-activated protein kinase
APC	Antigen presenting cell
αSMA	Alpha-smooth muscle actin
ATGL	Adipose tissue triacylglycerol lipase
BSA	Bovine serum albumin
CD40L	CD40 ligand
CE	Cholesterol ester
C/EBP(α, β, δ)	CCAAT/enhancer-binding protein (α, β, δ)
CGI-58	Comparative gene identification 58, a.k.a. ABHD5
ChREBP	Carbohydrate responsive element binding protein
CLS	Crown-like structure
CMA	Chaperone mediated autophagy
CTGF	Connective tissue growth factor
DG, DAG	Diglycerides, a.k.a. diacylglycerol
DNL	De novo lipogenesis
ECM	Extracellular matrix
ELISA	Enzyme-linked immunosorbent assay
Elk-1	ETS-like transcription factor 1
Elk-3	ETS-like transcription factor 3, also known as Net
Elk-4	ETS-like transcription factor 4, a.k.a. SAP-1 (SRF accessory protein 1)
ER	Endoplasmic reticulum
Ets	E-twenty-six
FA(s)	Fatty acid(s)
FABPc	cytoplasm fatty acid binding protein
FABPpm	plasma membrane fatty acid binding protein
FAS or FASN	Fatty acid synthase
FAT	Fatty acid translocase, a.k.a. CD36
FATP(1,4)	Fatty acid transport protein(1,4), a.k.a. fatty acyl-CoA synthetase
FBS	Fetal bovine serum
G3P	Glycerol-3-phosphate
GAG	Glycosaminoglycans

GC	Gas chromatography
GDP	Guanosine diphosphate
GLUT(1,4)	Glucose transporter(1,4)
GR	Glucocorticoid receptor
GTP	Guanosine triphosphate
HA	Hyaluronic acid, Hyaluronan
HAS	Hyaluronan synthases
hsc70	Heat shock cognate protein of 70 kDa, a.k.a. HSPA8
HSL	Hormone sensitive lipase
HUVEC	Human umbilical vein endothelial cells
IBMX	3-isobutyl-1-methylxanthine
IFN-γ	Interferon-gamma
IGF-1R	Insulin-like growth factor-1 receptor
IHC	Immunohistochemistry
IL-1(α, β)	Interleukin-1(α, β)
IL-4,5,6,8,10,12	Interleukin-4,5,6,8,10,12
LAL	Lysosomal acid lipase
LAMP-2A	Lysosome associated membrane protein type 2A
LDL	Low-density lipoprotein
LDs	Lipid droplets
LPA	Lysophosphatidic acid
MAG	Monoacylglycerol
MCP-1	Monocyte chemoattractant protein 1
MEF	Mouse embryonic fibroblasts
MGL	Monoacylglycerol lipase
MHC	Major histocompatibility complex
MRTF(A,B), MKL(1,2)	Myocardin-related transcription factors (A,B), a.k.a. megakaryoblastic leukemia (1,2)
MSC	Mesenchymal stem cell
nCEH	Neutral cholesterol ester hydrolase
NF-κB	Nuclear factor kappa-light-chain-enhancer of activated B cells
ORO	Oil-Red-O
PA	Phosphatidic acid
PAT	including Perilipin, Adipose differentiation related protein, and Tail-interacting protein of 47 kDa
PC	Phosphatidylcholine
PDGF	Platelet-derived growth factor
PGE_2	Prostaglandin E_2
PI3K	Phosphatidylinositol-4,5-bisphosphate 3-kinase
PKA	Protein kinase A
PLIN(1~3)	Perilipin(1~3)

PMA	Phorbol-12-myristate-13-acetate
PPAR(α,γ)	Peroxisome proliferator activated receptor-(α,γ)
RFU	Relative fluorescence units
ROCK	Rho-associated kinase
SLC27A(1~6)	Solute carrier family 27 members A(1~6), a.k.a. FATP(1~6)
SMA	Smooth muscle actin
SRE	Serum response element
SREBP(1a,1c,2)	Sterol regulatory element binding protein(1a,1c,2)
SRF	Serum response factor
SVF	Stromal vascular fraction
TAZ	Transcriptional coactivator with PDZ-binding motif
TCFs	Ternary complex factors
TEADs	TEA domains
TED	Thyroid eye disease
TG, TAG	Triglycerides, a.k.a. Triacylglycerol
TGF-β	Transforming growth factor-β
TIP-47	Tail-interacting protein of 47 kDa
TNF-α	Tumour necrosis factor-α
TSH	Thyrotropin
TSHR	Thyrotropin receptor
YAP	Yes-associated protein

Chapter 1 Introduction

1.1 Thyroid Eye Disease

1.1.1 Clinical Perspectives of Thyroid Eye Disease

Thyroid eye disease (TED) is an autoimmune inflammatory ophthalmopathy related to thyroid dysfunction. The incidence is reported 16 per 100,000 women and 3 per 100,000 men (Bartley, 1994). The prevalence is 0.1~0.3% without ethnicity preference (Lazarus, 2012). Ninety percent of TED occurs in patients with Graves' disease, and the rest 3%, 1%, and 6% are from Hashimoto thyroiditis, primary hypothyroidism, and euthyroid, respectively. On the other hand, about 30% of Graves' disease patients develop TED (Holds, 2011-2012). The temporal relationship of the onset between TED and thyroid disease is close although not simultaneous. About 77% of patients have prior or concurrent thyroid disease on TED diagnosis, and 70% of the rest develop thyroid disease within 1 year (Wiersinga et al., 1988).

TED is characterised by the clinical signs of eyelid retraction (in 90% of patients), proptosis (in 60% patients), and limited extraocular muscle movements (in 40% patients). TED patients present symptoms ranging from mild eye irritation, periocular redness and swelling, double vision, to severe visual impairment. The diagnosis of TED requires thyroid function and antibody tests, periocular and orbital evaluation, and orbital radiographic imaging (**Table 1.1**). The clinical course of TED lasts as long as 1~3 years and comprises an initial deteriorating phase, a plateau period, and a slow and limited improvement phase, and these are graphed as the well-known Rundle's curve (**Figure 1.1**).

Table 1.1 Diagnostic criteria for Thyroid Eye Disease (TED).

Adapted from (Holds, 2011-2012)

Diagnostic criteria for TED

The diagnosis of TED is made when 2 of the following 3 signs of the disease are present:

1. Concurrent or recently treated immune-related thyroid dysfunction (≥1)

- **Graves hyperthyroidism**
- **Hashimoto thyroiditis**
- **Thyroid antibodies (+) but without dysthyroid state: TSH-receptor Ab (TRAb), thyroid-binding inhibitory immunoglobulins (TBII), thyroid-stimulating immunoglobulins (TSI), antimicrosomal Ab.**

2. Typical orbital signs (≥1)

- **Eyelid retraction with typical temporal flare (unilateral/bilateral)**
- **Proptosis (unilateral/bilateral)**
- **Restrictive strabismus in a typical pattern**
- **Compressive optic neuropathy**
- **Fluctuating eyelid oedema/erythema**
- **Chemosis/caruncular oedema**

3. Radiographic evidence of TED-unilateral/bilateral fusiform enlargement of muscle (≥1)

- **Inferior rectus muscle**
- **Medial rectus muscle**
- **Superior rectus/levator complex**
- **Lateral rectus muscle**

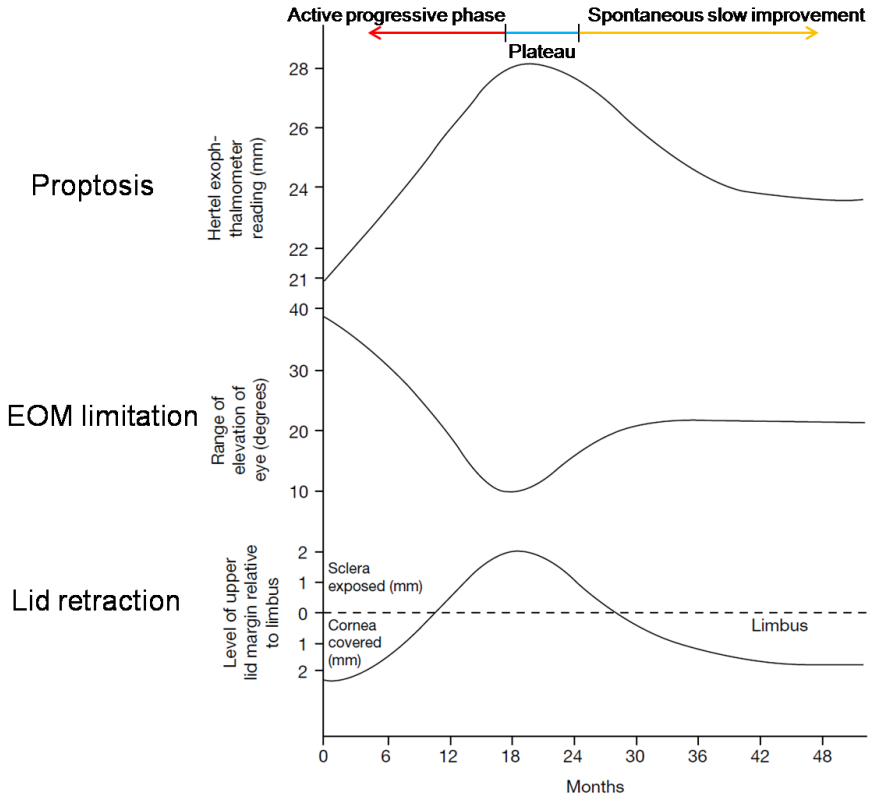

Figure 1.1 Rundle's curves presenting time course with clinical manifestations. Adapted from (Wiersinga and Kahaly, 2007)

The treatment of TED is complicated and depends on both TED disease activity and severity which are the most important two evaluations when approaching TED patients. A management algorithm has been developed by European Group On Graves' Orbitopathy (EUGOGO) as treatment guidelines (**Figure 1.2**). Management varies from routine follow-ups, topical lubricants, systemic glucocorticoids or immunosuppressants, radiation therapy, prism lenses, to multi-staged rehabilitative surgeries, according to disease status. If the disease has progressed to irreversible stage, surgeries are indicated to restore the appearance and function. Multi-staged surgeries especially the orbital decompression surgery, however, is destructive and risky. There is a new therapeutic regimen, teprotumumab, a human monoclonal antibody inhibitor of insulin-like growth factor-1 receptor (IGF-1R), recently reported to be effective to reduce clinical activity and proptosis (Smith et

al., 2017). Nevertheless, despite treatment, some severe cases still lose their vision due to compressive optic neuropathy. Therefore, understanding the biology of the disease would help develop feasible ways to prevent TED progression or to reverse TED.

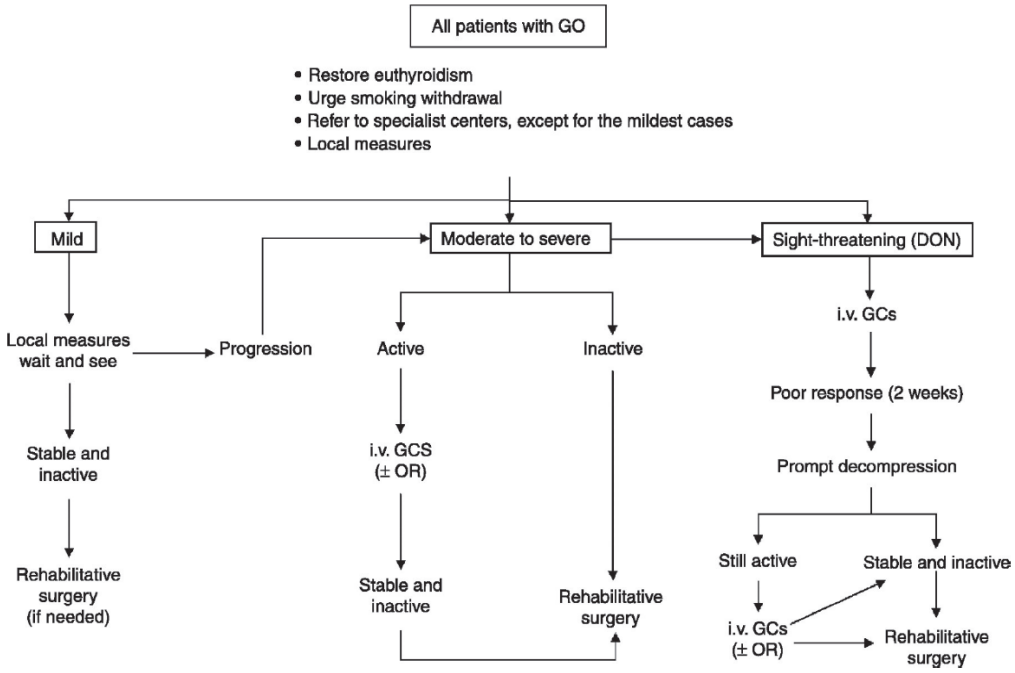

Figure 1.2 Algorithm for management of TED.

Adapted from (Bartalena et al., 2008)

1.1.2 Pathogenesis of Thyroid Eye Disease

Eyeball protrusion in TED patients is caused by an increase in soft tissue volume within the non-distensible orbital cavity bounded by orbital bones. The enlargement of extraocular muscle comes from the deposition of glycosaminoglycans (GAG), which also contributes to the retrobulbar fat and soft tissue expansion. Adipose tissue enlargement is thought to be due to adipogenesis. TED development is mediated by the underlying autoimmune reaction rather than by abnormal thyroid hormone levels (Bahn, 2010). The course of TED consists of an initiative immune reaction with inflammatory process, followed by GAG production,

adipogenesis, and a later fibrotic stage. Orbital fibroblasts, the key cell type involved in TED, expressing characteristic receptors make the orbit a distant and distinctive target organ from the TED initiating organ, the thyroid gland. Many immunocompetent, inflammatory cells with cell surface antigens and cytokines are involved in development of TED. T cells, predominantly CD4+, are the main immune cells found in TED (Forster et al., 1998). CD8+ T cells are also revealed to recognise orbital fibroblasts to initiate the signalling in pathogenesis of TED (Grubeck-Loebenstein et al., 1994). The potential stimuli and responsive molecules contributing to TED pathogenesis are summarised in **Table 1.2** (Dik et al., 2016). Following interaction with T cells, orbital fibroblasts are activated to increase secretion of interleukin-1 alpha (IL-1α), interleukin-6 (IL-6), and interleukin-8 (IL-8). T cells also stimulate proliferation, hyaluronic acid (HA) production, and adipogenesis in fibroblasts. Cytokines like interleukin-1 beta (IL-1β), interferon-gamma (IFN-γ), and platelet-derived growth factors (PDGFs) enhance HA production while having various effects on adipogenesis through other inflammatory mediators (**Table 1.2, Figure 1.3**)

Table 1.2 Various factors linked to TED pathology and their effects on orbital fibroblasts. Adapted from (Dik et al., 2016)

Stimulus	Effect on orbital fibroblasts							
	Inflammatory mediator production	Adhesion molecule expression	Co-stimulatory molecule expression	Proliferation	Hyaluronan production	TSHR expression	Adipogenesis	Myofibroblast differentiation
Inflammatory mediators/growth factors								
IL-1α		↑: ICAM-1		↑			–	
IL-1β	↑: IL-6, IL-8, IL-16, CCL2, PGE_2	↑: ICAM-1			↑		↑	
IL-4				↑	↑		–	
IL-6				–		↑	↑	
IFN-γ	↑: CCL2, CXCL9, CXCL10,CXCL11	↑: ICAM-1	↑: CD40		↑	↓	↓	
IGF-1				↑	↑			
Leukoregulin	↑: PGE_2				↑			
PDGF-AA	↑: IL-6			↑	↑	↓		
PDGF-AB	↑: IL-6			↑	↑	↑		
PDGF-BB	↑: IL-6, IL-8, CCL2, CCL5, CCL7			↑	↑	↑		
PGD_2					↑		↑	
PGE_2	↑: IL-6							
TGF-β				↑, –	↑	↓	–	↑
TNF-α	↑: IL-6, IL-8	↑: ICAM-1			↑	↓	↓	
Cellular interaction								
T cells	↑: IL-1α, IL-6, IL-8, CCL2, PGE_2	↑: ICAM-1		↑	↑		↑	
Mast cells	↑: PGE_2				↑			
Autoantibodies								
TSHR	↑: IL-6, IL-8, CCL2, CCL3, CCL4, CCL5, CXCL10, G-CSF, TNF-α	↑: ICAM-1			↑		↑	
IGF-1R	↑: IL-16, CCL5				↑			
Other factors								
Pressure							↑	↑
Smoking							↑	

↑ represents inducing effect, ↓ represents inhibitory effect, – represents no effect.

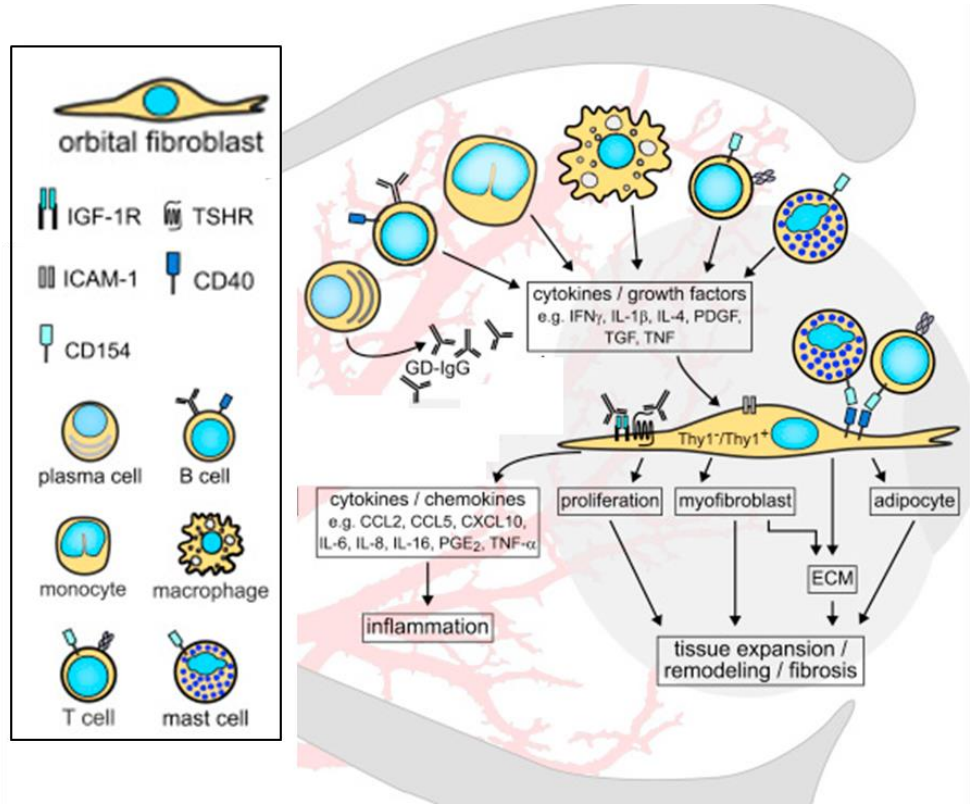

Figure 1.3 Pathogenesis of TED

Orbital fibroblasts are immune-activated by (1) cytokines and growth factors secreted by various immune cells, (2) CD40 which is expressed on their surface interact directly with CD40L (CD154) on T cells, (3) autoantibodies (GD-IgG) binding to TSHR and IGF-1R on orbital fibroblasts. Their activation further result in adipogenesis (adipocyte formation), HA secretion (ECM), myofibroblast transformation, and proliferation, and these contribute to the tissue remodelling and fibrosis in TED progress. Activated orbital fibroblasts also secrete cytokines and chemokines to induce further local inflammation. Adapted from (Dik et al., 2016).

1.1.2.1 Fibroblasts

Orbital fibroblasts differ from fibroblasts of other anatomic origin in morphology and features relating to functions. Morphologically, orbital fibroblasts tend to be spindle-shaped with cytoplasmic granules whereas dermal ones are more angular and less granular (Smith et al., 1989). Both normal and TED orbital fibroblasts but not dermal fibroblasts express CD40, a surface antigen which interacts with CD40 ligand (CD40L)-expressing T lymphocytes and mast cells to activate IL-6 and IL-8 upregulation (Sempowski et al., 1998). This makes orbital fibroblasts sensitive to T lymphocytes and triggers further inflammatory reactions. Orbital fibroblasts also uniquely express thyrotropin receptor (TSHR) and IGF-1R, both with higher expression in TED than control (Pritchard et al., 2003). As circulating thyrotropin receptor antibodies (TSHR-Ab) target thyroid follicular cells which express TSHRs, orbital fibroblasts share these antigenic epitopes on their surface and are thus reactive to TSHR-Ab and make the orbit a distinctive site for thyroid disease. With regard to GAG production, it is significantly induced in orbital fibroblasts, but not in dermal or subcutaneous fibroblasts, by IFN-γ or adipocyte differentiation medium (Smith et al., 1991; Zhang et al., 2012). These characteristics make orbital fibroblasts sensitive to the autoimmune stimulations and lead to the pathogenesis of TED comprising adipogenesis, HA production and fibrosis.

Orbital fibroblasts are heterogeneous in phenotypes and functions. Thy-1, a cell-surface glycoprotein, also known as CD90, can categorise orbital fibroblasts into two different subgroups (Koumas et al., 2002; Li et al., 2014). Thy-1^+ cells are capable of differentiating into myofibroblasts after transforming-growth-factor β (TGF-β) treatment, whereas Thy-1^- cells are prone to adipogenesis and cytoplasmic lipid droplets (LDs) formation after stimulation with peroxisome proliferator-activated receptor-γ (PPARγ) agonist (Koumas et al., 2003). Other properties of orbital fibroblasts include the response to prostaglandin E_2 (PGE_2) treatment

where 37% (range 22~50%) of cells presented shape change into more stellate and central elevated (Smith et al., 1995; Smith et al., 1994), and a preadipocyte subpopulation of 5~10% cells being able to be differentiated into adipocyte after stimulation with adipogenic differentiation medium (Sorisky et al., 1996). From the perspective of stem cells, fibroblasts are indistinguishable from mesenchymal stem cells (MSCs) in morphology, surface marker or immunophenotypes (Denu et al., 2016). Recent studies have revealed that both control and TED orbital fibroblasts express surface markers fulfilling MSC criteria, and show the potential to multilineage differentiations. This property may explain the diverse phenotypes of orbital fibroblasts in TED (Brandau et al., 2015; Kozdon et al., 2015).

1.1.2.2 Autoimmunity and Inflammation

TED is initiated with autoimmunity and inflammation. In early histochemical studies, infiltrating immunocompetent cells including mainly T lymphocytes (predominantly CD4+) and macrophages, with few B cells found in active TED orbits (Heufelder and Bahn, 1993; Weetman et al., 1989). B cells are involved more in the very early stage of TED as being antigen-presenting cells (APCs) and Ab-secreting cells and are followed by recruitment of T cells. B cells and T cells closely interact with each other for TED development. TED autoimmunity is originated from the intolerance of T cells to TSHR with unknown cause, and followed by B cells functioning as APCs. APCs recognise specific antigens (TSHR in autoimmune thyroid diseases), internalise them and present fragments of antigen peptides via human major histocompatibility complex (MHC) class II molecules to CD4+ helper T cells. Helper T cells have surface T cell antigen receptors (TCR) to connect with antigen/MHC (HLA complex) and are then activated. These activated helper T cells further reciprocally activate B cells and differentiate them into TSHR-Ab-producing plasma cells. While B cells express CD40 on their surface, they can bind to

CD40L of T cells to activate T cells as well (Bahn, 2010; Rydzewska et al., 2018) (**Figure 1.4**). The activated helper T cells are further divided with subtypes. Th1 cells secrete IL-2, IFN-γ, tumour necrosis factor-α (TNF-α), and IL-12, mainly for cellular immunity, whereas Th2 cells secrete IL-4, IL-5, IL-6, and IL-10 for humoral immunity. These cytokines enhance the orbital inflammation (Huang et al., 2019).

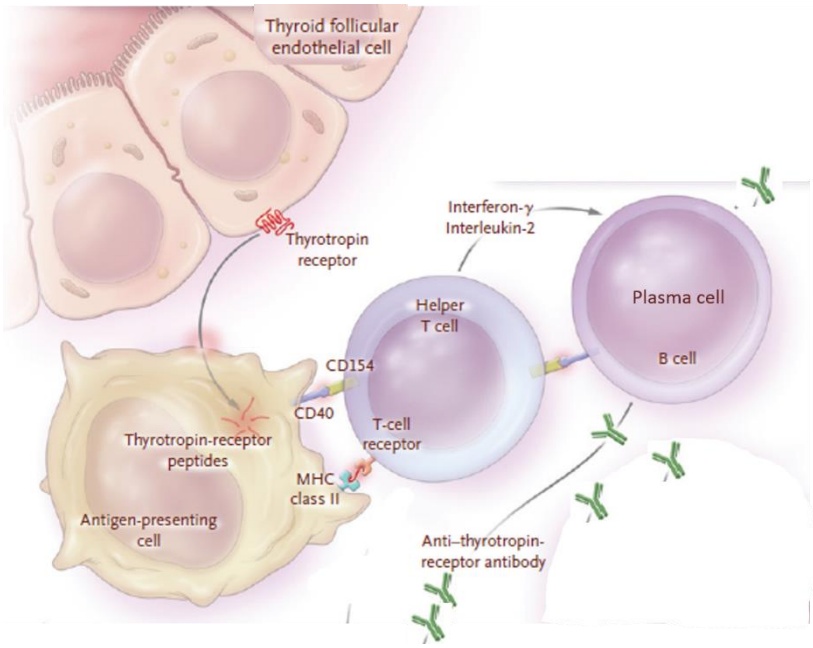

Figure 1.4 Diagram of initiation of TED autoimmunity

B cells functioning as antigen-presenting cells (APCs) internalise TSHR and present TSHR fragment on their surface as an antigen. This signal is passed to helper T cells and T cells activate B cells to produce TSHR Ab. Adapted from (Bahn, 2010)

When the B cell-secreted TSHR-Abs bind to TSHR on thyroid follicular epithelial cells, the thyroid produces uncontrolled amount of thyroid hormones as well as gets tissue hyperplasia. Similarly, these TSHR-Abs bind to TSHR on orbital fibroblasts, and in association with T cells, macrophages, and cytokines, TED orbital tissue remodelling is triggered (Bahn, 2010). As aforementioned, T lymphocytes, by expressing CD40L, interact with orbital fibroblasts directly by making CD40-CD40L bridges

(Sempowski et al., 1998). This engagement stimulates nuclear factor kappa-light-chain-enhancer of activated B cells (NF-κB) translocation in orbital fibroblasts, IL-6, IL-8 (Sempowski et al., 1998), and PGE_2 (Cao et al., 1998) synthesis in orbital fibroblasts and further aggravates inflammation. The secreted cytokines are capable of recruiting more lymphocytes to inflamed orbit. The CD40-CD40L ligation also promotes fibroblasts proliferation (Feldon et al., 2005) and HA synthesis (Cao et al., 1998) and thus contributes to TED tissue remodelling (**Figure 1.5**).

Based on these immunopathogenesis, immunotherapies targeting TSHR, IGF-1R, cytokines (TNF-α, IL-6, IL-1), B cells and T cells have been developed (Salvi, 2014). Rituximab, a monoclonal antibody against B cell surface antigen CD20, has been used to deplete B cells in order to treat some autoimmune diseases (Anolik et al., 2003; Leandro et al., 2002). It was reported that treatment with rituximab decreased the TED activity and progression effectively (Salvi et al., 2007; Salvi et al., 2015; Ueki et al., 2011), but another randomised controlled study showed rituximab not more effective than placebos (Stan et al., 2015). The differences between sampling, measurement, and reporting bias might have contributed to the discrepancy (Stan and Salvi, 2017). Recently, teprotumumab, an IGF-1R antagonist, has shown promising results in treating TED. It was given once every 3 weeks, and was more effective than placebo in improving CAS and proptosis over the course of 24 weeks. It is currently undergone phase 3 trial (Smith et al., 2017).

The involvement of macrophages in TED is evidenced by histopathological studies (Chen et al., 2008) and upregulation of macrophage-derived cytokine gene expression in TED tissues (Kumar and Bahn, 2003), but further information from *in vitro* studies are lacking and detailed mechanisms are still unknown. The more details about macrophages will be discussed in Section 1.4.

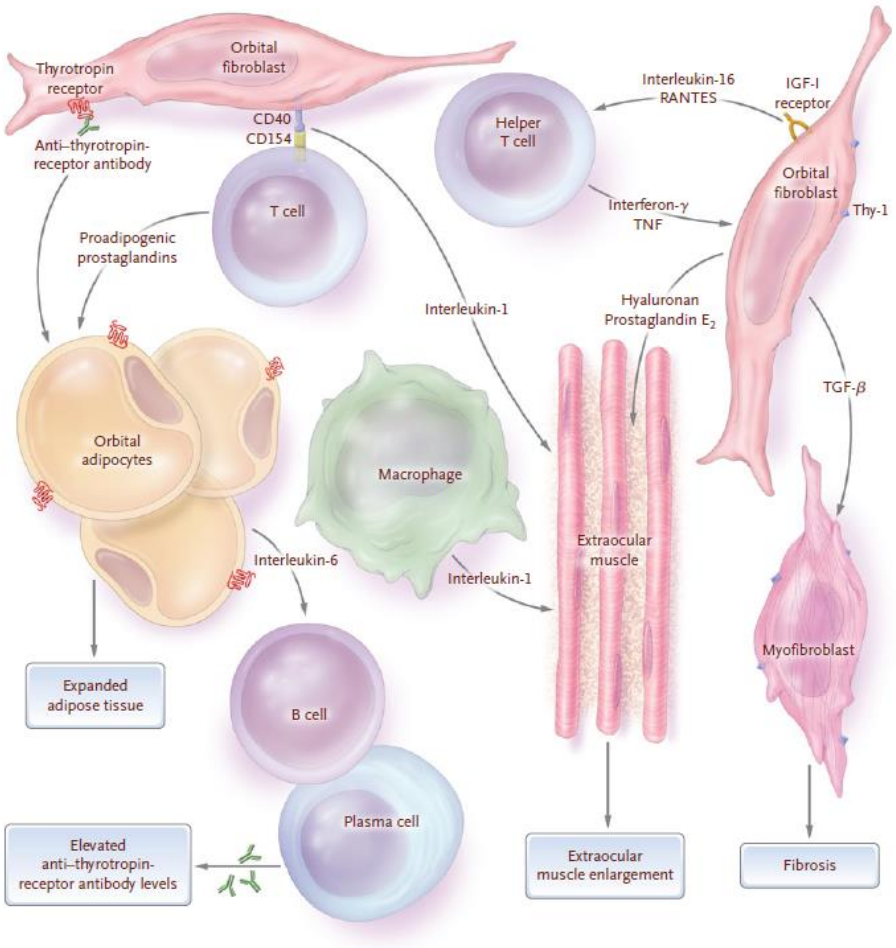

Figure 1.5 The correlation of immunocompetent cells with orbital fibroblasts in activation of TED.

The binding of TSHR Ab to TSHR on orbital fibroblasts, and interaction between orbital fibroblast and T cells through CD40-CD40L, promote adipogenesis and fat expansion. Activated helper T cells secreting TNF and IFNγ, and macrophages secreting IL-1, both stimulate orbital fibroblasts to produce HA. IGF-1R activation on orbital fibroblasts also triggers HA secretion which contributes to the enlargement of fat tissue and extraocular muscle. Orbital fibroblasts exposed to TGF-β are transformed into myofibroblasts to promote fibrosis. The adipocytes secreted IL-6 matures B-cell into plasma cells and increases TSHR Ab production. Adapted from (Bahn, 2010)

1.1.2.3 Fat Expansion

The characteristic clinical feature of TED is adipose tissue expansion. Orbital fibroblasts were shown to be capable of adipocyte differentiation, and adipogenesis has been considered the mechanism for TED fat enlargement since then (Sorisky et al., 1996). However, the exact nature of adipogenesis in TED is still unclear. PPARγ is the main transcription factor in adipogenesis, and its gene expression is increased in orbital tissues obtained from active TED stage compared to non-active TED and healthy controls by gene array (microarray) and quantitative polymerase chain reaction (PCR) assay (Kumar et al., 2005; Mimura et al., 2003). Since active TED tissues may contain immune cells like macrophages which express high levels of PPARγ, the increase in PPARγ seen in TED tissue may not be exclusively from adipogenesis of orbital fibroblasts, but it has not been proven by histology yet. In addition, the evidence for adipogenic late markers, such as lipoprotein lipase (LPL) and adiponectin, is not consistent in studies from patient samples. In a microarray study, both LPL and adiponectin showed increased gene expression in TED patients compared to control individuals (Kumar et al., 2005). However, in a more recent study, adiponectin protein concentration from TED orbital fat was not significantly different from samples from healthy individuals by enzyme-linked immunosorbent assay (ELISA) (Soiberman et al., 2013). *In vitro*, orbital fibroblasts derived from TED orbital adipose tissue are prone to differentiation into adipocytes and increased gene expression of PPARγ, leptin, and adiponectin upon chemical differentiation (Kumar et al., 2004; Sorisky et al., 1996). The adipogenesis differentiation is more likely to occur in Thy-1^- subpopulation cells (Lehmann et al., 2010; Smith et al., 2002). Adipogenesis following chemical differentiation was shown to induce TSHR expression in both orbital fibroblasts (TED and control) (Valyasevi et al., 1999) and fibroblasts from abdominal fat (Starkey et al., 2003). The link between TSHR expression and adipogenesis was further

revealed by increasing gene expression of adipogenic markers after gain-of-function mutation in TSHR (Zhang et al., 2006). These indicate that the adipogenic phenotype in TED *in vitro* differentiation model may be mediated by TSHR on orbital fibroblasts. In addition, IGF-1 was reported to induce lipid formation and adipogenic markers upregulation in TED orbital fibroblasts, and adipogenesis could be decreased by IGF-1R antibody and PI3K inhibitor, showing that IGF1-R may be also involved in adipogenesis via the PI3K-Akt signalling pathway (**Figure 1.6**) (Zhao et al., 2013).

1.1.2.4 Hyaluronic Acid Production

The histopathological examination of TED orbit reveals oedematous tissue, with GAG, mainly HA, accumulation surrounding muscle cells and connective tissues. This is attributed to another pathognomonic feature of TED, tendon-spared muscle enlargement (Riley, 1972). *In vitro*, orbital fibroblasts derived from both TED patients and normal individuals produce GAG upon stimulation with IL-1, TGF-β, IFN-γ, and PDGF (Korducki et al., 1992; Smith et al., 1991; van Steensel et al., 2012). In addition to cytokines, IGF-1, human recombinant TSH, bovine TSH, and human stimulatory monoclonal anti-TSHR antibody M22 have been reported to induce HA production, indicating both TSHR and IGF-1R play critical role in TED tissue remodelling (Iyer and Bahn, 2012; Kumar et al., 2012; Smith and Hoa, 2004). More recent studies revealed that TSHR and IGF-1R act synergistically on HA secretion (Krieger et al., 2015; Krieger et al., 2016). For the downstream signalling, PI3K-Akt-mTOR pathway was reported to be the one linking IGF-1 signalling to HA, but it is not involved in TSH signalling to HA (**Figure 1.6**). The production of HA is regulated by hyaluronan synthases (HASs) and UDP-glucose dehydrogenase, and HAS2 gene expression is best correlated with HA production in orbital fibroblasts (Zhang et al., 2012).

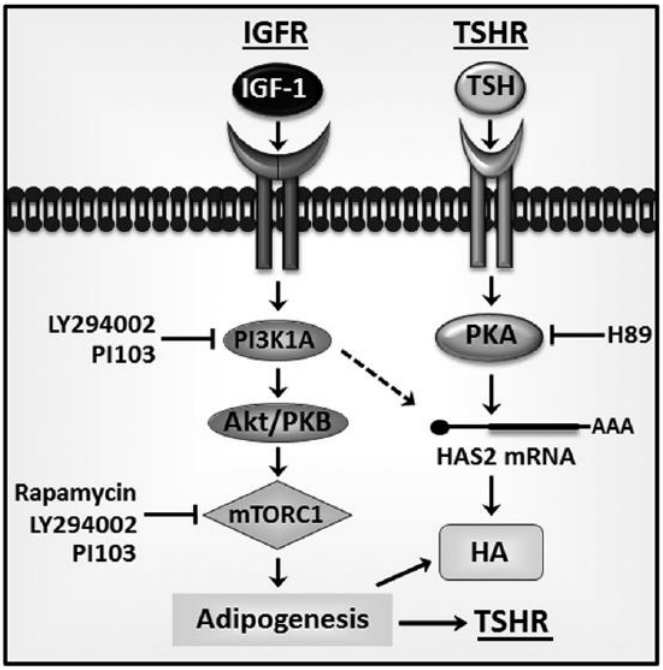

Figure 1.6 TSHR and IGFR signalling for HA production in orbital fibroblasts.

Both TSHR and IGFR signalling contributes to the production of HA, and PI3K/Akt/mTOR is the downstream of IGF-1 signalling. Adapted from (Zhang et al., 2012)

1.1.2.5 Fibrosis

On histopathological examinations, orbital connective tissue of late stage TED is inactive but fibrotic with dense scar revealed by Masson's trichrome positive staining (Hufnagel et al., 1984). Fibrosis is always regarded as a chronic and irreversible stage, and only surgery can correct the morbidity. Fibrosis is characterised by excessive extracellular matrix (ECM) deposition, and TGF-β is considered the main regulator in fibrosis. The immunohistochemical (IHC) staining of orbital connective tissue showed co-localisation of TGF-β expression with fibrotic regions, and the intensity of TGF-β expression correlates well with TED clinical activity and severity (Pawlowski et al., 2014). *In vitro*, Thy-1^+ orbital fibroblasts exposed to TGF-β can differentiate into myofibroblasts

expressing high level of alpha-smooth muscle actin (αSMA), a known fibrosis marker (Koumas et al., 2003). Furthermore, upon TGF-β activation, fibroblasts secrete connective tissue growth factor (CTGF), another profibrotic protein, which stimulates fibroblasts proliferation and matrix contraction (Leask and Abraham, 2004). The evidence for involvement of CTGF in TED has recently been reported showing that TED orbital fibroblasts express higher levels of CTGF mRNA and protein than control ones do. The amount of CTGF protein correlates with TED activity and severity scores (Huang et al., 2016). In addition, TGF-β1 upregulates CTGF, fibronectin and αSMA expression in TED orbital fibroblasts, and the silencing of CTGF reduces fibronectin and αSMA expression, suggesting CTGF is an important mediator in TGF-β1-stimulated myofibroblasts transformation in TED fibrosis (Tsai et al., 2018).

1.2 Mechanotransduction

Mechanotransduction is the concept that tissues and cells are able to sense mechanical stimuli, convert them into biochemical signals, and then respond biologically. In general, cells may experience mechanical stimuli from surrounding ECM and neighboring cells via cell-substrate contact (integrin) and cell-cell contact (cadherin), respectively, and this force transduces via cytoskeleton network to nucleus to modulate gene expression (Vining and Mooney, 2017). This is especially true for stem cells, whose survival, proliferation, organization, migration, and differentiation can be regulated by mechanical factors (Li et al., 2011). There are three basic kinds of mechanical forces including compression, tension and shear force contributing to stimulation on tissues (Butcher et al., 2009). *In vitro*, MSCs at low magnitude of tensile strain differentiate toward osteogenic phenotype, at higher tension differentiate toward cardiovascular phenotype, and at compressive strain differentiate toward chondrogenic phenotype (Schmelter et al., 2006; Simmons et al., 2003;

Takahashi et al., 1998). On the other hand, the ECM stiffness has been reported to determine the differentiation of MSCs. MSCs tend to differentiate into the lineage whose physiological stiffness matches the substrate stiffness the MSCs are grown. For instance, MSCs grown on rigid matrix differentiate toward bone, and on medium or soft matrix turn into muscle or neuron lineage (Engler et al., 2006; Huebsch et al., 2010). Moreover, modulating ECM stiffness together with chemical factors triggers more pronounced expression of differentiation markers than conditions with solely chemical factors. This suggests that elastic and chemical growth factors work synergistically on cellular differentiation (Tan et al., 2014).

Orbital tissues in TED encounter mechanical stimulation. TED occurs in the inextensible orbital cavity, and thus the volume increase of orbital contents due to HA production and fat expansion results in increased intraorbital pressure. The rise of intraorbital pressure may cause severe visual impairment because of optic nerve ischemia secondary to poor blood flow from high tissue pressure (Bahn, 2010; Daley et al., 2008; Fletcher and Mullins, 2010). Therefore, mechanical factors affect TED clinically, but whether TED development is mediated by mechanotransduction is yet to be studied. Previous work in our lab revealed spontaneous LD formation of orbital fibroblasts in a 3D *in vitro* model, and the pressure load enhanced the LDs (Li et al., 2014). Since orbital fibroblasts have properties of stem cells and the matrix elasticity may mediate cell differentiation (Brandau et al., 2015; Feng et al., 2010; Kozdon et al., 2015), we hypothesised that soft matrix in 3D promotes spontaneous LD formation by mechanotransduction.

1.2.1 3D Culture Model

Classical cell studies have been performed on glass or plastics where rigidity is at 10^9 Pascal levels, but most cells *in vivo* are at the stiffness of

1 to 10^6 Pascal (Mendez and Janmey, 2012) (**Figure 1.7**). Since cellular differentiation and behaviour are strongly determined by mechanical force (Butcher et al., 2009; Engler et al., 2006), it is ideal to have *in vivo* model for experimental research. Building an *in vivo* model for TED has been explored for decades, however, it has always been difficult to obtain all TED human manifestations including thyroid dysfunction, thyroid disease, and orbitopathy at the same time in one mouse model (Banga et al., 2015; Wiesweg et al., 2013). The immunisation method used in recent models delivered a human TSHR A-subunit plasmid to mice intramuscularly followed by electroporation. They yielded variable thyroid function, but better consistency in orbital features such as HA deposition at extraocular muscle, fat expansion, orbital fibrosis (Gortz et al., 2016; Moshkelgosha et al., 2013). However, the reproducibility is still unsatisfying, and it was reported owing to the difference in gut microbiota composition (Berchner-Pfannschmidt et al., 2016; Masetti et al., 2018). It is still more easily accessible to study TED *in vitro*. To simulate *in vivo* conditions, it is important to perform *in vitro* experiments in an appropriate elastic environment similar to the normal physiological status. Orbital fibroblasts reside within orbital tissue which is mainly composed of orbital fat. The stiffness of fat is around 1 kPa (**Figure 1.7**). The stiffness of orbital fat was measured as 250~500 Pa and 500~900 Pa in calf and monkey, respectively (Schoemaker et al., 2006). Our group has developed a three-dimensional (3D) *in vitro* model in which cells are cultured in collagen gels as a mimic for the *in vivo* soft orbital environment. We use type I collagen to make gels at a final collagen concentration of 1.5 mg/mL which predictably gives 100~500 Pa according to previous reports (Jin et al., 2016; Joshi et al., 2018) and unpublished results from the lab. This elasticity is more similar to the physiological stiffness compared to 2D culture in dish. Furthermore, in our TED 3D model, weights can be applied mimicking the increased orbital pressure after retrobulbar volume expansion. The 3D model also enables the observation of gel contraction as a parameter of fibrosis

evaluation. Our most striking finding is that TED orbital fibroblasts in 3D model spontaneously differentiate into LD expressing cells, whereas in 2D culture this phenomenon only occurs after triggering differentiation with differentiation medium (Li et al., 2014). The nature of this spontaneous differentiation remains to be clarified, but the preferred adipocyte differentiation in soft matrix suggests that mechanoresponsive pathways may be involved.

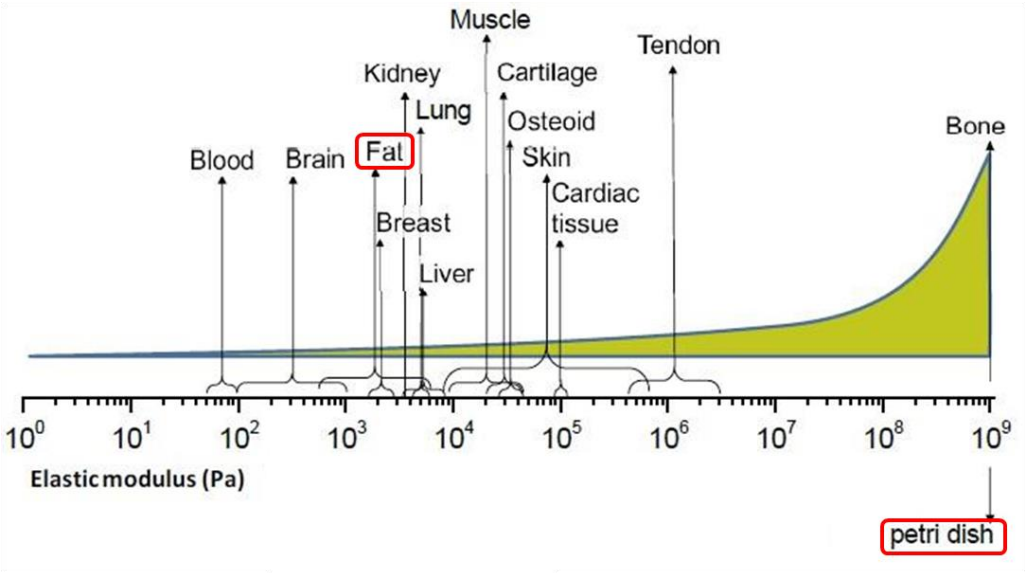

Figure 1.7 Elastic modulus of various tissues

Adapted from (Sachot et al., 2014)

1.2.2 MRTF

The Myocardin-Related Transcription Factors (MRTFs, or megakaryoblastic leukemia MKL)/Serum Response Factor (SRF) pathway is one of the well-known mechanosignalling pathways. SRF is a transcription factor which binds to the serum response element (SRE) in promoter region of target genes, and SRF target genes are characterised by the presence of CArG box. MRTFs, including myocardin, MRTF-A/MKL1/MAL22, and MRTF-B/MKL2/MAL16, are transcription coactivators that function together with SRF to regulate target gene

expression. MRTF/SRF target genes such as ACTA2 (αSMA) and CTGF can induce fibrosis or myofibroblast differentiation (Gressner and Gressner, 2008; Rockey et al., 2013; Tsou et al., 2014). MRTF shuttles between nucleus and cytoplasm, and this process is regulated by G-actin levels. The link between MRTF and mechanical force can be traced to mechanosensors, integrin and cadherin sensing mechanical stimuli from ECM and neighbour cells, respectively. The engagement of integrin and cadherin activates Rho family of GTPases which is composed of Rho, Rac, and Cdc42, to remodel actin cytoskeleton (Mui et al., 2016). RhoA is activated by phosphorylation, and further phosphorylates ROCK (Rho-associated kinase). There are also LIM kinases and cofilin joining into the downstream to form this force-Rho-ROCK-LIM kinases-cofilin pathway which regulates actin cytoskeleton. Actin cytoskeleton presents as either monomer G-actin or linear polymer F-actin form. The force-Rho-ROCK-LIM kinases-cofilin inhibits actin depolymerisation meaning promoting F-actin polymerisation (Parmacek, 2007). When actin polymerises into F-actin, the level of G-actin decreases, and MRTF becomes free to translocate into the nucleus, where SRF downstream genes are activated (Guettler et al., 2008; Miralles et al., 2003; Velasquez et al., 2013; Zhao et al., 2007) to mediate fibrosis or myofibroblast differentiation. In contrast, at high levels of G-actin, MRTF remains largely in cytoplasm, favouring white and brown adipogenesis (McDonald et al., 2015; Nobusue et al., 2014) (**Figure 1.8**). The mechanism for cytoplasmic MRTF promoting adipogenesis has not been well understood, but there was a report showing that MRTF-A interacts with PPARγ in nucleus and thus possibly regulates adipogenesis (Rosenwald et al., 2017).

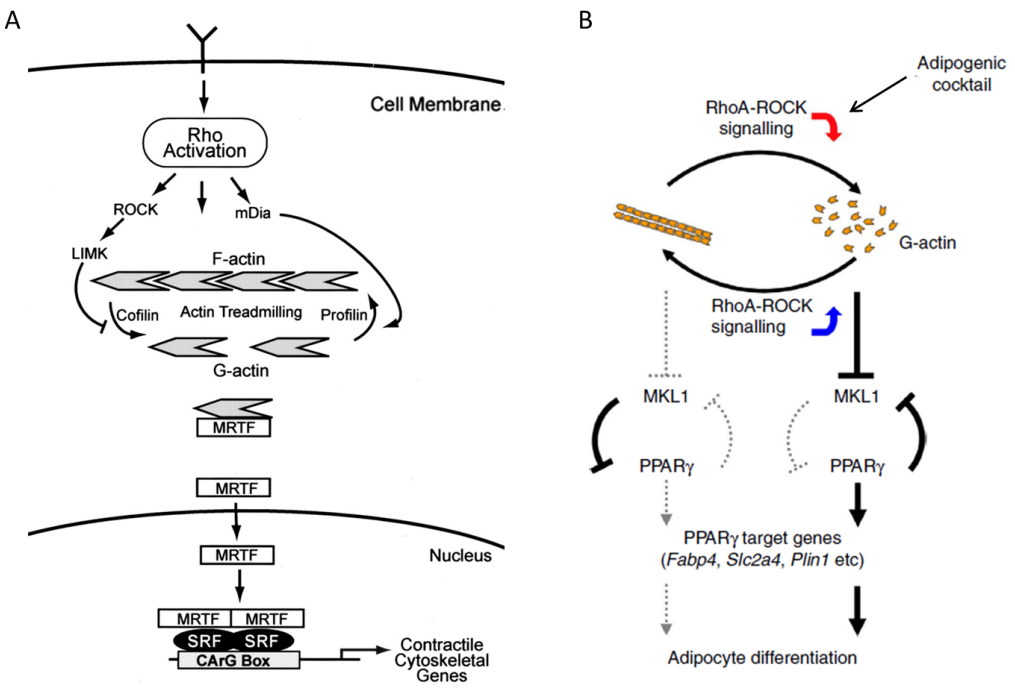

Figure 1.8 MRTF upstream and downstream regulations.

(A) Actin polymerisation is the main determinant for MRTF localisation. Rho-ROCK activation inhibits cofilin which depolymerises F-actin into G-actin, so increases F-actin. This frees MRTF to transfer into nucleus and triggers MRTF-SRF pathway and downstream contractile genes. (B) Adipogenic stimulus reduces Rho-ROCK signalling (red arrow pointing down means decrease) and increases depolymerisation of F-actin, so to increase G-actin which binds MRTF and retains the complex in cytoplasm (as (A) shows). This inhibits the MKL1 (MRTF-A) nuclear translocation and MRTF/SRF pathway. PPARγ gene is then upregulated, and cells are differentiated into adipocytes.

(A) Adapted from (Parmacek, 2007) (B) Adapted from (Nobusue et al., 2014)

In parallel with MRTF, there is another group of transcription co-activators, ternary complex factors (TCFs), including Elk-1 (ETS-like transcription factor), SAP-1 (SRF accessory protein 1, aliased as Elk-4) and Net (aliased as Elk-3), to regulate SRF target genes. TCFs are E-twenty-six (Ets) domain proteins which possess an Ets domain which makes sequence-specific interactions with DNA and a SRF interaction

domain. TCFs are known to be activated by Ras, phosphorylated by MAPK and ERK, and also to work with SRF on immediate-early transcriptional response (Hipskind et al., 1994; Posern and Treisman, 2006; Whitmarsh et al., 1995) (**Figure 1.9**). It is reported that TCFs and MRTFs compete to bind to SRF to regulate cell proliferation and contractility. When TCF-SRF is inactivated, many MRTF-SRF genes are enhanced and cells are more contractile in a mouse embryonic fibroblasts (MEFs) model (Gualdrini et al., 2016).

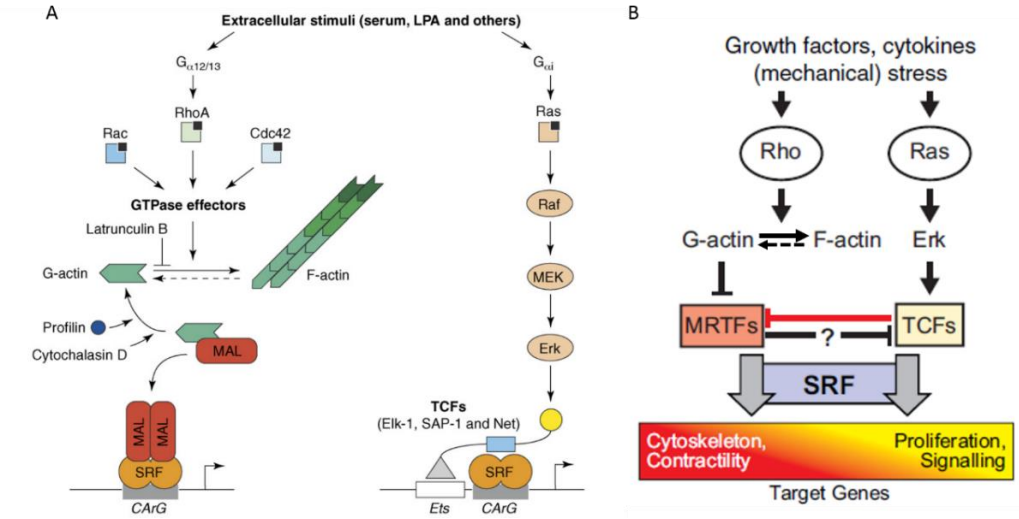

Figure 1.9 MRTFs and TCFs are both SRF regulators and complete to bind to SRF.

(A) Extracellular stimuli activate SRF by two separate signalling pathways: Rho/actin polymerisation/MRTFs, and Ras/Erk/TCFs. Yellow circle, transcriptional activation domain; blue rectangle, SRF interaction domain; grey triangle, ETS, DNA binding domain. (B) Model of MRTFs and TCFs antagonising each other and regulating different lineage of SRF target genes.

(A) Adapted from (Posern and Treisman, 2006) (B) Adapted from (Gualdrini et al., 2016)

1.2.3 YAP

Yes-associated protein (YAP) and transcriptional co-activator with PDZ-binding motif (TAZ) are another important mechanotransduction signalling transcriptional co-activators. Similar to MRTF, YAP/TAZ also shuttles between nucleus and cytoplasm in response to ECM stiffness, and mediates cell differentiation (Dupont et al., 2011; Halder et al., 2012). In the nucleus, YAP/TAZ interacts with TEA domains (TEADs) to regulate gene expression associated with proliferation, fibrosis, or osteogenesis. In a soft environment, YAP/TAZ remains in cytoplasm, and cells reside at growth arrest and preferably undergo adipogenesis (Dupont et al., 2011; Halder et al., 2012). The most striking finding of YAP/TAZ is that knockdown of YAP/TAZ and overexpression of YAP can overcome the mechanical cues to make adipogenesis occur on stiff ECM and rescue osteogenesis on soft substrates, respectively (Dupont et al., 2011), suggesting that YAP/TAZ is more determining than ECM for differentiation lineage. However, regulation of YAP/TAZ signalling is complex: 1) YAP/TAZ activity can be partially regulated by Rho-ROCK-F-actin tension. This is evidenced by using Rho and F-actin inhibitors, nuclear YAP/TAZ and downstream gene expression are effectively inhibited. But the overexpression of G-actin did not change YAP/TAZ activity or localisation (Dupont et al., 2011). 2) YAP/TAZ activity can be modulated by its phosphorylation status. Phosphorylated YAP is inactive and cytoplasmic, whereas unphosphorylated YAP is active and translocates to nucleus. Furthermore, Hippo/large tumor suppressor (LATS) signalling is often mentioned together with YAP/TAZ, because cytoplasmic YAP can be phosphorylated on serine 127 which is the target of LATS kinase of active Hippo pathway (Basu et al., 2003; Oka et al., 2008) (**Figure 1.10**). However, manipulation on LATS failed to overcome environmental mechanical cues suggesting that mechanotransduction of YAP/TAZ is independent from Hippo/LATS pathway (Dupont et al., 2011).

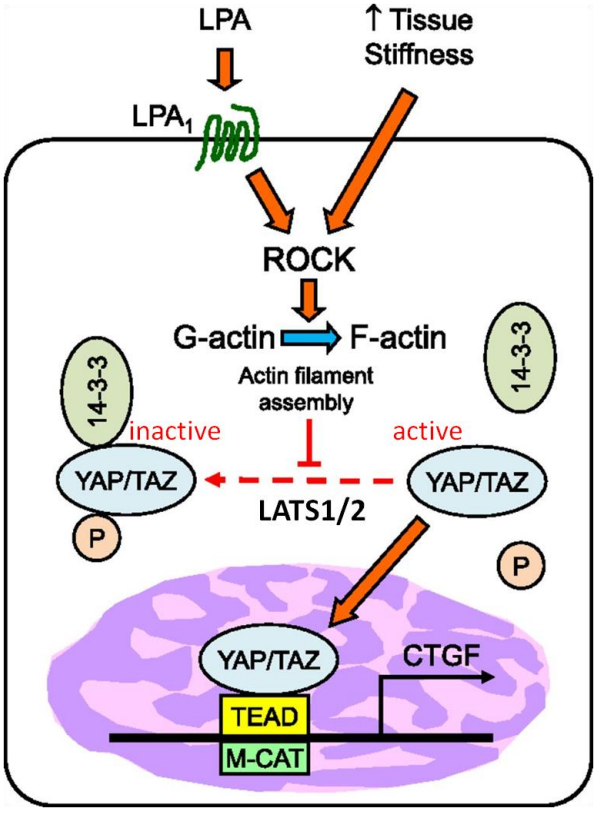

Figure 1.10 YAP/TAZ regulated by actin cytoskeleton and Hippo pathway.

The Rho-ROCK-F-actin signalling in stiff matrix or lysophosphatidic acid (LPA) stimulation activates YAP/TAZ nuclear accumulation and downstream gene expression. Activation of Hippo/LATS pathway phosphorylates and inactivates YAP/TAZ and leads to sequestration of YAP/TAZ in cytoplasm. Adapted from (Knipe et al., 2015)

3) YAP/TAZ is involved in Wnt signalling. When Wnt is off, YAP/TAZ is incorporated in the cytoplasmic destruction complex together with β-catenin. When Wnt is on, Wnt ligand disassembles the complex and frees YAP/TAZ and β-catenin to translocate to nucleus for downstream gene expressions (Piccolo et al., 2014) (**Figure 1.11**).

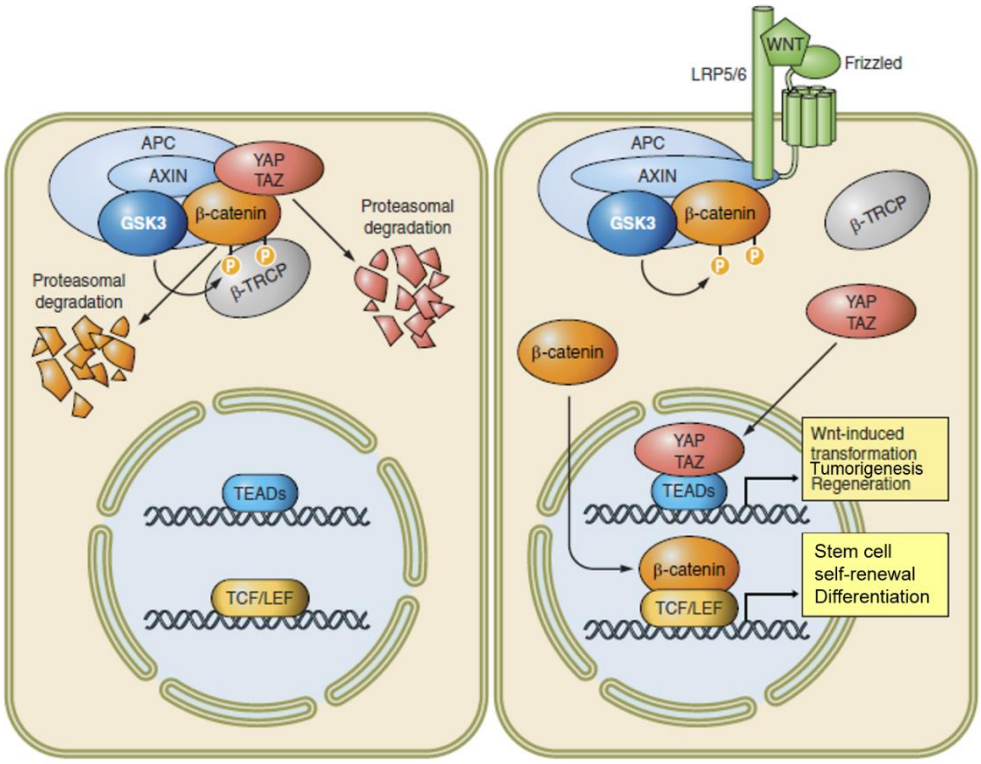

Figure 1.11 YAP/TAZ regulation by Wnt signalling.

In the Wnt-off state, YAP/TAZ is incorporated in the β-catenin destruction complex, and together with β-catenin is degraded in the cytoplasm. In the Wnt-on state, the Wnt ligand releases YAP/TAZ from the destruction complex and triggers YAP/TAZ nuclear accumulation to activate YAP/TAZ-dependent transcriptional responses. (APC, adenomatous polyposis coli; GSK3, glycogen synthase kinase-3; β-TRCP, β-transducin repeat containing protein; LRP, lipoprotein receptor-related protein; TEADs, TEA domains; TCF/LEF, T-cell factor/lymphoid enhancer factor) Adapted from (Piccolo et al., 2014)

1.3 Adipogenesis and Lipid droplet Metabolism

1.3.1 Adipogenesis

There are two kinds of adipose tissue, white and brown, being responsible for energy storage and heat generation, respectively (Saely

et al., 2012). The mature white adipocytes have single large lipid droplet (LD) accounting for more than 90% of the cell area, whereas brown adipocytes have multiple small vacuoles. The majority of fat in human body is composed of white adipose tissue. Brown adipose tissue is distributed at interscapular area in infants and disappears with age, and only small paravertebral and axillary depots are residual in adults (Sanchez-Gurmaches et al., 2016). Orbital adipose tissue has the characteristics of white adipose tissue, thus white adipogenesis is widely considered as the mechanism for retrobulbar fat expansion in TED. However, fat expansion can originate from two mechanisms, hyperplasia (cell number increase) and hypertrophy (cell size increase) (Hirsch et al., 1989; Kumar et al., 2004), and it has never been clarified in TED histopathology.

Adipogenesis is defined as the process whereby preadipocytes differentiate into adipocytes. Preadipocytes are distributed in adipose tissue, and derived from pericytes (Cawthorn et al., 2012). As **Figure 1.12** shows, ECM stiffness and related mechanotransduction factors contribute to adipogenesis at the initial stage where MSCs are committed into preadipocytes (Cristancho and Lazar, 2011). MSCs originate from pericytes as well, consistent with the pericyte origin of preadipocytes (Crisan et al., 2008). The committed preadipocytes undergo two stages of adipogenesis when being further exposed to adipogenic inducers. The protocols for *in vitro* adipogenic differentiation vary widely but there are three components generally used in adipogenic differentiation medium, including insulin, dexamethasone, and 3-isobutyl-1-methylxanthine (IBMX) (Saben et al., 2014; Scott et al., 2011). Other additional components may also be used, such as rosiglitazone (PPARγ agonist) and indomethacin. It was later reported that only dexamethasone with rosiglitazone are adequate and necessary to induce adipogenic differentiation (Contador et al., 2015). The usage of these chemicals is not mimic of natural physiological conditions, but is to activate transcription factors based on the mechanism of adipogenesis. Complete

adipogenesis requires stages of transcription factors activation. In addition to glucocorticoid receptor (GR) activation, activation of CCAAT/enhancer-binding protein β and δ (C/EBPβ and C/EBPδ), the first two transcription factors in adipogenesis, contribute to the first stage of adipogenesis which occurs hours following treatment with adipogenic inducers. The second stage of adipogenesis starts from the activation of intermediate and main transcription factors of adipogenesis -- PPARγ and C/EBPα, occurs days following the initial induction (Lefterova et al., 2014). As preadipocytes are getting more mature, LDs are formed and merged into a large droplet, and genes for adipocyte-specific proteins, such as leptin, adiponectin, LPL, and aP2 are expressed. This step matures adipocytes and finalises adipogenesis (Fonseca-Alaniz et al., 2007).

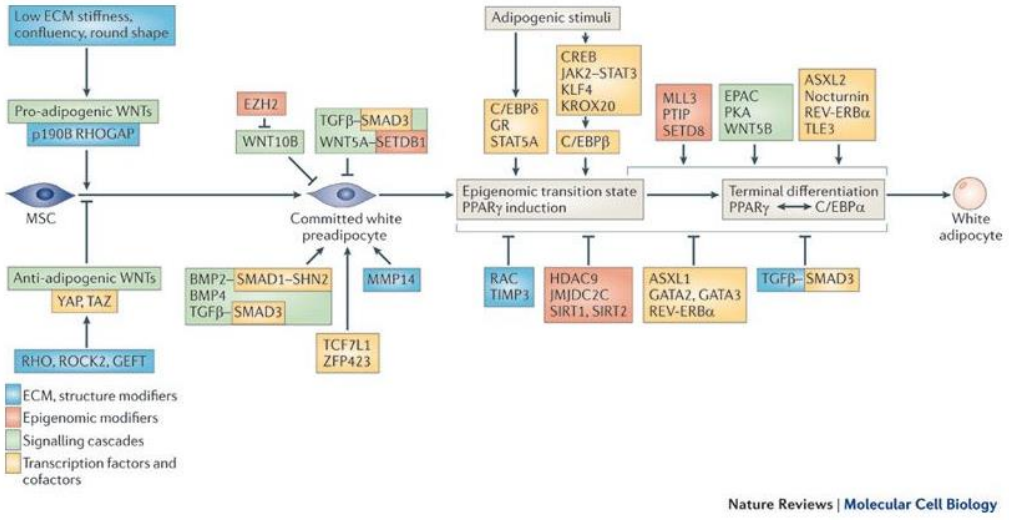

Figure 1.12 Cues involved in the differentiation of MSCs to mature white adipocytes.

MSCs are transitioned to committed white preadipocyte by soft ECM, inhibition of Rho-ROCK and YAP/TAZ. The further addition of adipogenic stimuli activates C/EBPδ and C/EBPβ, as first stage of adipogenesis. The activation of PPARγ leads to terminal differentiation, as second stage of adipogenesis, and mature white adipocytes are formed. Adapted from (Cristancho and Lazar, 2011)

Dexamethasone is an inducer of C/EBPβ and C/EBPδ, it also binds to GR, thus activates the first stage of activation of transcription factors (Scott et al., 2011). Rosiglitazone, a potent PPARγ ligand, directly increases PPARγ transcriptional activity and speeds adipogenesis (Benvenuti et al., 2007). Insulin enhances the expression of sterol regulatory element binding protein-1 (SREBP1) which further induces PPARγ (Fajas et al., 1999; Kim et al., 1998a; Kim et al., 1998b). The activation of PPARγ involves ligand binding, heterodimerisation of PPARγ with retinoic X receptor (RXR), and some coactivator proteins. Without ligand binding, PPAR/RXR is bound to co-repressors, preventing PPAR/RXR binding to PPAR response element (PPRE) on promoters (Leonardini et al., 2009) (**Figure 1.13**).

Previous TED studies have successfully induced adipogenesis markers such as C/EBPβ, C/EBPα, PPARγ, leptin, adiponectin, LPL, and aP2 by stimulating orbital fibroblasts with adipocyte differentiation medium. Nevertheless, it is unknown if there is any other lipid metabolism pathway contributing to fat expansion in TED.

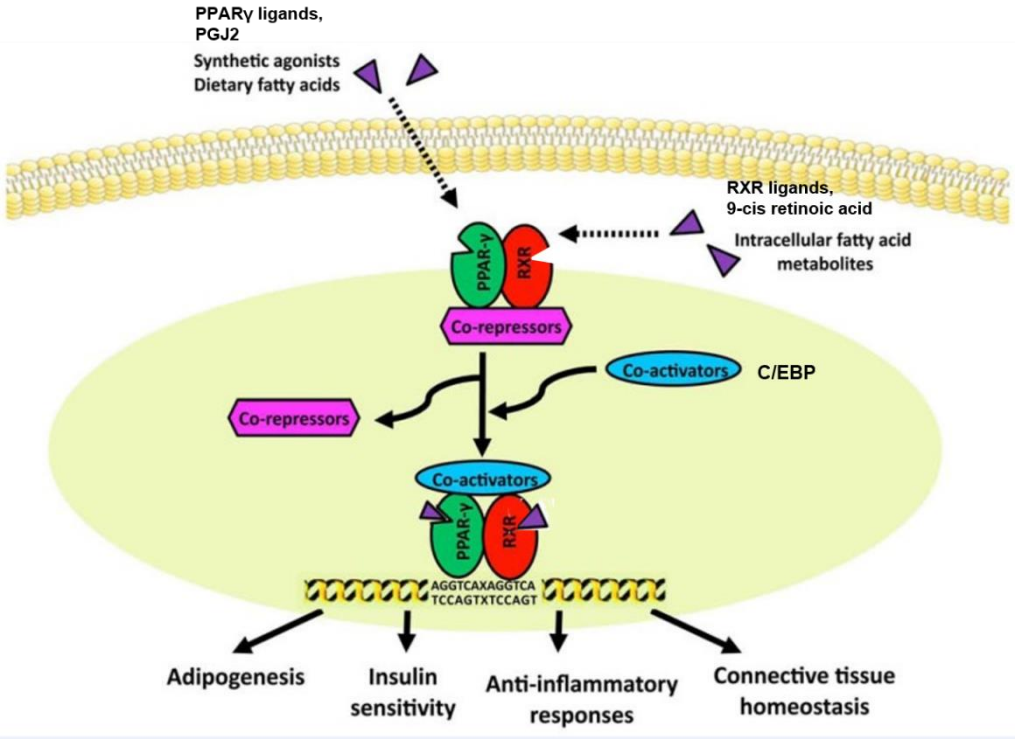

Figure 1.13 Mechanism of PPARγ activation.

PPARγ activation requires ligand binding to PPARγ and RXR, heterodimerisation of PPARγ and RXR, and the binding of co-activators to this dimer, and the whole complex binds to target gene to induce transcription. Adapted from (Wei et al., 2012)

1.3.2 Lipid Droplet Formation and Degradation

All mammalian cells have LDs within their cytoplasm (van Meer, 2001). LDs are an intracellular reservoir of neutral lipids to maintain energy homeostasis, and are regarded as dynamic cellular organelles (Guo et al., 2009). LDs are formed by the endoplasmic reticulum (ER), and interact with other organelles, such as ER, mitochondria, endosomes and plasma membrane to balance lipid storage and usage (Fujimoto et al., 2008; Goodman, 2008; Murphy et al., 2009). These LDs are composed of a central core of neutral lipids, mainly triglycerides (TGs,

a.k.a. triacylglycerols, TAGs) and sterol esters, and an outer envelope of monolayer of phospholipids. There are also proteins coating on LDs, including perilipin family proteins, membrane trafficking proteins--Rab, lipid-synthesis enzymes, and lipases (Blanchette-Mackie et al., 1995; Martin and Parton, 2006). TG is composed of one glycerol and three fatty acids (FAs), and is synthesized from glycerol-3-phosphate (G3P) and FAs. The G3P undergoes acylation and forms phosphatidic acid (PA) which turns into diglycerides (DG, a.k.a. diglycerides, DAGs) after dephosphorylation by an enzyme called Lipin. DG may turn into TG or phosphatidylcholine (PC), a phospholipid for plasma membrane and LD outer envelope (Itabe et al., 2017). The FAs of TGs may be formed by 2 mechanisms, 1) extracellular FAs entering cells and 2) carbohydrates, such as glucose, entering cells and then synthesizing FAs. The sterols of LDs are taken up into cells through endocytosis (Guo et al., 2009) (**Figure 1.14**). All of these result in increase of intracellular FAs and sterols and trigger the formation of LDs in ER (Blanchette-Mackie et al., 1995; Martin and Parton, 2006).

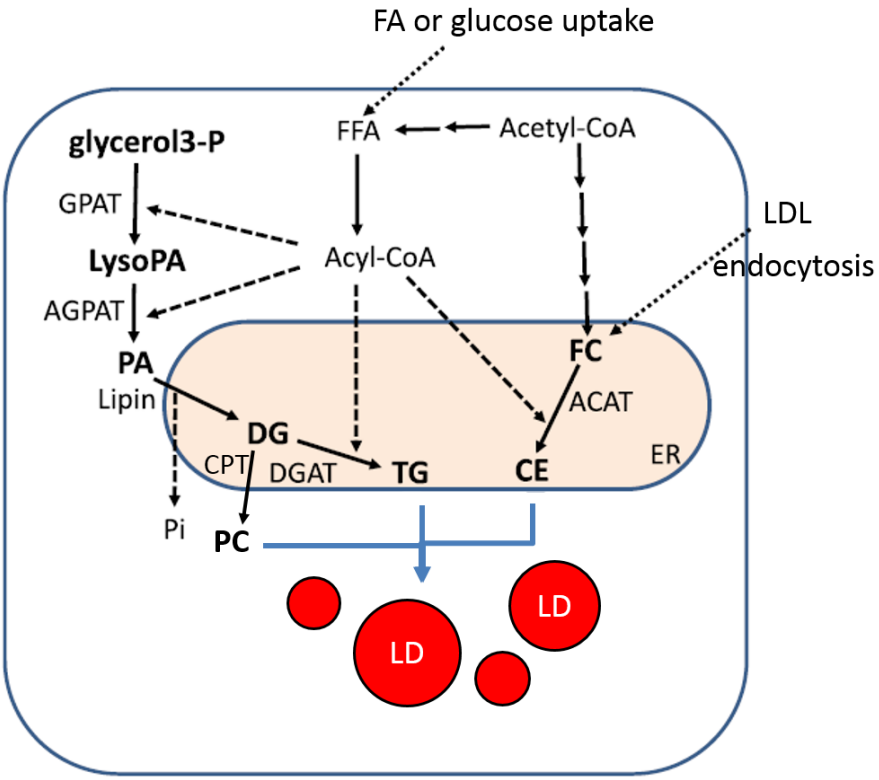

Figure 1.14 Diagram of lipid droplet formation

Lipid droplet (LD) is composed of (1) triglycerides (TG) from fatty acid (FA) and diglycerides (DG), and FAs may be de novo made from glucose or directly uptaken extracellularly while DG is from glycerol-3-phosphate (glycerol3-P, G3P) (2) cholesterol ester (CE) from endocytosis, (3) phosphatidylcholine (PC) from glycerol3-P. (glycerol3-P, glycerol-3-phosphate; GPAT, glycerol-3-phosphate acyltransferase; LysoPA, lysophosphatidic acid; AGPAT, 1-acylglycerol-3-phosphate O-acyltransferase; PA, phosphatidic acid; Pi, phosphate ion; DG=DAG, diglycerides=diacylglycerol; CPT, cholinephosphotransferase; DGAT, diacylglycerol acyltransferase; PC, phosphatidylcholine; FFA, free fatty acid; TG=TAG, triglycerides=triacylglycerol; LD, lipid droplet; FA, fatty acid; FC, free cholesterol; ACAT, acyl-CoA cholesterol acyltransferase; CE, cholesterol ester; ER, endoplasmic reticulum; LDL, low-density lipoprotein) Adapted from (Itabe et al., 2017)

FAs are formed of carbon and hydrogen molecules. FAs without double bonds are saturated FAs, and those with one double bond are monounsaturated whereas with more than one double bonds are polyunsaturated. Types of FAs differ in the numbers of carbon atoms and double bonds, and the location of the double bonds in the hydrocarbon chain. These can be simply named in the form of C:D (n-x or ω-x), where C refers to the number of carbon atoms, D is the number of double bonds, and n-x or ω-x refers to the location of double bond on x^{th} carbon counted from the methyl carbon end. The length of FAs hydrocarbon chain can be elongated with fatty acid elongase, and double bonds can be formed to desaturate FAs with desaturase (Ahmad, 2017; Naudí et al., 2012) (**Figure 1.15**). The main functions of FAs are energy storage, cellular membrane constitution, and signalling pathway regulation where FAs are precursors for prostaglandins, thromboxanes, and leukotrienes to mediate inflammation and coagulation (Calder, 2015). FA composition of fat depot is linked to diet and endogenous elongation and desaturation processes. FA composition profiles as well as lipogenic gene expression were shown different between visceral adipose tissue and abdominal subcutaneous adipose tissue in obese patients (Petrus et al., 2017). Therefore, FA composition may give insight into the pathophysiological change in fat tissue.

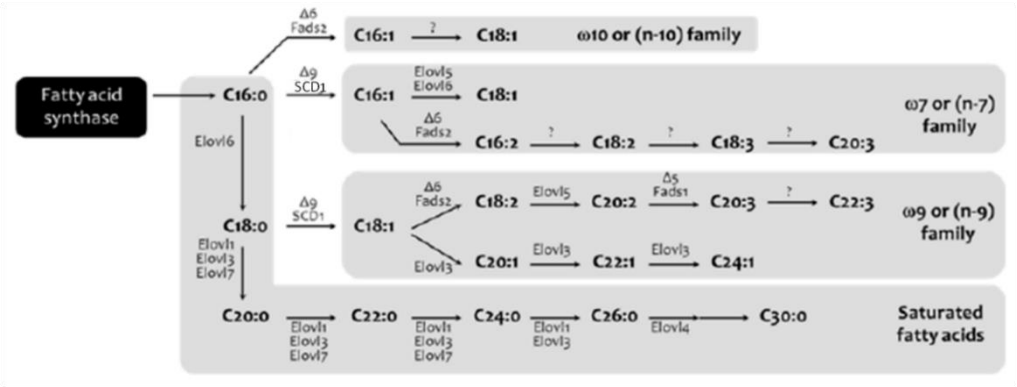

Figure 1.15 Pathway of long-chain fatty acid synthesis

Saturated FA C16:0 is produced by fatty acid synthase, and can be added with 2 more carbons under the action of fatty acid elongase 6 (ELOVL6) to become FA C18:0, and further addition of 2 more carbons makes FA C20:0. Under the function of stearoyl-CoA desaturase 1 (SCD-1), C16:0 can be desaturated into C16:1. Further desaturation or elongation makes C16:1 into C16:2 or C18:1, respectively. These are ω7 or n-7 family meaning the first double bond is at the 7th carbon counted from the methyl carbon end. Similar elongation and desaturation rules apply to other families. Adapted from (Naudí et al., 2012)

On the other hand, LDs undergo degradation while cells are in demand for energy, or upon hormonal or inflammatory stimulations. LD degradation mechanism can be categorised into (1) lipolysis: using cytoplasmic lipases to hydrolyse LDs at neutral pH, and (2) lipophagy: the autophagic degradation of LDs, also known as acidic lipolysis where LDs are transported to lysosome and hydrolysed by lysosomal acid lipase (LAL) at low pH (Zechner et al., 2017) (**Figure 1.16**). It is not clearly known what regulates LDs hydrolysis by lipolysis or degrade by lipophagy. The dysregulation of LD formation and degradation can lead to metabolic diseases, such as diabetes and obesity (Lazar, 2005). Although adipogenesis has been widely studied in TED, it is not known whether TED cells have more LD accumulation. The LDs we observed in our 3D *in vitro* model are small-sized LDs within cytoplasm, without

fibroblasts morphological change (Li et al., 2014), unlike the large LDs and round-up of fibroblasts seen in classical adipogenesis. Therefore, it would be informative to investigate the role of LDs in TED, especially using the 3D *in vitro* model. We hypothesised that in addition to classical adipogenesis, TED orbital fibroblasts may form LDs through FA uptake, carbohydrate utilisation and endocytosis or display altered LD degradation.

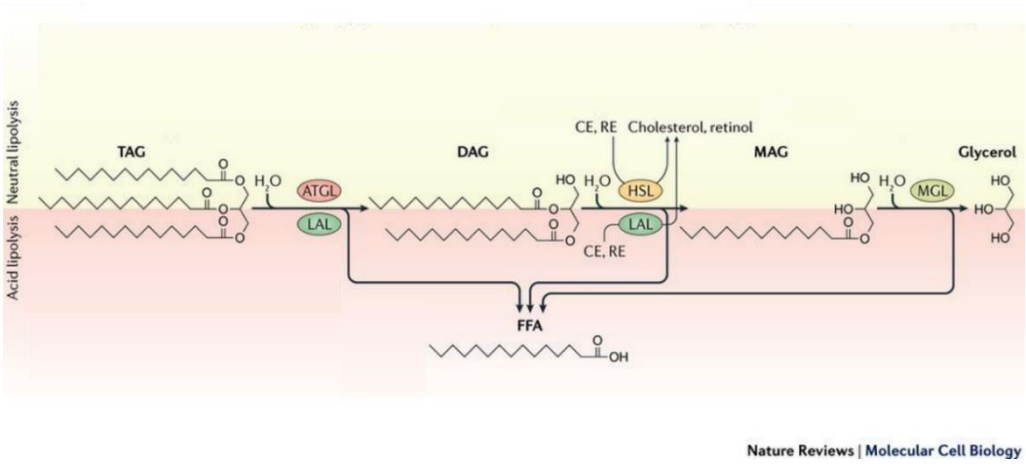

Figure 1.16 Lipid degradation pathway

By neutral lipolysis, TAG (TG) is degraded into DAG (DG) and FA by adipose tissue triacylglycerol lipase (ATGL), DAG is degraded into monoacylglycerol (MAG) and FA by hormone sensitive lipase (HSL), and MAG is degraded into glycerol and FA by monoacylglycerol lipase (MGL, MAGL). Cholesterol ester (CE) can be degraded into cholesterol by HSL as well. By acid lipolysis, lysosomal acid lipase (LAL) can degrade TAG, DAG and CE. Adapted from (Zechner et al., 2017)

1.3.2.1 Extracellular Fatty Acid entry into Cells

In the circulation, most fatty acids (FAs) are bound to transport protein, such as albumin. These bound FAs dissociate from albumin before entering into cells. No additional protein is needed for movements by simple diffusion. Alternatively, there are some proteins on plasma

membranes involved in free FA influx, including fatty acid translocase (FAT, also known as CD36), fatty acid transport protein (FATP, also known as fatty acyl-CoA synthetases), and plasma membrane fatty acid binding protein (FABPpm) (Glatz et al., 2010; Thompson et al., 2010). These different FATPs and FABP selectively facilitate entry of FAs of different chain lengths and degree of saturation (**Figure 1.17**).

FATP family has 6 subtypes named FATP1~6 encoded by gene “solute carrier family 27 members A1~6” (SLC27A1~6). Each subtype has different tissue distribution preference, for instance, FATP1 distributes within brown and white adipose tissue, heart, skeletal muscle, skin, brain, kidney and endothelial cells, whereas FATP5 expression is restricted to the liver (Anderson and Stahl, 2013). As FATPs are enzymes, the way they transport FAs is by direct converting of FAs into acyl-CoA ester, which is further processed in lipid storage (LD formation) or energy production (β-oxidation) (Lobo et al., 2007). White adipose tissue predominantly expresses FATP1 and FATP4 (Anderson and Stahl, 2013). FATP1 knockdown in 3T3L1 differentiated adipocytes showed decreased FA uptake and TG synthesis by tracing isotope-labelled FAs (Lobo et al., 2007). And overexpression of FATP1 in stable cell line C8 revealed increased TG synthesis from increased uptake and incorporation of isotope-labelled FAs (Hatch et al., 2002). *In vivo*, transgenic mice with cardiac-specific overexpression of FATP1 demonstrated increased FA uptake and FA accumulation in cardiomyocytes resulting in lipotoxic cardiomyopathy (Chiu et al., 2005). These suggest the functional role of FATP1 in FA transport. On the other hand, FATP4 overexpression in HEK293 cells increased FA uptake, and FATP4 gene silencing by antisense oligonucleotide decreased FA uptake in primary enterocytes (Stahl et al., 1999). However, the FATP4 knockdown by siRNA in differentiated 3T3L1 adipocytes did not decrease FA uptake (Lobo et al., 2007). In addition to this controversy in FA uptake function, FATP4 was reported to be localised to the ER rather than plasma membrane (Milger et al., 2006). Therefore, the mechanism FATP4 regulating FA uptake is

thought to be depletion of intracellular FAs, since it has acyl-CoA synthetase function for esterification FA with CoA, which then triggers FA uptake through plasma membrane (Digel et al., 2009).

CD36 is expressed in adipocytes, endothelial cells, cardiac and skeletal myocytes. *In vivo*, FA uptake was reduced in adipocytes (Febbraio et al., 1999), and smaller adipocyte size and lower number of adipocytes were found in CD36 knockout mice (Vroegrijk et al., 2013). CD36 gene mutation in human decreased palmitate (one kind of FA) uptake in muscle, adipose tissue, and cardiac tissue, but not hepatic tissue, detected by ^{11}C palmitate positron emission tomography (PET) scan (Hames et al., 2014). *In vitro*, FA uptake is positively correlated with CD36 surface expression in human preadipocytes in stromal vascular fraction (SVF) (Gao et al., 2017). CD36 was also found to be associated with cancer. CD36 expression as well as FA uptake and intracellular LD area were increased in human ovarian cancer cells after co-culture with omental adipocytes, and the effect can be abolished by CD36 inhibitor and shRNA. Adipocytes provide FAs for tumour growth via CD36. The CD36 knockdown decreased co-culture-induced invasion and migration, indicating that CD36 may regulate tumour progression (Ladanyi et al., 2018). CD36 may work independently or interact with FABPpm to facilitate FA entry. But unlike the enzymatic role of FATPs, CD36 appears to be membrane protein, and provides the extracellular attachment site for FAs. As FAs pass through the bilayer of plasma membrane, CD36 functions as a docking site for cytoplasm fatty acid binding protein (FABPc) or acyl-CoA synthetases at the intracellular side for further FA metabolism (Glatz and Luiken, 2018).

The total FA uptake has contributions from several membrane proteins. An analysis in human preadipocytes in SVF showed that cells express CD36 also have consistently higher level of FATP1 and FATP4 expression compared to cells negative for CD36 by flow cytometry. The CD36 inhibitor decreased total FA uptake, but it was not known whether

the functions of FATPs were affected (Gao et al., 2017). Another study revealed that cardiomyocytes of CD36 knockout mice had compensatory upregulation of FATP1, and this resulted in unchanged FA uptake (Habets et al., 2007). Since multiple transporters are involved, FA uptake is unpredictable when manipulating these transporters and compensatory effects should be considered in data interpretation.

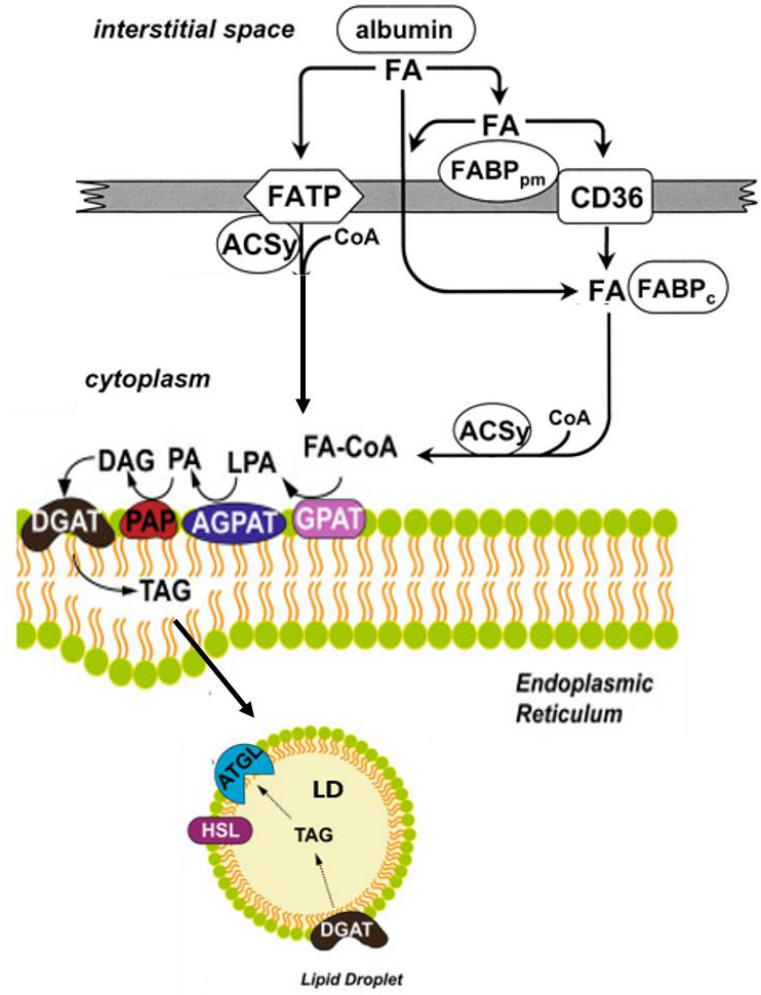

Figure 1.17 Molecular mechanisms for transmembrane cellular uptake of fatty acids.

Fatty acids (FAs) dissociate from albumin, and may cross plasma membrane directly by passive diffusion, or utilise FA transport related proteins such as FATPs, CD36, FABPpm, and FABPc to facilitate the entry. Adapted from (Azzazy et al., 2006; Chen and Li, 2016)

1.3.2.2 Carbohydrates Utilisation (De Novo Lipogenesis)

LDs may also originate from converting glucose into TGs through Krebs cycle and followed by synthesis of FAs. This mechanism is known as de novo lipogenesis (DNL), occurring in hepatocytes, adipocytes, and pathologically, cancer cells, and is related to fatty liver disease, obesity, type 2 diabetes, metabolic syndrome, and cancer (Ameer et al., 2014; Menendez and Lupu, 2007). DNL modulates glucose homeostasis. The DNL process involves glucose entry into cells through glucose transporters (GLUTs) on plasma membrane. There are 14 types of GLUTs found, and GLUT4 is primarily on adipocytes and is insulin-regulated (Cushman and Wardzala, 1980). DNL is not active during fasting, but post-prandial elevation of blood glucose and insulin levels stimulate DNL. It is triggered through increased substrate availability and insulin-activated insulin receptor which further activates GLUT4 to uptake glucose (Song et al., 2018). After entry into cells, glucose undergoes glycolysis, Krebs cycle in mitochondria, and the FA synthesis pathway (**Figure 1.18**). There are two key enzymes involved in DNL pathway which include acetyl-CoA carboxylase (ACC) and fatty acid synthase (FAS or FASN). The upregulation of FASN, the enzyme responsible for terminal catalytic step in DNL, is also observed in most malignancies and some viral infections (Ameer et al., 2014). FASN is transcriptionally regulated by SREBP-1c and carbohydrate-responsive element-binding protein (ChREBP) which are activated in response to insulin and glucose, respectively (Iizuka et al., 2004; Shimomura et al., 1999). DNL is more energy-costly than direct utilisation of FA in lipid deposition (Solinas et al., 2015). For the same caloric consumption of carbohydrate and fat, DNL (carbohydrate) produces fewer lipids per calorie than fats do. Some cell types rely on FA uptake more while other cell types use DNL mechanism more (Li and Cheng, 2014). The role of DNL in adipose tissue in TED has never been mentioned in literature. Which LD formation mechanism

(FA uptake or DNL) orbital fibroblasts utilise or whether TED and control orbital fibroblasts have different preference for LD formation is unknown. In addition, it was also reported that DNL and adipogenesis are linked. Adipogenesis was reduced in low glucose adipocyte differentiation medium evidenced by ORO staining, PPARγ and aP2 gene expression in both 3T3L1 and C3H10T1/2 cell lines. ChREBP may be the link between DNL and adipogenesis because ChREBP not only activates FASN but also upregulates PPARγ to induce adipogenesis. Constitutively active ChREBP enhances adipogenesis whereas dominant negative ChREBP impaired adipogenesis (Witte et al., 2015). Since TED orbital fibroblasts are prone to adipogenesis, it is possible DNL is involved in TED development.

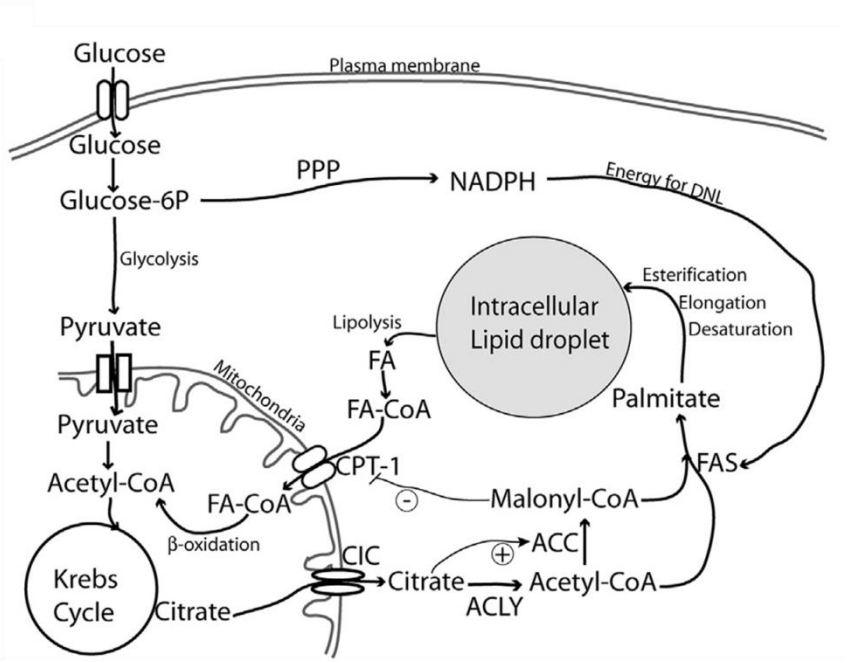

Figure 1.18 De novo lipogenesis (DNL) regulating metabolic homeostasis in a cell

Glucose enters the cell through glucose transporters (GLUT) on plasma membrane. It is converted to pyruvate via glycolysis, and enters mitochondria for Krebs cycle. Citrate leaves mitochondria and activates acetyl-CoA carboxylase (ACC) which converts acetyl-CoA to malonyl-CoA. Fatty acid synthase (FAS, FASN) further converts malonyl-CoA into palmitate (FAs) to form LDs. Adapted from (Solinas et al., 2015)

1.3.2.3 Sterols Taken Up Through Endocytosis

Plasma membranes are composed of sphingolipids and sterols to form lipid bilayer, and endocytosis presenting as invagination of plasma membrane therefore intakes sterols. Sterols are another core component of LDs in addition to TG, and they are generally produced in ER, sent to Golgi and then either formed into LDs or transported to the plasma membrane (Pichler and Riezman, 2004). Endocytosis internalises

plasma membrane with engulfed molecules to fuse with early endosomes. Some components of early endosomes are sent to the plasma membrane, ER or Golgi engaged to lipid recycling, whereas some form late endosomes and are sent to lysosomes for degradation. There are several types of endocytosis including macropinocytosis which engulfs large particles and extracellular fluid, clathrin-mediated endocytosis which internalises transferrin, LDL, and epidermal growth factor (EGF), and caveolae-mediated endocytosis which internalises integrin and lipids (**Figure 1.19**) (Bastiani and Parton, 2010; Lakadamyali et al., 2006; Mayor and Pagano, 2007).

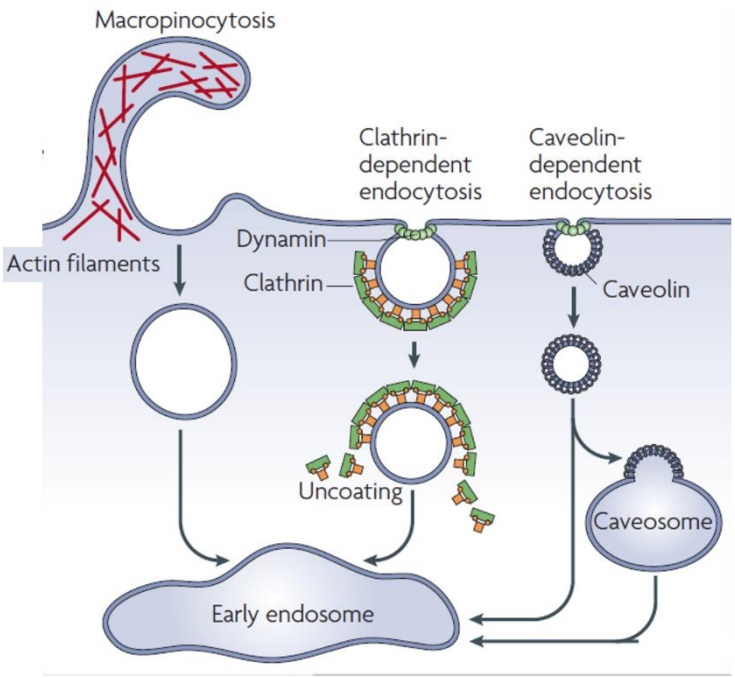

Figure 1.19 Endocytosis patterns

Particles may enter cells by endocytosis with mechanisms: (1) macropinocytosis (2) clathrin-dependent endocytosis or (3) caveolin-dependent endocytosis. Adapted from (Mayor and Pagano, 2007)

Caveolae are flask-shaped invaginations at plasma membrane presenting in adipocytes, fibroblasts, muscle cells and endothelial cells (Echarri and Del Pozo, 2015; Fielding and Fielding, 2000). The essential

structural proteins constituting caveolae are caveolins which are distributed at plasma membrane, Golgi apparatus and may move to LDs in response to cholesterol stimulations or elevated caveolin level at ER (Le Lay et al., 2006; Ostermeyer et al., 2001). There are three caveolin isoforms, Cav1-3, and caveolin-1 (Cav1) and caveolin-2 (Cav2) are more widely expressed (Thompson et al., 2010). Caveolae can act as FA transporters to uptake FAs and convert them into TG and store in LDs (**Figure 1.20**). The expression level of Cav1 was positively correlated with amount of FA transport through plasma membrane in HEK293 cells (Meshulam et al., 2006). Inhibition of caveolae by caveolin inhibitor filipin III and antisense oligonucleotide of Cav1 reduced FA uptake in HepG2 hepatoma cell line (Pohl et al., 2002). *In vivo*, Cav1 knockout mice showed decreased TG in liver and decreased LDs in hepatocytes (Fernandez et al., 2006). Cav1 knockout mice were resistant to obesity but presented elevated TG and FA levels in serum (Razani et al., 2002). In addition to endocytosis and lipid metabolism, caveolae are also involved in mechanosensing and signal transduction (Parton and del Pozo, 2013). The association between caveolae and cytoskeleton was firstly proposed after the observation of proximity of caveolae and stress fibres in electron microscope (Rohlich and Allison, 1976). Later actin filaments were found to keep caveolae at the cell surface, and depolymerisation of actin induces Cav1 movement from cell surface inward to cytoplasm where Cav1 cluster and accumulate (Mundy et al., 2002). Another study also showed that in differentiated adipocytes, caveolae cluster and form rosette pattern in cytoplasm (Parton et al., 2002). Since actin depolymerisation is associated with adipogenesis, it is reasonable that actin depolymerisation, caveolae redistribution and adipogenesis are linked, but how caveolae is involved is unknown. Therefore, it would be of interest to know if fat expansion in TED is attributed to combined mechanisms from actin cytoskeleton, caveolae, and adipogenesis.

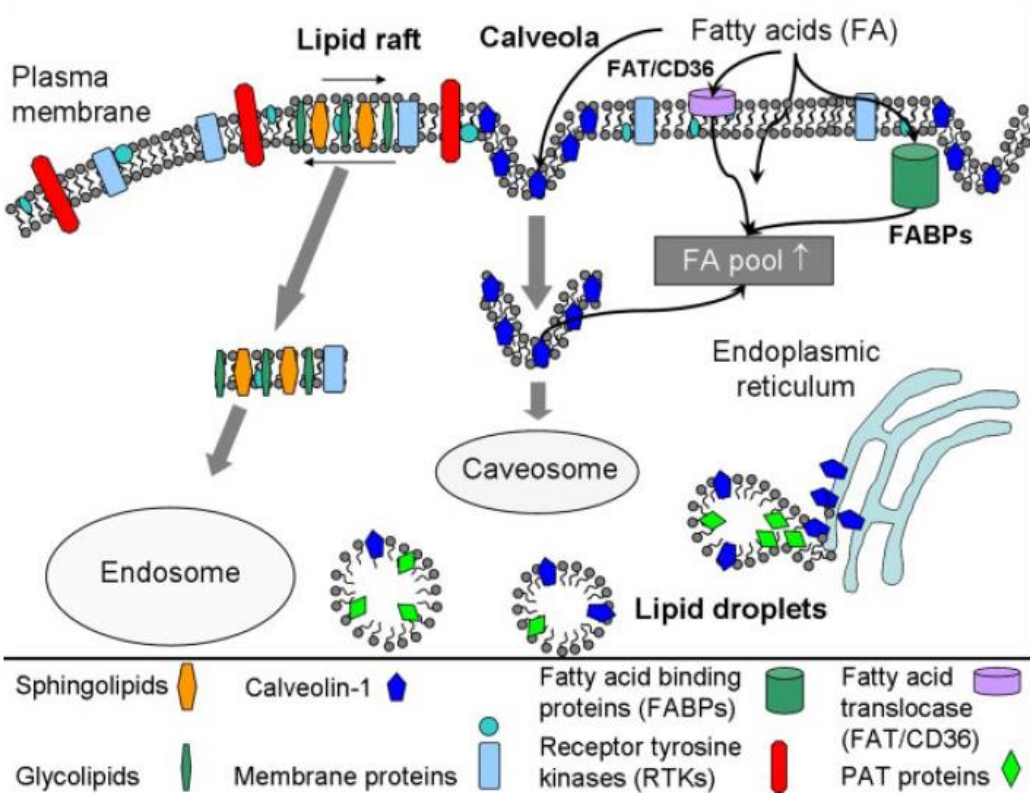

Figure 1.20 Diagram of FA transport through caveolae on plasma membrane.

Fatty acids (FAs) may influx via caveolae, which is formed by caveolin-1 at plasma membrane. FAs are then internalised to caveosome for processing. LDs are formed at ER, where caveolin-1 and PAT (perilipin, adipophilin, and TIP47) assist enveloping TG inside LDs. Adapted from (Anderson and Borlak, 2008)

1.3.2.4 Lipolysis and Perilipin

LDs are formed in excess of energy for future usage, and the breakdown of LDs provides fuel in the demand of energy. Therefore, lipid metabolism is balanced between formation and degradation of LDs. As LDs are composed of the neutral lipids core from TG and cholesterol ester (CE), the degradation comprises the breakdown of TG into FAs and glycerol, and CE into FA and cholesterol in neutral cytosolic hydrolysis and lipophagy (acidic hydrolysis). TG is hydrolysed into FA

and DG, monoacylglycerol (MAG), and glycerol by adipose tissue triacylglycerol lipase (ATGL), hormone sensitive lipase (HSL), and monoacylglycerol lipase (MGL or MAGL), respectively. CE is degraded into cholesterol by neutral cholesterol ester hydrolases (nCEHs), and HSL belongs to one of the nCEHs. By acid lipolysis (lipophagy), lysosomal acid lipase (LAL) can degrade TG, TG's intermediate products, and CE (Zechner et al., 2017) (**Figure 1.16**). On the other hand, proteins coated on the surface of LDs regulate lipolysis pathway by stabilising the LDs and prevent degradation. The essential surface proteins on LDs are the perilipin family, also known as PAT family, including perilipin (perilipin1, PLIN1), adipose differentiation related protein (ADRP, also known as adipophilin or perilipin2, PLIN2), tail-interacting protein of 47 kDa (TIP-47, also known as perilipin3, PLIN3), and S3-12 (Brasaemle, 2007; Greenberg et al., 1991). As the LDs enlarge and mature, the surface proteins of LDs change as well. For example, at the earliest stage with smallest LDs, S3-12 and TIP47 are found (Wolins et al., 2005; Wolins et al., 2003). When LDs grow into middle size, PLIN2 replaces TIP47; and as LDs enlarge at the later maturation stage, PLIN1 becomes the only of PAT family on LDs (Wolins et al., 2005). PLIN1 is mainly distributed in adipose tissue and is closely associated with HSL to regulate lipolysis. Under basal conditions, PLIN1 is unphosphorylated and resides on LDs protecting LDs from lipolysis. HSL is cytosolic and has little access to LDs. Upon catecholamines stimulation on β-adrenergic receptors, activated protein kinase A (PKA) phosphorylates PLIN1 and HSL and triggers a lipolysis signal (Brasaemle, 2007) (**Figure 1.21**). Phosphorylated PLIN1 is eventually degraded and released from LDs. PKA-phosphorylated HSL doubles lipolysis activity (Belfrage et al., 1981; Kawamura et al., 1981), whereas PKA-triggered translocation of HSL from cytosol to the surface of LDs hugely rises the lipolysis activity by 50~100 times (Clifford et al., 2000). However, the phosphorylation and translocation of HSL was independent of PLIN1 phosphorylation, but it failed to enhance lipolysis in the absence of PLIN1 phosphorylation

(Miyoshi et al., 2006). Therefore, the lipolysis is likely regulated by interaction of PLIN1 and HSL.

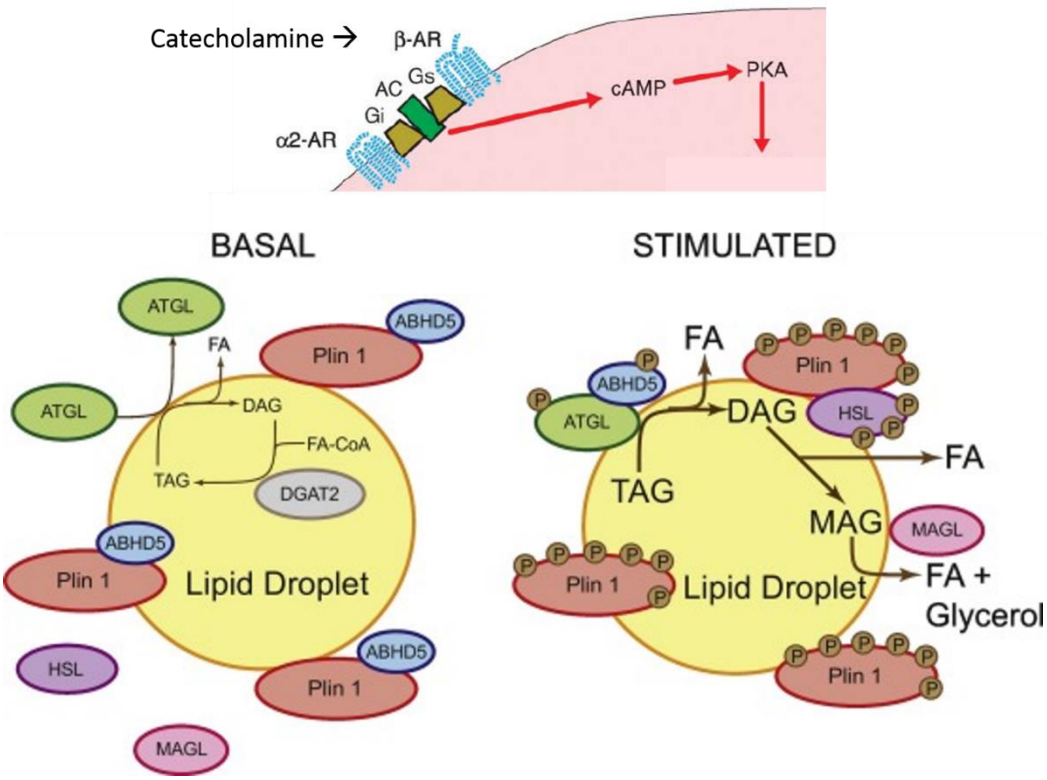

Figure 1.21 PLIN1 and lipolysis signals under basal and stimulated conditions.

Under basal conditions, PLIN1 is unphosphorylated, binds to alpha beta hydrolase domain protein 5 (ABHD5) and blocks ABHD5 from attaching to lipases. HSL and MAGL are not bound to LDs. When catecholamine stimulation activates PKA, PLIN1 is phosphorylated and ABHD5 is liberated to bind to ATGL. The ABHD5/ATGL complex hydrolyses TAG (TG). HSL is phosphorylated and moves to LDs to bind to phosphorylated PLIN1 and hydrolyses DAG (DG). Adapted from (Brasaemle, 2007; Sztalryd and Brasaemle, 2017)

PLIN2 (ADRP) is ubiquitously expressed in adipose tissue, skeletal muscle, heart muscle, liver, lung, mammary gland, and adrenal gland (Straub et al., 2013), and is pathologically associated with fatty liver (Motomura et al., 2006; Straub et al., 2008). Moreover, PLIN2 was also

found in macrophages in atherosclerotic plaques (Wang et al., 1999). Macrophage with LD accumulation form specific foam cells which are hallmark of atherosclerosis (Stary, 2000). PLIN2 is thus linked to LD accumulation in macrophages and atherosclerosis. *In vivo*, PLIN2 was increased on the surface of LDs in the liver of high fat diet fed mice (Motomura et al., 2006). PLIN2 knockout mice were protected from fatty liver when fed with normal diet or alcohol fed diet (Carr et al., 2014; Chang et al., 2006), and were resistant to obesity induced by high fat diet (McManaman et al., 2013). PLIN2 knockout mice also presented smaller atherosclerotic plaques with less LDs per unit area under microscope (Paul et al., 2008). *In vitro*, PLIN2 knockdown in THP-1 macrophages significantly decreased TG and CE levels, whereas PLIN2 overexpression in THP-1 macrophages and Swiss 3T3 significantly increased TG, CE, and LDs (Imamura et al., 2002; Larigauderie et al., 2004). Lipid (cholesterol) loading increased PLIN2 RNA and protein expression in *in vitro* macrophages (Paul et al., 2008), and so did FA loading in differentiated myotube system (Feng et al., 2017). The increased PLIN2 was accompanied with increased LDs amounts (Feng et al., 2017; Paul et al., 2008), indicating that PLIN2 presents a role closely correlated with the observed LDs.

PLIN2 itself is very unstable in the cytoplasm unless bound to LDs as it is otherwise degraded by ubiquitin/proteasome pathway (Masuda et al., 2006; Xu et al., 2005). The involvement of PLIN2 in LD degradation is regarded as the mechanism linking PLIN2 to LDs. However, unlike PLIN1, PLIN2 does not have PKA consensus sites on its structure (Brasaemle, 2007). Therefore, while PLIN1 is activated by catecholamine stimulation through phosphorylation, PLIN2 is not phosphorylated upon catecholamine stimulation (Macpherson et al., 2013). PLIN2 does not recruit HSL to LDs through protein interaction either (Macpherson et al., 2013; Miyoshi et al., 2006). There have been several models proposed showing different mechanisms of how PLIN2 might be regulating LD degradation. In HEK293 where endogenous PLIN2 is minimal, PLIN2

transfected cells dissociate ATGL from LDs, and retain more TG inside cells (Listenberger et al., 2007). This supports a role for PLIN2 in preventing neutral lipolysis by lipases (**Figure 1.16**). Moreover, another model proposed a role for both lipolysis and lipophagy in PLIN2 regulation on LDs in 3T3 cells (Kaushik and Cuervo, 2015; Kaushik and Cuervo, 2016) (**Figure 1.16**, **Figure 1.22**). PLIN2 was shown to be degraded by chaperone mediated autophagy (CMA) following AMP-activated protein kinase (AMPK)-mediated phosphorylation. AMPK inhibition increased PLIN2 level, suggesting that phosphorylation of PLIN2 promotes its degradation, but the association to CMA is not yet understood (Kaushik and Cuervo, 2016). CMA is a special type of autophagy that selectively degrades cytosolic proteins across lysosome membrane. The two major proteins in CMA are heat shock cognate protein of 70 kDa (hsc70 or HSPA8) and lysosome associated membrane protein type 2A (LAMP-2A). Hsc70 recognises and binds cytosolic proteins (PLIN2 here) bearing a specific motif, and the complex translocates to lysosome and binds to LAMP-2A which is a transmembrane protein on lysosome. The complex unfolds at lysosome, and the substrate translocates into lysosome for degradation (Alfaro et al., 2018). Impaired CMA decreased ATGL localisation on LDs, and this supports neutral lipolysis (Kaushik and Cuervo, 2015). This leads to more PLIN2 preserved on LDs, and PLIN2 prevents the association between ATGL and LDs as previously mentioned, and thus the lipolysis by lipases mechanism is thought to be involved. On the other hand, treatment with an autophagy inhibitor increased LDs number. Impaired CMA decreased the colocalisation of autophagy markers with LDs, indicating that the increased amount of PLIN2 on LDs prevents LDs being engulfed by autophagosome. These support the involvement of lipophagy mechanism in PLIN2 regulation on LDs (Kaushik and Cuervo, 2015) (**Figure 1.22**).

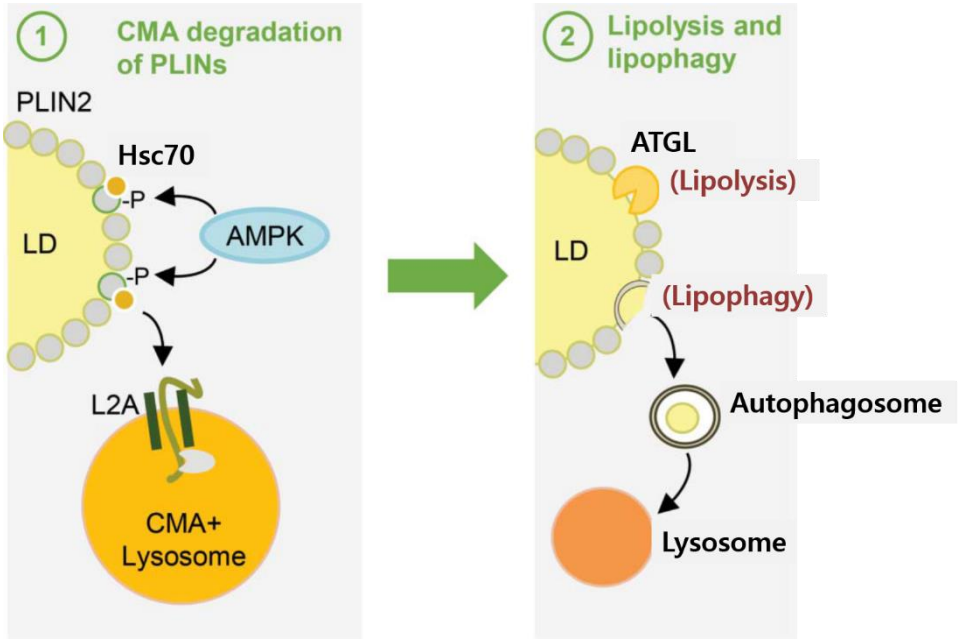

Figure 1.22 Model of PLIN2 regulation by chaperone mediated autophagy (CMA) and AMPK phosphorylation, and further LDs degradation.

Left figure: Heat shock cognate protein of 70 kDa (Hsc70) recognises PLIN2 and binds to PLIN2 on LDs. PLIN2 phosphorylation by AMPK is accompanied. The HSc70/PLIN2 complex leaves LDs and binds to lysosome associated membrane protein type 2A (L2A) on lysosome, and PLIN2 is degraded within lysosome. These constitute the chaperone mediated autophagy (CMA) process. Right figure: The absence of PLIN2 on LDs recruits ATGL to LDs for neutral lipolysis. Lacking PLIN2 on LDs also enables autophagy effectors to engulf LDs to form autophagosome which is sent to lysosome for further degradation as the lipophagy mechanism in LD degradation. Adapted from (Kaushik and Cuervo, 2016)

1.4 Macrophage

Macrophages are a type of leukocytes, and most of macrophages derive from circulating monocytes. They engulf foreign substances, pathogens, cancer cells, and cellular debris in response to tissue damage or infection, via the process of phagocytosis (Aderem and Underhill, 1999). They are also involved in immune reactions by secreting cytokines and recruiting other immune cells to modulate inflammation. After phagocytosis, macrophages digest the engulfed pathogens and present the antigen to helper T cell through pathogen-derived MHC class-II bound peptides to initiate adaptive immunity (Davis et al., 1998). The interaction with T cells in turn activates macrophages through cytokines produced by T cells. Macrophages are usually classified into M1 and M2 subtypes according to their surface markers and secreted cytokines (**Figure 1.23**). Bacterial infection, lipopolysaccharide (LPS), and Th1 cytokine IFNγ promote M1-polarised macrophages which secrete IL-6, IL-1β, and monocyte chemoattractant protein 1 (MCP-1) for proinflammatory and pathogen killing responses. Th2 cytokine IL-4 and IL-13 stimulate M2-polarised macrophages which secrete IL-10 and TGFβ for anti-inflammatory reactions (Atri et al., 2018). This M1/M2 classification is the observation based on cultured macrophages, but macrophages phenotypes *in vivo* are more diverse and may switch between different types (Oishi and Manabe, 2018).

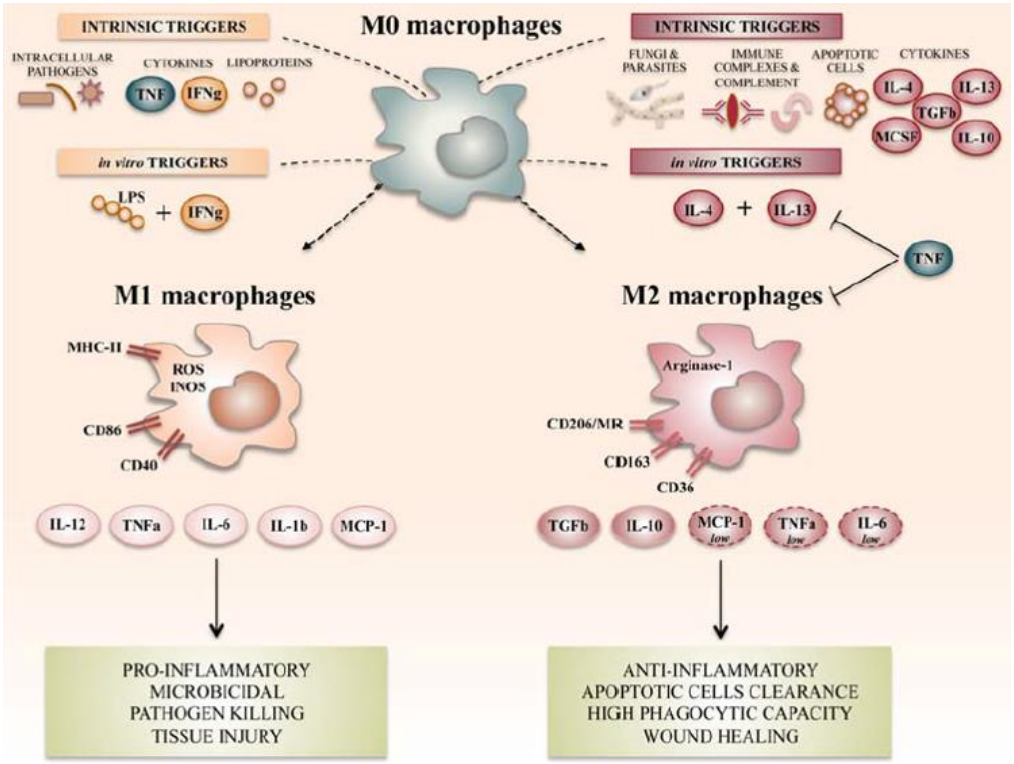

Figure 1.23 Macrophage polarisation stimulants and produced cytokines

Intracellular pathogen, LPS, and IFNγ stimulate M0 macrophages to be polarised into M1 macrophages for proinflammatory function. IL-4 and IL-13 stimulate M0 macrophages to be polarised into M2 macrophages for anti-inflammatory and wound healing reactions. Adapted from (Atri et al., 2018)

In tissue injury, macrophages function as mediators for a series of processes including inflammation, tissue repair, regeneration, and fibrosis. Following injury or pathogen invasion, the immune system is activated through recruitment of neutrophils and monocytes which may differentiate into macrophages. These macrophages are predominantly M1 macrophages for removing pathogens and debris. As pathogens and dead tissue are eliminated, the anti-inflammatory M2 macrophages replace M1 macrophages to become the predominant type. Thus the inflammation resolves, followed by wound healing and regeneration. Although M1 secreted cytokines IL-1, IL-6, TNFα and IFNγ are

proinflammatory function, blocking these cytokines impaired regeneration in muscle injury model (Oishi and Manabe, 2018), suggesting that M1 and its cytokines are also involved in initiation of tissue repair. The transition of M1 predominant to M2 predominant is important because persistent M1 function may cause tissue damage. The polarisation of macrophages is reversible *in vitro* (Porcheray et al., 2005), and this transition is regulated by the microenvironment cytokine shift from IFNγ and TNFα to IL-10, and regulatory T cells (Tregs, also known as suppressor T cells). M2 mediated repair is also well controlled for tissue homeostasis, and the dysregulation of persistent repair may lead to pathological fibrosis (Oishi and Manabe, 2018).

Fibrosis is characterised by fibroblasts proliferation and differentiation, together with excessive deposition of ECM. M2-like macrophages promote healing and fibrosis by recruiting fibroblasts and inflammatory cells, and secreting various kinds of growth factors and cytokines such as TGF-β1 and PDGF (Rappolee et al., 1988). TGF-β1 can activate fibroblasts into myofibroblasts which are the main cell type for fibrosis (Tomasek et al., 2002). Furthermore, macrophages secrete matrix metalloproteases (MMPs) that degrade basement membrane and attract more fibroblasts and inflammatory cells to the site to enhance fibrosis (Giannandrea and Parks, 2014). On the other hand, macrophages phagocytose the dying inflammatory cells, promote myofibroblast apoptosis and modulate ECM turnover by digesting ECM components, to terminate fibrosis (Wynn, 2008). Therefore, macrophages are a key regulator of fibrosis where they balance the pro- and anti- scarring activities.

1.4.1 Macrophage in Obesity Model

In addition to wound healing, macrophages are present in adipose tissue, and regulate adipose tissue remodeling. In lean adipose tissue,

macrophages constitute only 10% of the total cell counts (Weisberg et al., 2003), and M2 macrophages predominate and maintain the adipose tissue homeostasis. At the onset of obesity, proinflammatory M1 macrophages are recruited to adipose tissue and predominate the macrophage population (Lumeng et al., 2008). This results in large amounts of macrophages accumulation, making up to 50% of the cells in obese adipose tissue, and correspondingly makes obese adipose tissue as a site of inflammation (Weisberg et al., 2003). In the process of obesity development, adipocytes get hypertrophy (increased adipocytes size), secrete proinflammatory cytokines, and promote adipocyte death. The adipocyte death recruits more M1 macrophages to form crown-like structures (CLS) which contribute to adipose tissue fibrosis in association with myofibroblast and ECM deposition (Buechler et al., 2015; Cinti et al., 2005) (**Figure 1.24**).

On the other hand, preadipocytes in adipose tissue are regulated by macrophages to prevent obesity. Adipogenic differentiation in human primary cultured preadipocytes was significantly reduced by monocyte-derived macrophages with or without LPS activation (Lacasa et al., 2007). Polarised M1 macrophages decreased adipogenesis whereas polarised M2 macrophages did not change LDs or expression of PPARγ and C/EBPα in murine preadipocytes (Cheng et al., 2019). In nutrient and energy excess, M2 macrophages maintain preadipocyte survival by releasing PDGF (Molgat et al., 2009), and promote proliferation of these preadipocytes without inducing inflammation. Moreover, a mouse model demonstrated that M2 macrophages supported brown adipogenesis and adipose tissue remodeling by activating β3-adrenergic receptor. Noninflammatory M2 macrophages cleared dead white adipocytes and recruited preadipocytes by expressing osteopontin, a chemotactic factor. The following proliferation and brown adipogenesis of preadipocytes replaced the phagocytosed dead adipocytes to complete the remodelling (Lee et al., 2016; Lee et al., 2013). This confirms that M2 macrophages

contribute to adipocyte hyperplasia (increased adipocytes counts) which preserves adipose tissue function without inflammation or fibrosis.

Moreover, macrophages are involved in adipocyte lipolysis in response to energy demand. Lipolysis and increased free FA concentration activate macrophage accumulation for phagocytosis/uptake of lipids. During weight loss and in lean tissue, this is a temporary effect; however, in obese tissue, the chronic lipolysis and macrophage accumulation are associated with the pathological inflammation and impaired metabolism (Kosteli et al., 2010; Nguyen et al., 2011).

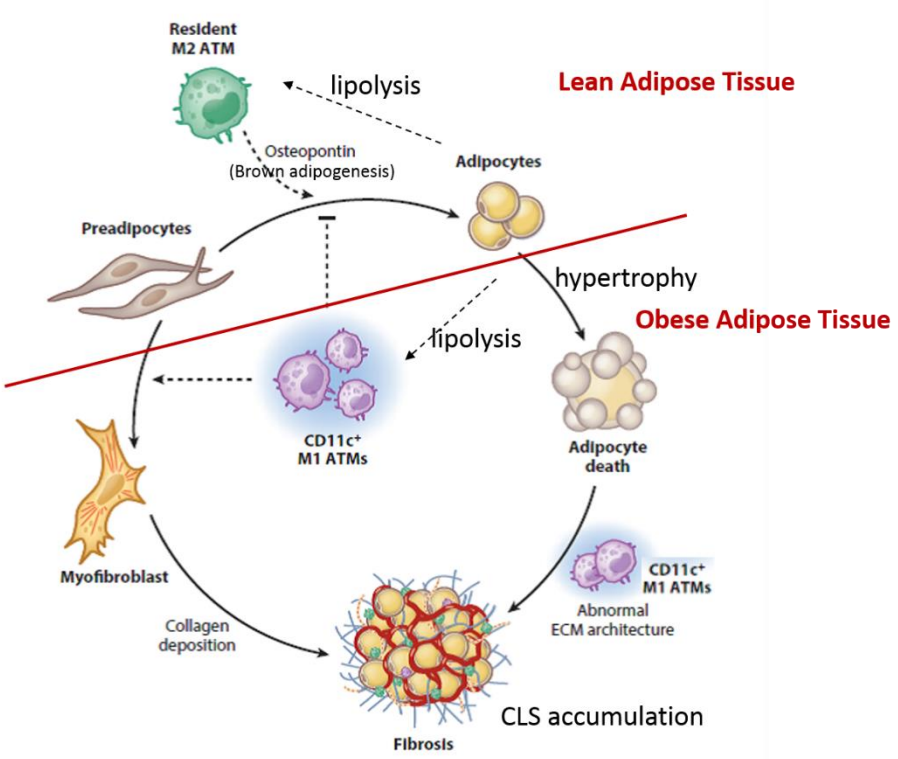

Figure 1.24 Adipose tissue macrophage (ATM) regulate adipose tissue remodelling

M2 ATM predominate in lean adipose tissue where they balance between adipogenesis and lipolysis. M1 ATM are recruited in obese adipose tissue and contribute to adipose tissue fibrosis. Adapted from (Martinez-Santibanez and Lumeng, 2014)

1.4.2 Macrophage in Thyroid Eye Disease

Macrophages are thought to participate in the immunological stage of TED. This was firstly suggested by a study showing upregulation of macrophage-derived cytokine gene expression in TED tissues (Kumar and Bahn, 2003). This was later confirmed by IHC and histopathological studies. Along with other immune cells, monocytes and activated macrophages were found in active TED fibrovascular septae and orbital tissues in IHC studies. As the disease enters inactive stage, the amount of activated macrophages decreases, but it remains higher in fibrovascular septae than in adipose tissue when compared to respective areas in control tissue (Eckstein et al., 2004). IHC staining of orbital fat for CD68, a specific antigen of macrophages, demonstrated higher positive staining in TED tissues than in controlled tissues, and CD68 expression correlates with TED severity (Chen et al., 2008; Pawlowski et al., 2014). The macrophage infiltration is found mainly around blood vessel walls, among adipocytes, and in fibrotic areas of adipose tissue. These suggest that macrophages may not only play a crucial role in early TED during the inflammatory process within adipose tissue, but are also linked to fibrosis in fibrovascular area in late TED.

Macrophages in TED are derived from monocytes (Eckstein et al., 2004) and are thought to be M1-like macrophages. As M1 macrophages are proinflammatory, this is consistent with the inflammatory role of macrophages in TED. Moreover, fat expansion and fibrosis are features in TED, and these are similar to the environment in obesity with adipose tissue fibrosis, in which M1 macrophages are involved. In obesity model, macrophages are recruited due to adipocyte hypertrophy and to cytokines secreted by adipocytes, and together they form CLS. This part may be different from the TED pathogenesis where activation of T cells initiates the inflammatory reactions and recruits macrophages before fat expansion. It is unknown if macrophages in TED regulate adipogenesis as the inhibitory effect M1 show in obesity model. But it will be interesting

to investigate if macrophages in TED promote adipose tissue fibrosis as M1 macrophages do in obesity, and if the profibrotic mechanism is regulated by differentiation of preadipocytes into myofibroblasts or by modulating ECM in adipose tissue.

1.5 Aims and Objectives

TED is characterised by immune/inflammation, adipogenesis, HA production, and fibrosis in the orbital cavity. As adipogenesis and HA production both result in soft tissue volume expansion, the intraorbital pressure is elevated, and contents in orbital cavity bear compression force. We have observed enhanced LD formation in orbital fibroblasts under pressure in our 3D *in vitro* TED model (Li et al., 2014). These suggest that mechanical factors are important in TED pathogenesis and may possibly mediate TED features. We hypothesised that orbital fibroblasts are regulating contractility and LD formation, and these features are perturbed through changes in mechanoregulation. Dysregulation of LD formation/adipogenesis, FA uptake, and LD degradation may lead to fat expansion, and macrophage promotes LD formation, HA production and fibrosis.

Firstly, to know if changes in extracellular mechanical forces regulate TED features, we aimed to study the involvement of MRTF/SRF pathway in fibrosis and adipogenesis in orbital fibroblasts. We compared the MRTF expression level and MRTF localisation between different mechanical environment, 2D and 3D, to understand if MRTF responds to ECM stiffness. We then manipulated MRTF and its antagonistic pathway TCF to see if contractility and LD formation were changed correspondingly.

Secondly, to understand the mechanisms of LD formation, we aimed to identify the molecular mechanisms of LD formation in 3D-cultured orbital fibroblasts. We explored adipogenesis and LDs metabolism including FA uptake, DNL, LDs surface protein—perilipin, using gene expression assay, functional assay, as well as inhibitors and gene silencing manipulations. We also examined the effect of inflammatory activation on perilipin expression.

Lastly, to clarify if macrophages alter the phenotypes of orbital fibroblasts, we aimed to culture orbital fibroblasts with and without macrophages in 3D *in vitro* model. LD formation, HA production, contractility, and cellular morphology of orbital fibroblasts, between the presence and absence of macrophages conditions were compared. Furthermore, potential pathways involved in macrophage-activated signalling were explored.

Chapter 2 Materials and Methods

2.1 Cell Culture

2.1.1 Primary Orbital Fibroblasts

Orbital fibroblasts were obtained from orbital adipose tissue through primary culture. Patient enrolment was approved by Ethics committee, and informed consent was obtained. Orbital fat was harvested from patients with active TED undergoing orbital decompression surgery or from control individuals undergoing orbital surgery unrelated to TED (**Table 2.1**). Adipose tissues were chopped into 1~2 mm^2 fragments and maintained in Dulbecco's modified Eagle's medium (DMEM, 4.5 g/L glucose, gibco, Life technologies, UK) supplemented with fetal bovine serum (FBS, 10% vol/vol, Sigma-Aldrich, UK and Labtech, UK), penicillin (100 U/mL, Gibco, Life technologies), streptomycin (100 μg/mL, Gibco, Life technologies), and L-glutamine (2mM, Gibco, Life technologies) and incubated at 37°C and 5% CO_2. After cells grew out of the tissue fragments and reached confluence, they were trypsinised (0.05% Trypsin-EDTA, Gibco, Life technologies) and maintained in the above medium in T75 tissue culture flasks (Corning, NY, USA). The resulting orbital fibroblasts from patients with TED were named as HO cell strains and from controls were CO cell strains. Cells were used between passage 3 and 9 for all experiments.

Table 2.1 Demographic data of donors of primary orbital fibroblasts cell lines from control individuals (CO) and TED patients (HO)

n/a: not applicable; DM: diabetes mellitus

Cell line	Age	Gender	Surgical procedure	TED duration (months)	CAS score	Systemic corticosteroid use (yes/no)	Steroid washout period	DM & PPARγ agonist use
CO3	68	F	Fat prolapse excision	n/a	n/a	no	n/a	no & no
CO4	49	M	Evisceration	n/a	n/a	no	n/a	no & no
CO5	80	M	Canthoplasty	n/a	n/a	no	n/a	no & no
CO6	56	F	Fat prolapse excision	n/a	n/a	no	n/a	no & no
CO7	33	M	Lacrimal Gland exploration	n/a	n/a	no	n/a	no & no
CO12	72	M	Fat prolapse excision	n/a	n/a	no	n/a	no & no
CO13	56	M	Fat prolapse excision	n/a	n/a	no	n/a	no & no
HO1	71	F	Orbital decompression	15	6	yes	no washout	no & no
HO2	60	M	Orbital decompression	8	5	yes	no washout	no & no
HO4	49	F	Orbital decompression	7	6	yes	no washout	no & no
HO6R	58	F	Orbital decompression	9	5	yes	no washout	no & no
HO8	62	F	Orbital decompression	28	6	yes	no washout	no & no
HO9R	54	M	Orbital decompression	9	4	yes	no washout	no & no

2.1.2 Macrophages

Macrophages were derived by phorbol-12-myristate-13-acetate (PMA, Promega Corporation, UK) activation of U937 monocytes. Human monocyte cell line U937 was kept in RPMI 1640 medium (Sigma-Aldrich, UK) supplemented with 10% FBS, penicillin (100 U/mL), streptomycin (100 µg/mL), and L-glutamine (2 mM). For differentiation, $2x10^6$ cells were stimulated with PMA (150 nM) in medium for 72 hours. The medium was then replaced with fresh RPMI without PMA and the cells left for another 48~72 hours to complete differentiation into macrophages.

2.2 Three-Dimensional (3D) Cultures

A 3D collagen gel culture environment was established by embedding cells in 1.5 mg/mL rat tail collagen type 1 matrix (First Link Ltd., Birmingham, UK). Gels were made from a mixture of 600 µL of rat tail collagen, 96 µL of concentrated medium mix [from 700 µL 10x DMEM (Sigma-Aldrich, UK), 70 µL L-glutamine, and 180 µL $NaHCO_3$ (Gibco, Life technologies, UK)], titrated with about 56 µL of 1M NaOH to reach neutral pH, and 60 µL cell suspension ($0.6x10^5$ cells for most experiments) before casting into dishes or wells before collagen polymerised. For free-floating gels as in contraction assay, gels were cast in the microwells of glass bottom MatTek dishes (MatTek Corporation, MA, USA) each with 150 µL gel solution and then detached (Li et al., 2014). For other experiments, gels were cast in 24 well plates (Nunc, Thermo, UK) with 210 µL gel solution and left attached. Co-culturing fibroblasts with macrophages was done in the same method after mixing, centrifuging and re-suspending the two cell types together.

2.3 Oil-Red-O staining

2.3.1 ORO for cells in 2D

After rinsing with PBS, cells were fixed in 10% formaldehyde (Sigma-Aldrich, UK) for 20 min followed by distilled water wash. After 5 min of incubation in 60% isopropanol (Fisher Scientific, UK), cells were incubated for 2 min in freshly filtered Oil-Red-O (ORO) [working solution made of 3:2 vol/vol dilution of ORO stock (3 mg/mL in 99% isopropanol) and distilled water] and then rinsed in water. Counterstaining was performed with hematoxylin (Gill No. 3, Sigma-Aldrich, UK) for 30 sec, followed by several long washes in tap water. Cells were imaged under microscope (Leica DMIL 20x objective) and lipid amounts were quantified by two ways. One method was evaluating the proportions of cells positively stained for ORO by cell counting, in which cells possessing more than 10 LDs were defined as ORO positive. The other method was quantified using Image J (http://rsb.info.nih.gov/ij/) to obtain “lipid droplet (LD) area per cell”. Images were adjusted in hue, saturation and brightness in “colour threshold” in “adjust” submenu under “image” menu until ORO stained lipid vesicles were all selected. Use the analysis “analyse particles” function, choosing particle size from 20 pixel^2 to exclude stained debris, and areas in pixel^2 were obtained by “measure” in “ROI manager”. The total LD area divided by manually obtained total cell counts in the field is “LD area per cell.”

2.3.2 ORO for cells in 3D

3D gels were rinsed with PBS and fixed in 10% formaldehyde for 20 min. Gels were then detached from the bottom of wells and washed in distilled water. After 5 min of incubation in 60% isopropanol, gels were stained for 2 min with freshly filtered ORO working solution. The gels were then

rinsed in water and counterstained with hematoxylin for 30 sec, followed by several long washes in tap water. Gels were topped with a 50% glycerol in tris-buffered saline (TBS) solution before observing and imaging. The ORO staining was quantified by counting ORO positive cells directly under the microscope (Leica DMIL 20x objective). A cell was deemed “ORO positive” when harbouring 10 or more LDs in its cytoplasm. A minimum of 100 cells were evaluated from 4~5 fields in each gel.

2.4 Western Blot

Cells in 2D monolayer culture were trypsinised, pelleted and resuspended in RIPA lysis buffer [made from 150 mM NaCl, 0.1% Triton X-100, 0.1% sodium dodecyl sulphate, 50 mM Tris-HCl pH8.0, 0.5% sodium deoxycholate, protease inhibitors (Roche, UK)]. Cells in 3D collagen gels were obtained by digesting the gels with 0.05% collagenase-D (Roche, UK) until completely liquefied. The digest was centrifuged and the cell pellet resuspended in RIPA buffer. Protein concentration was quantified by BCA assay (Thermo Fisher Scientific, UK), and the samples were denatured in sample buffer (Thermo Fisher Scientific, UK) at 95°C for 5 minutes. 7 µg of protein were loaded on 4-12% precast polyacrylamide gels (Novex™ Wedgewell™ or Bolt™, Invitrogen, Thermo Fisher Scientific, UK) for SDS-PAGE. Proteins were transferred to PVDF membranes (Thermo Fisher Scientific, UK), and then membranes were blocked for 1 hour at room temperature in 5% skimmed milk (for αSMA, GAPDH, MRTF-A, YAP) or 5% BSA (for MRTF-B, PLIN2, PPARγ) made in 0.1% Tween-20 in TBS (TBS-T) before overnight incubation with primary antibody (**Table 2.2**) in the respective blocking solution at 4°C. Membranes were washed with TBS-T before 1 hour incubation of secondary antibody (Peroxidase-AffiniPure donkey anti-mouse IgG (H+L), goat anti-rabbit IgG (H+L), or donkey anti-

goat IgG (H+L) Jackson Immunoresearch, PA, USA) diluted at 1:5000 in 5% milk in 0.1% TBS-T at room temperature. After another wash with TBS-T, membranes were developed using ECL (Pierce, Thermo Fisher Scientific, UK), X-ray film (Fujifilm, Japan) exposure in dark room and X-ray film processor (SRX-101A, Konica Minolta, NJ, USA). For loading control, membranes were probed with rabbit anti-GAPDH Ab (ab9485, abcam, UK) at 1:3000 in 5% milk. When the difference of molecular weights of the main target and GAPDH was big enough to have them clearly separated in the gel, membranes were cut for probing with the main target and GAPDH primary antibody separately but simultaneously. When the molecular weights of the target protein and GAPDH were close, the target protein was probed first, and after developing the membrane, the membrane was washed, stripped with stripping buffer (Thermo Fisher Scientific, UK), blocked with 5% milk, and then reprobed with anti-GAPDH primary antibody with steps aforementioned. Films were scanned and analysed using ImageJ software. Band intensities were normalised to GAPDH and then normalised to a reference sample which was loaded in each gel for comparing all cell strains and all independent experimental repeats.

Table 2.2 List of primary antibodies used in WB

Target protein	Dilution	Supplier	Cat. No
αSMA	1:3000	Sigma-Aldrich	A2547
GAPDH	1:3000	abcam	ab9485
MRTF-A	1:1000	Santa cruz	sc-21558
MRTF-B	1:1000	Bethyl laboratories	A302-768A
PLIN2	1:2000	Proteintech	15294-1-AP
PPARγ	1:1000	Santa cruz	sc-7273
YAP	1:2000	Santa cruz	sc-101199

2.5 Immunofluorescence

Table 2.3 List of primary antibodies used in IF

Target protein	Dilution	Supplier	Cat. No
αSMA	1:100	Sigma-Aldrich	A2547
MRTF-A	1:100	Santa cruz	sc-390324
PLIN2	1:100	Proteintech	15294-1-AP
YAP	1:100	Santa cruz	sc-101199

2.5.1 IF for cells in 2D

Coverslips (diameter 13 mm) were prepared by acid washing with 1 M HCl for 3-5 minutes, PBS rinse, 70% ethanol for 1-2 minutes, and another PBS rinse before seeding cells. For most targets except MRTF-A, after incubation, cells were fixed with 3.7% formaldehyde in PBS for 7 min, followed by 0.5% Triton-X 100 (Sigma-Aldrich, UK) permeabilisation for 20 min and 0.1 M Glycine (Sigma-Aldrich, UK) wash for 10 min. After rinse in 1% BSA in TBS pH 8.0 for 5 min, coverslips were transferred to a humidified dark chamber where they were blocked and stained for F-actin with Rhodamine-labeled Phalloidin (Molecular Probes, OR, USA) 1:20 dilution in TBS-1% BSA-1% FBS for 20 min at room temperature. The phalloidin/block was removed, and replaced with primary antibody diluted as indicated in (**Table 2.3**) in TBS-1% BSA for 1 hour at room temperature. After 3 times of washing in 1% BSA in pH 8.0 TBS, cells were incubated in secondary antibody (Alexa Fluor 488-Conjugated AffiniPure Donkey Anti-Mouse IgG; Jackson Immunoresearch laboratories, PA, USA) at a dilution of 1:100 for 1 hour at room temperature followed by washings. Coverslips were later mounted on slides with Fluoroshield mounting medium with DAPI (abcam, UK). Images were taken by Nikon Eclipse Ti microscope with NIS elements software with 10x Plan Fluor 0.30 NA objective or 20x S Plan Fluor ELWD 0.45 NA objective.

For MRTF-A in 2D, the protocol was slightly modified. Cells were blocked with 5% FBS and 5% BSA in PBS for 1 hr at room temperature before primary antibody overnight incubation at 4°C in a humidified chamber. After 3 times of washing in 0.1% Triton-X 100 in PBS, cells were incubated in secondary antibody at 1:100 and Rhodamine-phalloidin 1:20 diluted in 5 % FBS and 5% BSA in PBS for 2 hrs at room temperature in a humidified dark chamber, followed by washings in 0.1% Triton-X 100 in PBS before mounting.

2.5.2 IF for cells in 3D

Orbital fibroblasts cultured in gels were fixed with 3.7% formaldehyde for 30 min, followed by 0.5% Triton-X 100 permeabilisation for 30 min. After 0.1 M Glycine wash for 30 min and TBS-1% BSA-1% for 15 min, gels were transferred to eppendorfs for blocking and staining for F-actin with Rhodamine-phalloidin 1:20 in TBS-1% BSA-1% FCS for 30 min at room temperature. The gels were then incubated with primary antibody (**Table 2.3**) in TBS-1% BSA overnight at 4°C. After 3 times of 10 min washes, gels were incubated with secondary antibody for 2 hours at room temperature followed by another 3 times of 10 min washes. Gels were transferred back to MatTek dishes and mounted with Fluoroshield mounting medium with DAPI. Images were taken using Nikon Eclipse Ti microscope with 10x Plan Fluor 0.3 NA or 40x S Plan Fluor ELWD 0.60 NA objectives. For MRTF-A staining, protocols were modified as with in 2D, using 5% FBS and 5% BSA in PBS as blocking buffer and antibody dilution buffer, and 0.1% Triton-X 100 in PBS as washing buffer.

For 3D IF quantification, full stacks (50 µm in Z stack with 1 µm step) of 5-6 fields were acquired using the 10X objective and processed using the NIKON NIS Element Software. Maximal intensity projections were generated and background signal was corrected by subtracting the mean intensity from a selected ROI. Cells were manually traced at F-actin signal (TRITC) to get outlines as selected areas for calculations. The integrated density was obtained by dividing sum of fluorescence intensity for TRITC and FITC by the selected area. For representative single cell images, cells were imaged with 40x objective, processed by deconvolution, and shown as maximal intensity projections.

2.5.3 Co-localisation of PLIN2 with ORO

For co-localisation studies of LDs and PLIN2, cells were grown as a monolayer on top of the same soft gel matrix where LDs were produced

as well. Gels without cells were cast in the same way described earlier but using FBS instead of cell pellet suspended in FBS. $0.15x10^5$ cells in 750 µL culture medium were seeded into a well of 24 well plate, the cell counts were the same as which inside one gel.

The combined ORO and PLIN2 IF staining was modified from protocol suggested by manufacturer of PLIN2 primary antibody and article published by Koopman et al. (Koopman et al., 2001). After 24 hrs of culture, the medium was removed, and the cells were rinsed with PBS and fixed with cold 100% ethanol for 10 min at room temperature, followed by 3 times of PBS wash and 0.2% Triton-X 100 permeabilisation for 5 min and another 3 times of PBS wash. Blocking was performed with 5% FBS and 5% BSA in PBS for 1 hr at room temperature before incubation with primary antibody diluted in 1% BSA in PBS for 1.5 hr at room temperature. After primary antibody incubation, cells on gels were washed 3 times with PBS before incubation with secondary antibody (Alexa Fluor 488-Conjugated AffiniPure Donkey Anti-Rabbit IgG; Jackson Immunoresearch laboratories, PA, USA) diluted in 1% BSA in PBS for 1 hr at room temperature. After 3 times of washing in PBS, cells were incubated with filtered ORO working solution (section 2.3.1) at room temperature for 30 min followed by washings in distilled water for 3 times. Gels were transferred onto slides and mounted with Fluoroshield mounting medium with DAPI. Cells and LDs with surrounding PLIN2 were observed, in which ORO-stained LDs were visualised at TRITC channel, and imaged using Axioskop 2 microscope (ZEISS, Germany) at high power 63x Plan-Apochromat 1.4 oil objective.

2.6 Cytokines, Inhibitors and Gene Silencing

2.6.1 Cytokines and Chemicals

Cytokines and growth factors were diluted in culture medium at indicated concentrations (**Table 2.4**) before adding to culture dish. For 2D culture, cytokine medium replaced original medium after cells were seeded for 1 day, while cytokine or growth factor medium was added to 3D culture right after gels were cast.

Macrophage conditioned medium was prepared from monocytes stimulated with PMA as previously described. After completion of differentiation, RPMI-1640 medium was replaced with 10 mL of fresh 10% FBS DMEM for an extra day to allow cytokines and growth factors secreted from macrophages into medium. Medium was then transferred to centrifuge tube (Corning, NY, USA) for spinning down at 1500 rpm for 5 min to remove cell debris. The supernatant was used as macrophage conditioned medium after cells were seeded in 2D for 1 day.

Table 2.4 List of cytokines and growth factors

Cytokines	Concentration.	Supplier	Cat. No
IFN-γ	20 ng/mL	Peprotech	300-02
IGF-1	20 μM	R & D Systems	291-G1-200
IL-1β	10 ng/mL	Peprotech	200-01B
IL-6	20 ng/mL	Peprotech	200-06
TNF-α	10 ng/mL	Peprotech	300-01A

2.6.2 Inhibitors

Most inhibitors were used for 3D culture, and medium with inhibitors diluted at indicated concentrations (**Table 2.5**) was added onto gels right after gel casting without adding into gel mix. Only IGF-1R blocking

antibody was added to both culture medium and gel mix. CCG-203971 in 2D was added after cells were seeded for 1 day.

Table 2.5 List of inhibiting reagents (inhibitors and inhibiting Ab)

Inhibiting target	Inhibitor	Concentration.	Supplier	Cat. No
Macropino-cytosis	Amiloride HCl	0.2 mM	Sigma-Aldrich	A7410
FASN	(±)-C75	50 μM	Cayman	10005270
MRTF/SRF	CCG-203971	10, 25 μM in 3D 12 μM in 2D	Cayman	15075
Clathrin-mediated endocytosis	Dynasore	80 μM	Sigma-Aldrich	D7693
Caveolin-1	Filipin	5 μg/mL	Sigma-Aldrich	F9765
FASN	GSK2194069	1 μM	Sigma-Aldrich	SML1259
PPARγ	GW9662	10 μM	Sigma-Aldrich	M6191
IGF-1R	IGF-1R blocking antibody (1H7)	5 μg/mL in medium 10 μg/mL in gel mix	BioLegend	351804
PI3K	LY294002	10 μM	Cell signaling	9901
Caveolin-1	Methyl-β-cyclodextrin (MBCD)	5 mM	Sigma-Aldrich	332615
TGFβ	SB431542	10 μM	Caymen	13031
CD36	Sulfosuccinimidyl Oleate (SSO)	200 μM	Caymen	11211
YAP	Verteporfin	2.5 μM	Sigma-Aldrich	SML0534

2.6.3 Gene Silencing

Gene silencing experiments were performed using siRNAs to knockdown target genes, and non-target control of equal concentration (**Table 2.6**). Fibroblasts were plated in 60 mm ($1.2x10^5$ cells/dish) dishes, and treated with siRNA [5 nM for most of the single target knockdown, 2.5 nM of each siRNA when more than one gene was targeted (in dual knockdown for MRTFA+B and triple knockdown for ELK1+3+4), 10 nM for PLIN2], together with 3 μL/mL Hiperfect transfection reagent (Qiagen, Germany) for 3~4 days (3 days for most genes, 4 days for PLIN2) as manufacturer's instructions. After completion of transfection, cells were pooled together and used to cast 3D collagen gels for further experiments and prepare whole cell lysates for WB or RNA extraction for qPCR to confirm the efficiency of gene silencing.

Table 2.6 List of siRNA sequences

siRNAs	Supplier	Cat. No	Sequence
ACTA2	Dharmacon	M-003450-00-0005	
Oligo 1 D-003450-01		siGENOME	GGAAGGACCUCUAUGCUAA
Oligo 2 D-003450-02		SMARTpool	GCCGAGAUCUCACUGACUA
Oligo 3 D-003450-03			GGAGAAACUGUGUUAUGUA
Oligo 4 D-003450-04			UGAGAAGAGUUACGAGUUG
AllStars Negative Control siRNA	Qiagen	1027281	
Cav1	Dharmacon	M-003467-01-0005	
Oligo 1 D-003467-01		siGENOME	CUAAACACCUCAACGAUGA
Oligo 2 D-003467-02		SMARTpool	GCAGUUGUACCAUGCAUUA
Oligo 3 D-003467-03			AUUAAGAGCUUCCUGAUUG
Oligo 4 D-003467-05			GCAAAUACGUAGACUCGGA
CD36	Dharmacon	M-010206-01-0005	
Oligo 1 D-010206-03		siGENOME	CGACACAUAUAAAGGUAAA
Oligo 2 D-010206-04		SMARTpool	GGAGACCUGUGUACAUUUC
Oligo 3 D-010206-05			CAUAGGACAUACUUGGAUA
Oligo 4 D-010206-06			GUAUUUGAAUCCGACGUUA
ELK1	Dharmacon	M-003885-01-0005	
Oligo 1 D-003885-02		siGENOME	GCCAGAAGUUCGUCUACAA
Oligo 2 D-003885-04		SMARTpool	GCAAGAACAAGACCAACAU
Oligo 3 D-003885-17			ACGGGAUGGUGGUGAAUUC
Oligo 4 D-003885-18			UUUAAUGGGUUGGGAGUCU
ELK3	Dharmacon	M-010320-00-0005	
Oligo 1 D-010320-01		siGENOME	GAUCUCCUCUUUAAUGUUG
Oligo 2 D-010320-02		SMARTpool	GAACGAUGGUGAAUUCAAG
Oligo 3 D-010320-03			ACAAGAACAUCAUCAAGAA
Oligo 4 D-010320-04			GCACGAGCCGCAACGAAUA
ELK4	Dharmacon	M-010315-01-0005	
Oligo 1 D-010315-01		siGENOME	GCAGGAACCUCCCAGAACA
Oligo 2 D-010315-03		SMARTpool	GAUGGGCAGUUUAAGCUUU
Oligo 3 D-010315-04			CACCAUCUGUCAUCAAAUU
Oligo 4 D-010315-05			CCUCAGAUACUAUUAUGUA
MKL1(MRTF-A)	Dharmacon	M-015434-01-0005	
Oligo 1 D-015434-01		siGENOME	GGUGAACUAUCCCAAAGUA
Oligo 2 D-015434-03		SMARTpool	GGACAGAGGACUAUCUCAA
Oligo 3 D-015434-04			AAACUGAGCUGAUUGAGCG
Oligo 4 D-015434-17			CCAUGGACACCUCGGAAUU
MKL2(MRTF-B)	Dharmacon	M-019279-00-0005	
Oligo 1 D-019279-01		siGENOME	GAAAAGAGCUCGACUAGCA
Oligo 2 D-019279-02		SMARTpool	GAACGAGCCAGAACUGAAA

Oligo 3 D-019279-03 Oligo 4 D-019279-04			GGAUGGAACUUUACCCUCA UCAGAAGGGUGAGAAGAAU
PLIN2 Oligo 1 D-019204-01 Oligo 2 D-019204-02 Oligo 3 D-019204-03 Oligo 4 D-019204-04	Dharmacon siGENOME SMARTpool	M-019204-00-0005	 GAGGAGAGACUGCCUAUUC GAUAUGAUGAUACUGAUGA UGAAGGAUUUGAUCUGGUU GAAGCUAGAGCCGCAAAUU
SLC27A1(FATP1) Oligo 1 D-010759-01 Oligo 2 D-010759-02 Oligo 3 D-010759-03 Oligo 4 D-010759-04	Dharmacon siGENOME SMARTpool	M-010759-00-0005	 UUCCAGGAGUGGAGGGUAA AGACAGACGUGGCCGUCUA CGAUAUACCAGGAGCUGCA CCUUAAAUGAGGCAGUCUA
SLC27A4(FATP4) Oligo 1 D-007500-01 Oligo 2 D-007500-02 Oligo 3 D-007500-03 Oligo 4 D-007500-18	Dharmacon siGENOME SMARTpool	M-007500-02-0005	 GACAAGGGCUUCACAGAUA CAUCAGGCGCGAUAUCUUU AAGUACAACUGCACGAUUG GGCUGAGACUGACGGGUUU

2.7 Gene Expression Assay

2.7.1 RNA Extraction

For 2D monolayer culture, cells were trypsinised, centrifuged, and then resuspended in QIAzol lysis reagent (Qiagen, Germany) for homogenisation. For 3D collagen gel culture, gels were detached and transferred to QIAzol lysis reagent until completely dissolved. After phase separation, the aqueous phase was harvested and processed for RNA isolation using RNeasy Mini Kit (Qiagen, Germany) following manufacturer's instructions.

2.7.2 Reverse Transcription, and Quantitative-PCR

Total RNA was quantified using spectrophotometry (NanoDrop, Thermo Scientific, UK). Reverse transcription was performed using QuantiTect Reverse Transcription Kit (Qiagen, Germany) according to

manufacturer's protocol. Gene expressions were evaluated by quantitative PCR using commercialised TaqMan gene expression assay PCR primers with FAM dye labelled probes (Thermo Fisher Scientific, UK) (**Table 2.7**) and TaqMan gene expression master mix (Applied Biosystems, Thermo Fisher Scientific, UK) in accordance to supplier's protocol. The q-PCR experiments were performed on 7900HT Fast Real-Time PCR system and QuantStudio6 Flex Real-Time PCR system (Applied Biosystems, UK). Relative quantification method was used for analysis (ΔC_T method for characterisation of gene expression between different culture conditions and cell lines, and $\Delta\Delta C_T$ method for gene knockdown efficiency check in single cell line) (Livak and Schmittgen, 2001), and GAPDH gene was used as an endogenous reference gene.

Table 2.7 List of qPCR Taqman probes

Gene	Gene Symbol	Taqman Gene Expression Assay probes Identification Number
Adiponectin	ADIPOR1	Hs00360422_m1
C/EBPβ	CEBPB	Hs00942496_s1
Caveolin1	CAV1	Hs00971716_m1
CD36	CD36	Hs00354519_m1
ELK1	ELK1	Hs00901847_m1
ELK3	ELK3	Hs00987814_m1
ELK4	ELK4	Hs00360813_m1
FABP4	FABP4	Hs01086177_m1
FATP1	SLC27A1	Hs01587911_m1
FATP4	SLC27A4	Hs00192700_m1
GAPDH	GAPDH	NM_002046.3
GLUT1	SLC2A1	Hs00892681_m1
GLUT4	SLC2A4	Hs00168966_m1
LPL	LPL	Hs00173425_m1
MRTF-A	MKL1	Hs01090249_g1
MRTF-B	MKL2	Hs00401867_m1
PLIN1	PLIN1	Hs00160173_m1
PLIN2	PLIN2	Hs00605340_m1
PPARα	PPARA	Hs00947536_m1
PPARγ	PPARG	Hs01115513_m1

2.8 Contraction Assay

Gels were made in MatTek dishes for contraction assay as described in 2.2. Orbital fibroblasts at a concentration of $0.74x10^5$ cells/mL were used

in the presence of serum except for co-culture experiments, where orbital fibroblasts ($1.5x10^5$ cells/mL) and macrophages ($2.25x10^5$cells/mL) were cultured in serum-free medium. The gels were photographed with a Nikon Coolpix camera daily for 7 days. Gel area and microwell area in each photo were measured using ImageJ software. The daily contraction rate was expressed as the percentage of gel area decrease compared to the original gel area. The calculation formula is “100% x (1−ratio of gel area to microwell area)” with 1 representing the equal size of gel area and microwell area at the time point when gels were made (Li et al., 2014).

2.9 LDH Cytotoxicity

For cytotoxicity test, 3D collagen gels were made with orbital fibroblasts ($0.74x10^5$ cells/mL) and macrophages ($1.5x10^5$ cells/mL) in the presence of TGF-β inhibitor SB431542 and PI3K inhibitor LY294002, and with orbital fibroblasts only ($1.85x10^5$ cells/mL) for MRTF inhibitor CCG-203971 test. After 3-4 days (CCG, 4 days; SB & LY, 3 days) of incubation in phenol red-free medium (CCG, 10% FBS; SB & LY, serum-free), culture medium was transferred to 96-well plate and processed using Pierce LDH cytotoxicity assay kit (Thermo Fisher Scientific, UK) and cytotoxicity calculated following manufacturer’s instructions. Cells lysed with lysis buffer were used as maximum LDH activity controls (100% cytotoxicity).

2.10 Chemical Adipogenic Differentiation

Differentiation medium was made from DMEM with 10% FBS, 1% penicillin/streptomycin, and 1% L-glutamine, supplemented with dexamethasone (1 μM, Sigma-Aldrich, UK), rosiglitazone (1 μM, Sigma-

Aldrich, UK), and insulin (10 µg/mL, Sigma-Aldrich, UK) [protocol modified from (Guasti et al., 2012)]. For chemical adipogenic differentiation in MRTF inhibitor or gene silencing experiments, adipogenic differentiation medium was added 3 days after MRTF inhibitor or siRNA treatment. For other chemical adipogenic differentiation in 2D, cells were grown and kept at 100% confluency for 2 days in regular DMEM with 10% FBS before replacing the medium with differentiation medium. Differentiation was allowed to proceed for 2 weeks, and medium was changed twice a week. For chemical differentiation in 3D, cells were embedded in collagen gels at concentration of $1.5x10^5$ cells/mL and cultured in DMEM with 10% FBS for 2 days before replacement with differentiation medium. Differentiation was allowed to proceed for 10~14 days, and medium was exchanged twice a week. Control cultures were treated in the same way using DMEM with 10% FBS medium.

2.11 Sample Preparation for Gas Chromatography

Cells from three conditions were sampled for gas chromatography (GC) for lipidomics study. For analysis of 3D spontaneous lipid formation, $15x10^5$ cells were needed for one sample preparation, and in order to avoid cell crowding in gels, 36 gels were made. After 2 weeks of 3D culture in which the medium was refreshed once a week, the gels were digested in 0.05% collagenase-D and the cell pellets were resuspended in 150 µL cell lysis buffer (cOmplete Lysis-M, Roche, UK) and frozen at -80°C. For 2D chemical adipogenic differentiation, $2x10^5$ cells were seeded in one well of 6 well plate. Same as previous mentioned 2D chemical adipogenic differentiation, after 100% confluency for 2 days, cells were treated with adipogenic differentiation medium. After 2 weeks of differentiation, cell lysates were collected by scraping cells off in 150

µL cOmplete Lysis-M buffer and frozen at -80°C. For 3D chemical adipogenic differentiation, $3.5x10^5$ cells were used for making 10 gels. Adipogenic differentiation medium was added after gels were cast. After 2 weeks of 3D culture in chemical adipogenic differentiation medium, gels were digested in 0.05% collagenase and cell pellets were resuspended in 150 µL cOmplete Lysis-M and frozen at -80°C. Samples were further analysed by GC at the Oxford Centre for Diabetes Endocrinology and Metabolism (OCDEM). Lipids were extracted from samples using a mixture of 2:1 chloroform:methanol. Known amounts of glyceryl tripentadecanoate (15:0) were added to samples before lipid extraction as internal standard. FAs were methylated at 80°C for 2 hr with methanolic sulfuric acid to form fatty acid methyl esters (FAME) and analysed by GC using an Agilent 6890N GC and Agilent 7890B GC (Agilent Technologies, Stockport, UK). Individual FA concentrations were identified by reference to the known internal standard. Results were expressed as individual FA weight pg/10^5 cells which was summed up as total TG weight pg/10^5 cells. Percentage FA composition (mol%) for each lipid fraction was calculated.

2.12 Exogenous Fatty Acid Mixture Preparation

Three main FAs were reconstituted from sodium oleate (O7501, Sigma-Aldrich, UK), sodium palmitate (P9767, Sigma-Aldrich, UK), and linoleic acid sodium salt (L8134, Sigma-Aldrich, UK) dissolved in warm 10% FA-free BSA (A7030, Sigma-Aldrich, UK) in DMEM/F12 medium (D6421, Sigma-Aldrich, UK). Stock solutions of each FA were made at 10 mM, and filtered through 0.22 µm filters before confirming their concentrations using colorimetric non esterified fatty acids (NEFA) kit (FA115, Randox Laboratories, UK). Stock solutions were diluted 1 in 10 to fit the standard calibration curve which is composed of 6 concentrations range between

0 mM and 1 mM. Samples were loaded in 96 well plate and measured at absorbance mode wavelength 550 nm and reference wavelength 700 nm using microplate reader (SAFIRE F129073, TECAN, Austria). The concentrations for my oleate, palmitate, and linoleate stock solutions were 9.91 mM, 9.425 mM, and 9.78 mM, respectively. For FA supplement, stock solutions were added to culture medium to make final concentrations of oleate 90 μM, palmitate 60 μM, and linoleate 50 μM.

2.13 AdipoRed Assay to Semi-quantify 3D Lipid Formation

In addition to getting proportions of cells positively stained for ORO, modified AdipoRed assay was used to quantify LD formation after FA supplement. 10 gels were cast at cell concentration of $0.74x10^5$ cells/mL in 24 well plate, with 5 gels treated with regular culture medium as control and 5 gels treated with FA supplemented medium for 1 day. Four gels from each group were digested with 0.05% collagenase-D while the rest one gel was stained for ORO for observing under microscope. The gel digest was separated into 2 parts, 3/4 for AdipoRed dye staining, 1/4 for protein level quantification. After spinning down, the cell pellets for AdipoRed were resuspended with 400 μL of diluted AdipoRed Assay Reagent (1:40 in PBS, Lonza, MD, USA) and incubated at room temperature for 10~15 min to stain intracellular LDs. The cell suspension in AdipoRed reagent was loaded to 96 well plate in serial dilution in order to confirm the measurement was in good linear regression and not saturated, and any oversaturated point or outlier was excluded. Samples were measured at fluorescence mode with excitation at 485 nm and emission at 572 nm using microplate reader (SAFIRE F129073, TECAN), and diluted AdipoRed Reagent without cells were loaded for background subtraction. The cell pellets for protein quantification was lysed with lysis buffer and protein level was assessed by BCA assay.

The readout relative fluorescence units (RFU) were normalised to protein amount, in which the FA supplement samples always yielded higher RFU/µg protein levels compared to control samples without FA. But the absolute RFU/µg protein varied between experiments, therefore the results were expressed as the fold change of FA supplement group relative to control without FA group.

2.14 Fatty Acid Uptake Kit

To know if ability for FA uptake changes over time after cells grown in 3D, cells cultured in 3D gels for 24 hr, 6 hr, 2.5 hr and 0.5 hr were assessed using FA uptake kit (MAK156, sigma-aldrich, UK; and ab176768, abcam, uk). The FA uptake kit uses fluorescent FA analogue as substrate for transmembrane FA transport, and a cell membrane-impermeable quenching agent is included, which eliminates extracellular fluorescence and enables specific measurement of intracellular FA. The detected fluorescence signal is the uptaken FAs (Liao et al., 2005). Advance preparation started from seeding $1.35x10^5$ cells per 60 mm dish for 4 dishes 2 days prior first gel casting time point (24 hr). Cells were cast into 3 gels in 24 well plate and kept in 10% FBS DMEM for 24 hr, 6 hr, 2.5 hr and 0.5 hr before FA dye treatment. FA dye was prepared following manufacturer's instruction in which stock solution was made by dissolving TF-C12 FA (fluorescence labelled dodecanoic acid) in DMSO. Before FA treatment, fresh FA dye loading solution was made from 1:500 v/v stock solution:assay buffer. This FA dye loading solution was mixed with 10% FBS DMEM at 1:1 v/v ratio, and 240 µL of the mixture per well was given to replace culture medium. After 1 hr of incubation in 37°C 5% CO_2 incubator, gels were digested with 0.05% collagenase-D. Cells were pelleted and resuspended with cOmplete Lysis-M. Fluorescence of lysates were measured in 96 well plate at excitation wavelength 485 nm and emission wavelength 515 nm using microplate reader (SAFIRE

F129073, TECAN). Lysates were also used for protein quantification by BCA assay. The FA uptake was obtained by the measured RFU during the FA incubation (1 hr) normalised to the protein amount (μg), and expressed at the unit of RFU/μg protein.

2.15 Hyaluronic Acid Enzyme-Linked ImmunoSorbent Assay (ELISA)

Hyaluronic acid (HA) production was quantified with hyaluronan enzyme-linked immunosorbent assay (ELISA) (R & D Systems, MN, USA). 3D collagen gels were made with orbital fibroblasts at a concentration of $0.74x10^5$ cells/mL, with or without macrophages of $1.5x10^5$ cells/mL (1:2) or $3.7x10^5$ cells/mL (1:5) in serum-free medium. After 3 days, the culture medium was collected, and the gels were digested with 0.05% collagenase-D for 30 min at 37°C to extract any further HA trapped in the gel. The collagenase digest was centrifuged to remove cells and debris and the supernatant collected. The mixture of media and supernatant from digested gels was diluted in serum-free DMEM (1:30) to fit the standard calibration curve which was composed of 6 concentrations range between 0 ng/mL and 30 ng/mL. Samples were assayed according to manufacturer's instructions and detected at absorbance mode wavelength 450 nm and reference wavelength 570 nm using microplate reader (FLUOStar OPTIMA, BMG Labtech, Germany). Gels without cells, and gels with macrophages only, were used for baseline calibration.

2.16 Statistics

Most data presented were means averaged from at least three independent experiments ± standard error of the mean (SEM). Statistical

analysis was performed using two-tailed Student's t-test or one-way ANOVA with post-hoc Turkey's multiple comparison test on Prism 5 (GraphPad software). $P<0.05$ was considered statistically significant.

Chapter 3 MRTF/SRF role in TED

3.1 Introduction

The orbital cavity is a limited space bound by bony walls, and an increase in orbital contents volume may result in elevated intraorbital pressure. HA production and fat expansion contribute to the expansion of extraocular muscle and intraorbital fat in TED. Thus TED patients often have increased intraorbital pressure, and their vision may be threatened due to optic nerve ischemia secondary to poor blood flow from this high tissue pressure (Bahn, 2010; Daley et al., 2008; Fletcher and Mullins, 2010). These clinical manifestations suggest that orbital tissues in TED may be subjected to severe changes in their mechanical properties which may compound the pathology. Previous work in our lab revealed spontaneous LD formation in orbital fibroblasts in a 3D *in vitro* model in which cells were cultured in soft collagen matrix, whereas orbital fibroblasts grown in 2D stiff matrix did not produce LDs. Moreover, applying weight to simulate intraorbital pressure elevation enhanced the LD accumulation in this 3D model (Li et al., 2014). These suggest that orbital fibroblasts are mechanosensitive and may regulate LD formation in response to mechanical changes in their environment.

The mechanics of ECM stiffness and applied force in ECM are transmitted into cells and cells respond with internal force through cytoskeleton arrangement. In addition to generating internal force, cells regulate gene expressions in response to cytoskeleton and mechanics as mechanotransduction mechanism (Chen, 2008). MRTF/SRF and YAP/TAZ/TEAD are two well-known mechanotransduction signalling pathways, where MRTF and YAP/TAZ are important transcription co-activators. In rigid matrix like 2D tissue culture plastic, MRTF and YAP/TAZ shuttle to nucleus to bind their respective transcription factors and activate downstream SRF and TEAD pathways. MRTF/SRF

pathway regulates genes associated with cytoskeleton and contractility (Esnault et al., 2014; Gualdrini et al., 2016). YAP/TAZ/TEAD pathway regulates cell growth and proliferation, and CTGF is its important direct target gene (Zhao et al., 2008). Activation of both pathways is related to contractility and is profibrotic (Noguchi et al., 2018; Yu-Wai-Man et al., 2017). Oppositely, in soft environment like 3D, MRTF and YAP/TAZ are exported from the nucleus and cells favour adipogenic differentiation (Dupont et al., 2011; Nobusue et al., 2014; Tsou et al., 2014). We hypothesised that dysregulation of MRTF and YAP led to the more adipogenic and more fibrotic phenotype in TED orbital fibroblasts. We expected that MRTF and YAP activation would result in more contractile and less adipogenic phenotypes, while the deactivation would be less contractile and more adipogenic. In order to understand if MRTF and YAP are involved in TED development, we explored the expression and localisation of MRTF-A and YAP in orbital fibroblasts in our 3D model. Since there is no good MRTF-B antibody available, and MRTF-A and MRTF-B show functional redundancy (Cen et al., 2003), most of the work was focused on MRTF-A. We further observed the adipogenic and fibrotic phenotypes of orbital fibroblasts in response to MRTF manipulation.

3.2 Results

3.2.1 Orbital fibroblasts spontaneously produce LDs in 3D

We confirmed that orbital fibroblasts grown in 3D collagen matrix spontaneously form and accumulate LDs, whereas none of the cells in 2D showed visible LDs (**Figure 3.1**A), and cells obtained from TED patients generally yielded more LDs than those from control individuals

(**Figure 3.1**B). CO5 and CO6 cells had high proportions of ORO positivity compared to other COs and even HOs. It is unknown if this is due to any donor-related factor, but these two cells lines were derived from more anteriorly located fat, and some of our other control lines derived from septal fat also displayed high ORO positivity (data not shown). It is possible that phenotypes of orbital fibroblasts vary according to their original location, though we have not done a formal study.

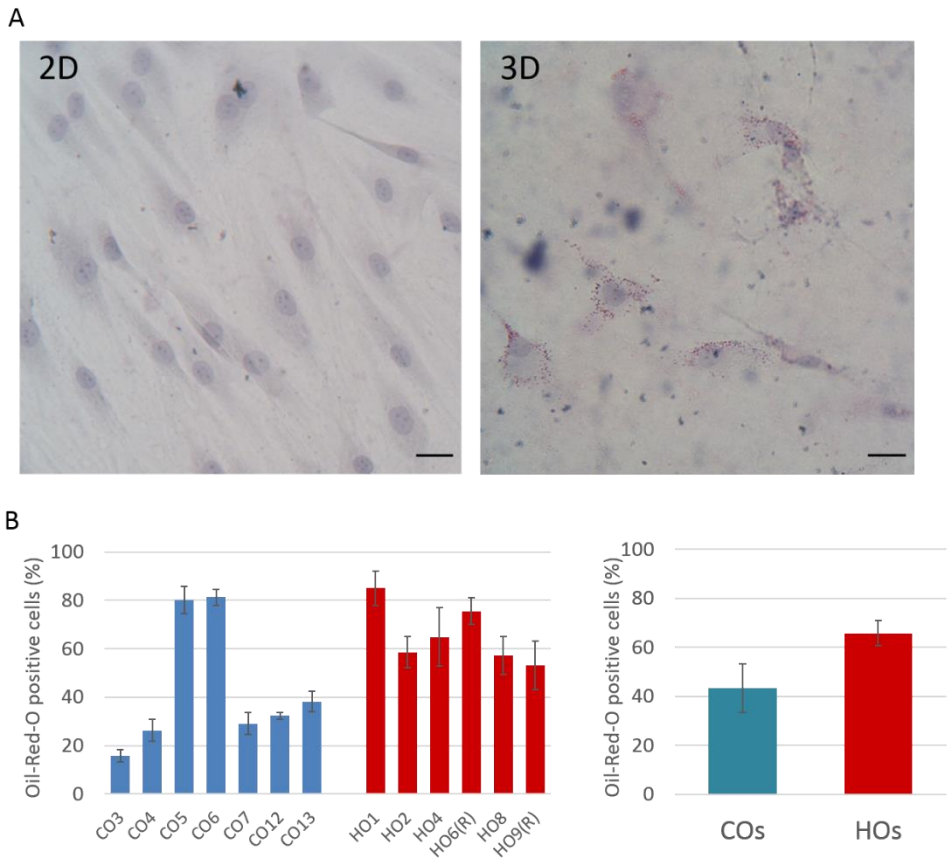

Figure 3.1 TED fibroblasts are more likely to produce LDs in 3D than control orbital fibroblasts

(A) Representative images of Oil-Red-O (ORO) stained HO2 orbital fibroblasts cultured in 2D (left image) and 3D for 7 days (right image) (scale bar: 25 μm) (B) Proportion of ORO positive cells of 7 control (COs: CO3, CO4, CO5, CO6, CO7, CO12, CO13) and 6 TED (HOs: HO1, HO2, HO4, HO6R, HO8, HO9R) orbital fibroblasts primary cell lines after 7 days of culture in 3D. Left: individual cell line ORO data. Right: averaged COs and HOs ORO data. (shown are mean ± SEM, each n≥3, no significant difference between COs and HOs, t-test)

3.2.2 MRTF in orbital fibroblasts

3.2.2.1 MRTF-A protein level expression is reduced in 3D culture

We examined if the levels of MRTF-A in orbital fibroblasts are altered in 3D culture. Protein samples were collected from control (COs: CO4, CO6, CO7, CO12) and TED (HOs: HO1, HO2, HO4, HO6R) cell lines in both 2D and 3D. Western blotting was performed for MRTF-A. It revealed that MRTF-A protein levels were decreased in 3D, though it is only statistically significant in averaged control cells rather than TED cells (**Figure 3.2**). Despite being significantly more adipogenic, TED cells did not show less MRTF-A protein, overall suggesting that LD accumulation is not linked to MRTF-A level.

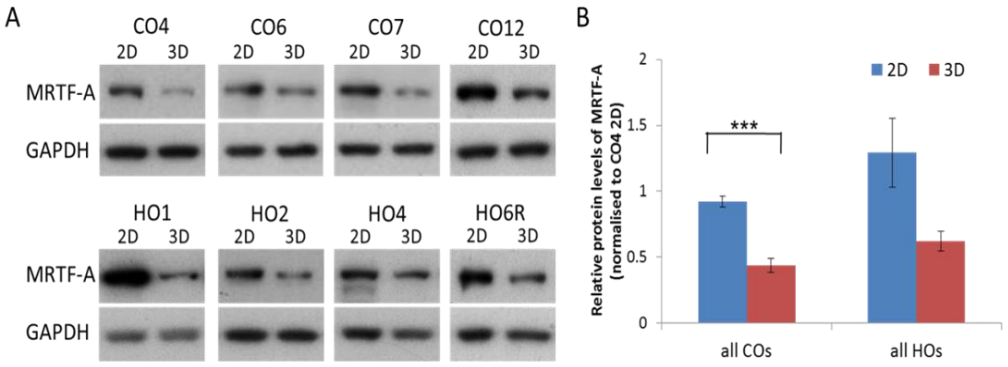

Figure 3.2 MRTF protein levels decreased in 3D.

(A) Representative Western blots of MRTF-A protein in 4 control (COs) and 4 TED (HOs) cell lines. (B) Relative MRTF-A protein levels for the same 4 COs and 4 HOs cell lines after 5-7 days culture in the presence of 10% serum in monolayers (2D) and in gels (3D) (n≥3; ***p<0.001, by t-test)

3.2.2.2 MRTF-A localisation is altered in 3D

Immunofluorescence (IF) for localisation of MRTF-A was done to compare orbital fibroblasts cultured in 2D and 3D in the presence of 10% serum. MRTF-A localised to the nucleus in the majority of cells in 2D, with no visible difference between TED (HOs: HO2, HO6R) and control (COs: CO7, CO12) orbital fibroblasts (**Figure 3.3**).

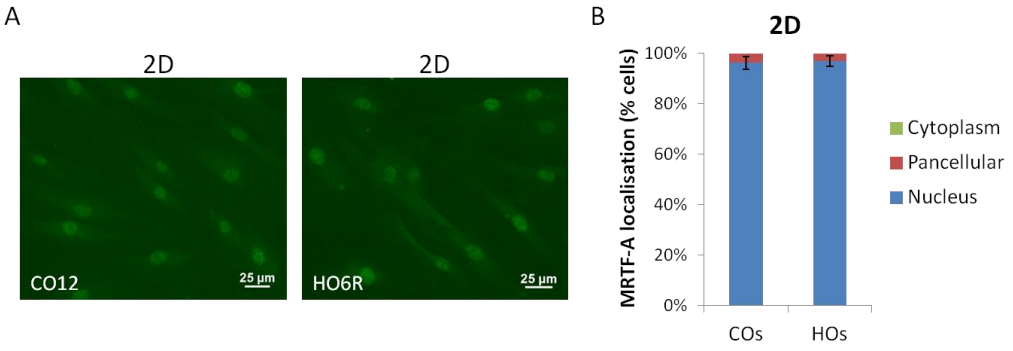

Figure 3.3 MRTF-A was nuclear in orbital fibroblasts in 2D

(A) Representative images of MRTF-A staining in CO12 (control) and HO6R (TED) fibroblasts cultured in 2D in the presence of 10% serum. Scale bar, 25 µm (B) Quantification of MRTF-A localisation in 2D was achieved by categorising more than 100 cells into nucleus, pancellular, or cytoplasm. COs were averaged from control orbital fibroblasts CO7, CO12; HOs were averaged from TED orbital fibroblasts HO2, HO6R (n=3).

The same TED (HOs: HO2, HO6R) and control (COs: CO7, CO12) orbital fibroblasts were used for MRTF-A localisation in 3D. Upon culture in 3D, MRTF-A localisation was altered. Within the soft matrix, MRTF-A moved out of the nucleus, with half of the cells showing pancellular MRTF-A on Day 1 (**Figure 3.4**A,B). The shift of MRTF-A from nucleus to more cytoplasmic in 3D seems to be consistent with previous work showing that stem cells differentiate towards adipocyte lineage in soft matrix, in line with our observation of increased LD formation in 3D soft matrix. 3D MRTF-A distribution patterns varied over time and appeared

to match at least partly the LD levels: MRTF-A significantly moved out of nucleus on Day 1 with concurrent high ORO, moved back to nucleus as ORO went down on Day 4 (**Figure 3.4**B,C). The increase in nuclear MRTF-A concurrent with the decrease in LDs on Day 4 is consistent with the idea that MRTF/SRF activation leads to the decrease of adipogenesis. However, the MRTF-A distribution pattern in COs and HOs was similar, while HOs presented higher proportions of ORO positive cells. Therefore, MRTF-A localisation might play a role but not be the key determinant for spontaneous LD formation in 3D orbital fibroblasts.

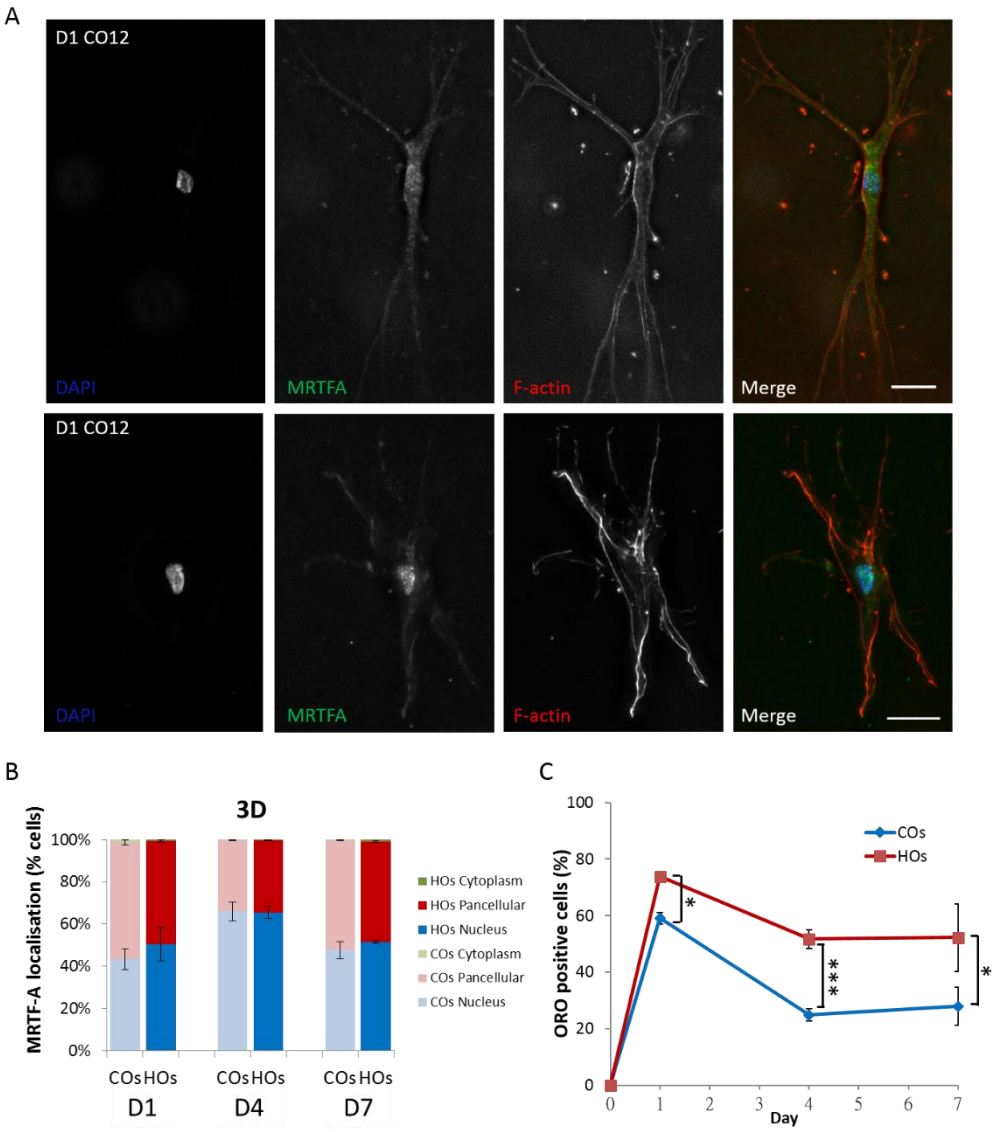

Figure 3.4 MRTF-A moved out of nucleus in 3D

(A) Representative IF images of CO12 (control) fibroblasts cultured in 3D gels for 1 day. Scale bar, 25 µm, Merge images are from DAPI (blue), MRTF-A (green), and F-actin (red). Top panel: pancellular MRTF-A; Bottom panel: nuclear MRTF-A (B) Quantification of MRTF-A localisation in cells cultured in 3D for 1 day, 4 days, and 7 days. More than 50 cells were observed and categorised into nucleus, pancellular, or cytoplasm in each independent experiment. COs averaged from control orbital fibroblasts CO7, CO12; HOs averaged from TED orbital fibroblasts HO2, HO6R (n=3). (C) Kinetic curves of proportion of ORO positive cells of the same COs (CO7, CO12) and HOs (HO2, HO6R) (n=3~4 for each cell line, *p<0.05, ***p<0.001, t-test). Cells for IF (B)

and ORO (C) assays of the same experiment were from the same 2D flasks and cast into 3D gels at the same time.

3.2.2.3 MRTF inhibition decreased orbital fibroblasts contractility

MRTF is a co-activator of SRF, which regulates the expression of a number of genes involved in fibrosis, such as αSMA, CTGF, and type I collagen (Haak et al., 2014). MRTF-A overexpression, in primary culture mouse cardiac fibroblasts upregulates αSMA gene and protein expression (Small et al., 2010), in human fetal lung fibroblast cell line IMR90 upregulates both type I collagen and smooth muscle actin (SMA) protein expression, indicating that activation of MRTF/SRF pathway promotes fibrosis. On the other hand, MRTF-A knockdown reduced type I collagen and SMA protein expression in IMR90 (Luchsinger et al., 2011). *In vivo* in a mouse model of myocardial infarction, in which ischemic cardiac myocytes trigger fibrosis and scar formation, MRTF-A knockout mice displayed significant smaller fibrotic scar size indicating that the depletion of MRTF gene reduces fibrosis (Small et al., 2010). Previous work in our lab also showed that MRTF inhibitors effectively reduced contractility and gene expression of αSMA and CTGF in human conjunctival fibroblasts (Yu-Wai-Man et al., 2017). Since MRTF localisation did not seem to be linked to the adipogenic phenotype in 3D, and MRTF was shown to regulate the fibrotic phenotype in conjunctival fibroblasts (Yu-Wai-Man et al., 2017), we investigated whether MRTF might regulate the fibrotic phenotype in orbital fibroblasts. Orbital fibroblasts were cultured in 3D in the same gels but in free-floating condition for using gel contraction as a readout of cell contractility as previously described (Li et al., 2014). CCG-203971, a second generation Rho/MRTF/SRF pathway inhibitor (Van De Water et al., 2013), was used to block MRTF activity as previously described (Yu-Wai-Man et al., 2017).

CCG-203971 10 μM did not reduce gel contraction, but CCG-203971 25 μM significantly reduced orbital fibroblasts contractility with 77.15% and 31.10% reduction compared to DMSO only mated control for CO7 (control) and HO6R (TED), respectively (**Figure 3.5**A,B). LDH cytotoxicity assay revealed minimal toxicity of CCG-203971 at both concentrations (**Figure 3.5**C). These suggest that MRTF inhibition by CCG-203971 effectively reduces the MRTF/SRF activated contractility in orbital fibroblasts.

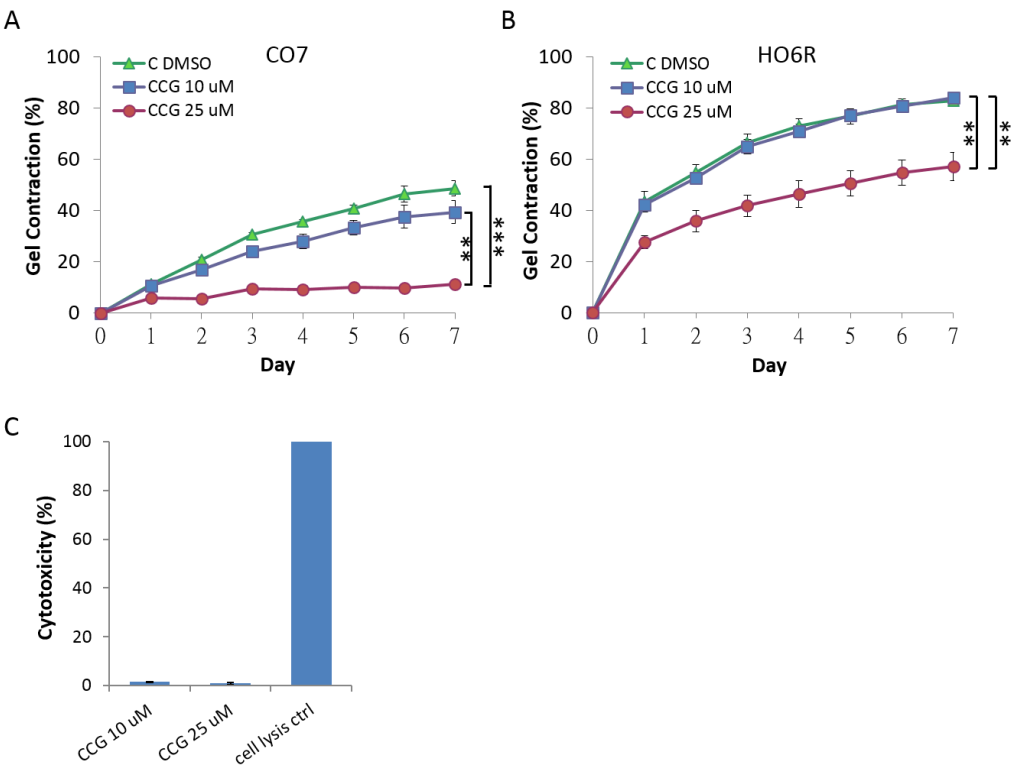

Figure 3.5 Inhibitor of MRTF, CCG-203971 at 25 μM, reduced gel contraction

Contraction assay of control (CO7) (A) and TED (HO6R) (B) orbital fibroblasts treated without CCG-203971 (DMSO added), or with CCG-203971 10 μM or 25 μM (shown are mean ± SE, D7 contractility by one-way ANOVA: CO7 $p<0.001$, post hoc C(DMSO) vs CCG 25 μM ***$p<0.001$, and CCG 10 μM vs CCG 25 μM **$p<0.01$; HO6R $p<0.01$, post hoc C(DMSO) vs CCG 25 μM **$p<0.01$, and CCG 10 μM vs CCG 25 μM **$p<0.01$, n=3, gels in triplicates) (C) LDH cytotoxicity assay showed minimal cytotoxicity of CCG-203971 10 μM and 25 μM after 3 days in 3D gels. Shown is calculated toxicity normalised to 100% cell lysis control. (n=3)

To confirm the involvement of MRTF in fibroblast contractility, we used siRNA to downregulate MRTF gene expression. To avoid redundancy between MRTF isoforms, we did a double knockdown of MRTF-A and MRTF-B, and the cells were then cast in free-floating gel matrix for contraction assay. Matrix contraction in both CO7 (control) and HO6R

(TED) orbital fibroblasts were significantly decreased by successful MRTF-A and MRTF-B gene silencing (**Figure 3.6**). Knockdown of MRTF-A and MRTF-B decreased Day 7 contractility by 73.69% and 34.97% compared to the control siRNA transfection in CO7 and HO6R, respectively. The reduction rates caused by siRNA are similar to those seen with the higher concentration of CCG, indicating that CCG 25 μM in blocking MRTF for contractility is as effective as knockdown of MRTF-A and MRTF-B. This again suggests that blocking MRTF function can reduce contractility of orbital fibroblasts and confirms the involvement of MRTF/SRF pathway in fibrotic phenotype in orbital fibroblasts. Moreover, CO7 seemed to be more sensitive than HO6R to the MRTF depletion on contractility. Since COs and HOs have similar MRTF-A protein levels and MRTF-A distribution in 3D, and the MRTF knockdown efficiency were similar in both CO7 and HO6R, it is less likely that intrinsic MRTF leads to this difference. It is possible that the more contractile HO6R has more or stronger profibrotic regulators for its contractility.

A

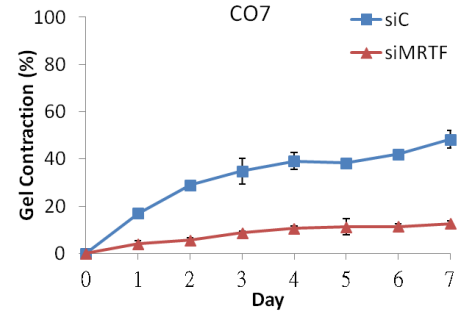

B

Relative gene expression Normalised to GAPDH Normalised to siControl	siControl	siMRTFA+siMRTFB
MRTFA	1	0.193 ± 0.042
MRTFB	1	0.209 ± 0.083

C

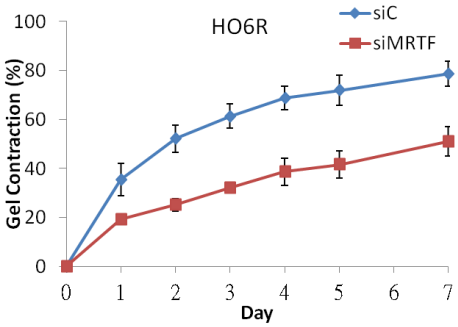

D

Relative gene expression Normalised to GAPDH Normalised to siControl	siControl	siMRTFA+siMRTFB
MRTFA	1	0.271 ± 0.066
MRTFB	1	0.228 ± 0.052

Figure 3.6 MRTF gene silencing reduced gel contraction

Contraction assay of control (CO7) and TED (HO6R) orbital fibroblasts transfected with control siRNA or MRTF-A + MRTF-B siRNAs. (A) Downregulating MRTF-A+MRTF-B decreased contractility of CO7 (shown are mean ± SE, Day 7 p<0.01, t-test, n=3, triplicates in each experiment) (B) MRTF-A and MRTF-B gene knockdown efficiency was quantified by qPCR gene expression assay normalised to GAPDH and then normalised to the mean of siControl (shown are mean ± SE, n=3) (C) Downregulating MRTF-A + MRTF-B decreased contractility of HO6R (Day 7 p<0.05, t-test, n=3, triplicates in each experiment) (Two repeats were done by undergraduate student Chiyun Lee, results of the three experiments are consistent) (D) MRTF-A and MRTF-B gene knockdown efficiency was quantified by qPCR gene expression assay normalised to GAPDH and then normalised to the mean of siControl (n=3) (Two repeats were done by undergraduate student Chiyun Lee, results of the three experiments are consistent)

3.2.2.4 Adipogenesis of orbital fibroblasts was not regulated by MRTF

.3.2.2.4.1. MRTF inhibitor increased lipid formation in 3D but MRTF gene silencing did not

Adipogenesis and contraction are often mutually exclusive and regulated by opposite effectors on the Rho/MRTF/SRF pathway. The inhibition of Rho/MRTF/SRF triggered adipogenesis in mouse preadipocyte 3T3-L1 cells and mouse dedifferentiated fat cells, which have higher potential to differentiate into adipocytes compared to preadipocytes (Nobusue et al., 2014). In addition, our localisation studies suggested that MRTF might indeed also function as an inhibitor of adipogenesis in orbital fibroblasts (**Figure 3.4**). We hypothesised that depletion of MRTF could induce adipogenesis in 3D orbital fibroblasts. Rho/MRTF/SRF inhibitor CCG-203971 25 μM was applied to 3D culture for 7 days, and lipid production was assessed by ORO staining and further cell counting for ORO positive rates. 3D spontaneous LD formation was significantly enhanced after CCG-203971 25 μM treatment in both control orbital fibroblasts CO7 and CO12. In TED orbital fibroblasts HO2 and HO6R, the CCG-203971 increased the ORO positive rates mildly though not reaching statistical significance (**Figure 3.7**), likely due to the fact that HOs were already very positive on ORO.

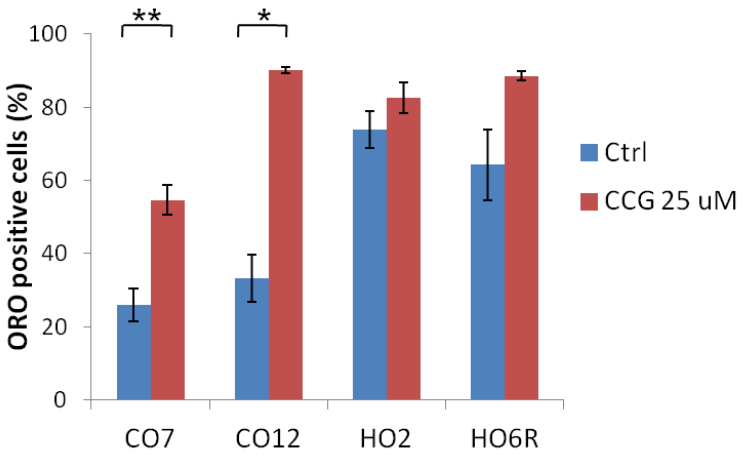

Figure 3.7 Inhibitor of MRTF, CCG-203971 at 25 μM, increased ORO positive rates in cells cultured in 3D

Proportion of cells positive for ORO from control (CO7, CO12) and TED (HO2, HO6R) orbital fibroblasts cultured in 3D with and without MRTF inhibitor CCG-203971 25 μM for 7 days was shown in mean ± SEM. (n=3, triplicates, *p<0.05, **p<0.01, by t-test)

We further used siRNA to knockdown MRTF expression and studied the same lipid formation after 7 days of 3D culture in a representative control orbital fibroblasts cell line, CO7. The gene silencing of MRTF was done targeting solely at MRTF-A, MRTF-B, or simultaneously at MRTF-A and MRTF-B (**Figure 3.8**A left). Despite an efficient knockdown of the proteins, neither MRTF-A, MRTF-B, or MRTFA+B silencing significantly affected lipid formation in CO7 cells as the inhibitor CCG-203971 did (**Figure 3.8**B). To exclude the possibility that MRTF gene expression recovered from knockdown within 7 days of incubation and thus failed to induce adipogenesis, the expression of MRTF-A and MRTF-B were evaluated in cells in Day 7 3D gels. There was no evidence of the downregulated genes returning to the level of control siRNA samples (**Figure 3.8**A right). MRTF does not appear to downregulate adipogenesis in our model as previously suggested, and MRTF inhibitor

possibly does not directly inhibit MRTF function. These suggest that 3D spontaneous LD formation of orbital fibroblasts might not be regulated by MRTF.

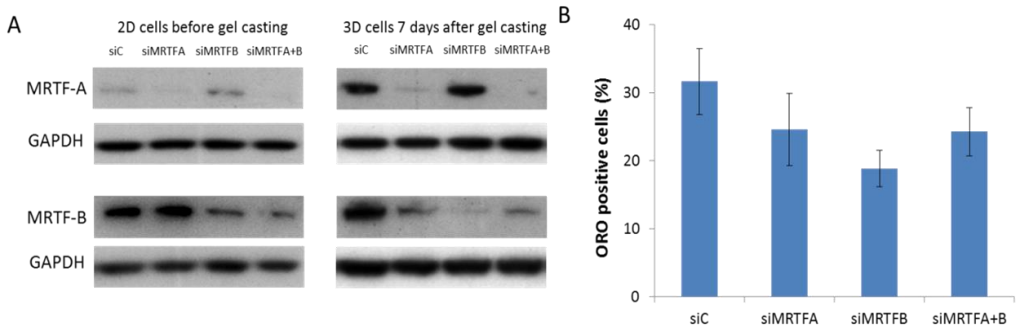

Figure 3.8 MRTF gene silencing did not increase ORO positive rates in 3D-cultured orbital fibroblasts

Control orbital fibroblasts CO7 were transfected with control siRNA, MRTF-A siRNA, MRTF-B siRNA, or MRTF-A + MRTF-B siRNAs, and then were cultured in 3D gels for 7 days for ORO staining. (A) Left: Representative Western blots probed for MRTF-A and MRTF-B levels showed the effects of siRNAs after 3 days of transfection and before transferring cells to 3D culture (n=3). Right: Western blots probed for MRTF-A and MRTF-B levels showed the lasting downregulation effect of the siRNA targeted genes (n=1). (B) MRTF gene silencing did not increase proportions of CO7 fibroblasts positive for ORO on Day 7 (n=3, triplicates).

.3.2.2.4.2. MRTF inhibition/ knockdown did not increase adipogenesis in 2D

Because some aspects of MRTF regulation appeared to be conserved in orbital fibroblasts like the MRTF localisation and the related LD formation (**Figure 3.3**, **Figure 3.4**), but not others such as MRTF knockdown in spontaneous LD formation in 3D (**Figure 3.8**), we further explored the MRTF involvement in classical 2D adipogenesis. Representative control

orbital fibroblasts CO7 were cultured in 2D using adipogenic differentiation medium composed of 1 μM dexamethasone, 1 μM rosiglitazone, and 10 μg/mL insulin, and the effect of Rho/MRTF/SRF inhibitor CCG-203971 and MRTF siRNA on 2D chemical adipogenesis was studied. CCG-203971 was added to the cells on the next day after cell plating and the concentration of CCG-203971 was adjusted to 12 μM because toxicity with some cell death was found using 25 μM in 2D culture for 16 days. As adipogenic differentiation protocols suggest, differentiation was commenced after cells reached confluency for 48 hours, which was Day 3 after our cell seeding, and the medium was refreshed twice a week. After completion of 14 days of differentiation, cells were stained with ORO, imaged, and the amount of lipid vesicles was quantified using image J in addition to the counting of ORO positive cells. Without adipogenic differentiation medium, no adipogenesis was observed in either presence or absence of MRTF inhibitor (**Figure 3.9**A left two images, **Figure 3.9**B). Consistent with previous work in the lab (Li et al., 2014), the control orbital fibroblasts were only moderately differentiated into adipocyte after chemical stimulation with about 20% cells positive for ORO (**Figure 3.9**C). Surprisingly, the MRTF inhibitor did not increase adipogenesis as expected (**Figure 3.9**A right two images, **Figure 3.9**B). Rather, it reduced the size of the LDs (**Figure 3.9**A right two images, **Figure 3.9**C). The discrepancy between different quantification methods results from that proportion of cells to produce lipids were not changed by MRTF inhibitor, but the sizes of lipid vesicles decreased after MRTF inhibitor treatment. In either method, this suggests that MRTF/SRF inhibition did not enhance adipogenesis of orbital fibroblasts in 2D.

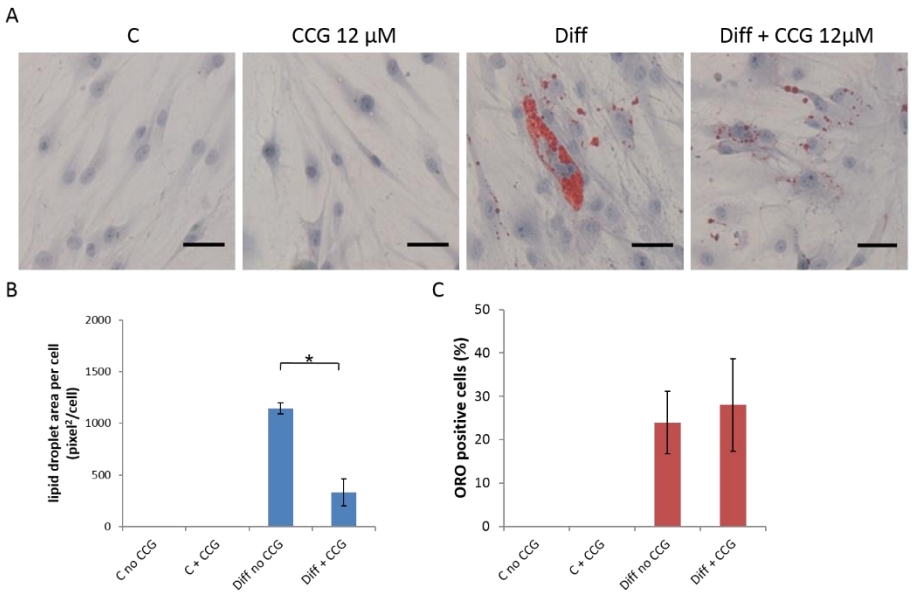

Figure 3.9 MRTF inhibitor CCG-203971 did not increase chemical adipogenesis in 2D

Control orbital fibroblasts CO7 were treated with or without CCG-203971 12 µM, and then cells were cultured in normal 10% FBS DMEM medium or adipogenic differentiation medium containing dexamethasone 1 µM, rosiglitazone 1 µM and insulin 10 µg/mL for 14 days with or without continuous CCG treatment. (A) Representative ORO and hematoxylin stained images of CO7 grown in normal medium without CCG (C), normal medium with CCG (CCG 12 µM), adipogenic differentiation medium without CCG (Diff), and adipogenic differentiation medium with CCG (Diff + CCG 12 µM) (scale bar, 25 µm) (B) ORO stained area quantified by image j was normalised to cell counts, shown as mean ± SEM (5 fields were analysed in each condition, n=3, *p<0.05, t-test) (C) Proportion of ORO positive cells was quantified by cell counting from the same images in above quantification (5 fields were analysed in each condition, n=3)

On the other hand, downregulating MRTF-A and MRTF-B appeared to slightly increase LD size but was not statistically significant, and it did not affect proportion of cells to produce lipids (**Figure 3.10**A,C,D), indicating downregulating MRTF did not affect size of lipid vesicles as MRTF

inhibitor did. Protein level of MRTF-A and MRTF-B did not recover after 2 weeks post completion of transfection (**Figure 3.10**B), consistent with the previous work in 3D (**Figure 3.8**A). This suggests that MRTF downregulation has a long-lasting effect. It was not common to have the lasting downregulation effect after removal of transfection reagent for this long, and whether it particularly happens in MRTF gene or in orbital fibroblasts is unknown, but it suggests that despite the MRTFs were downregulated, adipogenesis was not increased. Results from this section suggest that, while MRTF/SRF inhibitor increased LD formation in 3D but not in 2D, depletion MRTF levels did not affect either spontaneous adipogenesis in 3D or chemical adipogenesis in 2D in orbital fibroblasts.

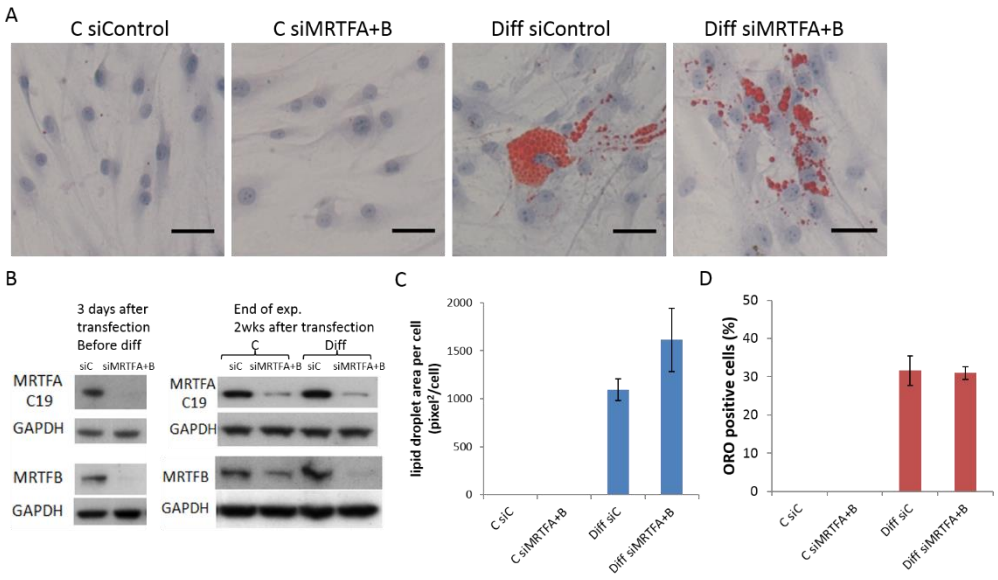

Figure 3.10 MRTF gene silencing did not change chemical adipogenesis in 2D-cultured cells

Control orbital fibroblasts CO7 were transfected with control siRNA or mixture of MRTF-A + MRTF-B siRNAs, and then cells were cultured in the presence or absence of adipogenic differentiation inducers (dexamethasone, rosiglitazone, and insulin) for 14 days (A) Representative ORO staining images of siControl or siMRTFA+B transfected cells cultured in normal medium (C) or adipogenic differentiation medium (Diff) (scale bar, 25 μm) (B) Representative Western blots probed for MRTF-A and MRTF-B before differentiation and at the end of differentiation showed effective MRTF-A and MRTF-B knockdown (n=3) (C) Quantification of ORO stained area normalised to cell counts of the above 4 conditions (5~6 fields were analysed in each condition, n=3) (D) Proportion of ORO positive cells was quantified by cell counting from the same images in above quantification (5~6 fields were analysed in each condition, n=3)

3.2.2.5 TCF gene silencing did not affect lipid formation in 3D

Previous work on MEFs has shown that knockout TCFs (including Elk-1, Elk-3, Elk-4) enhanced both MRTF and SRF genes (Gualdrini et al., 2016), and TCFs competed with MRTFs to bind SRF and regulate cell contractility. To know whether this balance also exists in orbital fibroblasts, we downregulated TCFs and expected to decrease LD formation by upregulating MRTFs indirectly. Triple knockdown of Elk-1, Elk-3, and Elk-4 was done by siRNA transfection in a representative TED orbital fibroblasts line, HO6R. Cells were then cultured in 3D for 7 days for spontaneous lipid formation. The knockdown of TCFs did not reduce the amount of ORO positive cells in 3D (**Figure 3.11**A) although the TCF genes were efficiently downregulated (**Figure 3.11**B), suggesting that TCFs did not regulate LD formation in TED orbital fibroblasts.

A

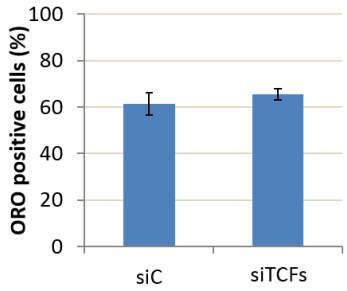

B

Relative gene expression normalised to GAPDH then normalised to siControl	siControl	siELK1+siELK3+siELK4
ELK1	1	0.150 ± 0.057
ELK3	1	0.141 ± 0.043
ELK4	1	0.253 ± 0.081

Figure 3.11 TCF gene silencing did not alter ORO positive rates in 3D-cultured orbital fibroblasts

TED orbital fibroblasts HO6R were transfected with control siRNA or a mixture of ELK1 + ELK3 + ELK4 siRNAs, and then cultured in 3D gels for 7 days for ORO staining. (A) TCF gene silencing did not decrease proportions of HO6R cells positive for ORO on Day 7 (n=3, triplicates) (B) ELK1, ELK3, and ELK4 gene knockdown efficiency was quantified by qPCR gene expression assay normalised to GAPDH and then normalised to the mean of siControl (shown are mean ± SEM, n=3)

3.2.3 YAP in orbital fibroblasts

3.2.3.1 YAP expression did not change between 2D and 3D

YAP is another transcription co-activator which has been implicated in mechanotransduction, and its localisation changes in response to ECM modulation and determines cell fate (Dupont et al., 2011). In order to understand the involvement of YAP in 3D lipid vesicle formation in orbital fibroblasts, we examined if the levels of YAP in orbital fibroblasts are altered in 3D culture. Protein samples were collected from control (COs: CO4, CO6, CO7) and TED (HOs: HO1, HO2, HO4) cell lines in both 2D and 3D. Western blotting was performed for YAP. YAP protein levels did not show any difference between 2D and 3D in control and disease cells (**Figure 3.12**).

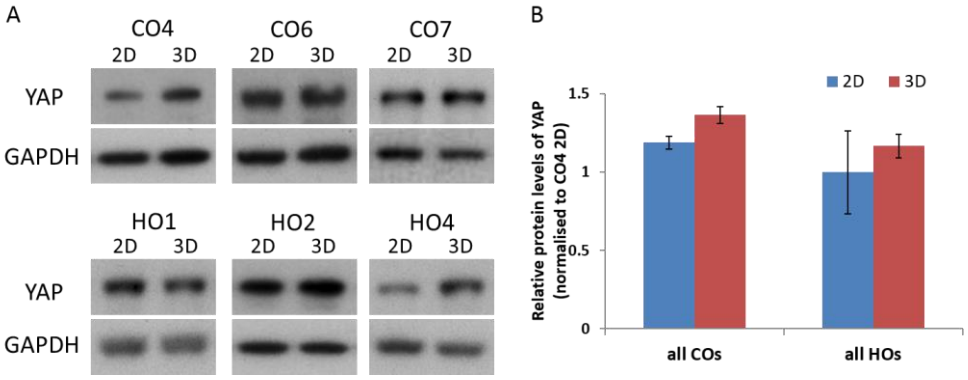

Figure 3.12 YAP protein levels did not change between 2D and 3D.

(A) Representative Western blots of YAP protein in 3 control (COs) and 3 TED (HOs) cell lines. (B) Relative YAP protein levels for the same 3 COs and 3 HOs cell lines after 5-7 days culture in the presence of 10% FBS in monolayers (2D) and in gels (3D) (shown are mean ± SEM, n≥3)

3.2.3.2 YAP localisation was altered in 3D

To understand YAP localisation in response to different matrix, YAP distribution was performed in one CO and one HO representative cell lines in 2D and 3D. YAP was mostly nuclear in TED cell line HO2 in 2D, but less nuclear with some pancellular pattern in control cell CO7 (**Figure 3.13**A,C). When cultured in 3D for one day, most cells displayed cytoplasmic or pancellular YAP (**Figure 3.13**B,D). This shift in YAP location from nucleus to more cytoplasmic is consistent with the soft nature of collagen gels and spontaneous LD formation observed in 3D collagen gel. But while the majority of cells were pancellular in 3D with very similar distribution between CO7 and HO2, the corresponding Day 1 ORO proportion was slightly lower in CO7 compared to HO2 (**Figure 3.13**D,E), not in line with the distribution. These suggest that YAP localisation does respond to ECM rigidity, but might not be directly linked to determine the spontaneous LD formation in 3D orbital fibroblasts.

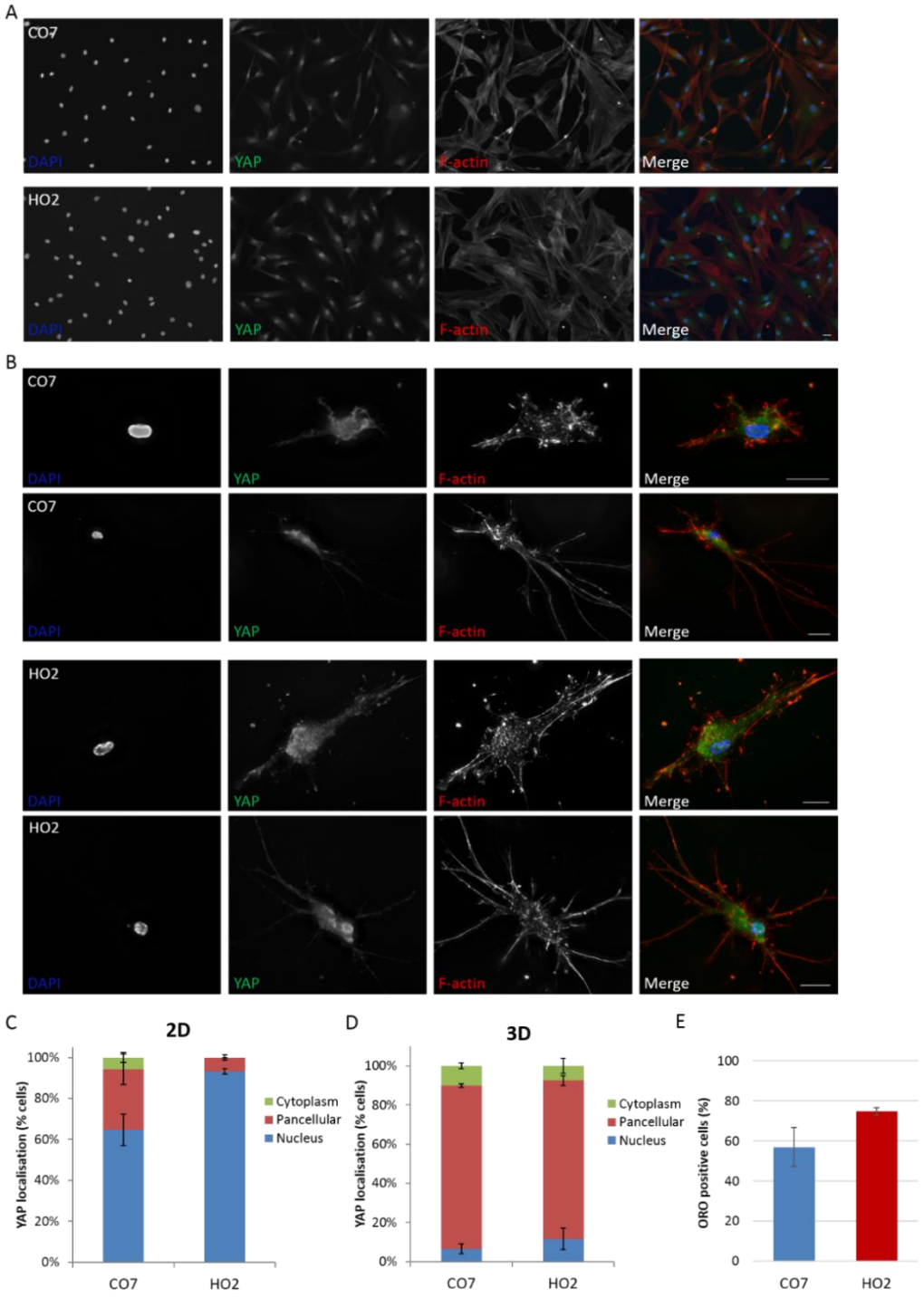

Figure 3.13 YAP moved out of nucleus in 3D

(A) Representative images of YAP staining in 2D cultured orbital fibroblasts CO7 (control) and HO2 (TED). Scale bar, 25 µm (B) Representative IF images of YAP staining in CO7 and HO2 cells cultured in 3D for 1 day. Images were taken with z stacks and then deconvolved. Scale bar, 25 µm, Merge images are from DAPI (blue), YAP (green), and F-actin (red) (C) Quantification of YAP

localisation in 2D by categorising more than 100 cells into nucleus, pancellular, or cytoplasm (n=3) (D) Quantification of YAP localisation in cells cultured in 3D for 1 day. More than 50 cells were categorised into nucleus, pancellular, or cytoplasm (n=3) (E) Proportion of CO7 and HO2 cells positive for ORO after culture in 3D for 1 day (n=3~4).

3.2.3.3 YAP inhibitor decreased lipid droplet formation in 3D

ECM stiffness regulates YAP/TAZ activity and localisation, and YAP/TAZ knockdown induced adipogenic differentiation in MSCs (Dupont et al., 2011). We did observe alteration in YAP localisation between 2D and 3D culture (**Figure 3.13**), although protein level were similar between 2D and 3D, as well as between TED and control cells (**Figure 3.12**). Here we examined if YAP inhibits lipid formation in 3D and expected YAP inhibitor would increase 3D lipid formation. Representative control cell CO7 and TED cell HO2 cultured in 3D were treated with verteporfin, an inhibitor of YAP/TEAD binding (He et al., 2018), and accessed for lipid formation by Day 7. Verteporfin significantly reduced lipid formation in 3D in HO2 cells (**Figure 3.14**).

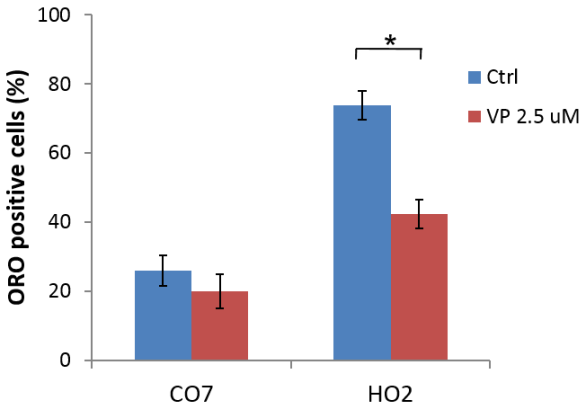

Figure 3.14 YAP inhibitor, verteporfin (VP) at 2.5 μM, decreased spontaneous LD formation in 3D

Proportion of ORO positive cells in control (CO7) and TED (HO2) orbital fibroblasts cultured in 3D with and without YAP inhibitor verteporfin 2.5 μM for 7 days (shown are mean ± SEM, n=3, triplicates, * p<0.05, by t-test)

3.3 Discussion

Extracellular mechanical forces transfer through the cytoskeleton to modulate intracellular signals, and gene expressions are altered to regulate cellular functions including proliferation, migration and differentiation (Daley et al., 2008). The internal forces control cellular behaviour as well through the arrangement of cytoskeleton, and it is known that cytoskeleton disruption and cell rounding promotes adipogenesis (Feng et al., 2010; Fletcher and Mullins, 2010; McBeath et al., 2004), while actin polymerisation is linked to contraction and fibrosis (Van De Water et al., 2013). TED is developed in an environment with increased pressure and is characterised by the presence of both adipogenesis and fibrosis. We studied the involvement of mechanotransduction transcription co-activators, MRTF and YAP, in the adipogenesis and fibrosis phenotypes of orbital fibroblasts. MRTF and YAP are mechano-effectors and regulate adipogenesis and contractility

according to their localisation (Finch-Edmondson and Sudol, 2016; Nobusue et al., 2014). We found that MRTF-A expression and localisation altered in response to matrix, whereas YAP only showed localisation change responding to matrix, and MRTF was involved in contractility of orbital fibroblasts.

3.3.1 MRTF-A localisation and expression are altered in 3D cultures

MRTF is a transcription co-activator on SRF pathway target genes, and itself is an SRF target gene as well (Esnault et al., 2014). MRTF accumulates at the nucleus when G-actin is depleted because of an increase in actin polymerisation, such as in stiff matrix or serum-stimulated, and conversely MRTF exports from nucleus when there is more G-actin (Nobusue et al., 2014; Vartiainen et al., 2007). MRTF-A appeared to behave similarly in orbital fibroblasts: nuclear in stiff plastic and moving out in soft gels. However, there was still a high proportion of cells with nuclear MRTF-A in our 3D gels in which we expected MRTF-A to come out of the nucleus because soft substrate presumably leads to less F-actin in the cells. Different cell lines might have various response to the matrix stiffness. MRTF-A expression in soft matrix was less prominent and less nuclear than stiff matrix but was not completely out of nucleus in a study in human colonic myofibroblasts (Johnson et al., 2014). This may be partly similar to our observation of some MRTF-A retained in nucleus in 3D soft matrix. On the other hand, MRTF gene expression level was shown to be higher in stiff matrix than in soft matrix in human colonic myofibroblasts (Johnson et al., 2014). Presumably, in stiff matrix, there is more nuclear MRTF to activate SRF and thus more MRTF may be expressed as MRTF being one of SRF target genes (Esnault et al., 2014). In orbital fibroblasts, MRTF-A was expressed at significantly lower protein levels in 3D compared to 2D, with the

difference more pronounced in control orbital fibroblasts, consistent with the lower level of nuclear MRTF-A in 3D. But we did not observe different MRTF-A levels between control and TED cells, suggesting MRTF-A of control and TED cells respond similarly to ECM mechanical force.

YAP, similar to MRTF-A, exports from nucleus in response to soft matrix, but is regulated by various pathways including Rho/actin, Hippo, and Wnt signalling (Basu et al., 2003; Dupont et al., 2011; Oka et al., 2008; Piccolo et al., 2014). In Hippo-regulated YAP, soft matrix induces phosphorylation and inactivation of YAP followed by retaining the phospho-YAP in cytoplasm, priming for degradation. YAP in Wnt-off pathway is incorporated in the β-catenin destruction complex and also degraded (**Figure 1.11**). Therefore, YAP protein expression levels are often lower in soft matrix compared to stiff matrix, for example in lung cancer cells, preosteoblasts, or human mammary epithelial cells (Codelia et al., 2014; Yuan et al., 2015; Zhang et al., 2018b). However, YAP protein levels in orbital fibroblasts remained unchanged from 2D to 3D. Interestingly, another type of ocular cells, human trabecular meshwork cells showed higher levels of YAP mRNA and protein on soft matrix compared to stiff matrix (Raghunathan et al., 2013). In addition, YAP/TAZ mRNA levels showed no difference between soft and stiff matrix in three different sourced lung fibroblasts including immortal lung fibroblasts, primary cultured fibroblasts from normal and idiopathic pulmonary fibrosis lungs (Liu et al., 2015). Therefore, it is likely that YAP levels may respond to stiffness variably in different cell types, and fibroblasts in particular may have a different regulation compared to epithelial and cancer cells. Moreover, while some studies showed that soft matrix promoted YAP phosphorylation and resulted in its exclusion from nucleus, YAP also responds to ECM rigidity in a phosphorylation-independent manner (Das et al., 2016). Thus it is also possible that YAP sequestered in cytoplasm without being phosphorylated or degraded in orbital fibroblasts in 3D, so the total YAP protein level was maintained. This is a limitation that we did not study which pathway was more

involved in regulating YAP in our 3D model. Additional studies exploring the upstream of YAP as well as phospho-YAP level may help to answer this question.

3.3.2 MRTF regulates contractility of orbital fibroblasts

Nuclear MRTF and YAP activate MRTF/SRF and YAP/TEAD pathway, respectively, to promote fibrosis (Johnson et al., 2014; Liu et al., 2015; Velasquez et al., 2013), while cytoplasmic MRTF and YAP tend to stimulate adipogenesis (Halder et al., 2012; Nobusue et al., 2014).

Using 3D collagen contraction assay, we showed that MRTF inhibitor CCG-203971 and MRTF-A with MRTF-B silencing reduced matrix contraction. CCG-203971 is thought to inhibit MRTF-A nuclear translocation and SRF responsive expression of CTGF, αSMA and collagen I, although detailed mechanism is not yet clearly known (Haak et al., 2017; Johnson et al., 2014). Since there were still a certain amount of nuclear MRTF-A in orbital fibroblasts in 3D gels, the reduction of nuclear MRTF-A by inhibitor would reduce SRF and its target genes activities, including contractility-related genes such as ACTA2 (αSMA) and CTGF. Inhibition of MRTF/SRF signalling by CCG-1423 (first generation) or CCG-203971 (second generation) has been shown to effectively reduce collagen I, CTGF, and SMA expression *in vitro* in scleroderma dermal fibroblasts (Haak et al., 2014; Shiwen et al., 2015), and in suppressing bleomycin-induced skin thickening and fibrosis in mice model (Haak et al., 2014). In human conjunctival fibroblasts *in vitro*, CCG-203971 decreased collagen gel contraction, CTGF and αSMA expression (Yu-Wai-Man et al., 2017). It is thus likely that MRTF is implicated in the contractile/fibrotic phenotype of orbital fibroblasts through the regulation of cytoskeletal SRF targets.

3.3.3 MRTF in adipogenesis in 3D

In both control and TED orbital fibroblasts, we found that both MRTF-A and YAP displayed nuclear localisation in 2D and moved out of nucleus in response to the soft matrix of 3D, consistent with previous reports (Halder et al., 2012; Huang et al., 2012). According to previous studies, Rho/F-actin/MRTF inhibition, leading to cytoplasmic MRTF, can promote adipocyte differentiation *in vitro* in mouse dedifferentiated fat cells (Nobusue et al., 2014). ROCK and MRTF/SRF inhibition also stimulate brown adipogenesis *in vitro* in a mouse embryo fibroblasts cell line C3H/10T1/2, and MRTF knockout mice showed increase brown adipogenesis in inguinal white adipose tissue (McDonald et al., 2015). Here we observed that CCG-203971 enhanced LD formation in 3D, but the MRTF-A and MRTF-B knockdown did not. CCG-203971 is the second generation MRTF inhibitor, similar to but less toxic than the first generation CCG-1423. Although the detailed mechanism of action is not known, they were demonstrated effective in inhibiting MRTF-A nuclear translocation without altering actin cytoskeleton (Haak et al., 2017; McDonald et al., 2015). Therefore, in our cells cultured in 3D with generally lower level of MRTF-A and partially localised in nucleus, we expected CCG-203971 treatment to increase MRTF-A retention in the cytoplasm, and consequently promote adipogenesis. Moreover, it was reported that the cytoplasmic sequestration of MRTF-A after interacting with G-actin is crucial for adipogenic differentiation. The mutant MRTF-A unbound to G-actin in cytoplasm was unable to induce adipogenesis as the G-actin bound MRTF-A did, although the further detailed mechanism is not known (Nobusue et al., 2014). CCG-203971 increased the amount of MRTF-A in cytoplasm might thus have increased the 3D spontaneous LD formation. On the other hand, the knockdown of MRTFs gene might have reduced the amount of MRTFs in both nucleus and cytoplasm but did not increase the cytoplasmic MRTF bound with G-actin, consequently

MRTFs silencing failed to increase 3D LD formation. It is also possible that CCG-203971 although not toxic at the concentration used in these experiments, it caused ER stress and induced LD formation (Evelyn et al., 2016; Han and Kaufman, 2016).

3.3.4 MRTF in adipogenesis in 2D

Adipogenesis requires less tension from the cytoskeleton, and disrupting the actin cytoskeleton promote adipogenesis (McBeath et al., 2004). Adipogenic induction in 2D cultured mouse dedifferentiated fat cells caused F-actin depolymerisation, and increase of G-actin concentration, accompanied by MRTF-A export from nucleus, resulting in adipogenesis (Nobusue et al., 2014). It was expected that CCG-203971, in conjunction with adipogenic differentiation, would enhance the adipogenesis since it blocks MRTF-A from nuclear accumulation. However, CCG-203971 had little effect on fibroblasts undergoing chemical adipogenesis in 2D, merely decreasing the size of lipid vesicles. This is consistent with previous report showing that first generation MRTF inhibitor CCG-1423 ranging from 1 to 16 μM did not increase lipid positive cells in mice white preadipocytes underwent adipogenic differentiation (Rosenwald et al., 2017). The same CCG-1423 concentration even decreased lipid formation in brown preadipocytes underwent adipogenic differentiation (Rosenwald et al., 2017), although there was evidence of CCG-1423 increasing brown adipogenesis in MSCs (McDonald et al., 2015). The cells used in our study were fibroblasts derived from white adipose tissue. Therefore, the effect of CCG on promoting adipogenesis may be variable among different cell types and may not increase adipogenesis as expected.

Knockdown of MRTF-A was shown to induce lipid formation in the absence of adipogenic differentiation medium in mouse dedifferentiated fat cells and mouse preadipocytes 3T3-L1, upregulating adipogenic

markers effectively in dedifferentiated fat cells (Nobusue et al., 2014). In the presence of brown and white adipogenic differentiation medium, MRTF-A knockdown increased the percentage of lipid-positive cells in brown and white preadipocytes derived from mice brown and white adipose tissue respectively (Rosenwald et al., 2017). Our dual knockdown of MRTF-A and MRTF-B slightly increased areas of LD formation in chemical adipogenesis. However, this increase was only minor compared to the stimulation of adipogenesis triggered by MRTF-A and MRTF-B gene silencing in other models (Nobusue et al., 2014; Rosenwald et al., 2017). It is possible due to different cellular models, as those studies used mouse dedifferentiated fat cells, 3T3-L1 preadipocytes, and immortalised preadipocytes from stromal-vascular fraction of white adipose tissue.

PPARγ is the key transcription factor in both white and brown adipogenesis, and these studies also revealed PPARγ upregulation accompanying lipid formation after MRTF-A silencing (Nobusue et al., 2014; Rosenwald et al., 2017). However, it is not yet well understood how the MRTF-A regulates adipogenesis through PPARγ. Interestingly, Rosenwald et al. demonstrated that MRTF-A interacted with PPARγ in both white and brown adipogenesis using co-immunoprecipitation technique from nuclear extracts, suggesting nuclear MRTF-A interacts directly with PPARγ to inhibit PPARγ activity (Rosenwald et al., 2017). This supports the hypothesis that ablation of nuclear MRTF-A induces PPARγ activation. It is a limitation that we have not studied the PPARγ levels in these CCG treatment and MRTFs knockdown conditions. It would provide more information and better evidence about adipogenesis in MRTF inhibition.

3.3.5 TCFs in 3D adipogenesis

TCFs and MRTFs are the two groups of co-activators controlling SRF, and their bindings to SRF is mutually exclusive (Gualdrini et al., 2016). MEFs from TCFs knockout mice showed upregulation of MRTF and SRF genes, as well as enhanced cytoskeleton and contractility compared to wild type MEFs, indicating MRTF/SRF signalling was upregulated upon knockout TCFs (Gualdrini et al., 2016). We hypothesised that downregulating TCFs would upregulate MRTFs and enhance contractility while reducing adipogenesis. Previous studies have shown that knockdown of Elk1 decreased LDs and adipogenesis markers expression following adipogenic differentiation in 3T3L1 cells (Wang et al., 2009). Elk3 and Elk4 silencing also reduced lipid formation in both white and brown adipogenesis (Rosenwald et al., 2017). However, our 3D spontaneous lipid formation did not decrease in response to TCFs knockdown although there was efficient gene silencing. The related experiments of investigating associated genes in 3D HO6R cells (performed by former master student Leslie Nitsche and undergraduate student Chiyun Lee) showed that TCFs knockdown elevated MRTFs levels but not significant due to wide error bars (**Figure 3.15**A). The MRTF/SRF target genes, ACTA2 and CTGF, were elevated but only ACTA2 reached statistical significance. Therefore, the absence of change in LDs in TCFs knockdown may be due to the insignificant upregulation of MRTFs and MRTF/SRF target genes or because TCFs and MRTFs are not antagonising each other in orbital fibroblasts. Similarly, downregulating TCFs was expected to enhance MRTF/SRF activity and increase contractility, which was not found in our contractility assay. The TCFs knockdown even decreased the contractility in both CO7 (control) and HO6R (TED) orbital fibroblasts (experiments performed by former master student Leslie Nitsche and undergraduate student Chiyun Lee) (**Figure 3.15**B-E). Therefore, we conclude from our data that downregulating TCFs did not significantly upregulate

MRTF/SRF signalling, and thus did not decrease 3D spontaneous LD formation or increase contractility. It is unknown whether this was directly linked to the failure of upregulating MRTFs or TCFs could function independently from MRTFs. In that case, TCFs possibly were not involved in adipogenesis and independently could regulate contractility.

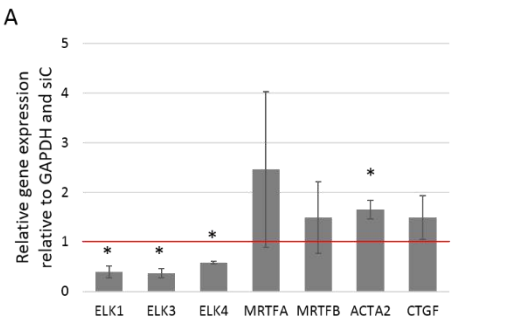

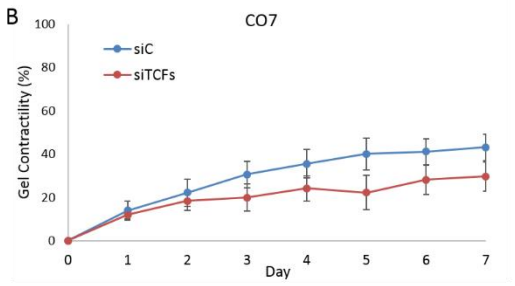

C

Relative gene expression normalised to GAPDH then normalised to siControl	siControl	siELK1+siELK3+siELK4
ELK1	1	0.34 ± 0.24
ELK3	1	0.23 ± 0.09
ELK4	1	0.43 ± 0.32

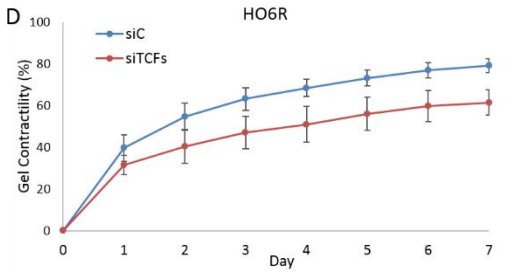

E

Relative gene expression normalised to GAPDH then normalised to siControl	siControl	siELK1+siELK3+siELK4
ELK1	1	0.18 ± 0.05
ELK3	1	0.11 ± 0.03
ELK4	1	0.22 ± 0.06

Figure 3.15 knockdown of TCFs decreased fibroblasts contractility

(A) Gene expression levels of HO6R cells after triple knockdown of TCFs (ELK1, ELK3, ELK4) and then cultured in 3D for 7 days. Shown are mean ± SEM of gene expressions normalised to GAPDH and relative to control siRNA samples (n=4, *p<0.05, t-test) (B, D) Downregulating ELK1+ELK3+ELK4 decreased contractility of CO7 (B) and HO6R (D), though not statistically significant. (CO7 n=3, HO6R n=5) (C, E) ELK1, ELK3, and ELK4 gene knockdown efficiency of the same experiments of Figure B (CO7, C) and D (HO6R, E), quantified by qPCR gene expression assay normalised to GAPDH and then to control siRNA (CO7 n=3, HO6R n=5) (Experiments performed by Leslie Nitsche and Chiyun Lee)

3.3.6 YAP in 3D spontaneous adipogenesis

We observed nuclear YAP in 2D and YAP export from nucleus with a large proportion of cells presenting pancellular YAP in 3D. It is similar to previous reports where YAP was found largely nuclear on stiff substrate, and cytoplasmic on soft (Das et al., 2016; Dupont et al., 2011; Liu et al., 2015). Since the knockdown of YAP/TAZ was reported to induce adipogenesis in MSCs (Dupont et al., 2011), we hypothesised that YAP inhibition would increase LD formation in orbital fibroblasts. However, YAP inhibitor, verteporfin, failed to increase adipogenesis. Verteporfin is thought to block YAP binding to TEAD in nucleus, but it also upregulates 14-3-3σ to retain phospho-YAP in cytoplasm (Wang et al., 2016) and inhibits the YAP/TEAD mediated cell proliferation (Moroishi et al., 2015). Moreover, verteporfin was shown to upregulate PPARγ gene expression in MSCs (Talele et al., 2015), and enhance adipogenesis in SVF of adipose tissue (Zhang et al., 2018a). The verteporfin concentration required to reduce YAP level varied among different cells (Wang et al., 2016). Although we used a concentration similar to most publications, we did not confirm that it altered YAP and phospho-YAP levels, or increased cytoplasmic YAP in our cells. We have not studied the effects of YAP/TAZ knockdown, or downstream of YAP/TEAD signalling either. Most YAP/TEAD target genes (Kim et al., 2017) are anti-adipogenic, such as CTGF (Tan et al., 2008), CYR61 (cysteine-rich protein 61) (Yang et al., 2018), TGFβ2 (Macotela et al., 2012), ADAMTS1 (a disintegrin and metalloproteinase with thrombospondin motifs) (Chen et al., 2016), and PTGS2 (Prostaglandin-Endoperoxide Synthase 2, cyclooxygenase-2, COX2) (Fujimori et al., 2012). However, there are a few showing pro-adipogenic effects, which are SGK1 (serum and glucocorticoid-inducible kinase 1) (Di Pietro et al., 2010), DAB2 (disabled-2) (Tao et al., 2016), and EDN1 (endothelin-1) (Xiong et al., 2001). We do not know if verteporfin in our experiments particularly downregulates the pro-adipogenic genes so as to result in decreasing lipid formation, we are not

able to conclude if YAP is involved in the lipid formation in orbital fibroblasts.

3.3.7 Conclusion

We found that MRTF-A expression level of orbital fibroblasts responded to ECM, but there was no obvious difference between control and TED cells. While the MRTF/SRF pathway appeared to be modulating contractility in orbital fibroblasts, it did not seem to influence lipid vesicles formation. MRTF was not involved in orbital fibroblasts adipogenesis model in either 3D or 2D.

Chapter 4 Adipogenesis and Lipid Droplet Accumulation in 3D *in vitro* TED Model

4.1 Introduction

Adipogenesis has been regarded as one of the pathogenesis of TED because patients with TED show expansion of orbital fat. *In vitro*, orbital fibroblasts derived from patients with TED are able to undergo differentiation towards adipocyte lineage upon chemical stimulation using adipogenic differentiation medium which is composed of insulin, dexamethasone, IBMX, and rosiglitazone (a PPARγ agonist). Classical adipogenesis markers are found elevated after 10 days, and cells from TED respond better to adipogenic stimulation (Kumar et al., 2004). Cells gradually show typical adipocytic features such as rounding up and LD formation after 7-10 days and 40% TED cells display accumulation of LDs after 14 days (Li et al., 2014; Valyasevi et al., 2002). The successfully adipogenic induction indicates that orbital fibroblasts have preadipocyte features, but does not exclude other mechanisms which may also result in fat expansion in TED, since the composition of adipogenic differentiation medium is not a simulation of pathophysiological changes in TED orbits.

Previously in our 3D *in vitro* model, spontaneous LD formation was observed in orbital fibroblasts cultured in collagen matrix with TED cells significantly more efficient in producing vesicles compared to control orbital fibroblasts. In this chapter, I will detail mechanisms by which TED fibroblasts produce more LDs in 3D as opposed to TED cells in 2D and to control orbital fibroblasts in 3D. Lipid metabolism is balanced between formation via fatty acid (FA) uptake or glucose utilisation and lipolysis by lipases. I investigated whether adipogenesis markers, FA uptake

efficiency, FA transporters, glucose transporters, and LD surface proteins, were key determinants in TED orbital fibroblasts making more LDs.

4.2 Results

4.2.1 3D spontaneous formation of LDs is not classical adipogenesis

Orbital fibroblasts cultured in 2D generally produce no or very few LDs (**Figure 4.1** 2D), but clusters of LDs are formed after 7~10 days in the presence of adipocyte differentiation medium (**Figure 4.1** 2D diff.). Following culture in 3D gels, cells in regular medium spontaneously form lipid vesicles, which are smaller than the chemically induced ones in 2D (**Figure 4.1** 3D). Cells in 3D in adipocyte differentiation medium do not present synergistic effects from both phenomena but produce larger LDs compared to 3D spontaneously formed ones, and fewer big LDs compared to 2D chemically differentiated ones (**Figure 4.1** 3D diff.).

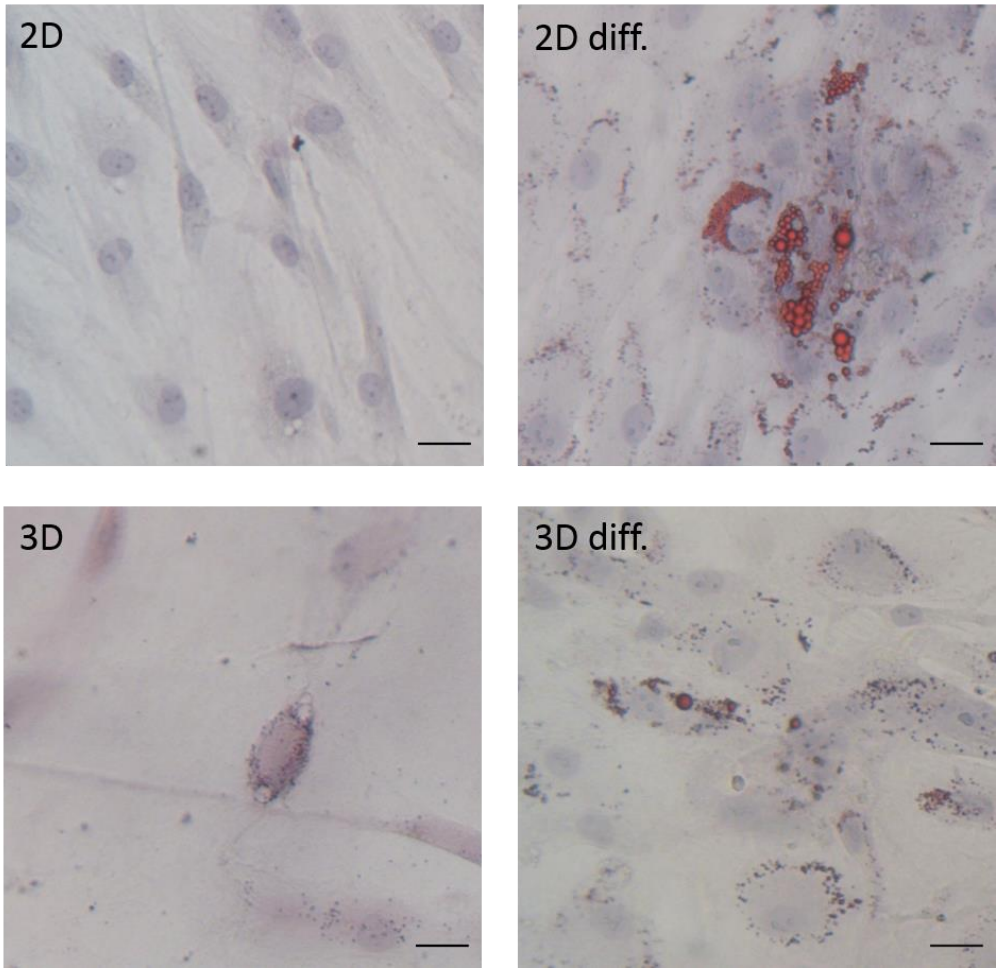

Figure 4.1 ORO staining of orbital fibroblasts cultured in different conditions

ORO staining of representative TED (HO2) cells in 2D in the absence (2D) and presence (2D diff) of adipocyte differentiation medium for 2 weeks after 100% confluency, and in 3D in the absence (3D) and presence (3D diff) of adipocyte differentiation medium for 10 days. Scale bar, 25 μm

The observation of smaller LDs spontaneously formed in 3D suggests that it could be early adipogenesis because large LDs in mature adipocytes are merged from multiple smaller LDs in young adipocyte (**Figure 4.2**).

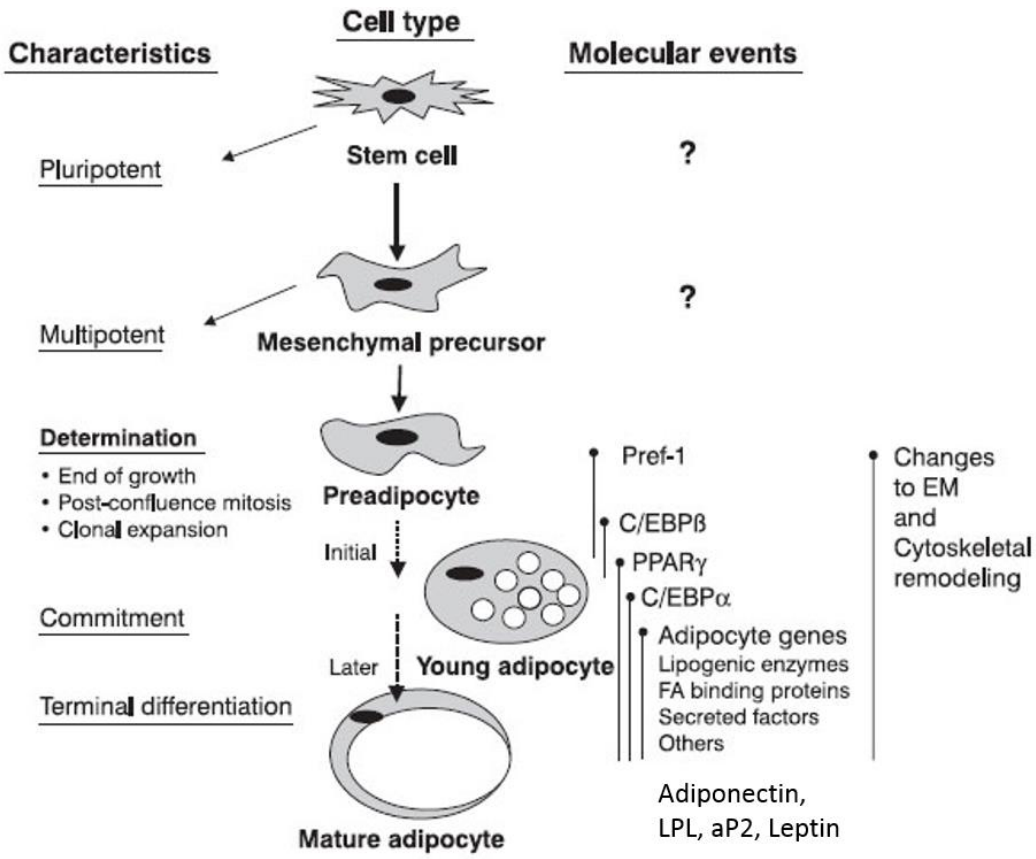

Figure 4.2 Pathway of adipocyte differentiation from stem cell

Classical adipogenesis comprises the determination and commitment of stem cells into preadipocytes with the involvement of early adipogenesis transcription factor—C/EBPβ, and intermediate and main transcription factors of adipogenesis—PPARγ. The following terminal differentiation matures the adipocytes characterised with LDs fusion into a large LD and upregulation of adiponectin, LPL and aP2 genes. Adapted from (Fonseca-Alaniz et al., 2007)

In order to clarify which transcription factors have been triggered in 3D spontaneous LD formation, messenger RNA samples were collected from control (COs: CO4, CO6, CO7) and TED (HOs: HO1, HO2, HO4) cell lines, cultured in 2D and 3D for 7 days. Gene expressions of lipid related markers including adipogenesis transcription factors PPARγ and C/EBPβ, and another transcription factor for lipid metabolism and FA oxidation—PPARα were analysed with real-time PCR. None of these markers showed significant difference in expression between TED and control orbital fibroblasts, or between 2D and 3D culture (**Figure 4.3**). Furthermore, late markers of adipogenesis such as adiponectin and LPL were not detectable in any conditions (data not shown). However, the response upon 3D varied among cell lines especially in PPARγ gene expression (**Figure 4.3**A) where CO4 and HO2 showed PPARγ upregulation while the rest cell lines downregulated PPARγ in 3D.

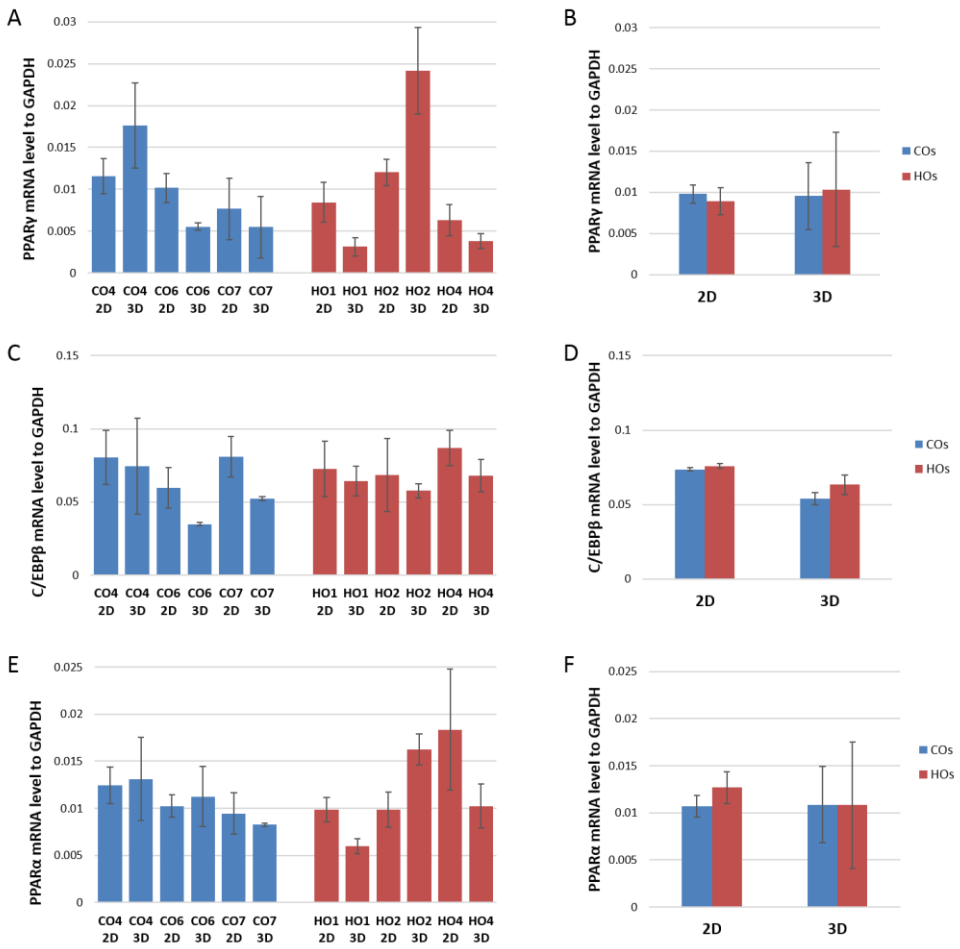

Figure 4.3 Orbital fibroblasts cultured in 3D for 1 week did not alter gene expression levels of PPARγ, C/EBPβ, and PPARα

RNA samples were collected from orbital fibroblasts cultured in 2D and 3D gels for 7 days. Gene expression levels of PPARγ (A,B), C/EBPβ (C,D), and PPARα (E,F) obtained by real-time PCR (qPCR) were normalised to GAPDH. Data of individual cell lines (control: CO4, CO6, CO7; TED: HO1, HO2, HO4) (A,C,E) were grouped and averaged (COs: CO4, CO6, CO7; HOs: HO1, HO2, HO4) (B,D,F) (Shown are mean ± SEM, n≥3).

Orbital fibroblasts spontaneously make LDs in 3D, but they do not display classical features of adipocytes. Also, as late markers of adipogenesis were undetectable in our 3D 7 days-cultured samples, this indicated that what we were observing was possibly still early adipogenesis, and this is consistent with most models of adipogenesis where people observed after 10~14 days of stimulation. To understand if the 3D environment works just as an initial trigger and longer 3D incubations are required for driving adipogenesis to a more mature stage, we monitored LD formation and gene expression in the TED cell line HO2 for 3 weeks in 3D. HO2 is the cell line which showed more prominent PPARγ upregulation in 3D, we expected it to be more prone to mature adipogenesis after longer 3D incubation. Adipogenic chemical differentiation in 2D for 2 weeks and 3D for 10 days were used as a comparison. Morphologically, cells grown in 3D chemical differentiation medium yielded larger LDs than those formed spontaneously in 3D (**Figure 4.1**), this might be due to the effect of adipogenesis inducers. But compared with LDs from 2D chemically differentiated cells, the 3D chemically induced LDs were smaller (**Figure 4.1**), indicating 3D matrix did not work synergistically with chemical differentiation. Gene expression studies showed that PPARγ gene was significantly upregulated after 2 weeks incubation and reached plateau at 3 weeks in 3D (**Figure 4.4**A). C/EBPβ was also slightly increased after 2 weeks (**Figure 4.4**B), while long-term 3D incubation did not significantly alter PPARα (**Figure 4.4**C). Chemical differentiation in either 2D or 3D yielded similar expression levels as long-term 3D in upregulating PPARγ. Although PPARγ expression was significantly higher after longer incubation, the late markers – adiponectin and LPL were still undetectable, whereas chemical differentiation samples in 2D and 3D both expressed detectable levels of adiponectin and LPL, and 3D levels were lower than 2D (**Figure 4.4**D), indicating 3D culture suppressed a full classical adipogenesis. In hindsight, using HO2 for long-term 3D

experiments may not have been representative for TED orbital fibroblasts although it appears to be more prone to PPARγ upregulation.

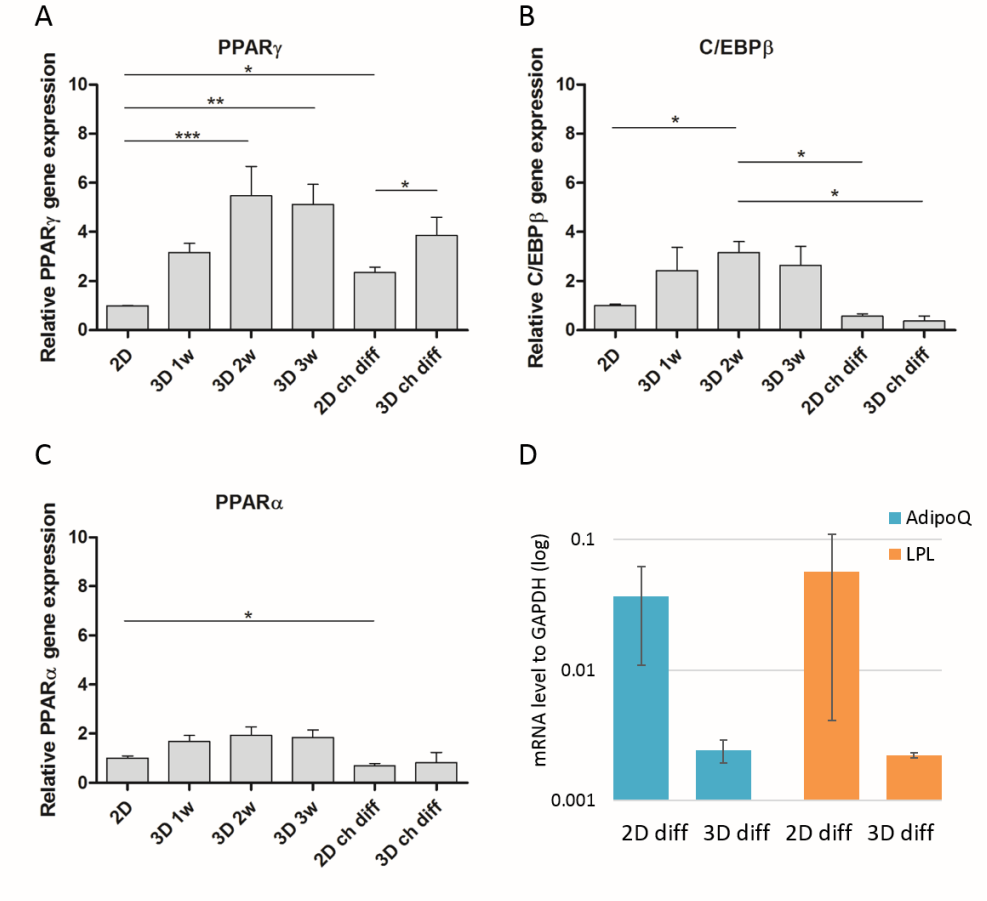

Figure 4.4 Long-term 3D culture rose higher PPARγ gene expression

RNA samples were collected from HO2 cells cultured in 2D, 3D for 1 week (3D 1w), 3D for 2 weeks (3D 2w), 3D for 3 weeks (3D 3w), 2D adipogenic differentiation medium for 2 weeks (2D ch diff), and 3D adipogenic differentiation medium for 10 days (3D ch diff). Gene expression levels of (A) PPARγ (B) C/EBPβ (C) PPARα obtained by real-time PCR (qPCR) were normalised to GAPDH and then referred to the mean 2D. (*p<0.05, **p<0.01, ***p<0.001, by one-way ANOVA and post-hoc.; n=3). (D) Gene expression levels of adiponectin (AdipoQ) and lipoprotein lipase (LPL) in chemical differentiation samples in 2D and 3D were normalised to GAPDH. (shown are mean ± SEM at log scale, 2D n=2, 3D n=3)

Gene expression does not always reflect protein levels, so PPARγ protein expression was also evaluated by Western blotting. In 3D, TED fibroblasts (HOs: HO1, HO2, HO4) expressed higher protein levels of PPARγ compared to control orbital fibroblasts (COs: CO4, CO6, CO7) (**Figure 4.5**A), suggesting that gene expression levels are not a good reflection of protein amount, and PPARγ protein level might be linked to LD formation in 3D. However, treatment with 10 μM of GW9662, an antagonist of PPARγ, did not reduce the ORO positive rates in 3D (**Figure 4.5**B), suggesting that PPARγ is not involved in LD formation in 3D. Overall, this work did not support that 3D LDs are products of classical adipogenesis.

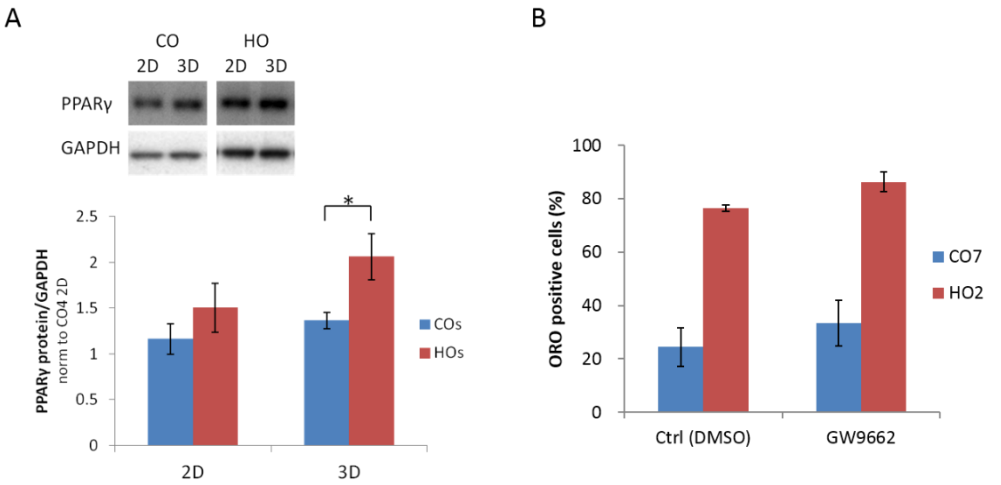

Figure 4.5 TED orbital fibroblasts expressed higher PPARγ protein levels than control orbital fibroblasts in 3D. Inhibiting PPARγ did not decrease the ORO positive cells in neither control nor TED orbital fibroblasts after 7 days culture in 3D.

(A) Top: Representative Western blots for PPARγ in 2D and 3D. Bottom: Quantification of Western blots from PPARγ protein level normalised to GAPDH and normalised to mean CO4 2D. Shown are mean ± SEM, averaged from 3 control cell lines (COs: CO4, CO6, CO7) and 3 TED cell lines (HOs: HO1, HO2, HO4). (*p<0.05, by t-test; n≥3). (B) ORO positive cell rates after 7 days of culture in 3D in the presence or absence of 10 μM of GW9662. (DMSO of equal volume of GW9662 was added to Ctrl wells, CO7 n=3, HO2 n=2)

4.2.2 The 3D spontaneous LD formation primarily originates from fatty acid uptake

4.2.2.1 LD formation in 3D is a fast process

TG is the main lipid component of LDs. In addition to lipid staining, measurement of TG levels and composition is another way to quantify

intracellular lipids. Since the above results revealed that 3D spontaneous LD formation might be different from classical adipogenesis, we investigated whether composition of LDs from 3D differs from LDs in 2D chemical differentiation. First, the total cellular TG levels were quantified by gas chromatography (GC) by our collaborator, Dr. Katherine Pinnick. The orbital fibroblasts cultured in 3D for 14 days for spontaneous LD formation (3D sp) presented much lower levels of TG compared to chemically differentiated cells in either 2D (2D ch) or 3D (3D ch) though not statistically significant (**Figure 4.6**A). There was no difference in TG levels between COs and HOs in any of the three culture conditions (COs: CO7, CO12, CO13; HOs: HO2, HO6R, HO9R). Representative cell lines CO7 and HO6R were picked up because of low and high for LD formation, respectively (**Figure 3.1**). The total TG levels on Day 1 were higher than those on D14 in CO7 and HO6R cells (**Figure 4.6**B). Single cell line data in **Figure 4.6**B showed higher levels of D14 TG of HO6R compared to CO7, but there was no difference between HOs and COs in pooled and averaged cell line data in **Figure 4.6**A because the levels between different cell lines varied. The decrease of TG level on D14 (**Figure 4.6**B) is contrary to classical adipogenesis where longer incubation accumulates more lipids, again indicating that spontaneous LD formation in 3D is not classical adipogenesis.

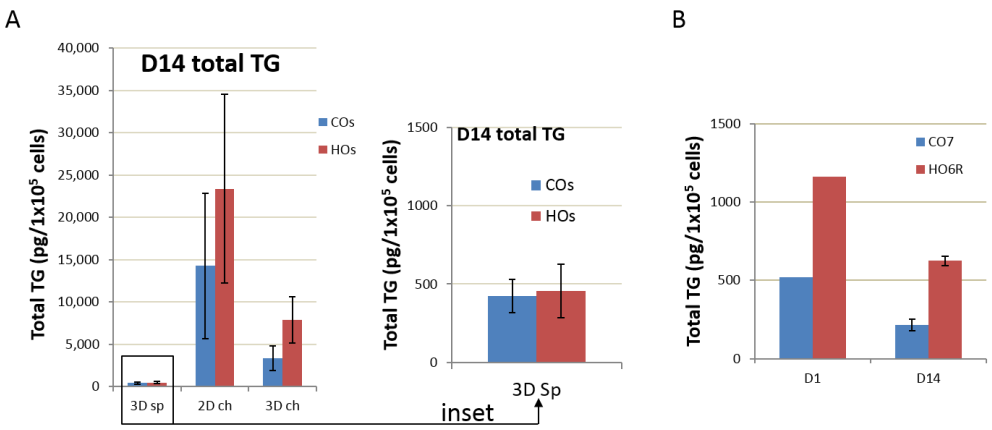

Figure 4.6 Total TG levels analysed by gas chromatography

Total TG levels were analysed by gas chromatography by our collaborator, Dr. Katherine Pinnick. Samples were collected by us. (A) Orbital fibroblasts were cultured in 3D normal 10% FBS DMEM medium (3D sp), 2D adipogenic differentiation medium (2D ch), 3D adipogenic differentiation medium (3D ch) for 14 days. 3 control and 3 TED orbital fibroblast cell lines were used. Magnified 3D sp data as inset is shown at the right. (COs: CO7, CO12, CO13; HOs: HO2, HO6R, HO9R; n=3) (B) CO7 (control) and HO6R (TED) cells were cultured in 3D normal 10% FBS DMEM (as 3D sp) for 1 day (D1) and 14 days (D14) (D1 n=1, D14 n=3)

As the amount of total TG appeared lower after two weeks, we investigated the kinetics of LD formation in 3D using ORO staining. The percentage of cells positively stained for ORO peaked at D1 in both averaged COs (CO3, CO7, CO12, CO13) and HOs (HO2, HO6R, HO8, HO9R) groups. HOs with overall producing more LDs consistently on D1, D4, and D7 (**Figure 4.7**A,B). The ORO positive fraction decreased by 30% from D1 to D7 in both COs and HOs, with the proportion in HOs remaining about 1.4 times higher than in COs on D1 and 1.8 times higher on D7. This suggested that the decrease of ORO might be an environmental effect influencing both COs and HOs. The fraction of cell positive for ORO peaked on Day1, consistent with the TG measurement in **Figure 4.6**B (**Figure 4.7**B). Therefore, short-term kinetics of ORO staining within 24 hours was further examined. HO2, HO6R, and CO7 cells cultured in 3D for 3 hours, 10.5 hours, and 24 hours showed a significant increase in cell positivity for ORO from 10.5h, indicating the 3D LD formation is a rapid response, presumably different from classical adipogenesis (**Figure 4.7**C). However, the fact that it is different between HOs and COs suggests that this reflects a functional dysregulation in lipid metabolism in TED.

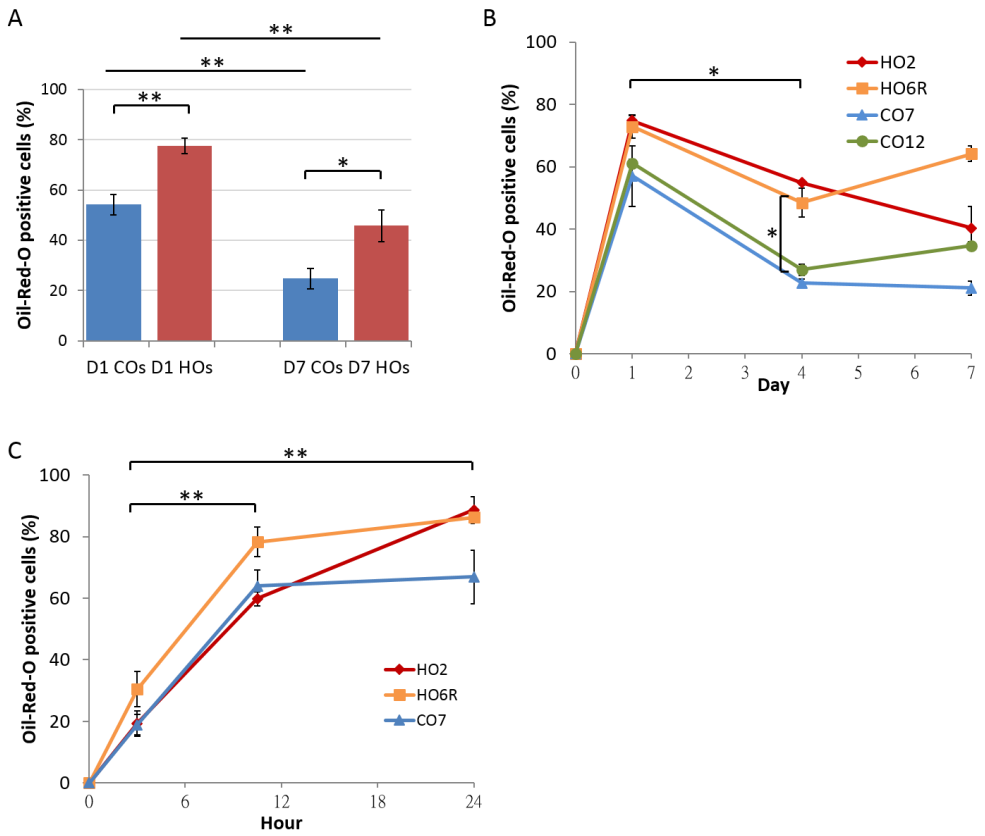

Figure 4.7 Fraction of cells positive for ORO peaked at 24 hours after cultured in 3D.

Orbital fibroblasts were cultured in 3D for different durations before ORO staining. (A) Averaged D1 and D7 ORO positive fractions of 4 control cell lines (COs: CO3, CO7, CO12, CO13) and 4 TED cell lines (HOs: HO2, HO6R, HO8, HO9R). (*p<0.05, **p<0.01, by t-test, n=3-4) (B) The kinetics of proportion of cells positive for ORO in CO7, CO12, HO2, HO6R. There were more ORO positive cells on D1 than on D4 with statistical significance (p=0.029), and also more on D1 than on D7 but with borderline significance (p=0.053). More HOs cells were ORO positive than COs on D4 (p=0.029) (*p<0.05, t-test, n=3-4) (C) The fraction of cells positive for ORO in CO7, HO2, and HO6R increased over time from 3h to 10.5h, and 24h. (3h vs 10.5h, p=0.004; 3h vs 24h, p=0.005; **p<0.01; t-test, n=3)

4.2.2.2 Cells in 3D culture uptake FAs from culture medium

To further understand the difference between 3D spontaneous LD formation and classical adipogenesis, the composition of TG in these LDs was analysed by lipidomics gas chromatography by collaborator, Dr. Katherine Pinnick. Samples were collected on Day 14 from cells grown for 3D spontaneous LD formation, 2D chemical adipogenesis and 3D chemical adipogenesis. FA composition was similar between control (COs: CO7, CO12, CO13) and TED (HOs: HO2, HO6R, HO9R) orbital fibroblasts for chemical stimulation, regardless of whether the cells were in 2D (2D ch) or 3D (3D ch) (**Figure 4.8**A,B). However, FA composition, similar in CO and HO, was significantly different for spontaneous LD formation in 3D (3D sp), suggesting that spontaneous LD formation is a different mechanism. The main difference was seen at the molar percentages of 16:1 n-7 and 18:0 FAs, in which the 16:1 n-7 is lower in “3D sp” samples but higher in chemical differentiation ones, whereas 18:0 is higher in “3D sp” and lower in chemical differentiation ones (**Table 4.1**). However, the FA pattern of TG in spontaneous LD formation was strikingly similar to our experimental control (medium with 10% serum but no cells) (**Figure 4.8**C), suggesting that spontaneous LD formation is linked to uptake of external FAs. Moreover, more groups of long-chain FAs from TED cells showed statistical difference between 3D spontaneously formed LDs and chemical adipogenesis lipids. In TED cells, saturated FAs 16:0 and 18:0 were significantly lower whereas monounsaturated FAs 16:1 n-7 and 18:1 n-7 were higher in chemical differentiated cells than in “3D sp” cells. In control cell groups, only 16:1 n-7 higher and 18:0 lower were shown in “2D ch” sample, the “3D ch” sample presented a proportion level between “3D sp” and “2D ch” but not significant. These indicate that chemical differentiation produced more unsaturated FAs from saturated FAs, and TED cells responded more than control cells.

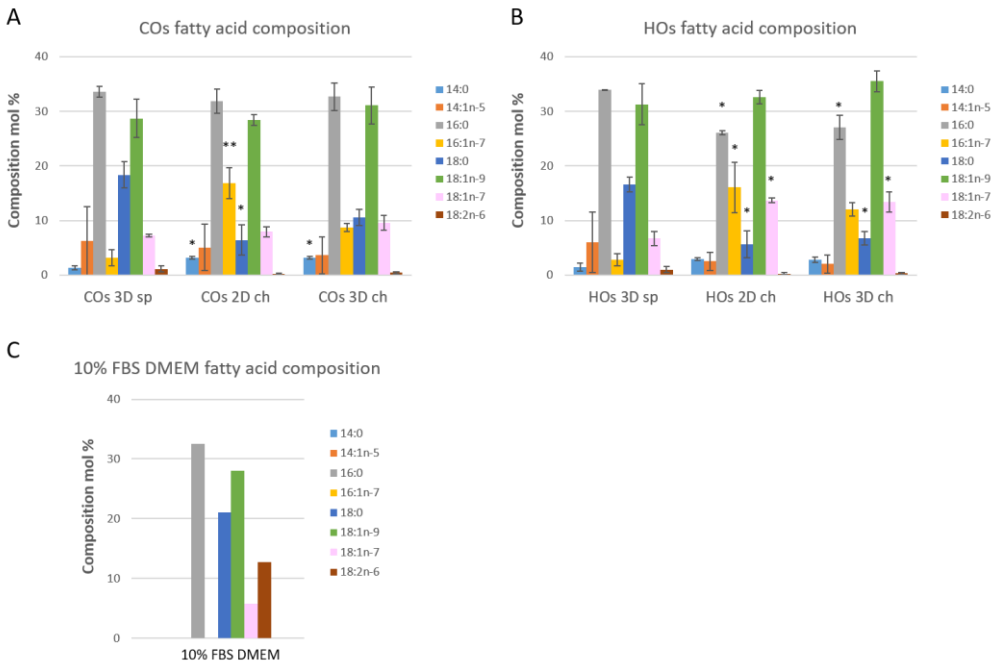

Figure 4.8 Fatty acid compositions of TG.

Fatty acid compositions of TG were analysed by gas chromatography by collaborators, samples were collected by us from orbital fibroblasts cultured for 14 days in 3D in 10% FBS DMEM for spontaneous LD formation (3D sp), in 2D in adipogenic differentiation medium (2D ch), or in 3D in adipogenic differentiation medium (3D ch). (A) The averaged mol% of FA compositions in COs: CO7, CO12, CO13 (each n=3) (B) The averaged mol% of FA compositions in HOs: HO2, HO6R, HO9R (each n=3) (C) The mol% of FA compositions of 10% FBS DMEM, culture medium for "3D sp" samples. (stars above bars meaning statistical significance compared to the same FA group in "3D sp" samples; *p<0.05, **p<0.01, by one-way ANOVA, post-hoc, n=3-4)

Table 4.1 FAs showing most variations with different culture conditions.

Mol% of FA	3D spontaneous	2D chemical	3D chemical
16:1 n-7	3	16	9~12
18:0	17	6	7~10

Molar percentage of 16:1 n-7 and 18:0 showed major difference in three culture conditions (3D sp, 2D ch, 3D ch) in orbital fibroblasts (COs and HOs pooled together)

To validate that orbital fibroblasts uptake FAs from medium which they incorporate into LDs, 200 μM of FAs [oleate 45% (90 μM), palmitate 30% (60 μM), and linoleate 25% (50 μM)] were added to the culture medium. FA concentration in culture medium contributed from FBS is minimal (12.8 μM, measured in **Figure 4.8**C), while physiological free-FA in human plasma is around 200~700 μM (Abdelmagid et al., 2015). LD formation was then analysed after 1 day, when LD formation peaks (**Figure 4.7**). FA supplement led to an increase in the proportion of cells positive for ORO in both control (COs: CO3, CO7, CO13) and TED (HOs: HO2, HO6R, HO9R) orbital fibroblasts although only CO groups showed statistical significance (*p<0.05) (**Figure 4.9**A). The effect was milder in HO cells as they already had a very high proportion of cells positive for ORO in regular medium. The ORO counting method only presents the proportion of cells positive for LDs, but does not reflect the amount of LDs within individual cells. Therefore, we used an AdipoRed assay to quantify total lipid formation. The FA supplement increased the cellular neutral lipids in both COs (CO3, CO7, CO13) and HOs (HO2, HO6R, HO9R) cells, consistent with the ORO staining. The increase was higher for HOs cells (44.28%) compared to COs cells (18.86%) (**Figure 4.9**B), suggesting that HOs present a greater capacity for FA uptake and processing into LDs.

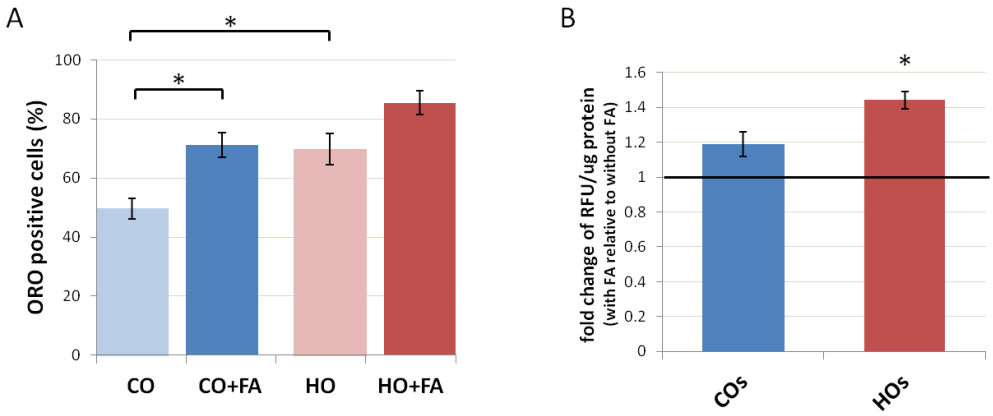

Figure 4.9 Fatty acid supplement increased lipid droplet formation in 3D cultured orbital fibroblasts.

Control orbital fibroblasts (COs: CO3, CO7, CO13) and TED cells (HOs: HO2, HO6R, HO9R) were cultured in 3D for 1 day in the presence or absence of the supplement of FA mixture (oleate, palmitate, and linoleate). (A) Gels were stained with ORO and the proportion of ORO positively stained cells were quantified. (*p<0.05, n=3-5) (B) Gels were digested, pelleted, and stained with AdipoRed before fluorometric analysis. The obtained RFU was normalised to protein level, and with FA supplement data was further referred to the without FA supplement data to obtain the fold change in response to FA supplement. (*p<0.05, n=3-4)

To determine whether the increase ability of HO cells to produce LDs was linked to increase FA uptake capacity, we examined early FA uptake in 3D using a standard FA uptake kit. The FA uptake kit utilises fluorescence labelled dodecanoic acid (a 12-carbon saturated FA) as substrate, and cell membrane-impermeable quenching agent is included in the composition to eliminate extracellular fluorescence. Only cells taking up dodecanoic acid show increased fluorescence intensity, and the measurement of fluorescence intensity therefore reflects the capability of FA uptake. The fluorescence intensity divided by the duration of FA treatment is FA uptake rate. The protocol was designed for cells cultured in 2D and measurement is usually performed directly as

a kinetic of FA accumulation from uptake. However, as our cells were cultured in 3D collagen, fluorescence measurement directly in the plate did not work. We thus modified the protocol to digest gels and lysed cells to get fluorescence intensity, but were not in this way able to assess cumulative kinetic measurements for the same sample. Instead, we measured the FA uptake within a given time window (1 hr) after seeding in 3D for different durations. Based on the kinetics of proportions of cells positive for ORO, orbital fibroblasts were seeded in gels for 0.5h, 2.5h, 6h, and 24h before fluorescent FA dye feeding for 1 hour. The FA uptake was obtained by measuring fluorescent intensities normalised to protein amounts. For example, we treated the cells in gels with FA dye for one hour after they were seeded in 3D for 2 hours, the measurement then reflecting the FA uptake amount between 2~3 hours after seeding in 3D. Data revealed that the FA uptake rate peaked early during 2.5h to 3.5h after 3D culture (**Figure 4.10**). The FA uptake rate change over time was minimal, however, with cells maintaining this FA uptake ability, potentially continuously accumulate FAs for the following 24 hrs. This is likely to contribute to the increase of ORO at 10.5h and peak at 24 hr (**Figure 4.7**C).

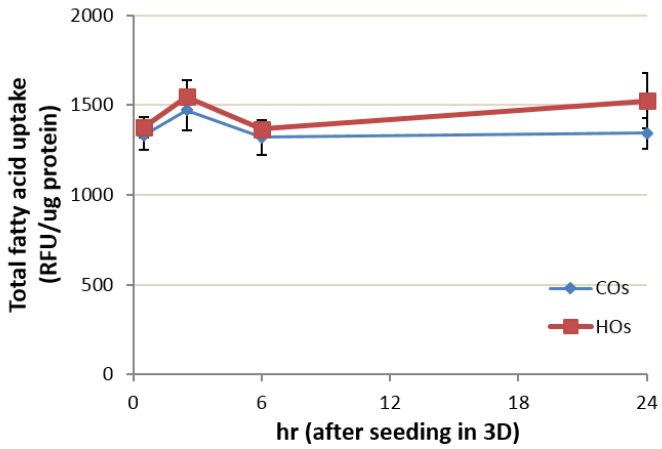

Figure 4.10 Fatty acid uptake ability of COs and HOs are at similar levels.

After 1 hour of fluorescent FA dye feeding in gels cast with orbital fibroblasts 0.5h, 2.5h, 6h, and 24h earlier, gels were digested, pelleted, and resuspended with lysis buffer before fluorometric analysis. The obtained RFU was normalised to protein level. Shown are mean ± SEM of total FA uptake per µg protein within 1 hr (averaged COs: from CO3, CO7, CO12, CO13; averaged HOs: from HO2, HO6R, HO8, HO9R, n=2-4)

4.2.2.3 3D spontaneous lipid droplet accumulation is not regulated by fatty acid transport proteins

To investigate the role of FA uptake in spontaneous LD formation, we examined FA transport proteins expression and knockdown. Gene expressions of the main FA transporters in 2D and early kinetics of 3D were explored in COs (CO3, CO7, CO12, CO13) and HOs (HO2, HO6R, HO8, HO9R). Romani et al. recently reported that cells in 2D produce minimal LDs, but the blockage of Rho/ROCK signalling by inhibitors or matrix softening significantly stimulates LD formation/accumulation in various cell types (Romani et al., 2019). This is consistent with our

observation of spontaneous LD formation in 3D, and thus 2D was used as a baseline comparison here. The authors also revealed the kinetics of upregulation of lipid synthesis related genes at 6 hours and more robust at 24 hours. We examined the gene expression at 0.5h, 6h, and 11h to fit our short-term ORO result (**Figure 4.7**C) and FA uptake rate (**Figure 4.10**) assuming that gene upregulation may precede uptake and LD formation. Orbital fibroblasts expressed all the investigated transmembrane fatty acid transporters, including fatty acid transport proteins 1 (FATP1), fatty acid transport proteins 4 (FATP4), CD36 (also known as fatty acid translocase), caveolin-1 (Cav1), and an intracellular transporter -- fatty acid binding protein 4 (FABP4). Cells expressed low levels of FATP1, and relatively higher levels of FATP4 and Cav1 (**Figure 4.11**). There was no significant difference between COs and HOs in expression of any of these genes, only FATP1 and Cav1 were slightly higher in HO. FATP1 and FATP4 were upregulated in 3D compared to 2D, suggesting that they may be involved in LD formation. Therefore, we next investigated the involvement of these FA transport proteins by inhibitors or knockdown their gene expression.

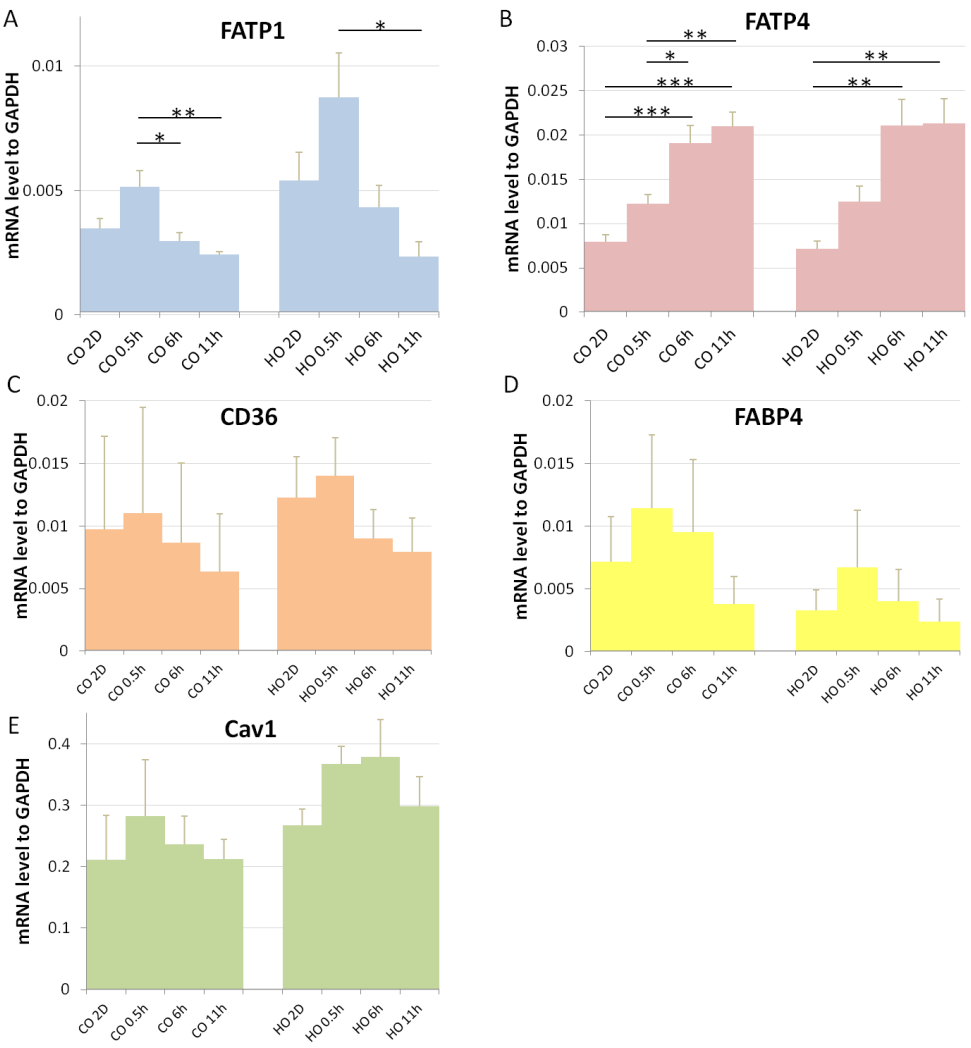

Figure 4.11 Gene expressions of fatty acid transporters

RNA samples were collected from orbital fibroblasts cultured in 2D and 3D gels for 0.5h, 6h, and 11h. Gene expression levels of (A) FATP1 (B) FATP4 (C) CD36 (D) FABP4 (E) Cav1 were obtained by real-time PCR (qPCR). Shown are mean ± SEM mRNA levels normalised to GAPDH, averaged from 4 control cell lines (COs: CO3, CO7, CO12, CO13) and 4 TED cell lines (HOs: HO2, HO6R, HO8, HO9R). (*p<0.05, **p<0.01, ***p<0.001, by t-test; n=3).

To assess the involvement of these FA transporters in 3D spontaneous LD formation, we used inhibitors and siRNAs downregulating FATP1, FATP4, CD36, or Cav1. Individual silencing of FATP1, FATP4, CD36, or Cav1 did not decrease the LDs, despite the knockdowns being efficient (**Figure 4.12**A,D,F). Considering a possible compensatory effect between FATP1 and FATP4, we knocked them down simultaneously. The dual knockdown of FATP1 and FATP4 did not decrease the LDs either (**Figure 4.12**B). However, the knockdown efficiency was not as good as single knockdowns, and this is possibly due to the half dose of siRNA used for each gene. Since the cells still retained 40% of gene expression level for both genes, the residual effect might be enough to preserve LD formation. None of the chemical inhibitors tested decreased the LD formation. The inhibitors tested were CD36 inhibitor (sulfosuccinimidyl oleate 200 μM), caveolin1 inhibitors (methyl-beta cyclodextrin (MBCD) 5 mM and filipin 5 μg/mL), and other endocytosis inhibitors including macropinocytosis inhibitor (amiloride-HCl 0.2 mM) and clathrin-mediated endocytosis inhibitor (dynasore 80 μM) (**Figure 4.12**C,E). Although blocked FA uptake transporters failed to reduce LD formation, we cannot completely rule out a role for uptake because the dual knockdown efficiency was not conclusive. These data suggested that the 3D spontaneous LD formation in orbital fibroblasts is not solely regulated by these FA uptake transporters.

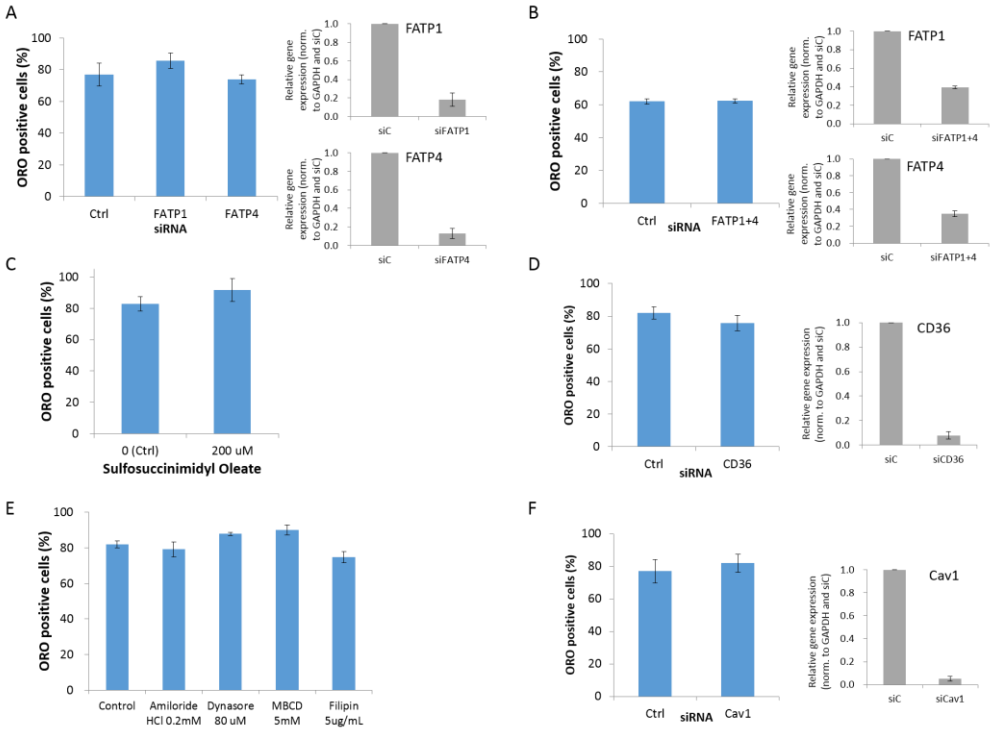

Figure 4.12 Inhibitors or gene silencing targeting for fatty acid transporters did not decrease LD formation.

(A-B) Representative TED orbital fibroblasts, HO6R cells, were transfected with control, FATP1 and FATP4 siRNAs separately (A), or control and the mixture of FATP1 and FATP4 together (B), in 2D for 3 days, and then cells were cultured in 3D gels for 1 day before ORO staining. Shown are mean ± SEM Day 1 fraction of cells positive for ORO. The KD efficiency was expressed as the mean ± SEM relative mRNA expression levels normalised to GAPDH and then normalised to control siRNA sample using qPCR. (n=3) (C) Mean ± SEM fraction of cells positive for ORO from representative TED orbital fibroblasts, HO2 cells, cultured in the absence (without DMSO either) or presence of sulfosuccinimidyl oleate 200 μM for 1 day. (n=3) (D) Fraction of cells positive for ORO of CD36 gene-silenced HO2 cells cultured in 3D for 1 day. The KD efficiency was expressed as the mean ± SEM relative mRNA expression levels normalised to GAPDH and then normalised to control siRNA using qPCR. (n=3) (E) Fraction of cells positive for ORO of HO6R cells cultured in various inhibitors blocking endocytosis for 1 day. (n=3, no DMSO in control sample) (F) Fraction of cells positive for ORO of Caveolin1 gene-silenced HO6R cells

cultured in 3D for 1 day for ORO staining. The KD efficiency was expressed as the mean ± SEM relative mRNA expression levels normalised to GAPDH and then normalised to control siRNA using qPCR. (n=3)

4.2.3 3D spontaneous lipid droplet accumulation does not reflect de novo lipogenesis

In addition to direct FA uptake, cells are capable of converting glucose into FAs in a mechanism known as de novo lipogenesis (DNL) (**Figure 1.18**). DNL has never been reported as mechanism for lipid formation in TED, but thyroid hormone T3, was reported to upregulate DNL in liver (Damiano et al., 2017). As TED is often clinically related to hyperthyroidism, we studied the involvement of DNL in LD formation in orbital fibroblasts. The transmembrane glucose transporter type 1 and type 4 (GLUT1 and GLUT4) are the main glucose transporter on adipocytes, and GLUT1, GLUT3, and GLUT4 were found on human dermal fibroblasts (Longo et al., 1990). We investigated the gene expressions of GLUT1 and GLUT4 in control (COs: CO3, CO7, CO12, CO13) and TED (HOs: HO2, HO6R, HO8, HO9R) orbital fibroblasts in 2D, 3D 0.5h, 3D 6h and 3D 11h. GLUT4 was almost undetectable in these samples (data not shown), whereas GLUT1 was upregulated after 6 hours of 3D culture in both COs and HOs (**Figure 4.13**A). Functional studies were performed in glucose deprivation 3D culture hypothesising that if the cells utilised DNL mechanism to produce LDs, glucose deprivation would lead to a decrease in LD formation. Representative control cell line CO7, and TED cell lines HO2 and HO6R, were cultured in 3D in low glucose DMEM (1000 mg/L glucose, 110 mg/L sodium pyruvate) and normal culture medium (high glucose 4500mg/mL DMEM).

Glucose-free medium was not used because of the concern that lower glucose decreases cell viability and increases apoptosis (Visagie et al., 2015). The low glucose DMEM also contains pyruvate which can be used as substrate for DNL. The proportion of ORO positive cells was consistently decreased in low glucose medium for both CO and HO cells on Day 1, but only moderately and not reaching statistical significance (**Figure 4.13**B). By Day 7, there was no more difference between high and low glucose (**Figure 4.13**C). This suggested that DNL is not involved in spontaneous LD formation, or only plays a minor part. To confirm this, we examined the effect of inhibitors of fatty acid synthase (FAS or FASN), the main enzyme of DNL pathway (**Figure 1.18**). Neither C75 50 μM (FASN inhibitor) nor GSK2194069 1 μM (FASN inhibitor) affected LD formation on Day1 in HO2 cells (**Figure 4.13**D), confirming that DNL is unlikely to be the mechanism accounting for spontaneous LD formation.

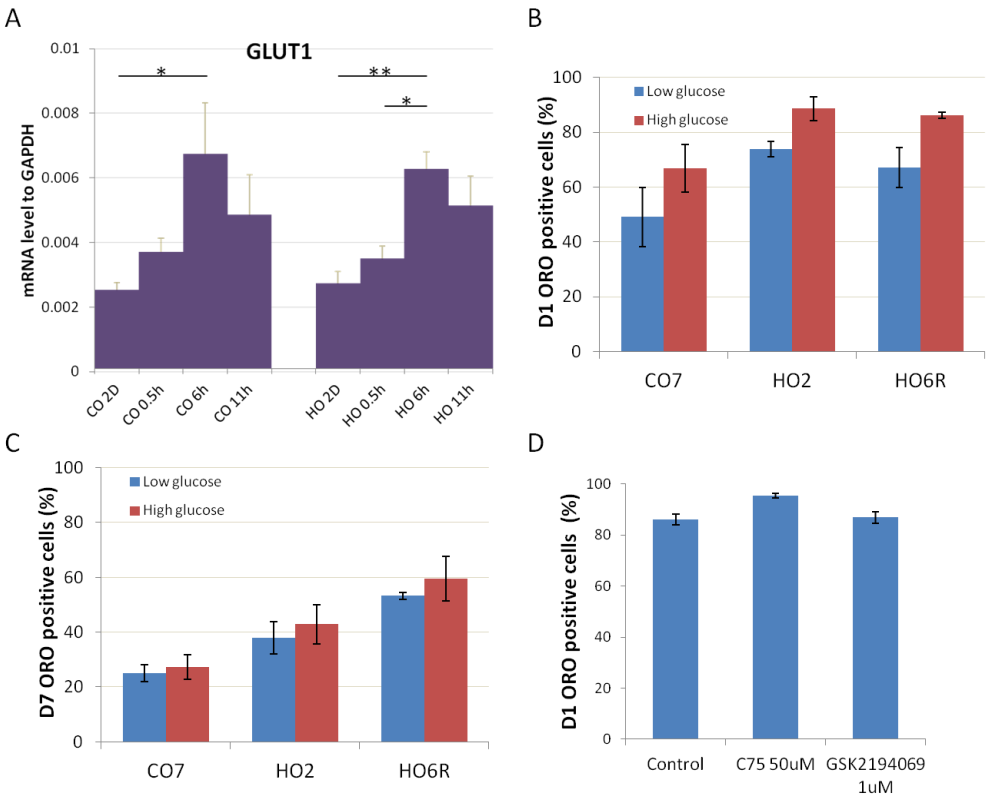

Figure 4.13 De novo lipogenesis (DNL) was not the key determinant for lipid formation in 3D

(A) Gene expression levels of GLUT1 from orbital fibroblasts cultured in 2D and 3D gels for 0.5h, 6h, and 11h by real-time PCR (qPCR). Shown are mean ± SEM mRNA levels normalised to GAPDH, averaged from 4 control cell lines (COs: CO3, CO7, CO12, CO13) and 4 TED cell lines (HOs: HO2, HO6R, HO8, HO9R). (*p<0.05, **p<0.01, by t-test; n=3). (B-C) Fraction of ORO positive cells of CO7, HO2 and HO6R cells cultured in low glucose (1000 mg/L) and high glucose (4500 mg/L) DMEM for 1 day (B) and 7 days (C). (D) Fraction of ORO positive cells of HO2 cells cultured in 3D for 1 day, treated with nothing as control (no DMSO) or FA synthase inhibitors, C75 50 μM and GSK2194069 1 μM. (Shown are mean ± SEM, n=3)

Finally, to exclude the possibility that FA uptake and DNL compensate each other for LD formation, we combined knockdown of FA transporters with glucose deprivation in TED cells. Although the proportion of ORO positive cells was lower in low glucose for all sets, there was no further reduction upon knockdown of the main FA transporters (**Figure 4.14**). This confirmed that neither FA uptake nor DNL is the key determinant in 3D spontaneous LD formation in orbital fibroblasts.

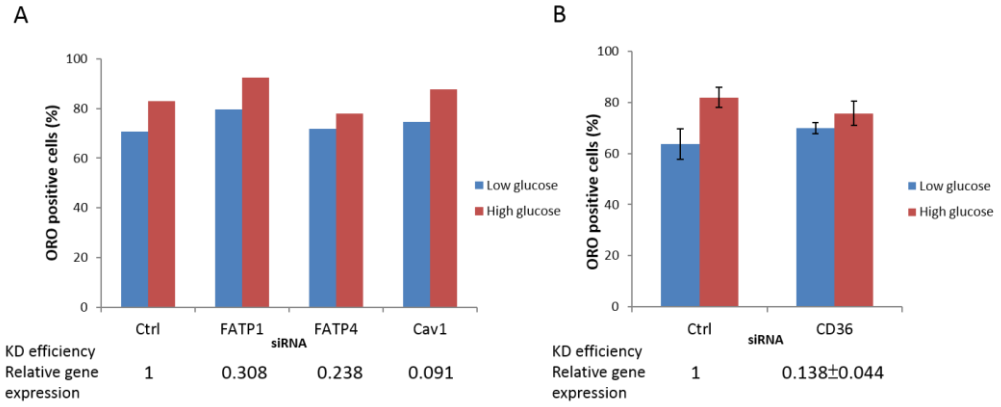

Figure 4.14 Gene silencing of fatty acid transporters in low glucose medium did not decrease lipid formation.

(A) Representative TED orbital fibroblasts, HO6R cells, were transfected with control, FATP1, FATP4, or Cav1 siRNAs. ORO positive cell rates were obtained after 1 day of 3D culture in low glucose and high glucose medium. The KD efficiency was expressed as the relative mRNA expression levels normalised to GAPDH and then normalised to control siRNA sample using qPCR. (shown are mean of triplicates, n=1) (B) Representative TED orbital fibroblasts, HO2 cells, were transfected with control, or CD36 siRNAs. ORO positive cell rates were obtained after 1 day of 3D culture in low glucose and high glucose medium. The KD efficiency was expressed as the mean ± SEM relative mRNA expression levels normalised to GAPDH and then normalised to control siRNA sample using qPCR. (n=2)

4.2.4 Lipid droplet protein - Perilipin 2 is overexpressed in TED orbital fibroblasts

The above results have shown that TED cells make more LDs in 3D compared to controls (**Figure 4.7**A). They may have a slightly higher rate of FA uptake but not high enough to explain the difference in LD accumulation. Since the exploration at the lipid formation aspects have not found a principle cause for LDs, we investigated another aspect of lipid metabolism, lipolysis (**Figure 4.15**). Lipid homeostasis is balanced between formation and degradation, and proteins on the surface of LDs regulate the lipases activities.

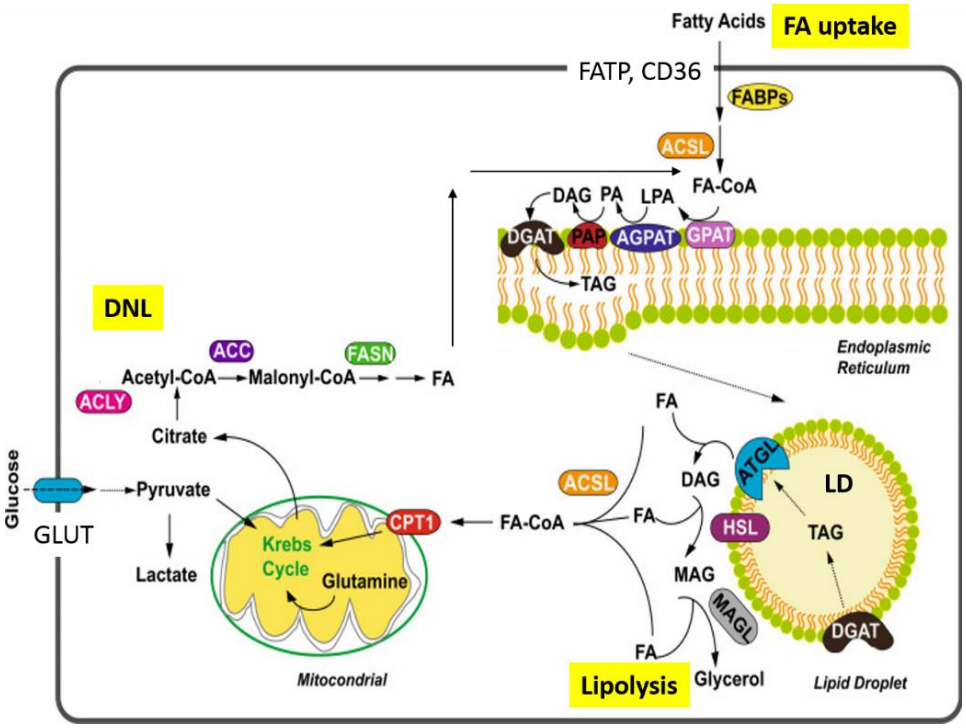

Figure 4.15 Diagram of lipid metabolism

Lipid metabolism is regulated by the formation and degradation of LDs. Intracellular FAs may come from FA uptake (extracellular FA entering cells through FATP or CD36) or DNL (glucose entering cells through GLUT and turned into FA) mechanisms. FAs are processed into TG and formed into LDs at ER. LDs can be hydrolysed by lipases (ATGL, HSL, MAGL). Adapted from (Chen and Li, 2016)

Proteins of the perilipin family are important LD surface proteins, which stabilise LDs by preventing hydrolysis. Therefore, the gene expressions of perilipin 1 (PLIN1) and perilipin 2 (PLIN2, also known as adipophilin or adipocyte differentiation related protein, ADRP) were investigated by qPCR in samples collected from 2D, 3D 0.5h, 3D 6h and 3D 11h from control orbital fibroblasts (COs: CO3, CO7, CO12, CO13) and TED orbital fibroblasts (HOs: HO2, HO6R, HO8, HO9R). PLIN1 levels were very low and without significant patterns (**Figure 4.16**A), whereas PLIN2 was significantly upregulated in HOs in both 2D and 3D 0.5h (p<0.05) (**Figure 4.16**B). Western blots in COs (CO4, CO6, CO7, CO12) and HOs (HO1, HO2, HO4, HO6R) in 2D and 3D (7 days) also consistently showed higher levels in HOs compared to COs (**Figure 4.16**C,D). PLIN2 protein expression was also higher in 3D compared to 2D for both COs and HOs although not reaching statistical significance for HOs (**Figure 4.16**C,D).

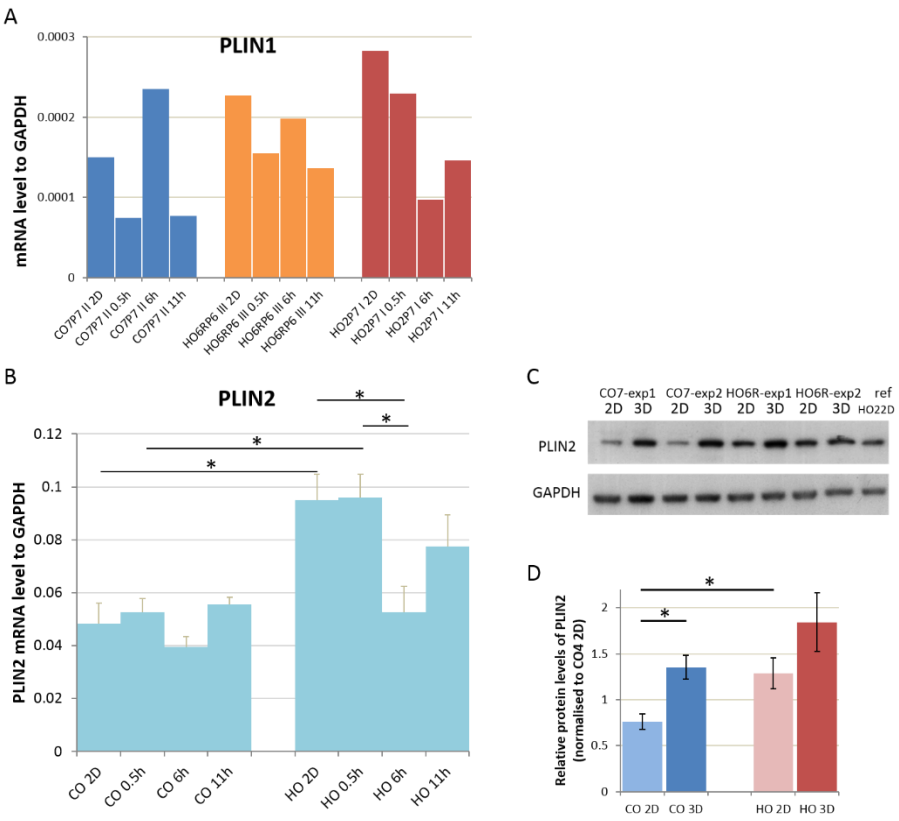

Figure 4.16 Perilipin 2 (PLIN2) levels were higher in HOs than COs.

(A) Gene expression levels of PLIN1 from CO7, HO6R, and HO2 cells cultured in 2D and 3D gels for 0.5h, 6h, and 11h analysed by real-time PCR (qPCR). Shown are mRNA levels normalised to GAPDH (n=1) (B) Gene expression levels of PLIN2 from orbital fibroblasts cultured in 2D and 3D gels for 0.5h, 6h, and 11h analysed by real-time PCR (qPCR). Shown are mean ± SEM mRNA levels normalised to GAPDH, averaged from 4 control cell lines (COs: CO3, CO7, CO12, CO13) and 4 TED cell lines (HOs: HO2, HO6R, HO8, HO9R). (*p<0.05, **p<0.01, by t-test; n=3). (C) Representative Western blots probed with PLIN2 and GAPDH, samples were from CO7 and HO6R in 2D and 3D for 7 days. (D) Quantification results of Western blots from PLIN2 protein level normalised to GAPDH and then normalised to mean CO4 2D level. Shown are mean ± SEM, averaged from 4 control cell lines (COs: CO4, CO6, CO7, CO12) and 4 TED cell lines (HOs: HO1, HO2, HO4, HO6R) in 2D and 3D 7 days. (*p<0.05, by t-test; n=2-4)

To assess whether PLIN2 was localised on LDs in orbital fibroblasts, representative TED cell line HO6R cells were seeded on top of the collagen gels. Immunofluorescence staining of PLIN2 followed by ORO staining was performed 1 day after cells seeded on soft matrix. Spontaneous LD formation was as well observed, and this monolayer of cells facilitated and improved the imaging quality. PLIN2 protein surrounding ORO-stained LDs was demonstrated (**Figure 4.17**).

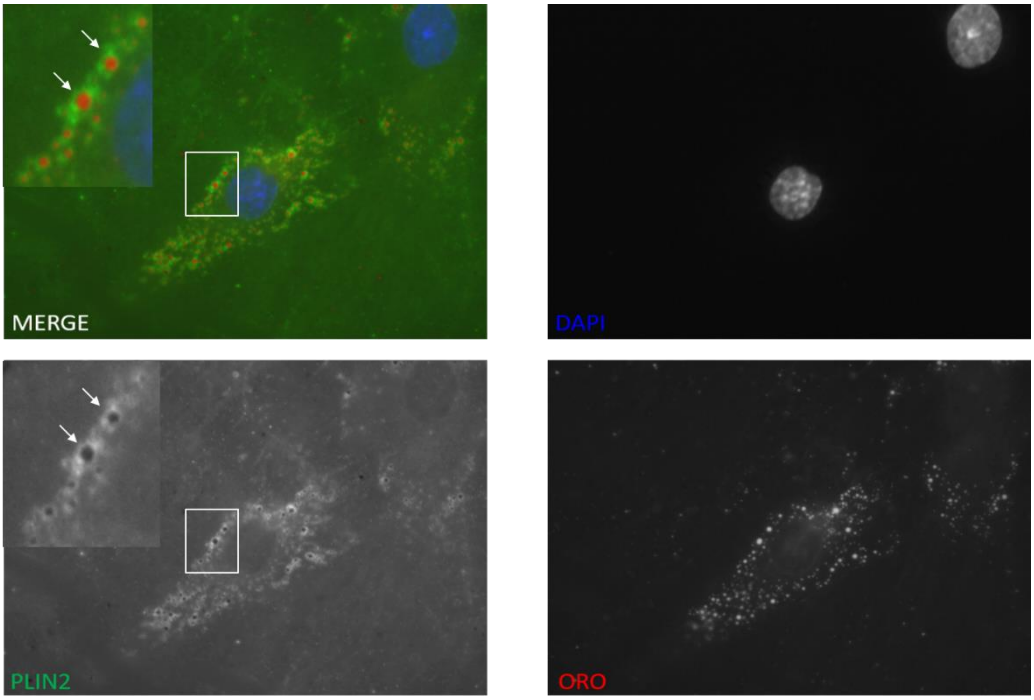

Figure 4.17 PLIN2 and lipid droplets localisation

Representative images were from HO6R cells cultured on top of soft matrix for 1 day followed by immunofluorescence staining for PLIN2 and ORO staining showing PLIN2 encircling around ORO stained LDs (arrows). Images were taken using Zeiss Axioskop2 microscope with 63x 1.4 oil objective. Merge image is from PLIN2 (green), ORO (red), and DAPI (blue).

4.2.5 Downregulating perilipin 2 decreased lipid droplet accumulation in 3D

PLIN2 expression was higher in TED cells and in 3D, suggesting a link to 3D LD formation. We used siRNA to downregulate PLIN2 in a representative TED cell line HO6R cells. ORO staining was done after 7 days of culture in 3D. PLIN2 protein expression was difficult to downregulate, with an average knockdown efficiency of only 30% despite trying multiple conditions (**Figure 4.18**A). However, it significantly decreased LD accumulation (**Figure 4.18**B). This indicates that PLIN2 level regulates 3D LD accumulation in orbital fibroblasts.

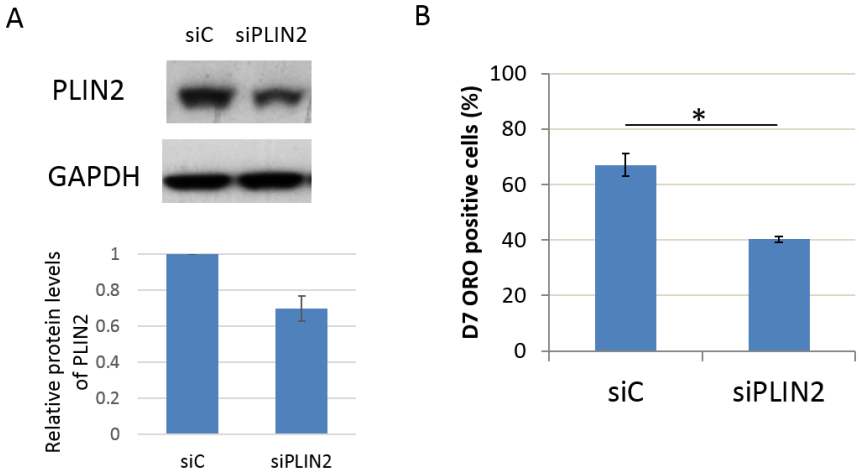

Figure 4.18 PLIN2 gene knockdown decreased ORO positive cells

(A) Representative Western blots and semi-quantification of PLIN2 levels showed the partial reduction of PLIN2 levels after transfection of PLIN2 siRNA in TED cells, HO6R (n=3) (B) Downregulating PLIN2 decreased the Day 7 fraction of HO6R cells positive for ORO by 40% (*p<0.05, t-test, n=3)

4.2.6 Increased perilipin 2 expression is linked to increased lipid droplet accumulation

We showed that PLIN2 is upregulated in TED orbital fibroblasts and in 3D, and the knockdown of PLIN2 decreases LD accumulation. This suggested a direct role for PLIN2 in LD regulation. TED development is initiated with inflammatory reactions and involvement of cytokines. On the other hand, previous studies have shown that a number of cytokines such as LPS, IL-6, IL-1α, and IFN-β lead to PLIN2 upregulation (Gu et al., 2008a). Therefore, we hypothesised that PLIN2 increased levels in TED fibroblasts may be a consequence of inflammation. We treated representative control cell line CO7 with various cytokines including IL-1β 10 ng/mL, IL-6 20 ng/mL, TNFα 10 ng/mL, IFNγ 20 ng/mL, and a mixture of these four together for 3 days in 2D. IL-1β alone and the mix significantly increased PLIN2 protein levels, whereas the others did not affect or mildly decreased PLIN2 level (**Figure 4.19**A). In addition, macrophage-conditioned medium was able to increase PLIN2 level in CO7 cells (**Figure 4.19**B). These suggested that the increased PLIN2 level in TED cells may indeed be the result of the inflammatory phase in TED, and this also gave us an experimental way of increasing PLIN2 levels in cells.

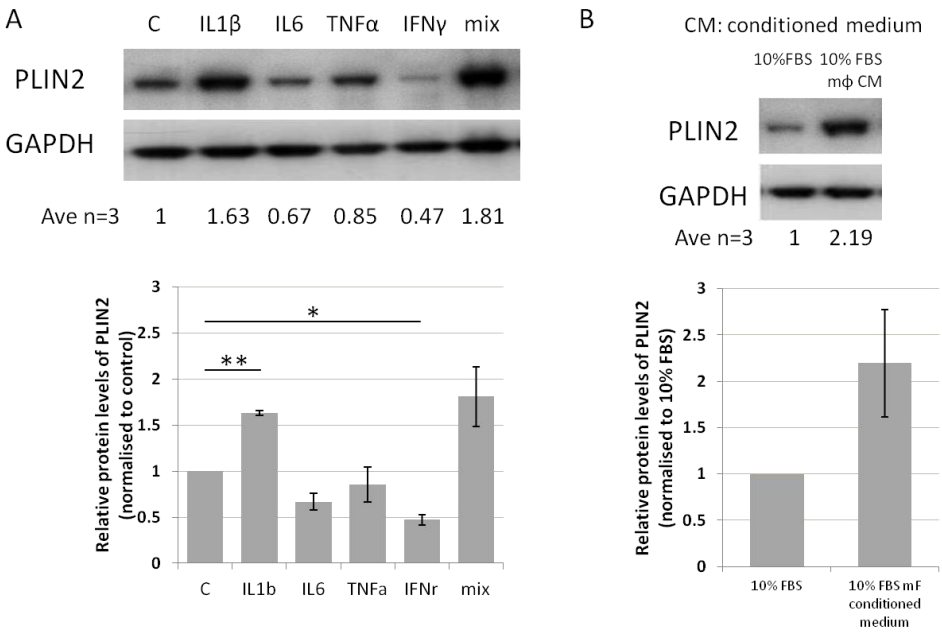

Figure 4.19 Cytokines and macrophage conditioned medium stimulate PLIN2 expression

Representative Western blots and semi-quantification of PLIN2 levels in response to cytokine treatment (A) or macrophage conditioned medium (B) for 3 days in control orbital fibroblast cell line CO7. Shown are mean ± SEM. (**p*<0.05, ***p*<0.01, t-test, n=3)

To further investigate whether an increase in PLIN2 levels is sufficient to increase the ability of fibroblasts to form LDs in 3D, we thus stimulated two control orbital fibroblasts cell lines CO7 and CO12 cells with cytokine mixture for 3 days, and then transferred to 3D culture in 10% FBS DMEM (without continuous cytokine stimulation) for another 7 days before ORO staining was performed. The cytokine mixture led to an increase in PLIN2 protein expression (**Figure 4.20**A) and subsequently increased the proportion of cells positive for ORO in 3D (**Figure 4.20**B). These indicated that PLIN2 may be an important mediator in regulating cytokine-stimulated cells to result in lipid metabolism disequilibrium and lead to the pathogenesis of fat expansion in TED development. When

cytokine stimulation was further given in 3D for 7 days, there were higher rates of cells positive for ORO regardless of previous cytokine treatment in 2D or not (**Figure 4.20**C). This suggested that PLIN2 may be a major contributor of LD formation in TED.

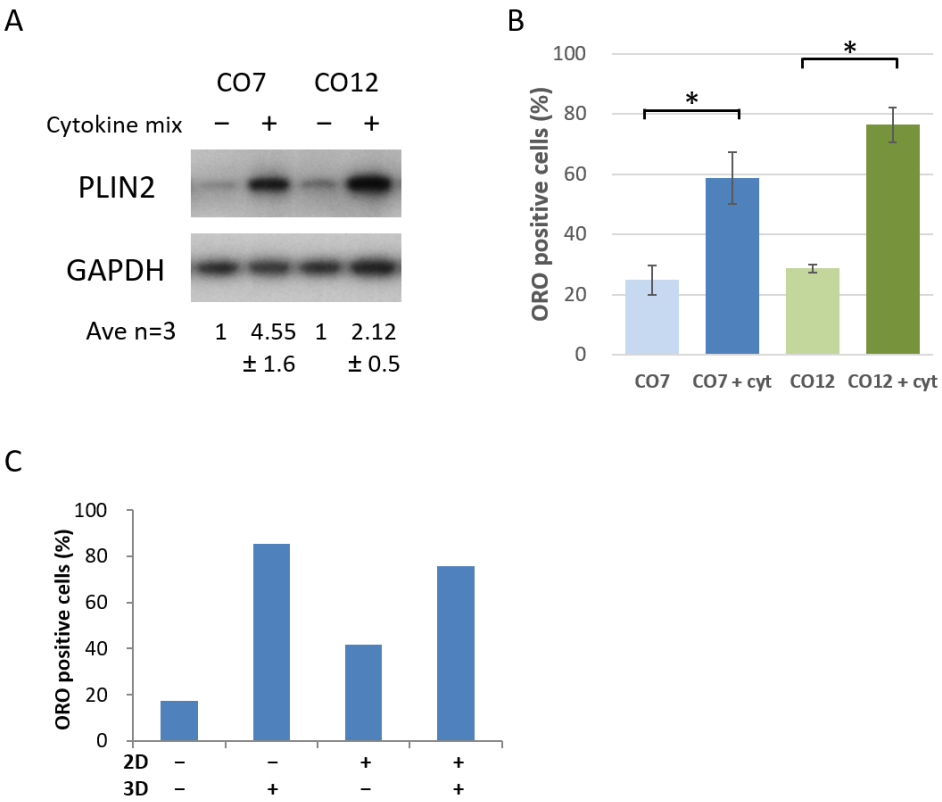

Figure 4.20 Cytokine stimulation increased LD accumulation in 3D

(A) Representative Western blots for PLIN2 levels in response to cytokines treatment in CO7 and CO12 for 3 days in the presence of 10% serum, quantified by normalisation to GAPDH and then to the control without cytokine sample and expressed as mean ± SEM (each n=3) (B) Cytokine-treated CO7 and CO12 cells showed higher proportions of ORO positive cells on Day 7 than those without cytokine treatment. (*p<0.05, t-test, n=3) (C) CO7 cells were cultured in 2D in 10% FBS with or without cytokine mixture for 3 days and followed by 3D culture with or without cytokine treatment for another 7 days before ORO staining. (2D- means no cytokine treatment in 2D, 2D+ means with cytokine treatment in 2D, 3D- means no cytokine treatment in 3D, 3D+ means with cytokine treatment in 3D) (Shown are mean of triplicates, n=1)

4.3 Discussion

Spontaneous LD formation is a key feature of orbital fibroblasts, with TED fibroblasts producing significantly more vesicles than control ones. Because of the literature linking TED and adipogenesis, we initially hypothesised that 3D culture triggered adipogenesis, especially in TED orbital fibroblasts, due to the mechanical cues. Adipogenesis is the differentiation of stem cells or preadipocytes into mature adipocytes which typically present with large unilocular LDs. Adipogenic transcription factors C/EBPβ, C/EBPδ, PPARγ and C/EBPα regulate adipogenesis and stimulate the expression of aP2, adiponectin, LPL and GLUT4. Our work on adipogenesis markers showed that the soft ECM was not sufficient to differentiate orbital fibroblasts into mature adipocytes, indicating that the observed LDs were not produced through classical adipogenesis. On the other hand, LDs can also be considered as organelles, which is a general process in all cells (Qi et al., 2017). The LDs are dynamically regulated through the balance between formation and degradation. We found that orbital fibroblasts uptake FAs to produce more LDs, suggesting that LD formation in 3D is more likely to reflect a general LD accumulation mechanism associated with FA uptake, and is different from adipogenesis. The transport proteins related to increase of intracellular FAs including FATP1, FATP4, CD36, Cav1, FABP4 and GLUT1 did not seem to determine the 3D LD formation in our model. Only the surface protein, PLIN2, was revealed upregulated in TED cells and in 3D (**Figure 4.21**). This is the first time lipid metabolism and LD accumulation were investigated in TED, and the significance of PLIN2 has never been reported in TED studies.

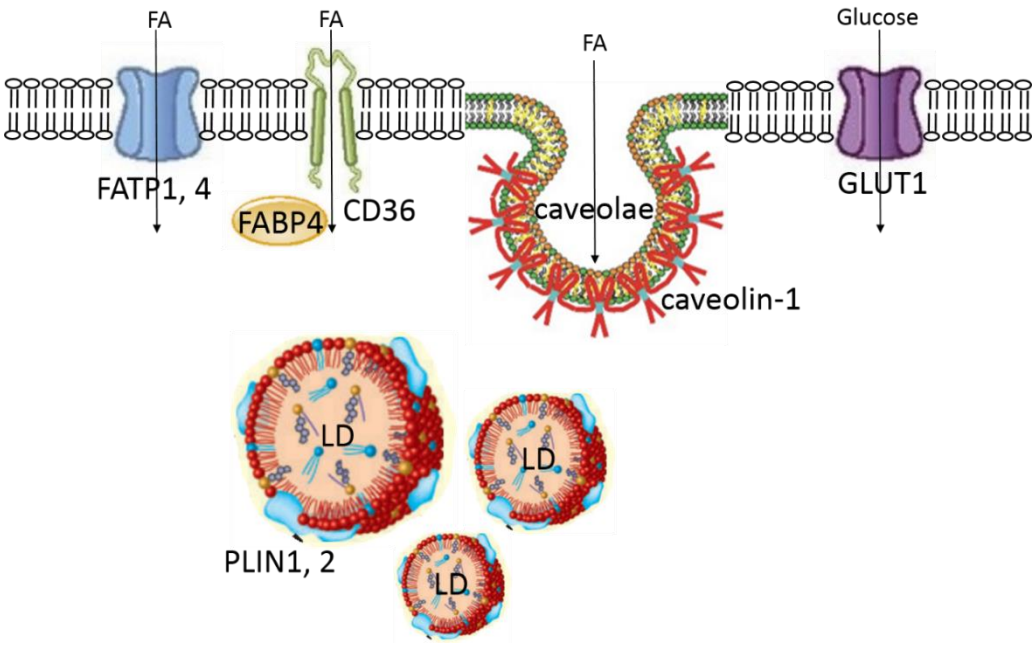

Figure 4.21 Diagram of lipid metabolism related molecules tested.

FA uptake related transport proteins FATP1, FATP4, CD36, FABP4, caveolin-1(cav1), glucose transporter GLUT1, and LDs surface proteins PLIN1 and PLIN2 were studied in this project. Components obtained from (Guo et al., 2009; Hagberg et al., 2013; Palestini et al., 2011; Razani, 2002)

4.3.1 Adipogenesis

We failed to prove our hypothesis that spontaneous LD formation in 3D was derived from adipogenesis. Our 3D cells produced only small LDs, were not rounded up morphologically, and did not show related adipogenesis markers compared to classical chemical adipogenesis cells. Although the importance of soft ECM in differentiation towards adipocyte lineage has been emphasized (Engler et al., 2006; Huebsch et al., 2010), ECM stiffness only contributes to the commitment of preadipocytes step in adipogenesis pathway (**Figure 1.12**). Further adipogenic induction and ligand binding are still required to complete the full adipogenesis (**Figure 1.12**, **Figure 1.13**). This is possibly why we did not get any significant difference in adipogenesis markers between 2D and 3D cells in the

absence of adipogenic differentiation medium (**Figure 4.3**, **Figure 4.5**), and we did not get detectable late markers of adipogenesis either. This indicates that our 3D culture probably is not sufficient to differentiate orbital fibroblasts into mature adipocytes in the absence of adipogenic inducers.

In addition to the necessity of adipogenic inducer, another prerequisite for successful *in vitro* adipogenic differentiation is cell confluency and contact inhibition of preadipocytes before adipogenic induction. When cells are confluent, they stop proliferating and are at the growth arrest G0/G1 in the cell cycle. The addition of adipogenic inducers make cells reenter cell cycle and express C/EBPβ and C/EBPδ to start the adipogenesis cascade (Patel and Lane, 2000). Adipogenic induction on subconfluent preadipocytes did not result in full adipogenesis (Frackelton et al., 2000). Cells grown in 3D often proliferate less, and their cell cycle progression is slowed down (Edmondson et al., 2014; Riedl et al., 2017), which is different from the nonproliferation and cell cycle arrest in 2D confluency.

There are very few reports presenting full adipogenesis derived from pure ECM modification without adipogenic inducers and which can successfully trigger adipogenic transcription factors – C/EBPs and PPARγ, terminal adipogenesis markers, and lipid vesicles formation. Successful adipogenesis induced by soft ECM without any additive chemicals was shown in human white adipose-derived adult stem cells (Young et al., 2013), but detailed mechanisms on how the soft ECM activated the whole adipogenesis process was not mentioned. The above study might be an exception, or the stem cells they used were more sensitive than orbital fibroblasts to adipogenic differentiation. We were not able to replicate this in our system.

We did not detect late adipogenic markers – adiponectin and LPL in any of the samples in the absence of adipogenic inducers despite longer incubation, but both adiponectin and LPL were detectable in cells

cultured in the presence of adipogenic inducers, indicating that adipogenic inducers are essential for full adipogenesis in our cells. When we compared the gene expression levels of adiponectin and LPL between 2D and 3D differentiated samples, 3D levels were consistently lower than 2D differentiated samples for both adiponectin and LPL, although 2D results presented with wide error bar and were repeated only twice (**Figure 4.4**D). This is in line with the LDs aspect under microscope where 3D chemical differentiated LDs were fewer and smaller compared to 2D counterparts (**Figure 4.1**), and is consistent with the total TG measurement on D14 where 3D chemical differentiated cells contained lower TG level compared to 2D ones (**Figure 4.6**A). But this is against the assumption that soft matrix contributes to the preadipocytes commitment, and the addition of adipogenic inducers should have synergistically enhanced the adipogenesis. This may be possibly due to the less confluency of 3D culture to mediate a full adipogenesis as aforementioned, or it is also possible that 3D environment has a mechanism preventing against adipogenesis.

4.3.2 Lipid droplet accumulation

Our work on adipogenesis did not support that 3D LDs are products from classical adipogenesis, and they must be produced from other mechanism. LDs are involved in both “adipogenesis” and “LD accumulation/growth” mechanisms, and these two are distinct mechanisms (Qi et al., 2017). LDs are considered as ubiquitous organelles for lipid storage, and their sizes range from <1 μm small lipid dots in all cells to >2 μm or up to 10 μm giant lipid vesicles in hepatocytes and adipocytes (Walther et al., 2017). Our 3D spontaneously-formed LDs are small ones ranging from <0.15 μm to 2 μm. Although LDs are regarded ubiquitous in all cells, we did not observe much in orbital fibroblasts grown in 2D. Only when orbital fibroblasts were cultured in 3D, LDs were prominently visualised after lipid staining.

This indicated a role for mechanical cues in LD accumulation. Recently, Romani et al. reported that ECM mechanical cues regulate LD accumulation as a general phenomenon in different types of cells (Romani et al., 2019). They demonstrated that LD accumulation increased in response to inhibiting Rho, ROCK, myosin light chain kinase (MLCK) or to soft ECM, whereas in stiff matrix in the absence of inhibitors of Rho, ROCK, or MLCK failed to induce LD accumulation. Their observation is consistent with our findings of the spontaneously LD formation in 3D soft ECM. The morphology and timescales of their LDs are similar to ours as well. They visualised LDs 6h after treating cells with those inhibitors, and the amount of LDs increased and was sustained for 48h. This is comparable to our visualisation of LDs 3.5h after cells seeded in 3D and the peak of LDs at 24h (**Figure 4.7**C). Furthermore, they revealed that mechanical cues-induced LD accumulation is regulated through SREBPs. SREBPs are known to regulate many lipogenic enzymes including acetyl CoA carboxylase, fatty acid synthase (FASN), HMG CoA synthase, HMG CoA reductase, mevalonate kinase, and thus regarded very important in the mechanism of LD formation (Horton et al., 2002). Romani et al. showed that the ECM responsive nuclear SREBP peaked at around 6h and started to fade at 24h. As LDs are dynamic organelles, the degradation of LDs will decrease the overall LDs if the upregulation genes such as SREBP do not last. This may possibly explain our prominent LDs appearance at 10.5h and peak at 24h, and then decrease gradually (**Figure 4.7**C), although we have not investigated if our 3D spontaneous LDs are regulated by SREBPs or any other genes to have a corresponding kinetic pattern.

4.3.3 Lipid droplet accumulation inhibits adipogenesis

From above, we have confirmed that orbital fibroblasts spontaneously produce LDs using a mechanism distinct from adipogenesis. The two pathways may counteract each other (**Figure 4.22**), and this is supported by our results: 1) inhibiting adipogenesis with PPARγ inhibitor increased LD formation (**Figure 4.5**B), and 2) cells cultured in 3D with chemical adipogenic differentiation produced smaller and fewer LDs (**Figure 4.1**), expressed lower levels of late adipogenesis markers (**Figure 4.4**D), contained lower levels of TG (**Figure 4.6**A), compared to cells cultured in 2D with chemical adipogenic differentiation. It is possible that 3D LD formation and adipogenesis antagonise each other, or at least, 3D LD formation antagonises adipogenesis. Such an antagonism between adipogenesis and LD accumulation could be mediated by seipin and phosphatidic acid (PA) (Qi et al., 2017). Seipin is an integral membrane protein in ER regulating lipid metabolism. The seipin gene knockout mice presented enlarged and enhanced LDs in adipocytes, but decreased adipogenesis related gene expression (Liu et al., 2014). The reduction in adipogenesis was attributed to the accumulation of PA in the absence of seipin since PA is a PPARγ antagonist which stabilises the binding of corepressor to PPARγ (Tsukahara et al., 2017). The possible explanation for the increase of LD size in seipin deficiency was adequate PA accumulation to provide enough phospholipids coat for LD growth. We have not explored whether seipin and Lipin-1 are decreased and PA is increased in our 3D soft ECM. But Romani et al. reported that Rho/ROCK/MLCK inhibition led to Lipin-1 decrease (Romani et al., 2019). Therefore, it will be interesting to study the effect of soft ECM on seipin, Lipin-1, PA, and SREBP in orbital fibroblasts using our 3D model.

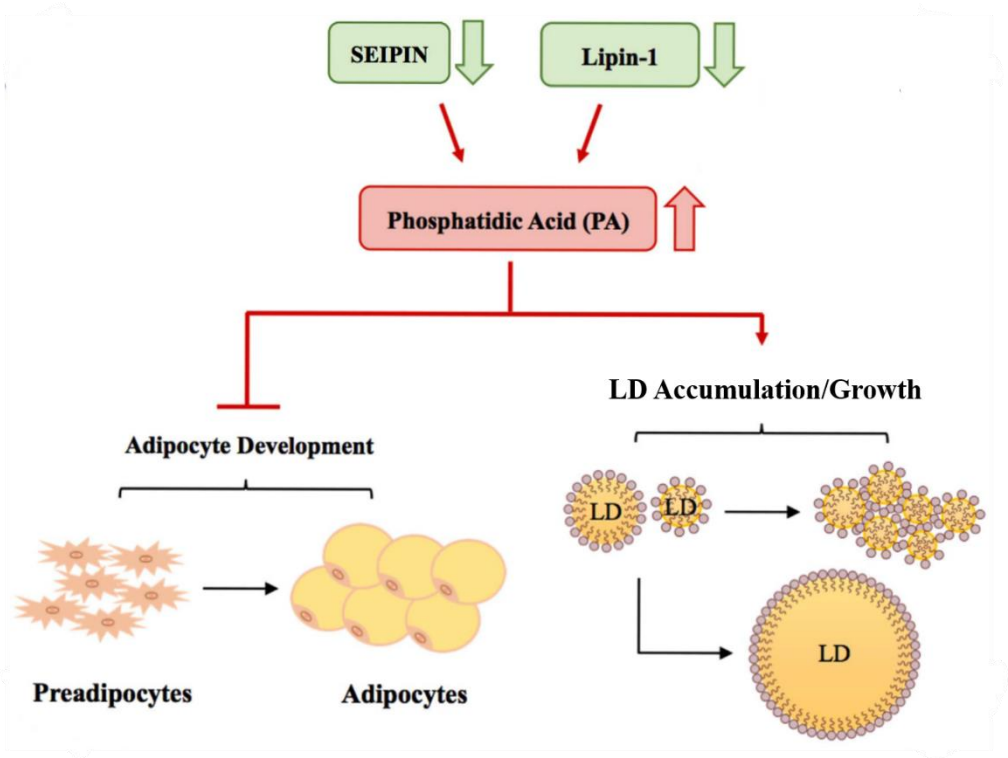

Figure 4.22 Adipogenesis and LD growth are two distinct processes

A loss of seipin or Lipin-1 increases phosphatidic acid (PA) accumulation, which may antagonise PPARγ in differentiating preadipocytes into mature adipocytes. PA level is positively correlated to LD size. PA promotes LD growth while inhibiting adipogenesis. Adapted from (Qi et al., 2017)

4.3.4 Long-chain fatty acids composition of TG

Our TG lipidomics analysis revealed that chemical adipogenic differentiation yielded a different pattern of FAs from those in 3D spontaneous LD formation (**Figure 4.8**). Chemical adipogenic differentiation not only increases cellular lipid contents, but also alters the FAs composition of lipids (Liaw et al., 2016). This is consistent with our observation. It was also reported that lipid profiles from 3T3-L1 undergoing adipogenic differentiation were overlapping but differed from those from *in vivo* WAT in mouse (Liaw et al., 2016). Moreover, in orbital fibroblasts, the TG analysis revealed that FA patterns in 3D chemical

adipogenic differentiation was generally more similar to 2D chemical adipogenic differentiation (**Figure 4.8**), but it was likely in the transition between 2D chemical adipogenic differentiation and 3D spontaneous LD accumulation, which was evidenced in 16:1 n-7 and 18:0 (**Table 4.1**). This is in line with the concept discussed earlier that 3D chemical adipogenic differentiation demonstrated a decreased effect in adipogenesis as cells were also making LDs using the spontaneous LD accumulation mechanism. It is a limitation that we did not have the TED and control orbital fat tissue to compare the lipid profiles, and we are not able to know whether cells cultured in the 3D *in vitro* model present a lipid profile more similar to *in vivo* orbital fat than the classical adipogenic differentiation model.

Lipidomics analysis of FA composition also revealed that chemical differentiated cells produced more unsaturated FAs from saturated FAs, which is more significant in TED cells. According to long-chain FA synthesis pathway, this desaturation requires stearoyl-CoA desaturase 1 (SCD1) (Paton and Ntambi, 2009) (**Figure 1.15**). SCD1 is regulated by the aforementioned SREBP, and related to metabolic syndrome. The SCD1 deficiency results in resistance to obesity, increases insulin sensitivity (ALJohani et al., 2017; Attie et al., 2002; Flowers and Ntambi, 2008). Functionally, unsaturated FAs are important substrates for synthesis of complex lipids. Here TED cells showing more robust response to adipogenic differentiation may be due to upregulated SCD1 gene. And as SCD1 gene is positively linked to obesity, this is in line with the fat expansion phenotype of TED.

4.3.5 Clarifying fatty acid or glucose uptake

We tried to clarify if FA uptake or DNL contributed to LD formation by observing LDs in response to depletion FA transport proteins and

glucose, but we did not find either to be the main determinant for 3D LD accumulation (**Figure 4.12**, **Figure 4.13**B-D, **Figure 4.14**). However, these are not straight-forward approaches, and we evaluated cell response by counting lipid-producing cells which could possibly be formed in any cellular stress condition. The weakness here is that manipulating one factor may cause compensatory effects from other contributors (Umbarawan et al., 2018). This is the reason we did FA transport protein knockdown and glucose deprivation simultaneously in **Figure 4.14**, but it was not straight-forward and not ideal either. Another possible issue is that any manipulation may be a stress to cells and thus LDs are produced. We observed more LDs in 3D cultured orbital fibroblasts in serum-free medium, and there was some evidence of autophagy in serum-free, suggesting a possible link between stress and LDs (data not shown). Therefore, a better way to clarify the contributions of FA uptake or DNL in LD synthesis is by using isotope tracers combined with subsequent mass spectrometry analysis. Cells *in vitro* are fed with isotope labelled carbohydrate substrates, and they incorporate isotope labelled carbohydrate into FAs, together with unlabelled FAs obtained from uptake, to make TG. By further spectrometry, the contributions from DNL (labelled) and uptake (unlabelled) can be quantified (Tumanov et al., 2015). The utilisation of FA or glucose to make TG and LDs varies among different tissues and cell types and is dynamic in response to stimulations like glucose, hypoxia, and excess FAs (Bensaad et al., 2014; Frayn et al., 2006). It is important to be able to clarify the effects from FA uptake or DNL, because different source of FAs may provide divergent functions. For example, in a CD36 knockout cardiac hypertrophy/fibrosis mouse model, glucose uptake surge compensated the FA uptake impairment in cardiac myocytes, and TG level remained unchanged in cardiac tissue. However, the ATP synthesis in CD36 knockout was decreased, suggesting that FAs produced from DNL were not utilised for providing energy (Umbarawan et al., 2018). When TED cells present more LDs than control cells, we do not know if

the proportion of contributions from FA uptake and DNL are conserved or altered. And if it is altered, it will be informative to know whether this alteration is associated with energy utilisation in TED.

4.3.6 PLIN2

We found that TED cells express higher levels of PLIN2 RNA and protein compared to control cells. But when comparing between 2D and 3D, 3D PLIN2 protein levels were higher than 2D in both TED and control, but PLIN2 gene expression in qPCR was not upregulated after shifted to 3D. This may be due to the difference in timescale in which mRNA was collected within 12 hrs of 3D culture in gels while 3D protein samples were from 7 days of incubation. It is also possible that PLIN2 protein in 3D and HOs are translated more efficiently or less degraded. This is consistent with reports showing that PLIN2 unbound to LDs is rapidly degraded by the proteasome (Masuda et al., 2006; Xu et al., 2005), and LDs acting as a post-translational control of PLIN2 protein levels. In such case, if PLIN2 proteins are less degraded in 3D and maintained at higher level, this will also support the positive correlation of PLIN2 level with LDs quantity in 3D (**Figure 4.7**A).

The PLIN2 knockdown efficiency was poor and maximally at just 30% decrease in TED cell line HO6R in various conditions tried (**Figure 4.18**). When we silenced PLIN2 in control cell lines CO7 and CO12, the knockdown efficiency was slightly better at 44% and 64%, respectively (data not shown). But the same silencing of PLIN2 in CO7 and CO12 in the presence of cytokine mixture where PLIN2 was significantly upregulated, the knockdown rate was decreased to 26~39% again (data not shown), suggesting that the higher PLIN2 level cells express, the more difficult it is to knock PLIN2 down. On the other hand, even though the knockdown efficiency was not satisfying in HO6R cells, partial silencing still reduced the LD accumulation (**Figure 4.18**). Therefore, the

LDs are closely related with PLIN2 level, but we have not investigated how they are linked yet.

Furthermore, we have found that IL-1β upregulated PLIN2 expression and promoted LD accumulation in our control orbital fibroblasts (**Figure 4.19, Figure 4.20**). In previous studies, inflammatory molecules LPS, IL-6, IL-1α, and IFN-β were shown to increase PLIN2 expression (Gu et al., 2008b; Ohhira et al., 2007), although lipid accumulation was not investigated. In addition, IL-1β and TNF-α were reported to enhance the intracellular TG and cholesterol accumulation in lipid-loaded macrophages to promote foam cell formation, and were found to suppress lipid turnover and efflux in macrophages (Persson et al., 2008). Since LD accumulation is associated with PLIN2 (Motomura et al., 2006; Straub et al., 2008), possibly IL-1β upregulates PLIN2 and then reduces lipid turnover to cause LD accumulation.

There are two possible mechanisms linking PLIN2 to LDs, and they have not been thoroughly clarified yet. One is that LDs are produced first and followed by more PLIN2 being preserved, and this is supported by evidence of degradation of unbound PLIN2 (Masuda et al., 2006; Xu et al., 2005). The other is PLIN2 being upregulated first and then more LDs being sequestered. This is based on the mechanism of PLIN2 preventing lipolysis (Listenberger et al., 2007; Sapiro et al., 2009). We do not know how PLIN2 and LDs are correlated with each other in 2D and 3D, and in control and TED cells. Future work will be needed to investigate the role of PLIN2 in LD accumulation in orbital fibroblasts in: (1) proteasome degradation of PLIN2, (2) lipolysis, and (3) ATGL, HSL association with PLIN2 and LDs (**Figure 4.23**).

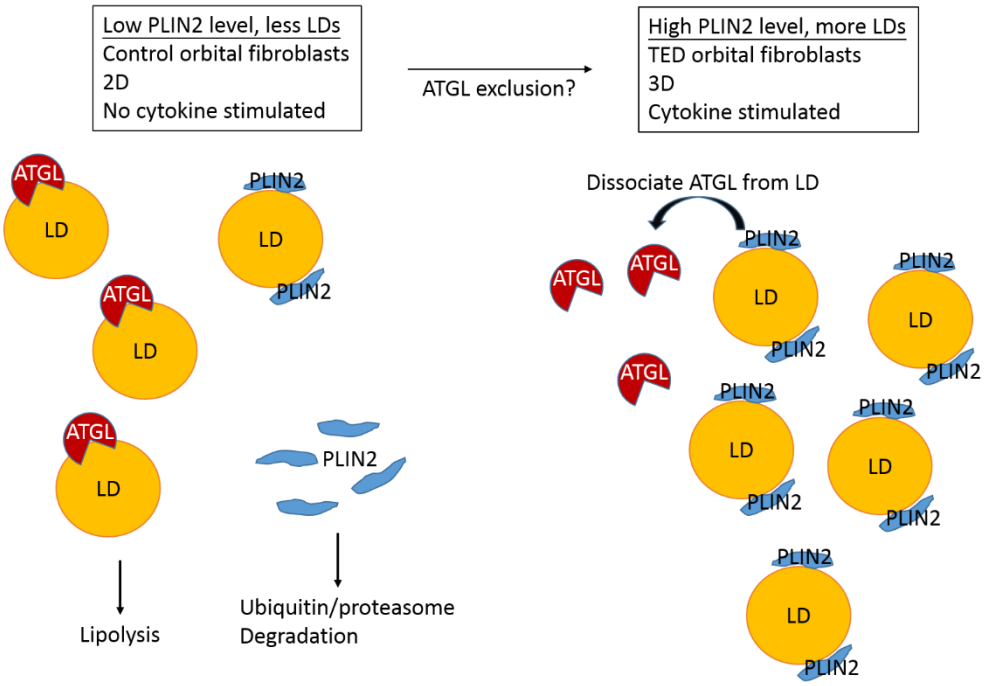

Figure 4.23 Proposed model for PLIN2 and LD accumulation in orbital fibroblasts.

Left: When PLIN2 and LDs levels are low (possibly in control orbital fibroblasts, 2D, or no cytokine stimulated conditions), unbound PLIN2 are degraded by ubiquitin/proteasome pathway, and ATGL can access LDs and hydrolyse LDs. Right: When PLIN2 and LDs levels are high (possibly in TED orbital fibroblasts, 3D, or cytokine stimulated conditions), PLIN2 dissociates ATGL from LDs and thus prevents lipolysis.

4.3.7 Conclusion

We clarified that the more prominent spontaneous LDs in 3D culture in TED orbital fibroblasts is not from classical adipogenesis. These LDs are products from FA uptake in lipid metabolism. While TED and control fibroblasts showed similarity in FA uptake, PLIN2, a surface protein on LDs, was expressed at significant higher levels in TED cells than control ones. PLIN2 expression could be enhanced by cytokine stimulation and

followed by LDs increase, simulating the inflammatory reactions resulting in fat expansion in TED. The decrease of PLIN2 expression was found to reduce LDs, therefore PLIN2 may represent a new marker of TED progression.

Chapter 5 Macrophage involvement in TED

5.1 Introduction

Macrophages are involved in immune reactions in phagocytosis and secretion of cytokines, and they interact with T cells by presenting antigens to T cells and being activated by T cells. TED is an autoimmune disease mainly initiated by T cell reactions, and macrophage involvement in TED was reported in IHC studies (Chen et al., 2008; Pawlowski et al., 2014), but detailed mechanisms have not been revealed. In obesity model, macrophages have been complicated in adipogenesis and fibrosis (Martinez-Santibanez and Lumeng, 2014), with features comparable to TED pathogenesis. CD11c+ M1 subtype macrophages inhibit adipogenesis and promote inflammation and fibrosis, whereas CD11c- M2 macrophages promote adipogenesis (Lumeng et al., 2008; Martinez-Santibanez and Lumeng, 2014). Therefore, we hypothesised that macrophages might play a role in orbital fat of TED similar to that in obesity model with respect to adipogenesis and fibrosis. We co-cultured macrophages with TED or control orbital fibroblasts *in vitro* in 3D (Kechagia et al., 2016; Li et al., 2014), and examined lipid formation, HA production and fibrosis via ORO staining, HA ELISA and contraction assay, respectively. We further explored the possible downstream pathways involved in the macrophage-related lipid formation, HA secretion and fibrosis.

5.2 Results

5.2.1 Macrophages do not affect spontaneous lipid formation in 3D orbital fibroblasts

In order to understand if macrophages promote lipid formation in orbital fibroblasts, the 3D culture system was used to study the interaction between macrophages and orbital fibroblasts after mixing orbital fibroblasts with macrophages as a co-culture. TED orbital fibroblasts (HOs: HO1, HO2, HO4, HO6R) and control orbital fibroblasts (COs: CO4, CO5, CO6, CO7) were co-cultured with monocyte-derived human macrophages (U937 line) at a 1:1 ratio for 7 days before ORO staining. Macrophages did not alter the ability of orbital fibroblasts to produce LDs (**Figure 5.1**A, B), although there was a trend for an increase in ORO positivity in the two control orbital fibroblast lines (CO4 and CO7) with low levels of LDs. Further increasing macrophage proportion in the co-culture up to five times more had a moderate effect, but without a statistically significant increase in LD formation (**Figure 5.1**C). This suggested that macrophages do not significantly modulate spontaneous LD formation in orbital fibroblasts in 3D.

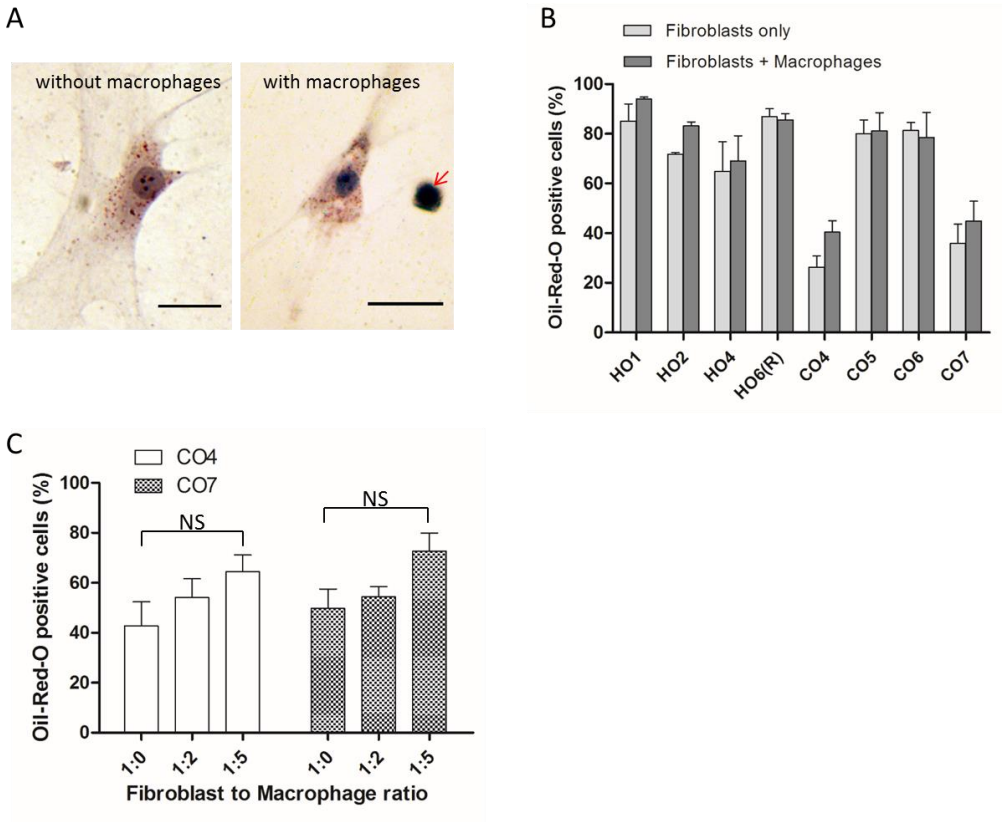

Figure 5.1 Macrophages do not significantly alter spontaneous lipid droplet formation in 3D-cultured orbital fibroblasts.

(A) Representative Oil-Red-O (ORO) staining of lipid-containing vesicles in orbital fibroblasts in 3D culture for 7 days: HO2 without macrophages (left) and CO6 with macrophages (right, arrow), at a 1:1 fibroblast:macrophage ratio. (scale bar, 25 μm) (B) Macrophages did not alter spontaneous LD formation in 3D culture. TED (HOs) or control (COs) fibroblasts ($0.74x10^5$ cells/mL) were cultured with macrophages ($0.74x10^5$ cells/mL) at a 1:1 fibroblast:macrophage ratio in the presence of 10% serum for 7 days. The fraction of ORO positive cells is shown as mean ± SEM. (n=3, no statistical difference between with and without macrophages) (C) ORO positive cells in control fibroblast lines, CO4 and CO7, did not significantly increase as the number of macrophages increased to $1.5x10^5$ cells/mL or $3.7x10^5$ cells/mL. (mean ± SEM; n=4, p=0.2162 (CO4) and p=0.0773 (CO7), one-way ANOVA)

5.2.2 Macrophages stimulate hyaluronic acid (HA) production in orbital fibroblasts

HA release in both 3D gels and medium was assessed using an ELISA assay. Four control (COs: CO4, CO5, CO6, CO7) and four TED (HOs: HO1, HO2, HO4, HO6(R)) fibroblast lines were cultured with/without macrophages at various ratios in 3D collagen gels in serum-free medium (as high HA levels are present in serum; data not shown). In the absence of macrophages, TED orbital fibroblasts secreted significantly higher levels of HA compared to control orbital fibroblasts, consistent with previous reports using cells cultured as 2D monolayers (Smith and Hoa, 2004). Co-culturing orbital fibroblasts with macrophages at 1:2 and 1:5 ratio significantly increased HA production in both control and TED fibroblasts, with higher HA levels for TED orbital fibroblasts (**Figure 5.2**A). IGF-1 working through IGF-1R on orbital fibroblasts has classically been reported to activate HA secretion (Krieger et al., 2015; Smith and Hoa, 2004). To determine whether macrophages stimulate HA production through IGF-1, a representative TED cell line, HO2, was co-cultured with macrophages at 1:2 fibroblast:macrophage ratio in the presence of IGF-1R blocking antibody. Inhibiting IGF-1R signalling did not affect macrophage-induced HA secretion, although as expected, it reduced IGF-1-mediated HA production in fibroblasts alone (**Figure 5.2**B) (Krieger et al., 2016; Smith and Hoa, 2004). This suggested that macrophages can stimulate HA production in orbital fibroblasts independently of IGF-1R signalling.

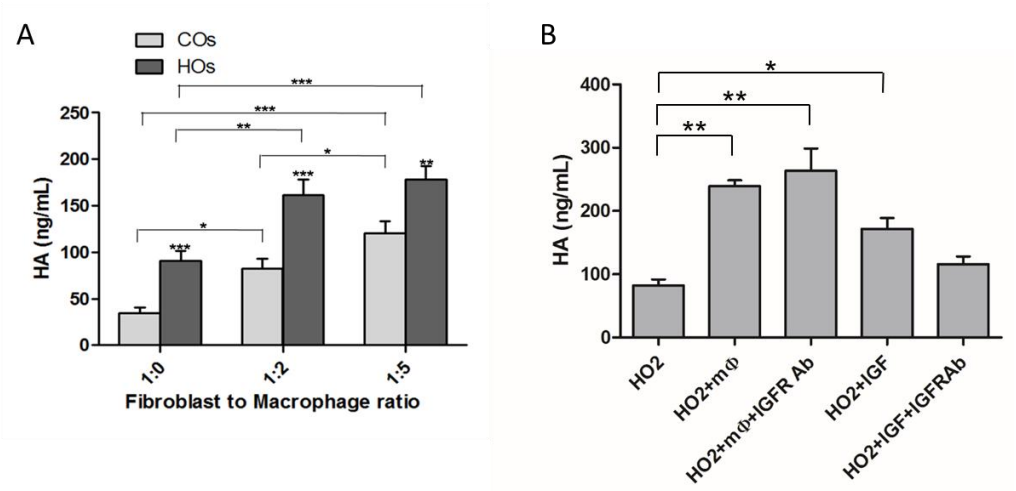

Figure 5.2 Macrophages stimulate hyaluronic acid (HA) production by orbital fibroblasts.

(A) Control (COs) and TED-derived (HOs) orbital fibroblasts were co-cultured in collagen gels in serum-free medium with macrophages at different ratios (fibroblasts $0.74x10^5$ cells/mL; macrophages $1.5x10^5$ cells/mL or $3.7x10^5$ cells/mL) and HA levels were measured from pooled medium and gel digest after 3 days (mean ± SEM; COs: CO4, CO5, CO6, CO7; HOs: HO1, HO2, HO4, HO6(R); 3~4 independent experiments each) (*p<0.05, **p<0.01, ***p<0.001, one-way ANOVA. Stars directly above HOs bars indicate the comparison between COs and HOs in that fibroblast:macrophage ratio group, t-test) (B) HO2 cells ($0.74x10^5$ cells/mL) were cultured with macrophages at 1:2 ratio (macrophages $1.5x10^5$ cells/mL) or in the presence of 20 μM IGF-1. IGF1 signalling was tested by adding IGF-1R blocking antibody 5 μg/mL in medium and 10 μg/mL in gel mix (n=3, *p<0.05, **p<0.01, one-way ANOVA) (no statistical significance between IGF-1 vs IGF-1+IGF-1R Ab p=0.057, t-test).

5.2.3 Macrophages promote orbital fibroblast contractility independently of alpha-smooth muscle actin expression

We previously showed that, in the presence of 10% serum, TED orbital fibroblasts contracted collagen matrix more efficiently than control

fibroblasts and were more responsive to pro-fibrotic and pro-inflammatory cytokines TGF-β1 and IL-1β (Li et al., 2014). To determine whether macrophages alone could stimulate orbital fibroblasts contractile properties as they do for other ocular fibroblasts (Kechagia et al., 2016), control (COs: CO4, CO6, CO7) and TED (HOs: HO1, HO2, HO4) orbital fibroblasts were co-cultured with macrophages in serum-free medium at a 2:3 fibroblast:macrophage ratio. The use of serum-free medium is to eliminate the effect from serum, and macrophages alone are unable to contract collagen gels (Kechagia et al., 2016). Orbital fibroblasts are poorly contractile in serum free medium (Li et al., 2014) and, therefore, higher numbers were needed to detect contraction, these higher numbers of fibroblasts limiting the amount of macrophages that can be added to co-cultures without overcrowding the gels. Nevertheless, macrophages significantly promoted contraction for both control and TED fibroblasts (**Figure 5.3**A).

As orbital fibroblasts are highly contractile in the presence of serum, and responsive to TGF-β1 (Li et al., 2014), which is a cytokine involved in promoting the myofibroblast fibrotic phenotype, we sought to determine whether orbital fibroblast contractility was linked to expression of the classical fibrosis marker αSMA, which is known to regulate fibroblast contractility (Hinz et al., 2001). We expected that the higher αSMA level cells expressed, the more contractile cells would be. Both control (COs: CO4, CO6, CO7) and TED (HOs: HO1, HO2, HO4) orbital fibroblasts expressed significant levels of αSMA when cultured in the presence of 10% serum, with αSMA expression being slightly higher in 3D as compared to 2D, and levels overall consistently higher in TED cells. As expected, αSMA levels were significantly reduced in serum-free medium, with TED (HO) cells retaining significantly more αSMA than control (CO) ones (**Figure 5.3**B).

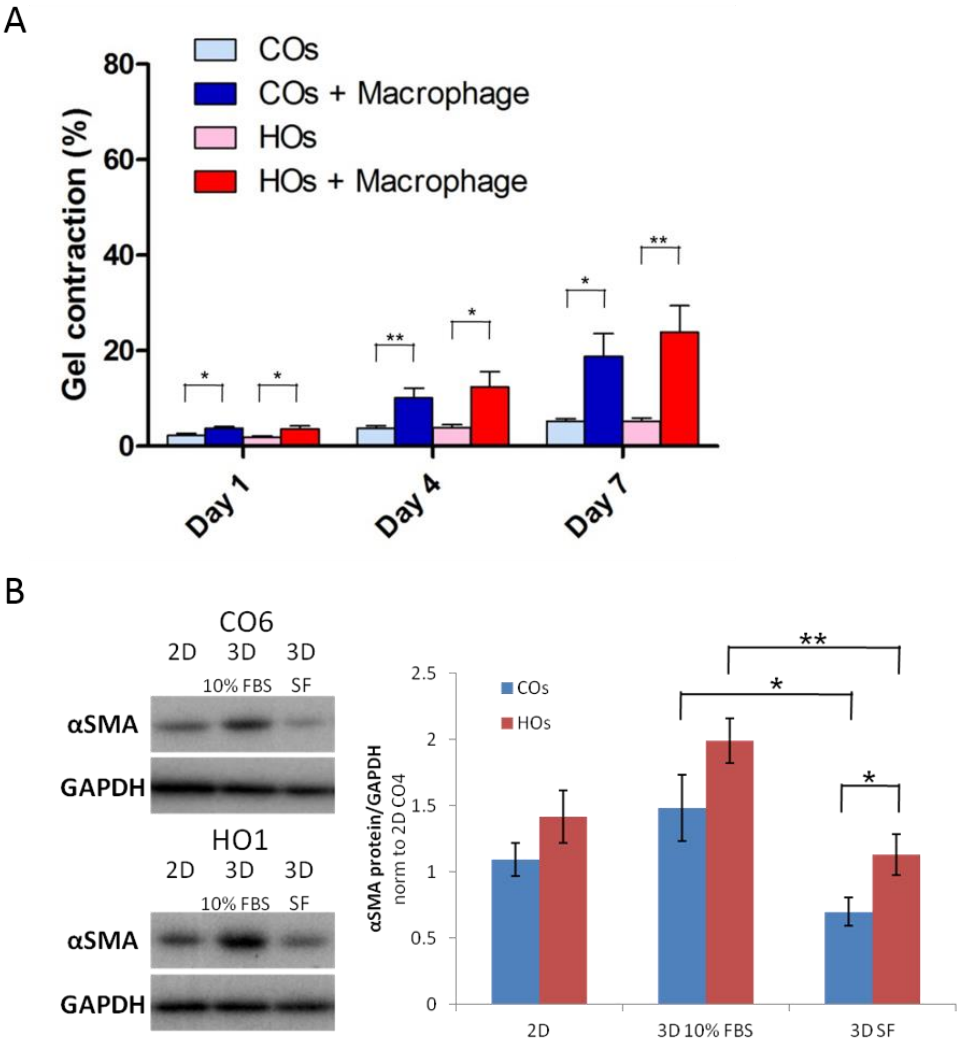

Figure 5.3 Macrophages promote orbital fibroblasts contractility.

(A) Orbital fibroblasts ($1.48x10^5$ cells/mL) were cultured with macrophages ($2.22 x10^5$ cells/mL) in serum-free medium for 7 days. Gel contraction is shown as mean ± SEM. Control (COs) and TED (HOs) fibroblasts are each averaged from 3 lines (COs: CO4, CO6, CO7; HOs: HO1, HO2, HO4) with n=3 and triplicates in each experiment. (*p<0.05, **p<0.01, t-test) (B) Representative Western blots and quantification of relative αSMA protein levels for the same 3 COs and 3 HOs cell lines after 5-7 days culture in the presence of 10% serum in monolayers (2D) and in gels (3D 10% FBS), and in serum-free medium in gels (3D SF) (n≥3; *p<0.05, **p<0.01, by one-way ANOVA and post-hoc.)

In contrast to the macrophage-induced contractility, 10% serum strongly induced fibroblast contractility, with gel contraction rates reaching 56-72% on Day 7 at low fibroblasts counts (**Figure 5.4**A). There is a trend of TED cells being more contractile than control cells as previously reported (Li et al., 2014), but no statistical significance was shown. In order to know if the serum-induced contractility in orbital fibroblasts is determined by the basic intrinsic αSMA protein levels in 3D in the presence 10% serum on Day 7, linear regression was done between gel contraction in 10% FBS and the αSMA protein levels in 3D in 10% FBS of each cell line. It showed that serum-induced contractility correlates well with intrinsic αSMA level in 3D 10% serum (R^2=0.84, *p*=0.01) (**Figure 5.4**B). Further linear regression was done between macrophage-induced contractility and intrinsic relative αSMA level in 3D 10% serum on Day 7. Poor correlation of macrophage-induced contractility with αSMA level in 3D in 10% serum was revealed (R^2=0.24, *p*=0.32) (**Figure 5.4**C), suggesting that macrophage-induced contractility is not comparable to serum-induced contractility and is not determined by the intrinsic αSMA level in 3D in 10% serum. These suggested that the regulating pathway for macrophage-induced contractility is different from that for serum-induced contractility, which may be partly determined by the intrinsic αSMA level in 3D in 10% serum.

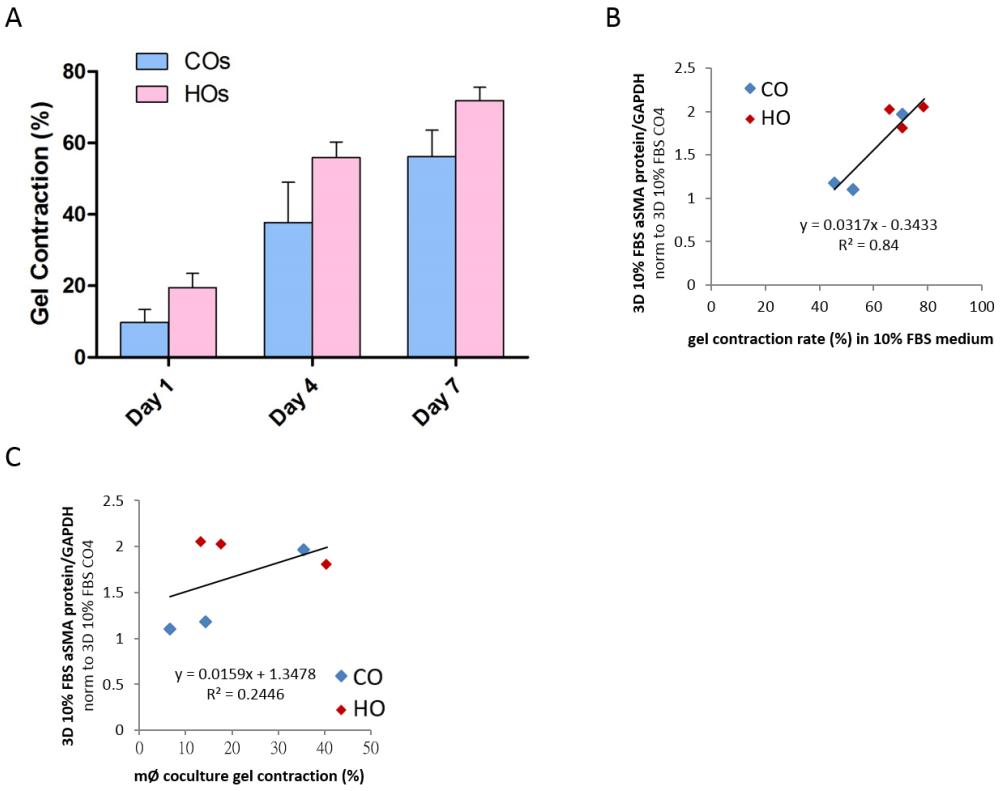

Figure 5.4 Serum-induced orbital fibroblast contractility is correlated with Day 7 intrinsic αSMA level.

(A) Orbital fibroblasts ($0.74x10^5$ cells/mL) in the presence of 10% serum are contractile on Day 7. Gel contraction is shown as mean ± SEM. (COs: CO4, CO6, CO7; HOs: HO1, HO2, HO4; each with n=3 and triplicates in each experiment) (B,C) Correlations of relative αSMA protein level in 3D in 10% serum and Day 7 fibroblast contractility [serum-induced (B); macrophage-induced (C)] were analysed by linear regression in 3 COs and 3 HOs (Each dot represents a cell line; COs in blue: CO4, CO6, CO7; HOs in red: HO1, HO2, HO4; each n=3).

To confirm a possible role for αSMA inducing orbital fibroblast contraction, gene silencing of αSMA was performed in a representative TED cell strain, HO2. Cells were then cultured in gels in medium with 10% serum or co-cultured with macrophages in serum-free medium to

observe gel contraction for 7 days. Downregulating αSMA to minimal levels using siRNA (**Figure 5.5**A) significantly reduced serum-mediated gel contraction in HO2 cells (**Figure 5.5**B), but did not affect macrophage-mediated contraction in the absence of serum (**Figure 5.5**C). This again confirmed that macrophage-induced orbital fibroblast contractility may be distinct from serum-induced contractility, and not directly linked to αSMA levels.

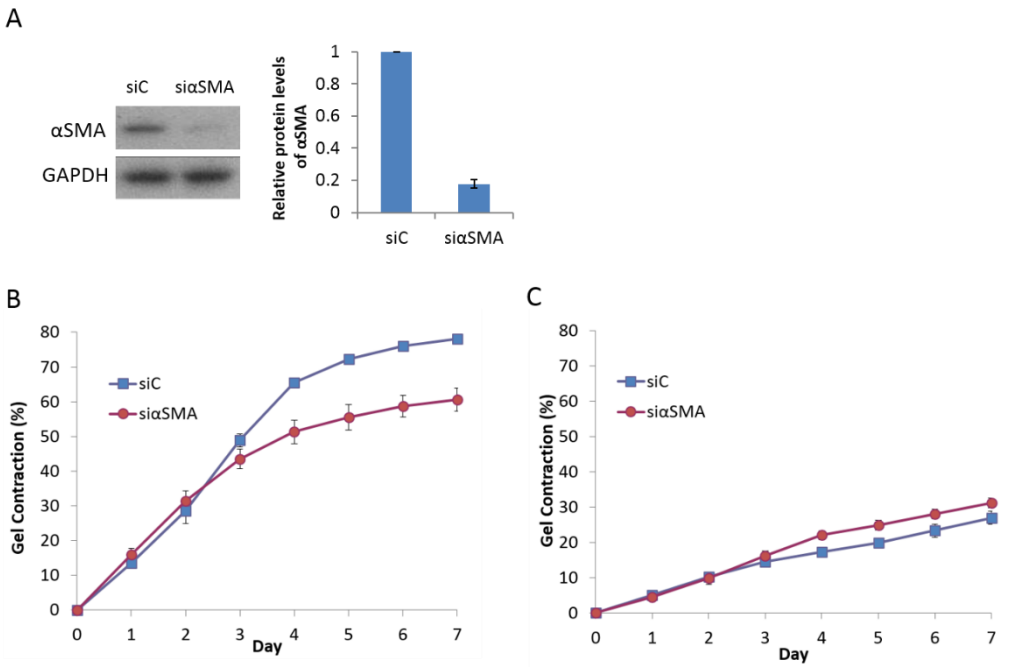

Figure 5.5 Downregulation of αSMA reduces serum-induced contractility, but not macrophage-induced contractility.

(A) Representative Western blot and semi-quantification of αSMA levels showed effective αSMA knockdown by siRNA in TED orbital fibroblasts HO2. (n=4) (B) Downregulating αSMA significantly decreased the contractility of HO2 fibroblasts ($0.74x10^5$ cells/mL) in the presence of 10% serum (n=3 and triplicates in each experiment, Day 7 $p<0.001$, t-test) (C) Downregulating αSMA did not decrease macrophage-stimulated contraction of HO2 orbital fibroblasts in serum-free medium (HO2 $1.48x10^5$ cells/mL, macrophages $2.22x10^5$ cells/mL, n=4 and triplicates in each experiment, Day 7 $p=0.077$, t-test).

5.2.4 Macrophages stimulate actin polymerisation and protrusive activity in orbital fibroblasts

To better understand how macrophages stimulate contraction, we examined morphology of fibroblasts in the gels during contraction. In the presence of serum, orbital fibroblasts adopted a “spread” morphology, with long, thick protrusions rich in filamentous and cortical actin, but lacking strong straight actin fibre bundles (**Figure 5.6**A). Alpha-SMA staining partly overlapped with actin filaments, but only a minute proportion of the cells (less than 3%) displayed αSMA in a typical “stress fibre” pattern distribution (**Figure 5.6**A,B), suggesting that orbital fibroblasts do not differentiate into classical myofibroblasts (Hinz et al., 2001; Meyer-Ter-Vehn et al., 2006; Tomasek et al., 2002) during contraction in 3D gels. Rather, in the majority of cells, αSMA was either cytoplasmic (in a perinuclear pattern), or partially co-localised to F-actin patterns (cortical fibres or intracellular bundles; **Figure 5.6**A,B). Under serum-free conditions, most cells displayed cytoplasmic perinuclear αSMA (**Figure 5.6**B). Upon macrophage co-culture, a significant increase in the proportion of cells with αSMA incorporation into actin bundles, with more than 50% of the cells showing partial co-localisation with F-actin was revealed (**Figure 5.6**).

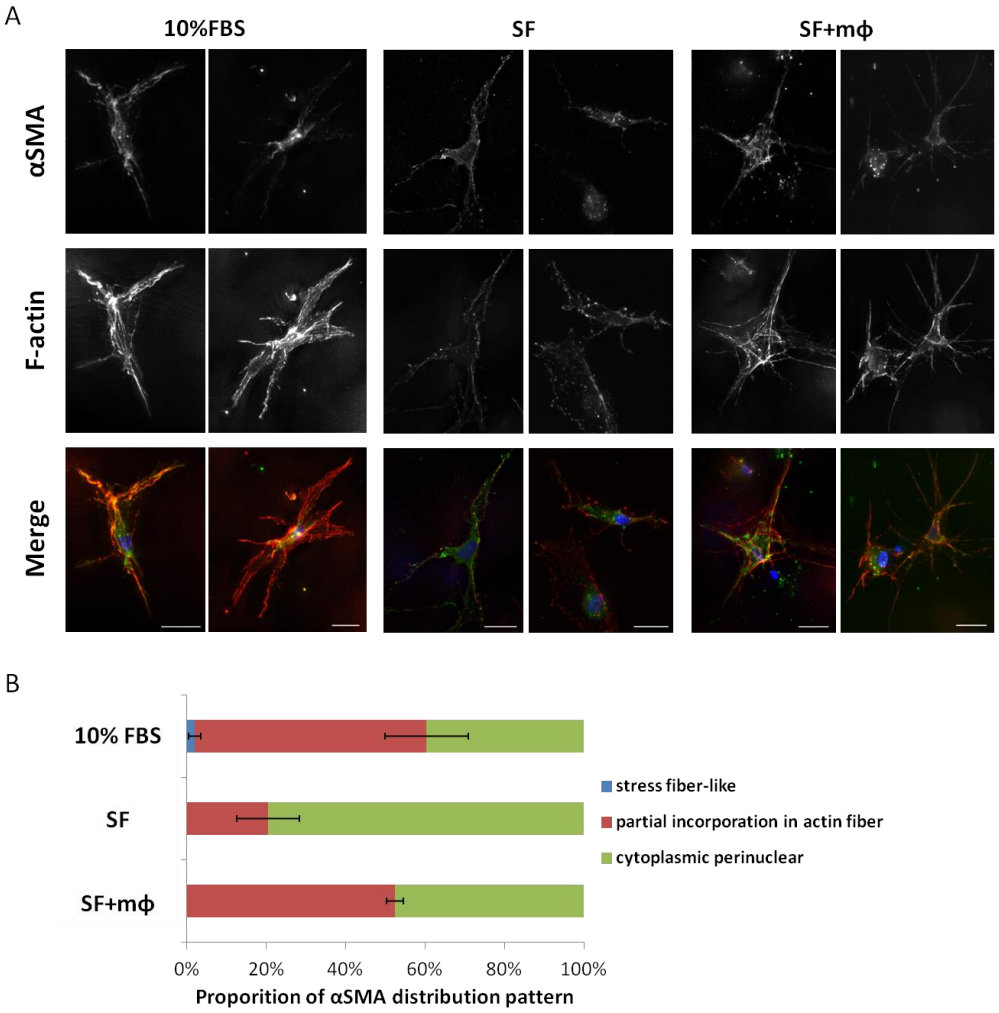

Figure 5.6 Macrophages increased αSMA incorporation in actin fibres.

(A) Representative images of αSMA and F-actin staining in HO2 fibroblasts ($1.48x10^5$ cells/mL) following 4 days of culture in gels in 10% serum (10%FBS), and in serum-free medium without (SF) and with macrophages ($2.22\ x10^5$ cells/mL) (SF+mφ). Scale bar, 25 μm, Merge images are from αSMA (green), F-actin (red), and DAPI (blue). (B) αSMA distribution in HO2 fibroblasts were categorised and proportioned in three patterns (>100 cells analysed, n=3).

Overall, αSMA levels (as measured by integrated fluorescence densities) were similar whether cells were in the presence of 10% serum, serum-free, or in macrophage co-culture (**Figure 5.7**A). On the other hand, F-actin levels were highest in 10% serum, lowest in serum-free, and the presence of macrophages significantly increased F-actin levels (**Figure 5.7**B). This matches the observation in **Figure 5.6**B where higher proportions of orbital fibroblasts showing αSMA incorporation into actin bundles in the presence of macrophages, suggesting that αSMA is randomly incorporated into actin fibres when they form as a result of the macrophage stimulation of actin polymerisation. Accordingly, macrophage co-culture resulted in significant changes in fibroblast morphology: while in serum-free medium, fibroblasts had few protrusions (**Figure 5.7**C,D), matching low levels of polymerised actin (**Figure 5.7**B), fibroblasts adopted a more “stellate” appearance, with more long thin protrusions in the presence of macrophages (**Figure 5.7**C,D). Thus, increased levels of F-actin and protrusion numbers upon co-culture with macrophages suggest that macrophages directly stimulate actin polymerisation and protrusion activity in fibroblasts, presumably driving the resulting gel contraction.

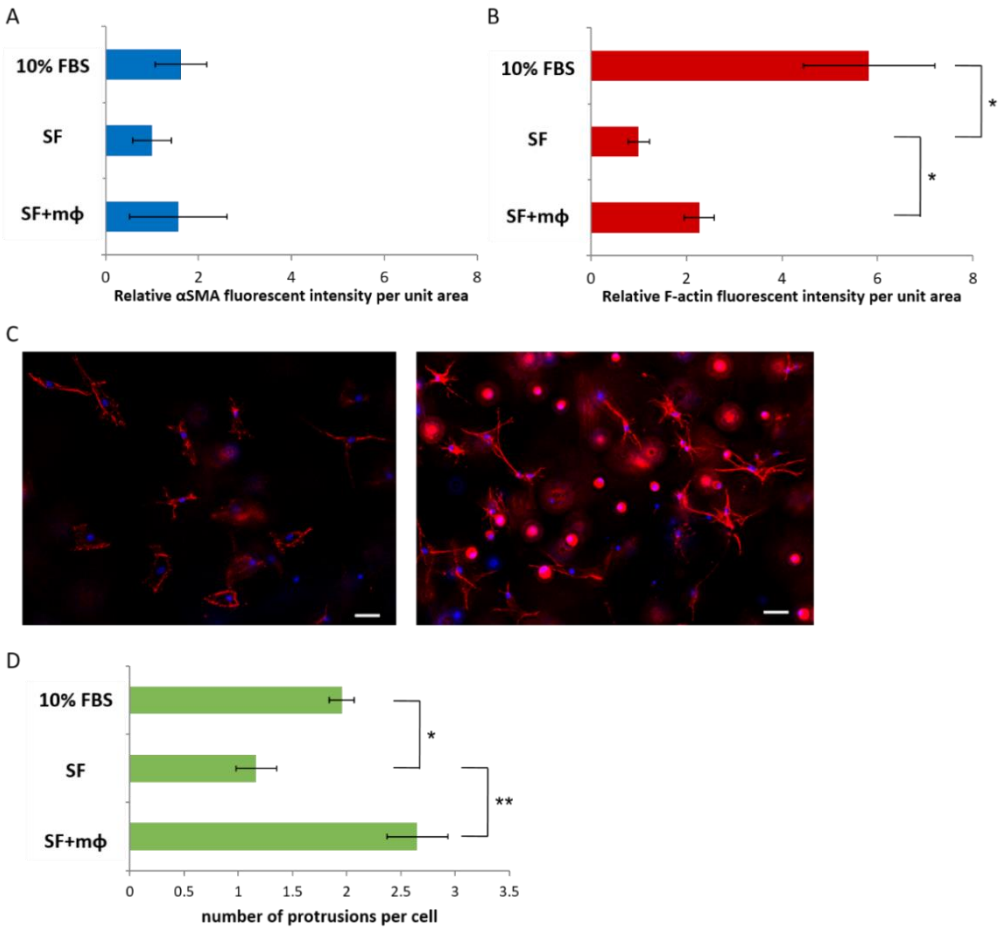

Figure 5.7 Macrophages increase F-actin levels and cell protrusions in orbital fibroblasts.

(A, B) Quantification of αSMA (A) and F-actin (B) levels in HO2 fibroblasts in gels in the presence of 10% serum, and in serum-free medium with/without macrophages; shown are fluorescence intensity measurements from maximum intensity projections normalised to the value of serum-free condition (n=4, *p<0.05, t-test). (C) Representative images of F-actin staining of HO2 fibroblasts in gels without (left) and with (right) macrophages in serum-free medium. Shown are maximal intensity projections of deconvolved image stacks. Scale bar, 50 µm. (D) Fibroblast protrusive activity with/without macrophage co-culture. Shown is the average number of protrusions per cell, as determined using F-actin staining. (n=4, *p<0.05, **p<0.01, t-test)

5.2.5 Macrophages drive the orbital fibroblasts pro-fibrotic phenotype through TGF-β and PI3K pathways

TGF-β signalling is reportedly involved in obesity (Yadav et al., 2011), HA production (Stuhlmeier and Pollaschek, 2004; Wang et al., 2005) and fibrosis in various organs (Biernacka et al., 2011; Meng et al., 2016). Similarly, phosphatidylinositol-4,5-bisphosphate 3-kinase (PI3K) has been implicated in lipid accumulation (Yu et al., 2008), and the PI3K-Akt pathway was previously shown to regulate HA production in TED fibroblasts (Zhang et al., 2014). Furthermore, whether as an independent pathway or through non-canonical TGF-β signalling, PI3K is the frequent target for anti-fibrotic therapies (Conte et al., 2011; Reilly et al., 2017). Activated macrophages can produce TGF-β and other pro-inflammatory cytokines that may activate these pathways in fibroblasts and promote fibrosis (Wynn and Barron, 2010). To determine whether either pathway could be modulating macrophages-mediated stimulation of orbital fibroblasts, we assessed the effect of TGF-β (SB131542, 10 μM) and PI3K (LY294002, 10 μM) inhibitors on LD formation, HA production and gel contraction using HO2 TED cells in the presence of macrophages. Neither inhibitor affected spontaneous LD formation (**Figure 5.8**A), but both SB131542 and LY294002 significantly decreased macrophage-induced HA production (**Figure 5.8**B), with minimal cytotoxicity (**Figure 5.8**C). However, only PI3K inhibition was able to significantly decrease macrophage-induced gel contraction (**Figure 5.8**D), suggesting that all three phenotypes do not result from exactly the same pathway.

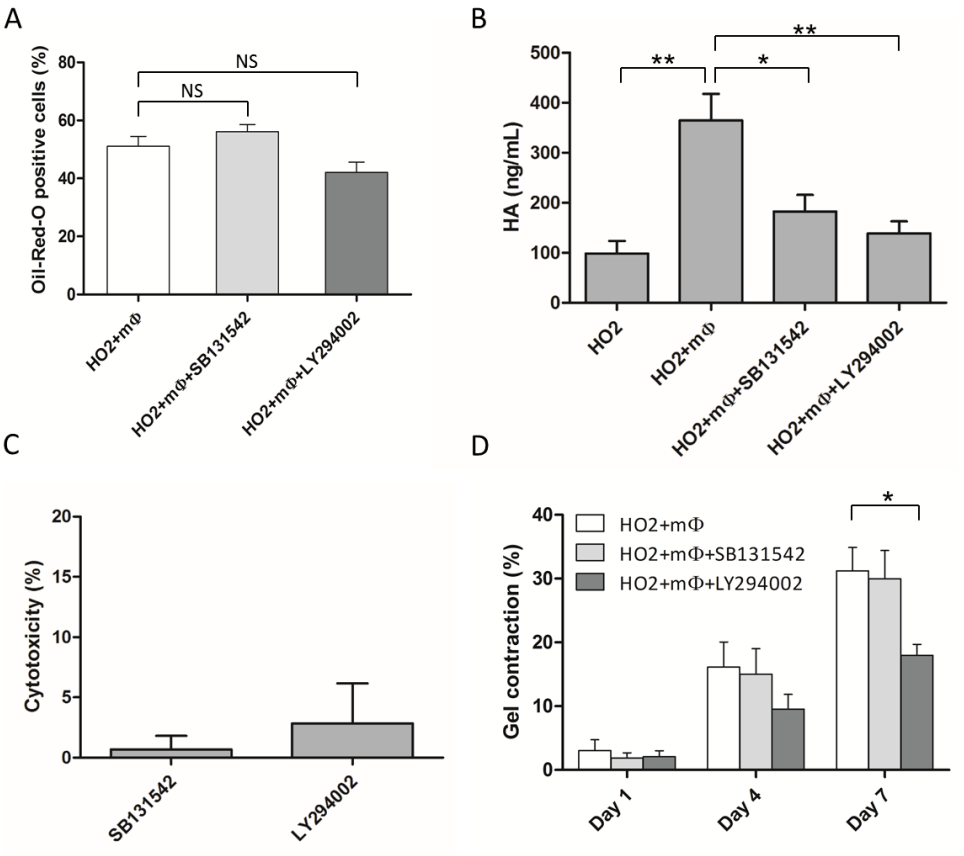

Figure 5.8 TGF-β and PI3K pathways differentially regulate macrophages' effect on orbital fibroblasts fibrotic phenotype.

(A) TGF-β (SB131542, 10 μM) and PI3K (LY294002, 10 μM) inhibitors did not alter LD formation in HO2 fibroblasts ($0.74x10^5$ cells/mL) co-cultured with macrophages ($0.74x10^5$ cells/mL) in gels for 7 days in the presence of 10% serum. (Shown are mean ± SEM proportion of cells containing LDs stained with ORO, n=4, p=0.2787 (SB131542) and p=0.1172 (LY294002), t-test) (B) Both TGF-β and PI3K inhibition prevented macrophage-mediated HA production. HO2 fibroblasts ($0.74x10^5$ cells/mL) were co-cultured with macrophages ($1.5x10^5$ cells/mL) at 1:2 fibroblast:macrophage ratio in gels with/without inhibitors and HA levels were measured after 3 days. (n=3, *p<0.05, **p<0.01, one-way ANOVA) (C) LDH assay showed minimal cytotoxicity of SB131542 and LY294002 after 3 days in 1:2 HO2:macrophage co-culture 3D gels. Shown is calculated toxicity normalised to 100% toxicity control. (n=2) (D) HO2 fibroblasts ($1.48x10^5$ cells/mL) were co-cultured with macrophages ($2.22\ x10^5$ cells/mL) in collagen gels in serum-free medium for 7 days for contraction assay, with/without TGF-β or PI3K inhibitors. Shown are mean ± SEM, n=4,

*p<0.05, t-test)

5.3 Discussion

Most TED studies have mainly focused on T and B cell activating inflammatory reactions (Feldon et al., 2005; Sempowski et al., 1998; Weetman et al., 1989), HA production (Krieger et al., 2015; Krieger et al., 2016; Zhang et al., 2012) and chemically differentiated adipogenesis (Sorisky et al., 1996; Zhao et al., 2013) after TSHR and IGFR activation. Little is known about either macrophage or fibrosis aspects in TED. Here, we show that macrophages do not significantly enhance LD formation in 3D but trigger HA production via TGF-β and PI3K signalling. Also, macrophages promote the orbital fibroblasts fibrotic phenotype which can be inhibited by PI3K signalling but not through TGF-β-αSMA regulation.

5.3.1 U937-derived macrophages as a model for activated tissue macrophages in TED

We used PMA to differentiate monocytes into macrophages in our experiments. PMA differentiates monocytes into macrophage-like cells (M0) which can be further polarised to M1 when incubated with IFN-α and LPS or M2 when incubated with IL-4 and IL-13 (Chanput et al., 2013; Genin et al., 2015). M1 are circulating macrophages whereas M2 are deemed residential ones (Mantovani et al., 2013). The PMA-differentiated macrophages used in our experiments are PMA-stimulated M0 only without further polarisation. However, we know from additional work in the lab (Kechagia et al., 2016) (Sharma et al., manuscript in preparation) that PMA-stimulated macrophages, similar to stimulated peripheral blood mononuclear cells, secrete a large range of cytokines

and can activate normal and fibrotic ocular fibroblasts. Moreover, tracing the origin of macrophages in TED in the study of Eckstein et al., large numbers of migrant monocytes including mature activated macrophages are found in active TED orbital tissues (Eckstein et al., 2004). Therefore, TED-related macrophages are migrant populations rather than residential ones, meaning possibly more M1 than M2 in TED tissue. With regard to the obesity model, M1 macrophages are pro-inflammatory and pro-fibrotic whereas M2 are anti-inflammatory and pro-adipogenic (Martinez-Santibanez and Lumeng, 2014). Interestingly, our results of orbital fibroblasts co-cultured with macrophages did not show increased LD formation but more fibrotic, and this is in line with the characteristics of M1 cells and consistent with the TED histopathology evidence (Eckstein et al., 2004).

5.3.2 Interaction of HA with macrophages

HA is a constituent of ECM, and HA level regulates the fibroblasts proliferation via TGF-β-SMAD3 pathway (Meran et al., 2008), thereby contributing to fibrosis (Albeiroti et al., 2015). In the process of fibrosis, there is dynamic synthesis and degradation of ECM. The synthesis of ECM leads to increased stiffness and fibrotic changes in tissues, while the degradation of ECM results in fragments which exhibit biological activities to regulate cell signalling, and HA is an example of ECM presenting this property (McKee et al., 1996). Macrophages express hyaluronan receptor CD44 on their surface (Jones et al., 2000; McKee et al., 1996), and macrophage activity can be regulated by HA working with chemokines (Horton et al., 1998). HA fragments were found to bind CD44, and induced gene expressions of macrophage inflammatory protein-1alpha (MIP-1α), -1beta (MIP-1β), and IL-8 in murine alveolar macrophage cell line and human bronchial alveolar macrophages (Jones et al., 2000; McKee et al., 1996). However, the observed HA secretion by

fibroblasts in response to stimulation of macrophages has never been reported. Our work shows for the first time that macrophages can trigger HA secretion in orbital fibroblasts, especially in TED orbital fibroblasts. This is possibly because of the cytokines secreted by macrophages. Interestingly, IL-1β was shown to induce HAS2 gene expression and HA production in orbital fibroblasts from TED patients (Chung et al., 2014; Kaback and Smith, 1999). The IL-1β stimulation on HA production is not exclusively in orbital fibroblasts, it was seen in HUVEC and primary human skin fibroblasts (Kennedy et al., 2000; Vigetti et al., 2010), and IL-1β can be secreted by macrophages (Arango Duque and Descoteaux, 2014). This macrophage-induced HA secretion may in turn activate macrophage activity, either through direct stimulation of HA receptor CD44 on the macrophage or by co-stimulation with chemokines, thus creating a positive feedback loop that may sustain and exacerbate fibrosis.

IGF1R stimulation has previously been linked to HA production in orbital fibroblasts (Smith and Hoa, 2004; Zhang et al., 2014), possibly through PI3K-A signalling (Zhang et al., 2014); consistent with this, we found macrophage-mediated HA secretion was prevented by a PI3K inhibitor (LY294002). However, blocking IGF-1R did not prevent HA secretion following macrophage stimulation, suggesting that fibroblasts can use a different upstream activator of PI3K-A signalling to trigger HA production and secretion. As evidenced by 1) macrophage-mediated HA production is inhibited by blocking TGF-β receptor, 2) a cross-talk between TGFβ1-TGFβ1 receptor/ALK5 and PI3K has been reported in a number of cell processes (Aki et al., 2015; Olieslagers et al., 2011; Yu et al., 2015) and 3) activated macrophages are known to secrete TGF-β1 (Wynn and Barron, 2010), macrophages may stimulate HA production in orbital fibroblasts through a non-canonical TGF-β1/PI3K pathway (Conte et al., 2011; Reilly et al., 2017). Whether this macrophage-induced HA production can be further linked to the macrophage-related fibrosis is still unknown.

5.3.3 αSMA and F-actin in fibrosis

An increase in fibroblast contractility is a hallmark of fibrosis, and our group has shown previously that fibrotic ocular fibroblasts, including TED orbital fibroblasts, display increased contractile features in our 3D model compared to their normal, non-diseased counterparts (Ezra et al., 2010; Kechagia et al., 2016; Li et al., 2014). Contractile fibrotic fibroblasts *in vivo* often present with characteristic cytoskeletal features, including expression of the specific actin isoform αSMA, defining the so-called myofibroblast phenotype (Eddy et al., 1988; Grinnell, 1994; Hinz et al., 2007). *In vitro*, αSMA incorporation into strong actin bundles and prominent stress fibres on stiff or "tensioned" substrates have traditionally been linked to fibroblast contractility and myofibroblast phenotype (Hinz et al., 2001). As orbital fibroblasts displayed cytoskeletal changes, including an increase in actin bundles, after co-culture with macrophages, we initially hypothesised that macrophage-induced orbital fibroblasts contractility might be mediated through the acquisition of a myofibroblast-like phenotype. However, while both control and TED orbital fibroblasts express αSMA, we found that macrophage-mediated stimulation of fibroblast contractility was not linked to αSMA expression; rather, macrophages stimulated actin dynamics in fibroblasts, with increased protrusive activity and actin polymerisation.

Moreover, TGF-β/Smad can trigger Rho activation and αSMA synthesis (Ji et al., 2014; Masszi et al., 2003; Vardouli et al., 2008) (**Figure 5.9**A), whereas Rac is more related to PI3K pathway in which there is a positive feedback loop between Rac and PI3K (Campa et al., 2015; Raftopoulou and Hall, 2004) (**Figure 5.9**B). Our results showed that PI3K inhibitor rather than TGF-β inhibitor reduced macrophage-induced contractility, suggesting that a PI3K/Rac pathway may be involved in macrophage-stimulated contraction. Interestingly, this is in agreement with the morphological results where the absence of myofibroblast pattern also

favours a non-TGFβ/Rho pathway. Therefore, instead of TGF-β signalling, which is the classical upstream pathway mediating the acquisition of the myofibroblast phenotype (Evans et al., 2003; Hu et al., 2003), PI3K may be mediating fibroblast contractility in the presence of macrophages.

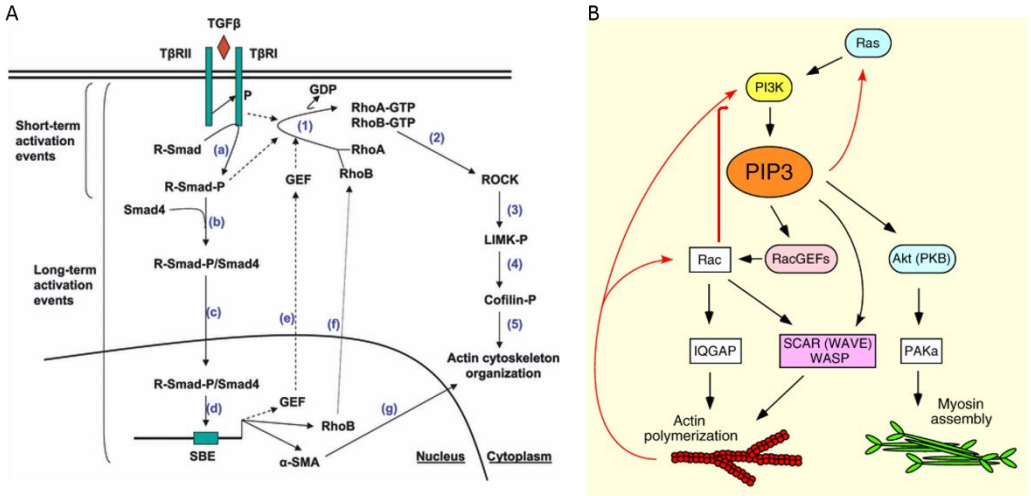

Figure 5.9 TGFβ and PI3K regulates actin polymerisation through Rho and Rac, respectively.

(A) Rho can be activated by TGFβ through Smad dependent and independent pathways, and further activates ROCK and actin cytoskeleton. (B) Ras/PI3K regulates actin polymerisation through Rac. (A) Adapted from (Vardouli et al., 2008) (B) Adapted from (Kölsch et al., 2008)

5.3.4 Conclusions

Our work demonstrates that macrophages stimulate HA production of orbital fibroblasts via TGF-β and PI3K signalling, and promote a fibrotic phenotype independent from αSMA through PI3K signalling rather than the classical TGF-β/αSMA pathway. The PI3K inhibitor, LY294002, decrease both macrophage-mediated HA production and contraction in orbital fibroblasts.

Chapter 6 General Discussion

TED causes periocular disfigurement and threatens vision. Current treatments mainly aim at inflammation control to prevent fat expansion. Once the inflammation subsides, the remaining soft tissue problems are less likely to resolve naturally or by medical approaches. Only invasive surgical interventions can restore normal appearance and functions, but despite treatment, some severe cases still lose their vision. The detailed mechanisms about soft tissue change have not been thoroughly understood, and this impedes the development of effective treatment to prevent or reverse TED progression.

In order to better understand TED pathogenesis, this study aimed to find the molecular determinants of TED at aspects of mechanotransduction, LD accumulation, and macrophage participation. We approached mechanotransduction through investigating MRTF, a transcriptional co-activator in MRTF/SRF mechanotransduction pathway, and found that orbital fibroblasts are mechanosensitised by exporting MRTF-A from nucleus and decreasing MRTF-A protein expression in response to 3D culture. MRTF is involved in contractility but not in lipid formation in orbital fibroblasts. The spontaneously formed LDs in 3D were shown to be linked to FA uptake and PLIN2 expression. PLIN2 is overexpressed in orbital fibroblasts from TED patients, and is upregulated by cytokine stimulation and leads to enhancement of LDs. This suggests an important regulating role of PLIN2 in TED, which is a novel discovery in orbital fibroblasts. In addition, macrophages are involved in TED development by stimulating HA secretion and contractility in orbital fibroblasts by promoting actin polymerisation through PI3K signalling.

6.1 Inflammation Triggers TED Features in Orbital Fibroblasts

While PLIN2 was found closely related to LD accumulation in orbital fibroblasts cultured in 3D, cytokines and in particular IL-1β, were shown to upregulate PLIN2 (**Figure 4.19**A, **Figure 4.20**A,B). This indicates that IL-1β is possibly an important trigger for LD accumulation in orbital fibroblasts and may contribute to fat expansion in TED. This is in line with previous report showing that IL-1β enhanced chemically induced adipogenesis in orbital fibroblasts (Yoon et al., 2011), although there was also a report showing opposite results, in which IL-1β inhibited mouse preadipocyte differentiation (Gregoire et al., 1992). Interestingly, macrophage conditioned medium also upregulated PLIN2 (**Figure 4.19**B), presumably influencing LD formation as well. However, this is not consistent with our results with macrophage and orbital fibroblasts co-culture experiments, where macrophage did not significantly alter 3D LD formation (**Figure 5.1**). Considering cell counts issue, cell counts of macrophage in conditioned medium were five times to fibroblasts, which is comparable to co-culture experiments where two and five times were used. It is possible that more repeats in co-culture experiments would have concluded an effect of macrophage. It is also possible that in co-culture, fibroblasts altered the macrophage response. For example, MIP-1α secretion by macrophages was shown dependent on the intercellular adhesion molecule 1 (ICAM-1) secreted by fibroblasts in a co-culture system (Steinhauser et al., 1998). Similarly, oral periodontal ligament fibroblasts downregulated TNF-α secretion by PMA differentiated THP-1 macrophages (Tzach-Nahman et al., 2017). Therefore, it is possible that orbital fibroblasts might change macrophages activation levels and attenuate their pro-lipogenic ability.

We found that macrophages stimulated HA secretion in orbital fibroblasts, and TED fibroblasts produced higher levels of HA compared to control

cells (**Figure 5.2**). This is also possibly related to cytokines secreted by macrophages. Macrophages can secrete IL-1β and TNFα (Atri et al., 2018). IL-1β, TNFα and TNFβ were reported to induce HA production through NFκB regulation in HUVEC (Vigetti et al., 2010), and IL-1β also induced HA accumulation in primary human skin fibroblasts (Kennedy et al., 2000). In particular, IL-1β increased HAS2 gene expression and HA secretion in TED orbital fibroblasts (Chung et al., 2014; Kaback and Smith, 1999). Therefore, it is likely that macrophages indirectly induced HA production in orbital fibroblasts by release of these cytokines. Moreover, we found that PI3K and TGFβ inhibitors reduce macrophage-induced HA. Interestingly, both PI3K/Akt and TGFβ crosstalk with NFκB signalling, and inhibiting PI3K/Akt and TGF-β signalling can inhibit NFκB activation (Ataie-Kachoie et al., 2013; Rogers et al., 2008). As 1) NFκB mediates cytokine-induced HA production, 2) PI3K/Akt and TGFβ crosstalk with NFκB and 3) our observation of PI3K and TGF-β inhibition reduced macrophage-induced HA production, all these together again support the possibility of macrophage-induced HA is via cytokine secretion. Nevertheless, TED cells are clearly more able to produce HA than control cells in both the presence and absence of macrophages, and this is likely due to intrinsic differences in other HA expression pathways.

Overall, our findings are consistent with an essential role of inflammation in initiating multiple aspects of the TED phenotypes.

6.2 3D Lipid Droplet Accumulation in TED

Fat expansion is an important pathological feature in TED. While most *in vitro* 2D model TED studies stated that adipogenesis in orbital fibroblasts contributes to fat expansion (Kumar et al., 2005; Sorisky et al., 1996), our group previously demonstrated spontaneous LD formation more prominent in TED orbital fibroblasts than control counterparts in 3D

model (Li et al., 2014). Adipogenesis refers to the formation of mature adipocytes differentiated from MSCs, and usually requires chemical adipogenic differentiation medium to trigger the differentiation process. Our LDs are spontaneously formed in 3D in the absence of chemical adipogenic differentiation medium. In this study, we found that spontaneous LD accumulation in 3D results from a mechanism different from that drives classical adipogenesis. It is more consistent with a pathway recently published – LD accumulation as a ubiquitous phenomenon in a wide variety of cells in response to ECM stiffness (Romani et al., 2019). Extracellular mechanical cues transmit to cells and change internal cellular structure (cytoskeleton) and intracellular force (Chen, 2008). The Golgi apparatus appears to be the sensor for this mechanical force and modulates SREBP localisation by Lipin-1 which is a negative regulator of lipid formation (Romani et al., 2019). Romani et al. reported that in soft matrix or inhibition of Rho, ROCK, or MLCK, the Golgi senses the extracellular and intracellular force and inactivates Lipin-1, this further enhances SREBP translocation to nucleus, activates lipid related genes and LD formation. How the Golgi apparatus senses the force to regulate Lipin-1 activity is unknown. The upregulated genes are related to metabolism of cholesterol, FA, and TG, and are different from adipogenesis genes. This pathway links mechanotransduction to LD formation, in line with our findings that LDs are formed spontaneously in 3D and related to FA uptake.

In MRTF/SRF or YAP mechanotransduction signalling, soft matrix, inhibiting Rho/ROCK, or interfering MRTF/SRF or YAP pathway contributes to adipogenesis (Dupont et al., 2011; Nobusue et al., 2014). This and the aforementioned pathway has some factors in common, 1) soft matrix or Rho/ROCK inhibition as initiator, 2) related to intracellular force which is downstream of Rho/ROCK, and 3) lipid formation as end product although one is LD formation, and the other is adipocyte differentiation. We failed to show that the downregulation of MRTF or inhibiting YAP could increase adipogenesis in our MRTF and YAP

experiments. There are some possible reasons for this: 1) MRTF or YAP hypothesis is based on adipogenesis, but our 3D LD formation is proven not to be adipogenesis, the two pathways do not coexist in our 3D model, 2) Romani et al. also showed that the LD formation is independent from YAP/TAZ signalling (Romani et al., 2019), indicating the two pathways are different, 3) the adipogenesis induced by depleting MRTF or YAP is cell type specific because we could not reproduce increase of adipogenesis by depleting MRTF in 2D neither in the presence nor absence of chemical adipogenic differentiation medium.

Romani et al. reported that SREBP and its target genes are involved in LD accumulation, and those are genes regulating lipogenic enzymes (Horton et al., 2002), but we have not yet investigated these genes in our 3D model. Those genes are mediators in the aspect of lipid formation, however, we have not found much difference between TED and control cells in molecules regulating FA uptake or DNL, suggesting that LD formation ability might be similar in TED and control cells, and SREBP related genes may not be the key determinant in TED phenotype. But the most significant determinant we found in TED 3D LD accumulation is PLIN2, a LD surface protein. LDs and PLIN2 appear to stabilise each other mutually, as LDs preserve PLIN2 from being degraded by proteasome, and PLIN2 stabilises LDs from hydrolysis. PLIN2 unbound to LDs is easily degraded by ubiquitin/proteasome pathway (Xu et al., 2005), and PLIN2 plays a role in preventing LD degradation (Feng et al., 2017). While we observed more PLIN2 in TED orbital fibroblasts and in cytokine-stimulated cells, we have not investigated if there is less PLIN2 degradation or less lipolysis associated. Future work on PLIN2 degradation and lipolysis can help understand the detailed mechanism about how PLIN2 is upregulated in TED. Interestingly, PLIN2 is also linked to PPARγ activation in adipogenic differentiation. PLIN2 has PPRE in its promoter region where heterodimer of PPAR/RXR bound to (Targett-Adams et al., 2005). The activation of PPAR can result in PLIN2 transcription, thus PLIN2 is a PPAR target gene. Therefore, higher

PLIN2 level in TED orbital fibroblasts is not only linked to lipid formation in our 3D model, but also possibly in 2D chemical adipogenesis model although it has never been studied. This indicates the significance of PLIN2 in TED phenotype.

6.3 Orbital Fibroblast Contractility

Fibroblast contractility is the presentation of intrinsic cellular force which cells respond to extracellular mechanical tension for maintaining tensional homeostasis (Brown et al., 1998). Intrinsic cellular force is regulated by actomyosin contractility and cytoskeletal assembly (Vining and Mooney, 2017). Alpha-SMA upregulation and incorporation in stress fibres is a common character in myofibroblast mediated contraction mechanism (Tomasek et al., 2002). In this study, we found that contractility of orbital fibroblasts in the presence of serum was decreased by silencing αSMA, MRTF, and TCF genes. TCFs and MRTFs compete to bind SRF to regulate contractility, and Gualdrini et al. reported that TCFs knockout increased contractility in MEFs (Gualdrini et al., 2016), thus we expected silencing TCFs would have similar effects in orbital fibroblasts. But we observed MRTF and TCF silencing both decreased serum-stimulated contractility in orbital fibroblasts. It is likely that serum-induced contractility is mediated by MRTF and TCF/SRF/αSMA pathway. However, in the presence of serum, downregulating αSMA to 10% residue of expression level reduced gel contraction rate from 70% to 50% only. Although it was not complete knockdown, it suggested that αSMA is not the only regulator in serum-stimulated contraction. On the other hand, in the absence of serum, orbital fibroblasts contractility was much reduced, and could be induced by macrophages through F-actin polymerisation but independent of αSMA, indicating that actin polymerisation dynamics rather than αSMA expression regulates macrophage-induced contractility in the absence of serum.

In addition to the stress fibre pattern in myofibroblast differentiation, there are other mechanisms regulating fibroblast-mediated collagen gel contraction. Fibroblasts in free-floating gels mainly retain a fibroblast phenotype without differentiating into myofibroblasts. They more likely contract gels by contacting collagen fibres directly with protrusion and retractions (Dahlmann-Noor et al., 2007; Dallon and Ehrlich, 2008). Previous work in the lab has shown that, in human corneal, tenon, and scleral fibroblasts cultured in 3D collagen matrix, collagen fibres were pulled towards cells as cells extended protrusions. These generated force to contract gels, suggesting that gel contraction is mediated by cell protrusive activity, which includes extension and retraction of cellular protrusions (Dahlmann-Noor et al., 2007). We found that macrophages induced orbital fibroblasts contractility through enhancing cell protrusions and F-actin polymerisation without transforming them into myofibroblasts, in line with the phenomenon observed in other ocular fibroblasts.

How macrophages promote actin polymerisation and protrusive activity is not known, although it is likely through cytokine release. A cytokine mixture of IL-1α, lL-6, and TNF-α in 0.3% serum increased F-actin level and led to rearrangement of the cytoskeleton in a stress fibre pattern, via Rho/ROCK in microvascular endothelial cells (Campos et al., 2009). MCP-1 also induced F-actin rearrangement into stress fibre via Rho/ROCK in mouse brain microvascular endothelial cells (Stamatovic et al., 2003), whereas IL-1β suppressed actin polymerisation in primary rat hippocampal neurons in an inflammation-Alzheimer disease model (Tong et al., 2018). We have shown that PI3K pathway is involved in macrophage-induced contractility without typical stress fibre formation, which is different from other cytokine-mediated contraction. Future investigations may focus on characterising the cytokine involvement as well as the interactions between macrophages and fibroblasts in macrophage-induced orbital fibroblast contractility.

ECM remodeling may also contribute to fibroblast contraction (Martin-Martin et al., 2011). Matrix degradation and deposition are dynamic processes to maintain tissue homeostasis, and their dysregulation may cause disease, such as fibrosis or non-healing wound. MMPs which can be secreted by fibroblasts and macrophages are the main regulator for proteolytic degradation of ECM (Lindner et al., 2012; Miteva et al., 2014). MMP production was found in Tenon's capsule fibroblasts during contraction in 3D collagen gel, and MMP inhibition reduced gel contraction (Daniels et al., 2003). Human peripheral blood-differentiated macrophages, upon co-incubation with human breast cancer cell line MCF-7 cells in transwell system, upregulate MMP2 and MMP9 gene expression in macrophages and result in secretion of these MMPs (Binder et al., 2004). We have not explored the involvement of MMPs in contraction of orbital fibroblasts or in fibroblast-macrophage co-culture system, and this can be investigated in future work for better understanding of macrophage-stimulated fibroblast contraction.

6.4 Conclusion and Future Work

This study gives new insights in the determinants of phenotype of orbital fibroblasts in TED. For the two main phenotypes, 1) adipogenesis, may not be classical adipogenesis in our model per se, and is likely mediated through inflammation by increasing PLIN2 expression, and 2) fibrosis as modeled with contraction, we showed that it is likely mediated by inflammation (macrophage) and mechanoregulation through MRTF/SRF. In summary, inflammation with cytokine increased PLIN2 level and LD formation, and promoted actin polymerisation and orbital fibroblasts contractility. Mechanotransduction was associated with orbital fibroblasts contractility, and since it was reported to be linked to LD accumulation, it could be involved in 3D spontaneous LD formation, although the mechanism with PLIN2 has not been characterised. We proposed a

model, in which inflammation is the initiator and mechanotransduction is the mediator, for both LD formation and contractility phenotypes of orbital fibroblasts in TED (**Figure 6.1**).

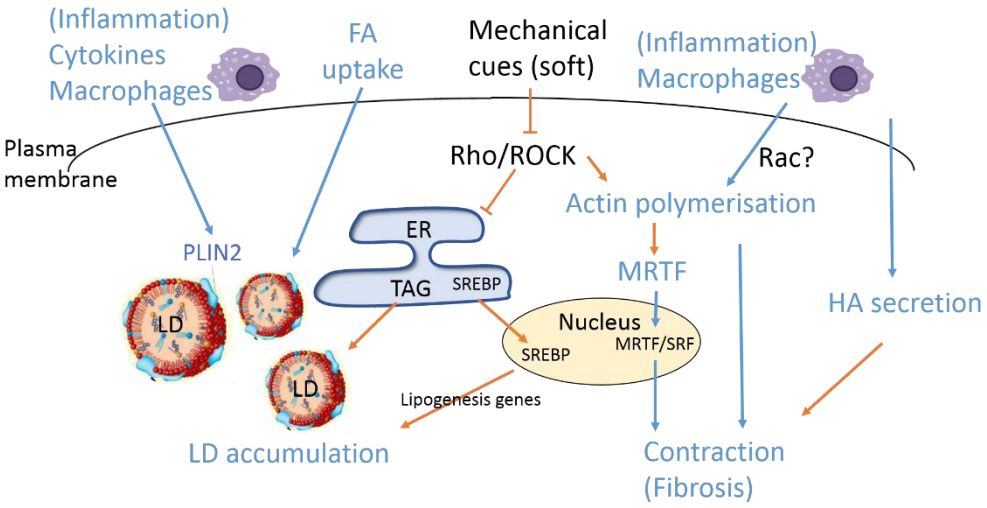

Figure 6.1 Proposed model for regulation of TED phenotype in orbital fibroblasts.

Cytokines and macrophages upregulate PLIN2 expression and increase LD accumulation which is also linked to FA uptake. MRTF which is known regulated by actin polymerisation mediates contractility. Macrophages stimulate contractility by promoting actin polymerisation, and promote HA production which can be linked to fibrosis as well. It has been reported that soft matrix inhibits Rho/ROCK signalling and translocates SREBP to nucleus to regulate lipid related genes and LD formation (Romani et al., 2019), whereas Rho/ROCK activation promotes actin polymerisation in stiff matrix. LD accumulation and contraction are divergent signalling in response to matrix stiffness or stimulants. (Blue arrows indicate pathways tested in this study. Orange arrows indicate the related published pathways which can be investigated in future work.) LDs element adapted from (Guo et al., 2009)

Future work can be directed towards

- To understand which receptor/signalling mediates upregulation of PLIN2 in orbital fibroblasts
    - The characteristic TSHR? or IGF-1R?
- To understand if lipogenic genes are involved in linking PLIN2 to LD formation
    - The gene expression levels of SREBPs and their target genes in TED and control cells, in 2D and 3D
- To clarify the relationship among PLIN2, lipases (ATGL, HSL), lipolysis, and proteasome degradation of PLIN2 on LD formation (as **Figure 4.23**)
    - Does the attenuation of proteasome degradation activity accompany the upregulation of PLIN2 level and more LD formation?
    - Do lipolysis activity and levels of lipases antagonise PLIN2 level?
    - Are lipases (ATGL, HSL) and PLIN2 both localised on LDs and with mutual exclusion effect?

Bibliography

Abdelmagid, S.A., S.E. Clarke, D.E. Nielsen, A. Badawi, A. El-Sohemy, D.M. Mutch, and D.W.L. Ma. 2015. Comprehensive profiling of plasma fatty acid concentrations in young healthy Canadian adults. *PloS one*. 10:e0116195-e0116195.

Aderem, A., and D.M. Underhill. 1999. Mechanisms of phagocytosis in macrophages. *Annu Rev Immunol*. 17:593-623.

Ahmad, M. 2017. Fatty Acids: Chemistry, Synthesis, and Applications. Academic Press and AOCS Press.

Aki, S., K. Yoshioka, Y. Okamoto, N. Takuwa, and Y. Takuwa. 2015. Phosphatidylinositol 3-kinase class II alpha-isoform PI3K-C2alpha is required for transforming growth factor beta-induced Smad signaling in endothelial cells. *J Biol Chem*. 290:6086-6105.

Albeiroti, S., A. Soroosh, and C.A. de la Motte. 2015. Hyaluronan's Role in Fibrosis: A Pathogenic Factor or a Passive Player? *Biomed Res Int*. 2015:790203.

Alfaro, I.E., A. Albornoz, A. Molina, J. Moreno, K. Cordero, A. Criollo, and M. Budini. 2018. Chaperone Mediated Autophagy in the Crosstalk of Neurodegenerative Diseases and Metabolic Disorders. *Front Endocrinol (Lausanne)*. 9:778.

ALJohani, A.M., D.N. Syed, and J.M. Ntambi. 2017. Insights into Stearoyl-CoA Desaturase-1 Regulation of Systemic Metabolism. *Trends Endocrinol Metab*. 28:831-842.

Ameer, F., L. Scandiuzzi, S. Hasnain, H. Kalbacher, and N. Zaidi. 2014. De novo lipogenesis in health and disease. *Metabolism*. 63:895-902.

Anderson, C.M., and A. Stahl. 2013. SLC27 fatty acid transport proteins. *Mol Aspects Med*. 34:516-528.

Anderson, N., and J. Borlak. 2008. Molecular mechanisms and therapeutic targets in steatosis and steatohepatitis. *Pharmacol Rev*. 60:311-357.

Anolik, J., I. Sanz, and R.J. Looney. 2003. B cell depletion therapy in systemic lupus erythematosus. *Curr Rheumatol Rep*. 5:350-356.

Arango Duque, G., and A. Descoteaux. 2014. Macrophage cytokines: involvement in immunity and infectious diseases. *Front Immunol*. 5:491.

Ataie-Kachoie, P., S. Badar, D.L. Morris, and M.H. Pourgholami. 2013. Minocycline Targets the NF-κB Nexus through Suppression of TGF-β1-TAK1-IκB Signaling in Ovarian Cancer. *Molecular Cancer Research*. 11:1279.

Atri, C., F.Z. Guerfali, and D. Laouini. 2018. Role of Human Macrophage Polarization in Inflammation during Infectious Diseases. *International journal of molecular sciences*. 19:1801.

Attie, A.D., R.M. Krauss, M.P. Gray-Keller, A. Brownlie, M. Miyazaki, J.J. Kastelein, A.J. Lusis, A.F. Stalenhoef, J.P. Stoehr, M.R. Hayden, and J.M. Ntambi. 2002. Relationship between stearoyl-CoA desaturase activity and plasma triglycerides in human and mouse hypertriglyceridemia. *J Lipid Res*. 43:1899-1907.

Azzazy, H.M., M.M. Pelsers, and R.H. Christenson. 2006. Unbound free fatty acids and heart-type fatty acid-binding protein: diagnostic assays and clinical applications. *Clin Chem*. 52:19-29.

Bahn, R.S. 2010. Graves' ophthalmopathy. *N Engl J Med*. 362:726-738.

Banga, J.P., S. Moshkelgosha, U. Berchner-Pfannschmidt, and A. Eckstein. 2015. Modeling Graves' Orbitopathy in Experimental Graves' Disease. *Horm Metab Res*. 47:797-803.

Bartalena, L., L. Baldeschi, A.J. Dickinson, A. Eckstein, P. Kendall-Taylor, C. Marcocci, M.P. Mourits, P. Perros, K. Boboridis, A. Boschi, N. Curro, C. Daumerie, G.J. Kahaly, G. Krassas, C.M. Lane, J.H. Lazarus, M. Marino, M. Nardi, C. Neoh, J. Orgiazzi, S. Pearce, A. Pinchera, S. Pitz, M. Salvi, P. Sivelli, M. Stahl, G. von Arx, and W.M. Wiersinga. 2008. Consensus statement of the European group on Graves' orbitopathy (EUGOGO) on management of Graves' orbitopathy. *Thyroid*. 18:333-346.

Bartley, G.B. 1994. The epidemiologic characteristics and clinical course of ophthalmopathy associated with autoimmune thyroid disease in Olmsted County, Minnesota. *Trans Am Ophthalmol Soc*. 92:477-588.

Bastiani, M., and R.G. Parton. 2010. Caveolae at a glance. *Journal of Cell Science*. 123:3831.

Basu, S., N.F. Totty, M.S. Irwin, M. Sudol, and J. Downward. 2003. Akt phosphorylates the Yes-associated protein, YAP, to induce interaction with 14-3-3 and attenuation of p73-mediated apoptosis. *Mol Cell*. 11:11-23.

Belfrage, P., G. Fredrikson, N.O. Nilsson, and P. Stralfors. 1981. Regulation of adipose-tissue lipolysis by phosphorylation of hormone-sensitive lipase. *Int J Obes*. 5:635-641.

Bensaad, K., E. Favaro, C.A. Lewis, B. Peck, S. Lord, J.M. Collins, K.E. Pinnick, S. Wigfield, F.M. Buffa, J.L. Li, Q. Zhang, M.J.O. Wakelam, F. Karpe, A. Schulze, and A.L. Harris. 2014. Fatty acid uptake and lipid storage induced by HIF-1alpha contribute to cell growth and survival after hypoxia-reoxygenation. *Cell Rep*. 9:349-365.

Benvenuti, S., I. Cellai, P. Luciani, C. Deledda, S. Baglioni, C. Giuliani, R. Saccardi, B. Mazzanti, S. Dal Pozzo, E. Mannucci, A. Peri, and M. Serio. 2007. Rosiglitazone stimulates adipogenesis and decreases osteoblastogenesis in human mesenchymal stem cells. *J Endocrinol Invest*. 30:RC26-30.

Berchner-Pfannschmidt, U., S. Moshkelgosha, S. Diaz-Cano, B. Edelmann, G.E. Gortz, M. Horstmann, A. Noble, W. Hansen, A. Eckstein, and J.P. Banga. 2016. Comparative Assessment of Female Mouse Model of Graves' Orbitopathy Under Different Environments, Accompanied by Proinflammatory Cytokine and T-Cell Responses to Thyrotropin Hormone Receptor Antigen. *Endocrinology*. 157:1673-1682.

Biernacka, A., M. Dobaczewski, and N.G. Frangogiannis. 2011. TGF-beta signaling in fibrosis. *Growth factors (Chur, Switzerland)*. 29:196-202.

Binder, C., F.R. Balkwill, L. Trümper, M. Schulz, S.C. Robinson, and T. Hagemann. 2004. Enhanced invasiveness of breast cancer cell lines upon co-cultivation with macrophages is due to TNF-α dependent up-regulation of matrix metalloproteases. *Carcinogenesis*. 25:1543-1549.

Blanchette-Mackie, E.J., N.K. Dwyer, T. Barber, R.A. Coxey, T. Takeda, C.M. Rondinone, J.L. Theodorakis, A.S. Greenberg, and C. Londos. 1995. Perilipin is located on the surface layer of intracellular lipid droplets in adipocytes. *J Lipid Res*. 36:1211-1226.

Brandau, S., K. Bruderek, K. Hestermann, G.E. Gortz, M. Horstmann, S. Mattheis, S. Lang, A. Eckstein, and U. Berchner-Pfannschmidt. 2015. Orbital Fibroblasts From Graves' Orbitopathy Patients Share Functional

and Immunophenotypic Properties With Mesenchymal Stem/Stromal Cells. *Invest Ophthalmol Vis Sci*. 56:6549-6557.
Brasaemle, D.L. 2007. Thematic review series: adipocyte biology. The perilipin family of structural lipid droplet proteins: stabilization of lipid droplets and control of lipolysis. *J Lipid Res*. 48:2547-2559.
Brown, R.A., R. Prajapati, D.A. McGrouther, I.V. Yannas, and M. Eastwood. 1998. Tensional homeostasis in dermal fibroblasts: mechanical responses to mechanical loading in three-dimensional substrates. *Journal of cellular physiology*. 175:323-332.
Buechler, C., S. Krautbauer, and K. Eisinger. 2015. Adipose tissue fibrosis. *World journal of diabetes*. 6:548-553.
Butcher, D.T., T. Alliston, and V.M. Weaver. 2009. A tense situation: forcing tumour progression. *Nat Rev Cancer*. 9:108-122.
Calder, P.C. 2015. Functional Roles of Fatty Acids and Their Effects on Human Health. *JPEN. Journal of parenteral and enteral nutrition*. 39:18s-32s.
Campa, C.C., E. Ciraolo, A. Ghigo, G. Germena, and E. Hirsch. 2015. Crossroads of PI3K and Rac pathways. *Small GTPases*. 6:71-80.
Campos, S.B., S.L. Ashworth, S. Wean, M. Hosford, R.M. Sandoval, M.A. Hallett, S.J. Atkinson, and B.A. Molitoris. 2009. Cytokine-induced F-actin reorganization in endothelial cells involves RhoA activation. *American journal of physiology. Renal physiology*. 296:F487-F495.
Cao, H.J., H.S. Wang, Y. Zhang, H.Y. Lin, R.P. Phipps, and T.J. Smith. 1998. Activation of human orbital fibroblasts through CD40 engagement results in a dramatic induction of hyaluronan synthesis and prostaglandin endoperoxide H synthase-2 expression. Insights into potential pathogenic mechanisms of thyroid-associated ophthalmopathy. *J Biol Chem*. 273:29615-29625.
Carr, R.M., G. Peralta, X. Yin, and R.S. Ahima. 2014. Absence of perilipin 2 prevents hepatic steatosis, glucose intolerance and ceramide accumulation in alcohol-fed mice. *PLoS One*. 9:e97118.
Cawthorn, W.P., E.L. Scheller, and O.A. MacDougald. 2012. Adipose tissue stem cells meet preadipocyte commitment: going back to the future. *Journal of lipid research*. 53:227-246.
Cen, B., A. Selvaraj, R.C. Burgess, J.K. Hitzler, Z. Ma, S.W. Morris, and R. Prywes. 2003. Megakaryoblastic Leukemia 1, a Potent Transcriptional Coactivator for Serum Response Factor (SRF), Is Required for Serum Induction of SRF Target Genes. *Molecular and Cellular Biology*. 23:6597.
Chang, B.H., L. Li, A. Paul, S. Taniguchi, V. Nannegari, W.C. Heird, and L. Chan. 2006. Protection against fatty liver but normal adipogenesis in mice lacking adipose differentiation-related protein. *Mol Cell Biol*. 26:1063-1076.
Chanput, W., J.J. Mes, H.F. Savelkoul, and H.J. Wichers. 2013. Characterization of polarized THP-1 macrophages and polarizing ability of LPS and food compounds. *Food Funct*. 4:266-276.
Chen, C.S. 2008. Mechanotransduction - a field pulling together? *J Cell Sci*. 121:3285-3292.
Chen, M.H., S.L. Liao, T.C. Chang, and L.M. Chuang. 2008. Role of macrophage infiltration in the orbital fat of patients with Graves' ophthalmopathy. *Clin Endocrinol (Oxf)*. 69:332-337.
Chen, S.Z., L.F. Ning, X. Xu, W.Y. Jiang, C. Xing, W.P. Jia, X.L. Chen, Q.Q. Tang, and H.Y. Huang. 2016. The miR-181d-regulated

metalloproteinase Adamts1 enzymatically impairs adipogenesis via ECM remodeling. *Cell Death And Differentiation*. 23:1778.
Chen, Y., and P. Li. 2016. Fatty acid metabolism and cancer development. *Science Bulletin*. 61:1473-1479.
Cheng, H., J. Luan, D. Mu, Q. Wang, J. Qi, Z. Li, and S. Fu. 2019. M1/M2 Macrophages Play Different Roles in Adipogenic Differentiation of PDGFRalpha(+) Preadipocytes In Vitro. *Aesthetic plastic surgery*. 43:514-520.
Chiu, H.C., A. Kovacs, R.M. Blanton, X. Han, M. Courtois, C.J. Weinheimer, K.A. Yamada, S. Brunet, H. Xu, J.M. Nerbonne, M.J. Welch, N.M. Fettig, T.L. Sharp, N. Sambandam, K.M. Olson, D.S. Ory, and J.E. Schaffer. 2005. Transgenic expression of fatty acid transport protein 1 in the heart causes lipotoxic cardiomyopathy. *Circ Res*. 96:225-233.
Chung, S.A., B.K. Jeon, Y.-H. Choi, K.O. Back, J.B. Lee, and K.H. Kook. 2014. Pirfenidone Attenuates the IL-1β–Induced Hyaluronic Acid Increase in Orbital Fibroblasts From Patients With Thyroid-Associated OphthalmopathyPirfenidone Decreases Hyaluronic Acid. *Investigative Ophthalmology & Visual Science*. 55:2276-2283.
Cinti, S., G. Mitchell, G. Barbatelli, I. Murano, E. Ceresi, E. Faloia, S. Wang, M. Fortier, A.S. Greenberg, and M.S. Obin. 2005. Adipocyte death defines macrophage localization and function in adipose tissue of obese mice and humans. *J Lipid Res*. 46:2347-2355.
Clifford, G.M., C. Londos, F.B. Kraemer, R.G. Vernon, and S.J. Yeaman. 2000. Translocation of hormone-sensitive lipase and perilipin upon lipolytic stimulation of rat adipocytes. *J Biol Chem*. 275:5011-5015.
Codelia, V.A., G. Sun, and K.D. Irvine. 2014. Regulation of YAP by mechanical strain through Jnk and Hippo signaling. *Current biology : CB*. 24:2012-2017.
Contador, D., F. Ezquer, M. Espinosa, M. Arango-Rodriguez, C. Puebla, L. Sobrevia, and P. Conget. 2015. Dexamethasone and rosiglitazone are sufficient and necessary for producing functional adipocytes from mesenchymal stem cells. *Exp Biol Med (Maywood)*. 240:1235-1246.
Conte, E., M. Fruciano, E. Fagone, E. Gili, F. Caraci, M. Iemmolo, N. Crimi, and C. Vancheri. 2011. Inhibition of PI3K prevents the proliferation and differentiation of human lung fibroblasts into myofibroblasts: the role of class I P110 isoforms. *PLoS One*. 6:e24663.
Crisan, M., S. Yap, L. Casteilla, C.W. Chen, M. Corselli, T.S. Park, G. Andriolo, B. Sun, B. Zheng, L. Zhang, C. Norotte, P.N. Teng, J. Traas, R. Schugar, B.M. Deasy, S. Badylak, H.J. Buhring, J.P. Giacobino, L. Lazzari, J. Huard, and B. Peault. 2008. A perivascular origin for mesenchymal stem cells in multiple human organs. *Cell stem cell*. 3:301-313.
Cristancho, A.G., and M.A. Lazar. 2011. Forming functional fat: a growing understanding of adipocyte differentiation. *Nat Rev Mol Cell Biol*. 12:722-734.
Cushman, S.W., and L.J. Wardzala. 1980. Potential mechanism of insulin action on glucose transport in the isolated rat adipose cell. Apparent translocation of intracellular transport systems to the plasma membrane. *J Biol Chem*. 255:4758-4762.
Dahlmann-Noor, A.H., B. Martin-Martin, M. Eastwood, P.T. Khaw, and M. Bailly. 2007. Dynamic protrusive cell behaviour generates force and drives early matrix contraction by fibroblasts. *Experimental cell research*. 313:4158-4169.

Daley, W.P., S.B. Peters, and M. Larsen. 2008. Extracellular matrix dynamics in development and regenerative medicine. *J Cell Sci*. 121:255-264.
Dallon, J.C., and H.P. Ehrlich. 2008. A review of fibroblast-populated collagen lattices. *Wound repair and regeneration : official publication of the Wound Healing Society [and] the European Tissue Repair Society*. 16:472-479.
Damiano, F., A. Rochira, A. Gnoni, and L. Siculella. 2017. Action of Thyroid Hormones, T3 and T2, on Hepatic Fatty Acids: Differences in Metabolic Effects and Molecular Mechanisms. *International journal of molecular sciences*. 18.
Daniels, J.T., A.D. Cambrey, N.L. Occleston, Q. Garrett, R.W. Tarnuzzer, G.S. Schultz, and P.T. Khaw. 2003. Matrix Metalloproteinase Inhibition Modulates Fibroblast-Mediated Matrix Contraction and Collagen Production In Vitro. *Investigative Ophthalmology & Visual Science*. 44:1104-1110.
Das, A., R.S. Fischer, D. Pan, and C.M. Waterman. 2016. YAP Nuclear Localization in the Absence of Cell-Cell Contact Is Mediated by a Filamentous Actin-dependent, Myosin II- and Phospho-YAP-independent Pathway during Extracellular Matrix Mechanosensing. *J Biol Chem*. 291:6096-6110.
Davis, M.M., J.J. Boniface, Z. Reich, D. Lyons, J. Hampl, B. Arden, and Y. Chien. 1998. Ligand recognition by alpha beta T cell receptors. *Annu Rev Immunol*. 16:523-544.
Denu, R.A., S. Nemcek, D.D. Bloom, A.D. Goodrich, J. Kim, D.F. Mosher, and P. Hematti. 2016. Fibroblasts and Mesenchymal Stromal/Stem Cells Are Phenotypically Indistinguishable. *Acta Haematologica*. 136:85-97.
Di Pietro, N., V. Panel, S. Hayes, A. Bagattin, S. Meruvu, A. Pandolfi, L. Hugendubler, G. Fejes-Tóth, A. Naray-Fejes-Tóth, and E. Mueller. 2010. Serum- and glucocorticoid-inducible kinase 1 (SGK1) regulates adipocyte differentiation via forkhead box O1. *Molecular endocrinology (Baltimore, Md.)*. 24:370-380.
Digel, M., R. Ehehalt, W. Stremmel, and J. Fullekrug. 2009. Acyl-CoA synthetases: fatty acid uptake and metabolic channeling. *Molecular and cellular biochemistry*. 326:23-28.
Dik, W.A., S. Virakul, and L. van Steensel. 2016. Current perspectives on the role of orbital fibroblasts in the pathogenesis of Graves' ophthalmopathy. *Exp Eye Res*. 142:83-91.
Dupont, S., L. Morsut, M. Aragona, E. Enzo, S. Giulitti, M. Cordenonsi, F. Zanconato, J. Le Digabel, M. Forcato, S. Bicciato, N. Elvassore, and S. Piccolo. 2011. Role of YAP/TAZ in mechanotransduction. *Nature*. 474:179-183.
Echarri, A., and M.A. Del Pozo. 2015. Caveolae - mechanosensitive membrane invaginations linked to actin filaments. *J Cell Sci*. 128:2747-2758.
Eckstein, A.K., B. Quadbeck, S. Tews, K. Mann, C. Kruger, C.H. Mohr, K.P. Steuhl, J. Esser, and R.K. Gieseler. 2004. Thyroid associated ophthalmopathy: evidence for CD4(+) gammadelta T cells; de novo differentiation of RFD7(+) macrophages, but not of RFD1(+) dendritic cells; and loss of gammadelta and alphabeta T cell receptor expression. *Br J Ophthalmol*. 88:803-808.
Eddy, R.J., J.A. Petro, and J.J. Tomasek. 1988. Evidence for the nonmuscle nature of the "myofibroblast" of granulation tissue and hypertropic scar. An immunofluorescence study. *Am J Pathol*. 130:252-260.

Edmondson, R., J.J. Broglie, A.F. Adcock, and L. Yang. 2014. Three-dimensional cell culture systems and their applications in drug discovery and cell-based biosensors. *Assay and drug development technologies*. 12:207-218.

Engler, A.J., S. Sen, H.L. Sweeney, and D.E. Discher. 2006. Matrix elasticity directs stem cell lineage specification. *Cell*. 126:677-689.

Esnault, C., A. Stewart, F. Gualdrini, P. East, S. Horswell, N. Matthews, and R. Treisman. 2014. Rho-actin signaling to the MRTF coactivators dominates the immediate transcriptional response to serum in fibroblasts. *Genes & Development*. 28:943-958.

Evans, R.A., Y.C. Tian, R. Steadman, and A.O. Phillips. 2003. TGF-beta1-mediated fibroblast-myofibroblast terminal differentiation-the role of Smad proteins. *Experimental cell research*. 282:90-100.

Evelyn, C.R., E.M. Lisabeth, S.M. Wade, A.J. Haak, C.N. Johnson, E.R. Lawlor, and R.R. Neubig. 2016. Small-Molecule Inhibition of Rho/MKL/SRF Transcription in Prostate Cancer Cells: Modulation of Cell Cycle, ER Stress, and Metastasis Gene Networks. *Microarrays (Basel, Switzerland)*. 5.

Ezra, D.G., J.S. Ellis, M. Beaconsfield, R. Collin, and M. Bailly. 2010. Changes in fibroblast mechanostat set point and mechanosensitivity: an adaptive response to mechanical stress in floppy eyelid syndrome. *Invest Ophthalmol Vis Sci*. 51:3853-3863.

Fajas, L., K. Schoonjans, L. Gelman, J.B. Kim, J. Najib, G. Martin, J.C. Fruchart, M. Briggs, B.M. Spiegelman, and J. Auwerx. 1999. Regulation of peroxisome proliferator-activated receptor gamma expression by adipocyte differentiation and determination factor 1/sterol regulatory element binding protein 1: implications for adipocyte differentiation and metabolism. *Mol Cell Biol*. 19:5495-5503.

Febbraio, M., N.A. Abumrad, D.P. Hajjar, K. Sharma, W. Cheng, S.F. Pearce, and R.L. Silverstein. 1999. A null mutation in murine CD36 reveals an important role in fatty acid and lipoprotein metabolism. *J Biol Chem*. 274:19055-19062.

Feldon, S.E., D.J. Park, C.W. O'Loughlin, V.T. Nguyen, S. Landskroner-Eiger, D. Chang, T.H. Thatcher, and R.P. Phipps. 2005. Autologous T-lymphocytes stimulate proliferation of orbital fibroblasts derived from patients with Graves' ophthalmopathy. *Invest Ophthalmol Vis Sci*. 46:3913-3921.

Feng, T., E. Szabo, E. Dziak, and M. Opas. 2010. Cytoskeletal disassembly and cell rounding promotes adipogenesis from ES cells. *Stem cell reviews*. 6:74-85.

Feng, Y.Z., J. Lund, Y. Li, I.K. Knabenes, S.S. Bakke, E.T. Kase, Y.K. Lee, A.R. Kimmel, G.H. Thoresen, A.C. Rustan, and K.T. Dalen. 2017. Loss of perilipin 2 in cultured myotubes enhances lipolysis and redirects the metabolic energy balance from glucose oxidation towards fatty acid oxidation. *J Lipid Res*. 58:2147-2161.

Fernandez, M.A., C. Albor, M. Ingelmo-Torres, S.J. Nixon, C. Ferguson, T. Kurzchalia, F. Tebar, C. Enrich, R.G. Parton, and A. Pol. 2006. Caveolin-1 is essential for liver regeneration. *Science*. 313:1628-1632.

Fielding, C.J., and P.E. Fielding. 2000. Cholesterol and caveolae: structural and functional relationships. *Biochim Biophys Acta*. 1529:210-222.

Finch-Edmondson, M., and M. Sudol. 2016. Framework to function: mechanosensitive regulators of gene transcription. *Cellular & molecular biology letters*. 21:28.

Fletcher, D.A., and R.D. Mullins. 2010. Cell mechanics and the cytoskeleton. *Nature*. 463:485-492.
Flowers, M.T., and J.M. Ntambi. 2008. Role of stearoyl-coenzyme A desaturase in regulating lipid metabolism. *Curr Opin Lipidol*. 19:248-256.
Fonseca-Alaniz, M.H., J. Takada, M.I. Alonso-Vale, and F.B. Lima. 2007. Adipose tissue as an endocrine organ: from theory to practice. *J Pediatr (Rio J)*. 83:S192-203.
Forster, G., E. Otto, C. Hansen, K. Ochs, and G. Kahaly. 1998. Analysis of orbital T cells in thyroid-associated ophthalmopathy. *Clin Exp Immunol*. 112:427-434.
Frackelton, A.R., Jr., P.A. Gruppuso, C.M. Boney, and R.A. Faris. 2000. The Critical Role of Shc in Insulin-Like Growth Factor-I-Mediated Mitogenesis and Differentiation in 3T3-L1 Preadipocytes. *Molecular Endocrinology*. 14:805-813.
Frayn, K.N., P. Arner, and H. Yki-Jarvinen. 2006. Fatty acid metabolism in adipose tissue, muscle and liver in health and disease. *Essays Biochem*. 42:89-103.
Fujimori, K., M. Yano, and T. Ueno. 2012. Synergistic suppression of early phase of adipogenesis by microsomal PGE synthase-1 (PTGES1)-produced PGE2 and aldo-keto reductase 1B3-produced PGF2α. *PloS one*. 7:e44698-e44698.
Fujimoto, T., Y. Ohsaki, J. Cheng, M. Suzuki, and Y. Shinohara. 2008. Lipid droplets: a classic organelle with new outfits. *Histochem Cell Biol*. 130:263-279.
Gao, H., F. Volat, L. Sandhow, J. Galitzky, T. Nguyen, D. Esteve, G. Astrom, N. Mejhert, S. Ledoux, C. Thalamas, P. Arner, J.C. Guillemot, H. Qian, M. Ryden, and A. Bouloumie. 2017. CD36 Is a Marker of Human Adipocyte Progenitors with Pronounced Adipogenic and Triglyceride Accumulation Potential. *Stem Cells*. 35:1799-1814.
Genin, M., F. Clement, A. Fattaccioli, M. Raes, and C. Michiels. 2015. M1 and M2 macrophages derived from THP-1 cells differentially modulate the response of cancer cells to etoposide. *BMC Cancer*. 15:577.
Giannandrea, M., and W.C. Parks. 2014. Diverse functions of matrix metalloproteinases during fibrosis. *Dis Model Mech*. 7:193-203.
Glatz, J.F., J.J. Luiken, and A. Bonen. 2010. Membrane fatty acid transporters as regulators of lipid metabolism: implications for metabolic disease. *Physiol Rev*. 90:367-417.
Glatz, J.F.C., and J. Luiken. 2018. Dynamic role of the transmembrane glycoprotein CD36 (SR-B2) in cellular fatty acid uptake and utilization. *J Lipid Res*. 59:1084-1093.
Goodman, J.M. 2008. The gregarious lipid droplet. *J Biol Chem*. 283:28005-28009.
Gortz, G.E., S. Moshkelgosha, C. Jesenek, B. Edelmann, M. Horstmann, J.P. Banga, A. Eckstein, and U. Berchner-Pfannschmidt. 2016. Pathogenic Phenotype of Adipogenesis and Hyaluronan in Orbital Fibroblasts From Female Graves' Orbitopathy Mouse Model. *Endocrinology*. 157:3771-3778.
Greenberg, A.S., J.J. Egan, S.A. Wek, N.B. Garty, E.J. Blanchette-Mackie, and C. Londos. 1991. Perilipin, a major hormonally regulated adipocyte-specific phosphoprotein associated with the periphery of lipid storage droplets. *J Biol Chem*. 266:11341-11346.
Gregoire, F., N. De Broux, N. Hauser, H. Heremans, J. Van Damme, and C. Remacle. 1992. Interferon-gamma and interleukin-1 beta inhibit

adipoconversion in cultured rodent preadipocytes. *Journal of cellular physiology*. 151:300-309.
Gressner, O.A., and A.M. Gressner. 2008. Connective tissue growth factor: a fibrogenic master switch in fibrotic liver diseases. *Liver Int*. 28:1065-1079.
Grinnell, F. 1994. Fibroblasts, myofibroblasts, and wound contraction. *J Cell Biol*. 124:401-404.
Grubeck-Loebenstein, B., K. Trieb, A. Sztankay, W. Holter, H. Anderl, and G. Wick. 1994. Retrobulbar T cells from patients with Graves' ophthalmopathy are CD8+ and specifically recognize autologous fibroblasts. *J Clin Invest*. 93:2738-2743.
Gu, J.-Q., S. Ikuyama, P. Wei, B. Fan, J.-i. Oyama, T. Inoguchi, and J. Nishimura. 2008a. Pycnogenol, an extract from French maritime pine, suppresses Toll-like receptor 4-mediated expression of adipose differentiation-related protein in macrophages. *American Journal of Physiology-Endocrinology and Metabolism*. 295:E1390-E1400.
Gu, J.Q., S. Ikuyama, P. Wei, B. Fan, J. Oyama, T. Inoguchi, and J. Nishimura. 2008b. Pycnogenol, an extract from French maritime pine, suppresses Toll-like receptor 4-mediated expression of adipose differentiation-related protein in macrophages. *Am J Physiol Endocrinol Metab*. 295:E1390-1400.
Gualdrini, F., C. Esnault, S. Horswell, A. Stewart, N. Matthews, and R. Treisman. 2016. SRF Co-factors Control the Balance between Cell Proliferation and Contractility. *Mol Cell*. 64:1048-1061.
Guettler, S., M.K. Vartiainen, F. Miralles, B. Larijani, and R. Treisman. 2008. RPEL Motifs Link the Serum Response Factor Cofactor MAL but Not Myocardin to Rho Signaling via Actin Binding. *Molecular and Cellular Biology*. 28:732.
Guo, Y., K.R. Cordes, R.V. Farese, Jr., and T.C. Walther. 2009. Lipid droplets at a glance. *J Cell Sci*. 122:749-752.
Haak, A.J., K.M. Appleton, E.M. Lisabeth, S.A. Misek, Y. Ji, S.M. Wade, J.L. Bell, C.E. Rockwell, M. Airik, M.A. Krook, S.D. Larsen, M. Verhaegen, E.R. Lawlor, and R.R. Neubig. 2017. Pharmacological Inhibition of Myocardin-related Transcription Factor Pathway Blocks Lung Metastases of RhoC-Overexpressing Melanoma. *Molecular cancer therapeutics*. 16:193-204.
Haak, A.J., P.S. Tsou, M.A. Amin, J.H. Ruth, P. Campbell, D.A. Fox, D. Khanna, S.D. Larsen, and R.R. Neubig. 2014. Targeting the myofibroblast genetic switch: inhibitors of myocardin-related transcription factor/serum response factor-regulated gene transcription prevent fibrosis in a murine model of skin injury. *The Journal of pharmacology and experimental therapeutics*. 349:480-486.
Habets, D.D., W.A. Coumans, P.J. Voshol, M.A. den Boer, M. Febbraio, A. Bonen, J.F. Glatz, and J.J. Luiken. 2007. AMPK-mediated increase in myocardial long-chain fatty acid uptake critically depends on sarcolemmal CD36. *Biochem Biophys Res Commun*. 355:204-210.
Hagberg, C., A. Mehlem, A. Falkevall, L. Muhl, and U. Eriksson. 2013. Endothelial fatty acid transport: role of vascular endothelial growth factor B. *Physiology (Bethesda, Md.)*. 28:125-134.
Halder, G., S. Dupont, and S. Piccolo. 2012. Transduction of mechanical and cytoskeletal cues by YAP and TAZ. *Nat Rev Mol Cell Biol*. 13:591-600.
Hames, K.C., A. Vella, B.J. Kemp, and M.D. Jensen. 2014. Free Fatty Acid Uptake in Humans With CD36 Deficiency. *Diabetes*. 63:3606.

Han, J., and R.J. Kaufman. 2016. The role of ER stress in lipid metabolism and lipotoxicity. *J Lipid Res*. 57:1329-1338.
Hatch, G.M., A.J. Smith, F.Y. Xu, A.M. Hall, and D.A. Bernlohr. 2002. FATP1 channels exogenous FA into 1,2,3-triacyl-sn-glycerol and down-regulates sphingomyelin and cholesterol metabolism in growing 293 cells. *J Lipid Res*. 43:1380-1389.
He, H., F. Du, Y. He, Z. Wei, C. Meng, Y. Xu, H. Zhou, N. Wang, X.G. Luo, W. Ma, and T.C. Zhang. 2018. The Wnt-beta-catenin signaling regulated MRTF-A transcription to activate migration-related genes in human breast cancer cells. *Oncotarget*. 9:15239-15251.
Heufelder, A.E., and R.S. Bahn. 1993. Detection and localization of cytokine immunoreactivity in retro-ocular connective tissue in Graves' ophthalmopathy. *Eur J Clin Invest*. 23:10-17.
Hinz, B., G. Celetta, J.J. Tomasek, G. Gabbiani, and C. Chaponnier. 2001. Alpha-smooth muscle actin expression upregulates fibroblast contractile activity. *Mol Biol Cell*. 12:2730-2741.
Hinz, B., S.H. Phan, V.J. Thannickal, A. Galli, M.L. Bochaton-Piallat, and G. Gabbiani. 2007. The myofibroblast: one function, multiple origins. *Am J Pathol*. 170:1807-1816.
Hipskind, R.A., D. Buscher, A. Nordheim, and M. Baccarini. 1994. Ras/MAP kinase-dependent and -independent signaling pathways target distinct ternary complex factors. *Genes Dev*. 8:1803-1816.
Hirsch, J., S.K. Fried, N.K. Edens, and R.L. Leibel. 1989. The fat cell. *Med Clin North Am*. 73:83-96.
Holds, J.B. 2011-2012. Orbit, Eyelids, and Lacrimal System. *In* Basic and Clinical Science Course. Vol. 7. American Academy of Ophthalmology.
Horton, J.D., J.L. Goldstein, and M.S. Brown. 2002. SREBPs: activators of the complete program of cholesterol and fatty acid synthesis in the liver. *J Clin Invest*. 109:1125-1131.
Horton, M.R., C.M. McKee, C. Bao, F. Liao, J.M. Farber, J. Hodge-DuFour, E. Pure, B.L. Oliver, T.M. Wright, and P.W. Noble. 1998. Hyaluronan fragments synergize with interferon-gamma to induce the C-X-C chemokines mig and interferon-inducible protein-10 in mouse macrophages. *J Biol Chem*. 273:35088-35094.
Hu, B., Z. Wu, and S.H. Phan. 2003. Smad3 mediates transforming growth factor-beta-induced alpha-smooth muscle actin expression. *Am J Respir Cell Mol Biol*. 29:397-404.
Huang, X., N. Yang, V.F. Fiore, T.H. Barker, Y. Sun, S.W. Morris, Q. Ding, V.J. Thannickal, and Y. Zhou. 2012. Matrix stiffness-induced myofibroblast differentiation is mediated by intrinsic mechanotransduction. *American journal of respiratory cell and molecular biology*. 47:340-348.
Huang, Y., S. Fang, D. Li, H. Zhou, B. Li, and X. Fan. 2019. The involvement of T cell pathogenesis in thyroid-associated ophthalmopathy. *Eye*. 33:176-182.
Huang, Y.M., P.C. Chang, S.B. Wu, H.C. Kau, C.C. Tsai, C.J. Liu, and Y.H. Wei. 2016. Expression and clinical significance of connective tissue growth factor (CTGF) in Graves' ophthalmopathy. *Br J Ophthalmol*.
Huebsch, N., P.R. Arany, A.S. Mao, D. Shvartsman, O.A. Ali, S.A. Bencherif, J. Rivera-Feliciano, and D.J. Mooney. 2010. Harnessing traction-mediated manipulation of the cell/matrix interface to control stem-cell fate. *Nat Mater*. 9:518-526.
Hufnagel, T.J., W.F. Hickey, W.H. Cobbs, F.A. Jakobiec, T. Iwamoto, and R.C. Eagle. 1984. Immunohistochemical and ultrastructural studies on the

exenterated orbital tissues of a patient with Graves' disease. *Ophthalmology*. 91:1411-1419.
Iizuka, K., R.K. Bruick, G. Liang, J.D. Horton, and K. Uyeda. 2004. Deficiency of carbohydrate response element-binding protein (ChREBP) reduces lipogenesis as well as glycolysis. *Proc Natl Acad Sci U S A*. 101:7281-7286.
Imamura, M., T. Inoguchi, S. Ikuyama, S. Taniguchi, K. Kobayashi, N. Nakashima, and H. Nawata. 2002. ADRP stimulates lipid accumulation and lipid droplet formation in murine fibroblasts. *Am J Physiol Endocrinol Metab*. 283:E775-783.
Itabe, H., T. Yamaguchi, S. Nimura, and N. Sasabe. 2017. Perilipins: a diversity of intracellular lipid droplet proteins. *Lipids in Health and Disease*. 16:83.
Iyer, S., and R. Bahn. 2012. Immunopathogenesis of Graves' ophthalmopathy: the role of the TSH receptor. *Best Pract Res Clin Endocrinol Metab*. 26:281-289.
Ji, H., H. Tang, H. Lin, J. Mao, L. Gao, J. Liu, and T. Wu. 2014. Rho/Rock cross-talks with transforming growth factor-beta/Smad pathway participates in lung fibroblast-myofibroblast differentiation. *Biomed Rep*. 2:787-792.
Jin, T., L. Li, R. Siow, and I.K.-K. Liu. 2016. Collagen matrix stiffness influences fibroblast contraction force. 047002 pp.
Johnson, L.A., E.S. Rodansky, A.J. Haak, S.D. Larsen, R.R. Neubig, and P.D.R. Higgins. 2014. Novel Rho/MRTF/SRF inhibitors block matrix-stiffness and TGF-β-induced fibrogenesis in human colonic myofibroblasts. *Inflammatory bowel diseases*. 20:154-165.
Jones, M., L. Tussey, N. Athanasou, and D.G. Jackson. 2000. Heparan sulfate proteoglycan isoforms of the CD44 hyaluronan receptor induced in human inflammatory macrophages can function as paracrine regulators of fibroblast growth factor action. *J Biol Chem*. 275:7964-7974.
Joshi, J., G. Mahajan, and C.R. Kothapalli. 2018. Three-dimensional collagenous niche and azacytidine selectively promote time-dependent cardiomyogenesis from human bone marrow-derived MSC spheroids. *Biotechnology and Bioengineering*. 115:2013-2026.
Kölsch, V., P.G. Charest, and R.A. Firtel. 2008. The regulation of cell motility and chemotaxis by phospholipid signaling. *Journal of Cell Science*. 121:551.
Kaback, L.A., and T.J. Smith. 1999. Expression of hyaluronan synthase messenger ribonucleic acids and their induction by interleukin-1beta in human orbital fibroblasts: potential insight into the molecular pathogenesis of thyroid-associated ophthalmopathy. *J Clin Endocrinol Metab*. 84:4079-4084.
Kaushik, S., and A.M. Cuervo. 2015. Degradation of lipid droplet-associated proteins by chaperone-mediated autophagy facilitates lipolysis. *Nat Cell Biol*. 17:759-770.
Kaushik, S., and A.M. Cuervo. 2016. AMPK-dependent phosphorylation of lipid droplet protein PLIN2 triggers its degradation by CMA. *Autophagy*. 12:432-438.
Kawamura, M., D.F. Jensen, E.V. Wancewicz, L.L. Joy, J.C. Khoo, and D. Steinberg. 1981. Hormone-sensitive lipase in differentiated 3T3-L1 cells and its activation by cyclic AMP-dependent protein kinase. *Proc Natl Acad Sci U S A*. 78:732-736.
Kechagia, J.Z., D.G. Ezra, M.J. Burton, and M. Bailly. 2016. Fibroblasts profiling in scarring trachoma identifies IL-6 as a functional component of a

fibroblast-macrophage pro-fibrotic and pro-inflammatory feedback loop. *Sci Rep*. 6:28261.
Kennedy, C.I., R.F. Diegelmann, J.H. Haynes, and D.R. Yager. 2000. Proinflammatory cytokines differentially regulate hyaluronan synthase isoforms in fetal and adult fibroblasts. *Journal of Pediatric Surgery*. 35:874-879.
Kim, J.B., P. Sarraf, M. Wright, K.M. Yao, E. Mueller, G. Solanes, B.B. Lowell, and B.M. Spiegelman. 1998a. Nutritional and insulin regulation of fatty acid synthetase and leptin gene expression through ADD1/SREBP1. *J Clin Invest*. 101:1-9.
Kim, J.B., H.M. Wright, M. Wright, and B.M. Spiegelman. 1998b. ADD1/SREBP1 activates PPARgamma through the production of endogenous ligand. *Proc Natl Acad Sci U S A*. 95:4333-4337.
Kim, T., D. Hwang, D. Lee, J.H. Kim, and S.Y. Kim. 2017. MRTF potentiates TEAD-YAP transcriptional activity causing metastasis. 36:520-535.
Knipe, R.S., A.M. Tager, and J.K. Liao. 2015. The Rho kinases: critical mediators of multiple profibrotic processes and rational targets for new therapies for pulmonary fibrosis. *Pharmacol Rev*. 67:103-117.
Koopman, R., G. Schaart, and M.K. Hesselink. 2001. Optimisation of oil red O staining permits combination with immunofluorescence and automated quantification of lipids. *Histochem Cell Biol*. 116:63-68.
Korducki, J.M., S.J. Loftus, and R.S. Bahn. 1992. Stimulation of glycosaminoglycan production in cultured human retroocular fibroblasts. *Invest Ophthalmol Vis Sci*. 33:2037-2042.
Kosteli, A., E. Sugaru, G. Haemmerle, J.F. Martin, J. Lei, R. Zechner, and A.W. Ferrante, Jr. 2010. Weight loss and lipolysis promote a dynamic immune response in murine adipose tissue. *J Clin Invest*. 120:3466-3479.
Koumas, L., T.J. Smith, S. Feldon, N. Blumberg, and R.P. Phipps. 2003. Thy-1 expression in human fibroblast subsets defines myofibroblastic or lipofibroblastic phenotypes. *Am J Pathol*. 163:1291-1300.
Koumas, L., T.J. Smith, and R.P. Phipps. 2002. Fibroblast subsets in the human orbit: Thy-1+ and Thy-1- subpopulations exhibit distinct phenotypes. *European Journal of Immunology*. 32:477-485.
Kozdon, K., C. Fitchett, G.E. Rose, D.G. Ezra, and M. Bailly. 2015. Mesenchymal Stem Cell-Like Properties of Orbital Fibroblasts in Graves' Orbitopathy. *Invest Ophthalmol Vis Sci*. 56:5743-5750.
Krieger, C.C., S. Neumann, R.F. Place, B. Marcus-Samuels, and M.C. Gershengorn. 2015. Bidirectional TSH and IGF-1 receptor cross talk mediates stimulation of hyaluronan secretion by Graves' disease immunoglobins. *J Clin Endocrinol Metab*. 100:1071-1077.
Krieger, C.C., R.F. Place, C. Bevilacqua, B. Marcus-Samuels, B.S. Abel, M.C. Skarulis, G.J. Kahaly, S. Neumann, and M.C. Gershengorn. 2016. TSH/IGF-1 Receptor Cross Talk in Graves' Ophthalmopathy Pathogenesis. *J Clin Endocrinol Metab*. 101:2340-2347.
Kumar, S., and R.S. Bahn. 2003. Relative overexpression of macrophage-derived cytokines in orbital adipose tissue from patients with graves' ophthalmopathy. *J Clin Endocrinol Metab*. 88:4246-4250.
Kumar, S., M.J. Coenen, P.E. Scherer, and R.S. Bahn. 2004. Evidence for enhanced adipogenesis in the orbits of patients with Graves' ophthalmopathy. *J Clin Endocrinol Metab*. 89:930-935.
Kumar, S., S. Iyer, H. Bauer, M. Coenen, and R.S. Bahn. 2012. A stimulatory thyrotropin receptor antibody enhances hyaluronic acid synthesis in

graves' orbital fibroblasts: inhibition by an IGF-I receptor blocking antibody. *J Clin Endocrinol Metab*. 97:1681-1687.
Kumar, S., A. Leontovich, M.J. Coenen, and R.S. Bahn. 2005. Gene expression profiling of orbital adipose tissue from patients with Graves' ophthalmopathy: a potential role for secreted frizzled-related protein-1 in orbital adipogenesis. *J Clin Endocrinol Metab*. 90:4730-4735.
Lacasa, D., S. Taleb, M. Keophiphath, A. Miranville, and K. Clement. 2007. Macrophage-secreted factors impair human adipogenesis: involvement of proinflammatory state in preadipocytes. *Endocrinology*. 148:868-877.
Ladanyi, A., A. Mukherjee, H.A. Kenny, A. Johnson, A.K. Mitra, S. Sundaresan, K.M. Nieman, G. Pascual, S.A. Benitah, A. Montag, S.D. Yamada, N.A. Abumrad, and E. Lengyel. 2018. Adipocyte-induced CD36 expression drives ovarian cancer progression and metastasis. *Oncogene*. 37:2285-2301.
Lakadamyali, M., M.J. Rust, and X. Zhuang. 2006. Ligands for clathrin-mediated endocytosis are differentially sorted into distinct populations of early endosomes. *Cell*. 124:997-1009.
Larigauderie, G., C. Furman, M. Jaye, C. Lasselin, C. Copin, J.-C. Fruchart, G. Castro, and M. Rouis. 2004. Adipophilin Enhances Lipid Accumulation and Prevents Lipid Efflux From THP-1 Macrophages. *Arteriosclerosis, Thrombosis, and Vascular Biology*. 24:504-510.
Lazar, M.A. 2005. How obesity causes diabetes: not a tall tale. *Science*. 307:373-375.
Lazarus, J.H. 2012. Epidemiology of Graves' orbitopathy (GO) and relationship with thyroid disease. *Best Pract Res Clin Endocrinol Metab*. 26:273-279.
Le Lay, S., E. Hajduch, M.R. Lindsay, X. Le Liepvre, C. Thiele, P. Ferre, R.G. Parton, T. Kurzchalia, K. Simons, and I. Dugail. 2006. Cholesterol-induced caveolin targeting to lipid droplets in adipocytes: a role for caveolar endocytosis. *Traffic*. 7:549-561.
Leandro, M.J., J.C. Edwards, and G. Cambridge. 2002. Clinical outcome in 22 patients with rheumatoid arthritis treated with B lymphocyte depletion. *Ann Rheum Dis*. 61:883-888.
Leask, A., and D.J. Abraham. 2004. TGF-beta signaling and the fibrotic response. *FASEB J*. 18:816-827.
Lee, Y.-H., S.-N. Kim, H.-J. Kwon, K.R. Maddipati, and J.G. Granneman. 2016. Adipogenic role of alternatively activated macrophages in β-adrenergic remodeling of white adipose tissue. *American journal of physiology. Regulatory, integrative and comparative physiology*. 310:R55-R65.
Lee, Y.H., A.P. Petkova, and J.G. Granneman. 2013. Identification of an adipogenic niche for adipose tissue remodeling and restoration. *Cell metabolism*. 18:355-367.
Lefterova, M.I., A.K. Haakonsson, M.A. Lazar, and S. Mandrup. 2014. PPARgamma and the global map of adipogenesis and beyond. *Trends Endocrinol Metab*. 25:293-302.
Lehmann, G.M., C.F. Woeller, S.J. Pollock, C.W. O'Loughlin, S. Gupta, S.E. Feldon, and R.P. Phipps. 2010. Novel anti-adipogenic activity produced by human fibroblasts. *Am J Physiol Cell Physiol*. 299:C672-681.
Leonardini, A., L. Laviola, S. Perrini, A. Natalicchio, and F. Giorgino. 2009. Cross-Talk between PPARgamma and Insulin Signaling and Modulation of Insulin Sensitivity. *PPAR Res*. 2009:818945.
Li, D., J. Zhou, F. Chowdhury, J. Cheng, N. Wang, and F. Wang. 2011. Role of mechanical factors in fate decisions of stem cells. *Regen Med*. 6:229-240.

Li, H., C. Fitchett, K. Kozdon, H. Jayaram, G.E. Rose, M. Bailly, and D.G. Ezra. 2014. Independent adipogenic and contractile properties of fibroblasts in Graves' orbitopathy: an in vitro model for the evaluation of treatments. *PLoS One*. 9:e95586.

Li, J., and J.X. Cheng. 2014. Direct visualization of de novo lipogenesis in single living cells. *Sci Rep*. 4:6807.

Liao, J., R. Sportsman, J. Harris, and A. Stahl. 2005. Real-time quantification of fatty acid uptake using a novel fluorescence assay. *J Lipid Res*. 46:597-602.

Liaw, L., I. Prudovsky, R.A. Koza, R.V. Anunciado-Koza, M.E. Siviski, V. Lindner, R.E. Friesel, C.J. Rosen, P.R. Baker, B. Simons, and C.P. Vary. 2016. Lipid Profiling of In Vitro Cell Models of Adipogenic Differentiation: Relationships With Mouse Adipose Tissues. *J Cell Biochem*. 117:2182-2193.

Lindner, D., C. Zietsch, P.M. Becher, K. Schulze, H.P. Schultheiss, C. Tschope, and D. Westermann. 2012. Differential expression of matrix metalloproteases in human fibroblasts with different origins. *Biochemistry research international*. 2012:875742.

Listenberger, L.L., A.G. Ostermeyer-Fay, E.B. Goldberg, W.J. Brown, and D.A. Brown. 2007. Adipocyte differentiation-related protein reduces the lipid droplet association of adipose triglyceride lipase and slows triacylglycerol turnover. *J Lipid Res*. 48:2751-2761.

Liu, F., D. Lagares, K.M. Choi, L. Stopfer, A. Marinkovic, V. Vrbanac, C.K. Probst, S.E. Hiemer, T.H. Sisson, J.C. Horowitz, I.O. Rosas, L.E. Fredenburgh, C. Feghali-Bostwick, X. Varelas, A.M. Tager, and D.J. Tschumperlin. 2015. Mechanosignaling through YAP and TAZ drives fibroblast activation and fibrosis. *American journal of physiology. Lung cellular and molecular physiology*. 308:L344-357.

Liu, L., Q. Jiang, X. Wang, Y. Zhang, R.C. Lin, S.M. Lam, G. Shui, L. Zhou, P. Li, Y. Wang, X. Cui, M. Gao, L. Zhang, Y. Lv, G. Xu, G. Liu, D. Zhao, and H. Yang. 2014. Adipose-specific knockout of SEIPIN/BSCL2 results in progressive lipodystrophy. *Diabetes*. 63:2320-2331.

Livak, K.J., and T.D. Schmittgen. 2001. Analysis of relative gene expression data using real-time quantitative PCR and the 2(-Delta Delta C(T)) Method. *Methods (San Diego, Calif.)*. 25:402-408.

Lobo, S., B.M. Wiczer, A.J. Smith, A.M. Hall, and D.A. Bernlohr. 2007. Fatty acid metabolism in adipocytes: functional analysis of fatty acid transport proteins 1 and 4. *J Lipid Res*. 48:609-620.

Longo, N., G.I. Bell, R.C. Shuster, L.D. Griffin, S.D. Langley, and L.J. Elsas. 1990. Human fibroblasts express the insulin-responsive glucose transporter (GLUT4). *Transactions of the Association of American Physicians*. 103:202-213.

Luchsinger, L.L., C.A. Patenaude, B.D. Smith, and M.D. Layne. 2011. Myocardin-related transcription factor-A complexes activate type I collagen expression in lung fibroblasts. *J Biol Chem*. 286:44116-44125.

Lumeng, C.N., J.B. DelProposto, D.J. Westcott, and A.R. Saltiel. 2008. Phenotypic switching of adipose tissue macrophages with obesity is generated by spatiotemporal differences in macrophage subtypes. *Diabetes*. 57:3239-3246.

Macotela, Y., B. Emanuelli, M.A. Mori, S. Gesta, T.J. Schulz, Y.-H. Tseng, and C.R. Kahn. 2012. Intrinsic Differences in Adipocyte Precursor Cells From Different White Fat Depots. *Diabetes*. 61:1691.

Macpherson, R.E., R. Vandenboom, B.D. Roy, and S.J. Peters. 2013. Skeletal muscle PLIN3 and PLIN5 are serine phosphorylated at rest and following lipolysis during adrenergic or contractile stimulation. *Physiol Rep*. 1:e00084.

Mantovani, A., S.K. Biswas, M.R. Galdiero, A. Sica, and M. Locati. 2013. Macrophage plasticity and polarization in tissue repair and remodelling. *J Pathol*. 229:176-185.

Martin-Martin, B., V. Tovell, A.H. Dahlmann-Noor, P.T. Khaw, and M. Bailly. 2011. The effect of MMP inhibitor GM6001 on early fibroblast-mediated collagen matrix contraction is correlated to a decrease in cell protrusive activity. *European Journal of Cell Biology*. 90:26-36.

Martin, S., and R.G. Parton. 2006. Lipid droplets: a unified view of a dynamic organelle. *Nat Rev Mol Cell Biol*. 7:373-378.

Martinez-Santibanez, G., and C.N. Lumeng. 2014. Macrophages and the regulation of adipose tissue remodeling. *Annu Rev Nutr*. 34:57-76.

Masetti, G., S. Moshkelgosha, H.L. Kohling, D. Covelli, J.P. Banga, U. Berchner-Pfannschmidt, M. Horstmann, S. Diaz-Cano, G.E. Goertz, S. Plummer, A. Eckstein, M. Ludgate, F. Biscarini, and J.R. Marchesi. 2018. Gut microbiota in experimental murine model of Graves' orbitopathy established in different environments may modulate clinical presentation of disease. *Microbiome*. 6:97.

Masszi, A., C. Di Ciano, G. Sirokmany, W.T. Arthur, O.D. Rotstein, J. Wang, C.A. McCulloch, L. Rosivall, I. Mucsi, and A. Kapus. 2003. Central role for Rho in TGF-beta1-induced alpha-smooth muscle actin expression during epithelial-mesenchymal transition. *Am J Physiol Renal Physiol*. 284:F911-924.

Masuda, Y., H. Itabe, M. Odaki, K. Hama, Y. Fujimoto, M. Mori, N. Sasabe, J. Aoki, H. Arai, and T. Takano. 2006. ADRP/adipophilin is degraded through the proteasome-dependent pathway during regression of lipid-storing cells. *J Lipid Res*. 47:87-98.

Mayor, S., and R.E. Pagano. 2007. Pathways of clathrin-independent endocytosis. *Nat Rev Mol Cell Biol*. 8:603-612.

McBeath, R., D.M. Pirone, C.M. Nelson, K. Bhadriraju, and C.S. Chen. 2004. Cell shape, cytoskeletal tension, and RhoA regulate stem cell lineage commitment. *Dev Cell*. 6:483-495.

McDonald, M.E., C. Li, H. Bian, B.D. Smith, M.D. Layne, and S.R. Farmer. 2015. Myocardin-related transcription factor A regulates conversion of progenitors to beige adipocytes. *Cell*. 160:105-118.

McKee, C.M., M.B. Penno, M. Cowman, M.D. Burdick, R.M. Strieter, C. Bao, and P.W. Noble. 1996. Hyaluronan (HA) fragments induce chemokine gene expression in alveolar macrophages. The role of HA size and CD44. *J Clin Invest*. 98:2403-2413.

McManaman, J.L., E.S. Bales, D.J. Orlicky, M. Jackman, P.S. MacLean, S. Cain, A.E. Crunk, A. Mansur, C.E. Graham, T.A. Bowman, and A.S. Greenberg. 2013. Perilipin-2-null mice are protected against diet-induced obesity, adipose inflammation, and fatty liver disease. *J Lipid Res*. 54:1346-1359.

Mendez, M.G., and P.A. Janmey. 2012. Transcription factor regulation by mechanical stress. *Int J Biochem Cell Biol*. 44:728-732.

Menendez, J.A., and R. Lupu. 2007. Fatty acid synthase and the lipogenic phenotype in cancer pathogenesis. *Nat Rev Cancer*. 7:763-777.

Meng, X.M., D.J. Nikolic-Paterson, and H.Y. Lan. 2016. TGF-beta: the master regulator of fibrosis. *Nat Rev Nephrol*. 12:325-338.

Meran, S., D.W. Thomas, P. Stephens, S. Enoch, J. Martin, R. Steadman, and A.O. Phillips. 2008. Hyaluronan facilitates transforming growth factor-beta1-mediated fibroblast proliferation. *J Biol Chem*. 283:6530-6545.
Meshulam, T., J.R. Simard, J. Wharton, J.A. Hamilton, and P.F. Pilch. 2006. Role of caveolin-1 and cholesterol in transmembrane fatty acid movement. *Biochemistry*. 45:2882-2893.
Meyer-Ter-Vehn, T., S. Gebhardt, W. Sebald, M. Buttmann, F. Grehn, G. Schlunck, and P. Knaus. 2006. p38 inhibitors prevent TGF-beta-induced myofibroblast transdifferentiation in human tenon fibroblasts. *Invest Ophthalmol Vis Sci*. 47:1500-1509.
Milger, K., T. Herrmann, C. Becker, D. Gotthardt, J. Zickwolf, R. Ehehalt, P.A. Watkins, W. Stremmel, and J. Fullekrug. 2006. Cellular uptake of fatty acids driven by the ER-localized acyl-CoA synthetase FATP4. *J Cell Sci*. 119:4678-4688.
Mimura, L.Y., S.M. Villares, M.L. Monteiro, I.C. Guazzelli, and W. Bloise. 2003. Peroxisome proliferator-activated receptor-gamma gene expression in orbital adipose/connective tissues is increased during the active stage of Graves' ophthalmopathy. *Thyroid*. 13:845-850.
Miralles, F., G. Posern, A.I. Zaromytidou, and R. Treisman. 2003. Actin dynamics control SRF activity by regulation of its coactivator MAL. *Cell*. 113:329-342.
Miteva, K., S. Van Linthout, and C. Tschöpe. 2014. Crosstalk between fibroblasts and inflammatory cells. *Cardiovascular Research*. 102:258-269.
Miyoshi, H., S.C. Souza, H.H. Zhang, K.J. Strissel, M.A. Christoffolete, J. Kovsan, A. Rudich, F.B. Kraemer, A.C. Bianco, M.S. Obin, and A.S. Greenberg. 2006. Perilipin promotes hormone-sensitive lipase-mediated adipocyte lipolysis via phosphorylation-dependent and -independent mechanisms. *J Biol Chem*. 281:15837-15844.
Molgat, A.S., A. Gagnon, and A. Sorisky. 2009. Preadipocyte apoptosis is prevented by macrophage-conditioned medium in a PDGF-dependent manner. *Am J Physiol Cell Physiol*. 296:C757-765.
Moroishi, T., C.G. Hansen, and K.L. Guan. 2015. The emerging roles of YAP and TAZ in cancer. *Nat Rev Cancer*. 15:73-79.
Moshkelgosha, S., P.W. So, N. Deasy, S. Diaz-Cano, and J.P. Banga. 2013. Cutting edge: retrobulbar inflammation, adipogenesis, and acute orbital congestion in a preclinical female mouse model of Graves' orbitopathy induced by thyrotropin receptor plasmid-in vivo electroporation. *Endocrinology*. 154:3008-3015.
Motomura, W., M. Inoue, T. Ohtake, N. Takahashi, M. Nagamine, S. Tanno, Y. Kohgo, and T. Okumura. 2006. Up-regulation of ADRP in fatty liver in human and liver steatosis in mice fed with high fat diet. *Biochem Biophys Res Commun*. 340:1111-1118.
Mui, K.L., C.S. Chen, and R.K. Assoian. 2016. The mechanical regulation of integrin–cadherin crosstalk organizes cells, signaling and forces. *Journal of Cell Science*. 129:1093.
Mundy, D.I., T. Machleidt, Y.S. Ying, R.G. Anderson, and G.S. Bloom. 2002. Dual control of caveolar membrane traffic by microtubules and the actin cytoskeleton. *J Cell Sci*. 115:4327-4339.
Murphy, S., S. Martin, and R.G. Parton. 2009. Lipid droplet-organelle interactions; sharing the fats. *Biochim Biophys Acta*. 1791:441-447.

Naudí, A., M. Jové, V. Ayala, O. Ramírez, R. Cabré, J. Prat, M. Portero-Otin, I. Ferrer, and R. Pamplona. 2012. Region Specific Vulnerability to Lipid Peroxidation in the Human Central Nervous System *In* IntechOpen.
Nguyen, K.D., Y. Qiu, X. Cui, Y.P. Goh, J. Mwangi, T. David, L. Mukundan, F. Brombacher, R.M. Locksley, and A. Chawla. 2011. Alternatively activated macrophages produce catecholamines to sustain adaptive thermogenesis. *Nature*. 480:104-108.
Nobusue, H., N. Onishi, T. Shimizu, E. Sugihara, Y. Oki, Y. Sumikawa, T. Chiyoda, K. Akashi, H. Saya, and K. Kano. 2014. Regulation of MKL1 via actin cytoskeleton dynamics drives adipocyte differentiation. *Nat Commun*. 5:3368.
Noguchi, S., A. Saito, and T. Nagase. 2018. YAP/TAZ Signaling as a Molecular Link between Fibrosis and Cancer. *International journal of molecular sciences*. 19:3674.
Ohhira, M., W. Motomura, M. Fukuda, T. Yoshizaki, N. Takahashi, S. Tanno, N. Wakamiya, Y. Kohgo, S. Kumei, and T. Okumura. 2007. Lipopolysaccharide induces adipose differentiation-related protein expression and lipid accumulation in the liver through inhibition of fatty acid oxidation in mice. *Journal of gastroenterology*. 42:969-978.
Oishi, Y., and I. Manabe. 2018. Macrophages in inflammation, repair and regeneration. *International immunology*. 30:511-528.
Oka, T., V. Mazack, and M. Sudol. 2008. Mst2 and Lats kinases regulate apoptotic function of Yes kinase-associated protein (YAP). *J Biol Chem*. 283:27534-27546.
Olieslagers, S., E. Pardali, V. Tchaikovski, P. ten Dijke, and J. Waltenberger. 2011. TGF-beta1/ALK5-induced monocyte migration involves PI3K and p38 pathways and is not negatively affected by diabetes mellitus. *Cardiovasc Res*. 91:510-518.
Ostermeyer, A.G., J.M. Paci, Y. Zeng, D.M. Lublin, S. Munro, and D.A. Brown. 2001. Accumulation of caveolin in the endoplasmic reticulum redirects the protein to lipid storage droplets. *J Cell Biol*. 152:1071-1078.
Palestini, P., L. Botto, I. Rivolta, and G. Miserocchi. 2011. Remodelling of membrane rafts expression in lung cells as an early sign of mechanotransduction-signalling in pulmonary edema. *Journal of lipids*. 2011:695369.
Parmacek, M.S. 2007. Myocardin-related transcription factors: critical coactivators regulating cardiovascular development and adaptation. *Circ Res*. 100:633-644.
Parton, R.G., and M.A. del Pozo. 2013. Caveolae as plasma membrane sensors, protectors and organizers. *Nat Rev Mol Cell Biol*. 14:98-112.
Parton, R.G., J.C. Molero, M. Floetenmeyer, K.M. Green, and D.E. James. 2002. Characterization of a distinct plasma membrane macrodomain in differentiated adipocytes. *J Biol Chem*. 277:46769-46778.
Patel, Y.M., and M.D. Lane. 2000. Mitotic Clonal Expansion during Preadipocyte Differentiation: Calpain-mediated Turnover of p27. *Journal of Biological Chemistry*. 275:17653-17660.
Paton, C.M., and J.M. Ntambi. 2009. Biochemical and physiological function of stearoyl-CoA desaturase. *Am J Physiol Endocrinol Metab*. 297:E28-37.
Paul, A., B.H. Chang, L. Li, V.K. Yechoor, and L. Chan. 2008. Deficiency of adipose differentiation-related protein impairs foam cell formation and protects against atherosclerosis. *Circ Res*. 102:1492-1501.
Pawlowski, P., J. Reszec, A. Eckstein, K. Johnson, A. Grzybowski, L. Chyczewski, and J. Mysliwiec. 2014. Markers of inflammation and

fibrosis in the orbital fat/connective tissue of patients with Graves' orbitopathy: clinical implications. *Mediators Inflamm*. 2014:412158.
Persson, J., J. Nilsson, and M.W. Lindholm. 2008. Interleukin-1beta and tumour necrosis factor-alpha impede neutral lipid turnover in macrophage-derived foam cells. *BMC Immunol*. 9:70.
Petrus, P., D. Edholm, F. Rosqvist, I. Dahlman, M. Sundbom, P. Arner, M. Rydén, and U. Risérus. 2017. Depot-specific differences in fatty acid composition and distinct associations with lipogenic gene expression in abdominal adipose tissue of obese women. *International Journal Of Obesity*. 41:1295.
Piccolo, S., S. Dupont, and M. Cordenonsi. 2014. The biology of YAP/TAZ: hippo signaling and beyond. *Physiol Rev*. 94:1287-1312.
Pichler, H., and H. Riezman. 2004. Where sterols are required for endocytosis. *Biochim Biophys Acta*. 1666:51-61.
Pohl, J., A. Ring, and W. Stremmel. 2002. Uptake of long-chain fatty acids in HepG2 cells involves caveolae: analysis of a novel pathway. *J Lipid Res*. 43:1390-1399.
Porcheray, F., S. Viaud, A.C. Rimaniol, C. Léone, B. Samah, N. Dereuddre-Bosquet, D. Dormont, and G. Gras. 2005. Macrophage activation switching: an asset for the resolution of inflammation. *Clinical and experimental immunology*. 142:481-489.
Posern, G., and R. Treisman. 2006. Actin' together: serum response factor, its cofactors and the link to signal transduction. *Trends Cell Biol*. 16:588-596.
Pritchard, J., R. Han, N. Horst, W.W. Cruikshank, and T.J. Smith. 2003. Immunoglobulin activation of T cell chemoattractant expression in fibroblasts from patients with Graves' disease is mediated through the insulin-like growth factor I receptor pathway. *J Immunol*. 170:6348-6354.
Qi, Y., L. Sun, and H. Yang. 2017. Lipid droplet growth and adipocyte development: mechanistically distinct processes connected by phospholipids. *Biochimica et biophysica acta. Molecular and cell biology of lipids*. 1862:1273-1283.
Raftopoulou, M., and A. Hall. 2004. Cell migration: Rho GTPases lead the way. *Dev Biol*. 265:23-32.
Raghunathan, V.K., J.T. Morgan, B. Dreier, C.M. Reilly, S.M. Thomasy, J.A. Wood, I. Ly, B.C. Tuyen, M. Hughbanks, C.J. Murphy, and P. Russell. 2013. Role of substratum stiffness in modulating genes associated with extracellular matrix and mechanotransducers YAP and TAZ. *Invest Ophthalmol Vis Sci*. 54:378-386.
Rappolee, D.A., D. Mark, M.J. Banda, and Z. Werb. 1988. Wound macrophages express TGF-alpha and other growth factors in vivo: analysis by mRNA phenotyping. *Science*. 241:708-712.
Razani, B., T.P. Combs, X.B. Wang, P.G. Frank, D.S. Park, R.G. Russell, M. Li, B. Tang, L.A. Jelicks, P.E. Scherer, and M.P. Lisanti. 2002. Caveolin-1-deficient mice are lean, resistant to diet-induced obesity, and show hypertriglyceridemia with adipocyte abnormalities. *J Biol Chem*. 277:8635-8647.
Razani, B.L., M. 2002. The Role of Caveolae and the Caveolins in Mammalian Physiology. *Reviews in Undergraduate Research*. 1:44-50.
Reilly, R., M.S. Mroz, E. Dempsey, K. Wynne, S.J. Keely, E.F. McKone, C. Hiebel, C. Behl, and J.A. Coppinger. 2017. Targeting the PI3K/Akt/mTOR signalling pathway in Cystic Fibrosis. *Sci Rep*. 7:7642.

Riedl, A., M. Schlederer, K. Pudelko, M. Stadler, S. Walter, D. Unterleuthner, C. Unger, N. Kramer, M. Hengstschlager, L. Kenner, D. Pfeiffer, G. Krupitza, and H. Dolznig. 2017. Comparison of cancer cells in 2D vs 3D culture reveals differences in AKT-mTOR-S6K signaling and drug responses. 130:203-218.

Riley, F.C. 1972. Orbital pathology in Graves' disease. *Mayo Clinic Proceedings*. 47:975-979.

Rockey, D.C., N. Weymouth, and Z. Shi. 2013. Smooth muscle alpha actin (Acta2) and myofibroblast function during hepatic wound healing. *PLoS One*. 8:e77166.

Rogers, R., G. Ouellet, C. Brown, B. Moyer, T. Rasoulpour, and M. Hixon. 2008. Cross-talk between the Akt and NF-κB Signaling Pathways Inhibits MEHP-Induced Germ Cell Apoptosis. *Toxicological Sciences*. 106:497-508.

Rohlich, P., and A.C. Allison. 1976. Oriented pattern of membrane-associated vesicles in fibroblasts. *J Ultrastruct Res*. 57:94-103.

Romani, P., I. Brian, G. Santinon, A. Pocaterra, M. Audano, S. Pedretti, S. Mathieu, M. Forcato, S. Bicciato, J.B. Manneville, N. Mitro, and S. Dupont. 2019. Extracellular matrix mechanical cues regulate lipid metabolism through Lipin-1 and SREBP. *Nat Cell Biol*.

Rosenwald, M., V. Efthymiou, L. Opitz, and C. Wolfrum. 2017. SRF and MKL1 Independently Inhibit Brown Adipogenesis. *PLoS One*. 12:e0170643.

Rydzewska, M., M. Jaromin, I.E. Pasierowska, K. Stozek, and A. Bossowski. 2018. Role of the T and B lymphocytes in pathogenesis of autoimmune thyroid diseases. *Thyroid research*. 11:2.

Saben, J., K.M. Thakali, F.E. Lindsey, Y. Zhong, T.M. Badger, A. Andres, and K. Shankar. 2014. Distinct adipogenic differentiation phenotypes of human umbilical cord mesenchymal cells dependent on adipogenic conditions. *Exp Biol Med (Maywood)*. 239:1340-1351.

Sachot, N., E. Engel, and O. Castano. 2014. Hybrid Organic-Inorganic Scaffolding Biomaterials for Regenerative Therapies. *Current Organic Chemistry*. 18:2299-2314.

Saely, C.H., K. Geiger, and H. Drexel. 2012. Brown versus white adipose tissue: a mini-review. *Gerontology*. 58:15-23.

Salvi, M. 2014. Immunotherapy for Graves' ophthalmopathy. *Current opinion in endocrinology, diabetes, and obesity*. 21:409-414.

Salvi, M., G. Vannucchi, I. Campi, N. Curro, D. Dazzi, S. Simonetta, P. Bonara, S. Rossi, C. Sina, C. Guastella, R. Ratiglia, and P. Beck-Peccoz. 2007. Treatment of Graves' disease and associated ophthalmopathy with the anti-CD20 monoclonal antibody rituximab: an open study. *Eur J Endocrinol*. 156:33-40.

Salvi, M., G. Vannucchi, N. Currò, I. Campi, D. Covelli, D. Dazzi, S. Simonetta, C. Guastella, L. Pignataro, S. Avignone, and P. Beck-Peccoz. 2015. Efficacy of B-cell targeted therapy with rituximab in patients with active moderate to severe Graves' orbitopathy: a randomized controlled study. *The Journal of clinical endocrinology and metabolism*. 100:422-431.

Sanchez-Gurmaches, J., C.M. Hung, and D.A. Guertin. 2016. Emerging Complexities in Adipocyte Origins and Identity. *Trends Cell Biol*. 26:313-326.

Sapiro, J.M., M.T. Mashek, A.S. Greenberg, and D.G. Mashek. 2009. Hepatic triacylglycerol hydrolysis regulates peroxisome proliferator-activated receptor alpha activity. *J Lipid Res*. 50:1621-1629.

Schmelter, M., B. Ateghang, S. Helmig, M. Wartenberg, and H. Sauer. 2006. Embryonic stem cells utilize reactive oxygen species as transducers of mechanical strain-induced cardiovascular differentiation. *FASEB J*. 20:1182-1184.

Schoemaker, I., P.P. Hoefnagel, T.J. Mastenbroek, C.F. Kolff, S. Schutte, F.C. van der Helm, S.J. Picken, A.F. Gerritsen, P.A. Wielopolski, H. Spekreijse, and H.J. Simonsz. 2006. Elasticity, viscosity, and deformation of orbital fat. *Invest Ophthalmol Vis Sci*. 47:4819-4826.

Scott, M.A., V.T. Nguyen, B. Levi, and A.W. James. 2011. Current methods of adipogenic differentiation of mesenchymal stem cells. *Stem Cells Dev*. 20:1793-1804.

Sempowski, G.D., J. Rozenblit, T.J. Smith, and R.P. Phipps. 1998. Human orbital fibroblasts are activated through CD40 to induce proinflammatory cytokine production. *Am J Physiol*. 274:C707-714.

Shimomura, I., Y. Bashmakov, S. Ikemoto, J.D. Horton, M.S. Brown, and J.L. Goldstein. 1999. Insulin selectively increases SREBP-1c mRNA in the livers of rats with streptozotocin-induced diabetes. *Proc Natl Acad Sci U S A*. 96:13656-13661.

Shiwen, X., R. Stratton, J. Nikitorowicz-Buniak, B. Ahmed-Abdi, M. Ponticos, C. Denton, D. Abraham, A. Takahashi, B. Suki, M.D. Layne, R. Lafyatis, and B.D. Smith. 2015. A Role of Myocardin Related Transcription Factor-A (MRTF-A) in Scleroderma Related Fibrosis. *PLoS One*. 10:e0126015.

Simmons, C.A., S. Matlis, A.J. Thornton, S. Chen, C.Y. Wang, and D.J. Mooney. 2003. Cyclic strain enhances matrix mineralization by adult human mesenchymal stem cells via the extracellular signal-regulated kinase (ERK1/2) signaling pathway. *J Biomech*. 36:1087-1096.

Small, E.M., J.E. Thatcher, L.B. Sutherland, H. Kinoshita, R.D. Gerard, J.A. Richardson, J.M. Dimaio, H. Sadek, K. Kuwahara, and E.N. Olson. 2010. Myocardin-related transcription factor-a controls myofibroblast activation and fibrosis in response to myocardial infarction. *Circ Res*. 107:294-304.

Smith, T.J., R.S. Bahn, and C.A. Gorman. 1989. Hormonal regulation of hyaluronate synthesis in cultured human fibroblasts: evidence for differences between retroocular and dermal fibroblasts. *J Clin Endocrinol Metab*. 69:1019-1023.

Smith, T.J., R.S. Bahn, C.A. Gorman, and M. Cheavens. 1991. Stimulation of glycosaminoglycan accumulation by interferon gamma in cultured human retroocular fibroblasts. *J Clin Endocrinol Metab*. 72:1169-1171.

Smith, T.J., and N. Hoa. 2004. Immunoglobulins from patients with Graves' disease induce hyaluronan synthesis in their orbital fibroblasts through the self-antigen, insulin-like growth factor-I receptor. *J Clin Endocrinol Metab*. 89:5076-5080.

Smith, T.J., G.J. Kahaly, D.G. Ezra, J.C. Fleming, R.A. Dailey, R.A. Tang, G.J. Harris, A. Antonelli, M. Salvi, R.A. Goldberg, J.W. Gigantelli, S.M. Couch, E.M. Shriver, B.R. Hayek, E.M. Hink, R.M. Woodward, K. Gabriel, G. Magni, and R.S. Douglas. 2017. Teprotumumab for Thyroid-Associated Ophthalmopathy. *N Engl J Med*. 376:1748-1761.

Smith, T.J., L. Koumas, A. Gagnon, A. Bell, G.D. Sempowski, R.P. Phipps, and A. Sorisky. 2002. Orbital fibroblast heterogeneity may determine the clinical presentation of thyroid-associated ophthalmopathy. *J Clin Endocrinol Metab*. 87:385-392.

Smith, T.J., G.D. Sempowski, H.S. Wang, P.J. Del Vecchio, S.D. Lippe, and R.P. Phipps. 1995. Evidence for cellular heterogeneity in primary cultures of human orbital fibroblasts. *J Clin Endocrinol Metab*. 80:2620-2625.

Smith, T.J., H.S. Wang, M.G. Hogg, R.C. Henrikson, C.R. Keese, and I. Giaever. 1994. Prostaglandin E2 elicits a morphological change in cultured orbital fibroblasts from patients with Graves ophthalmopathy. *Proceedings of the National Academy of Sciences*. 91:5094.

Soiberman, U., R. Levy, and I. Leibovitch. 2013. Adiponectin concentration in the orbital fat of patients with Graves' ophthalmopathy. *Clin Ophthalmol*. 7:1723-1726.

Solinas, G., J. Boren, and A.G. Dulloo. 2015. De novo lipogenesis in metabolic homeostasis: More friend than foe? *Mol Metab*. 4:367-377.

Song, Z., A.M. Xiaoli, and F. Yang. 2018. Regulation and Metabolic Significance of De Novo Lipogenesis in Adipose Tissues. *Nutrients*. 10.

Sorisky, A., D. Pardasani, A. Gagnon, and T.J. Smith. 1996. Evidence of adipocyte differentiation in human orbital fibroblasts in primary culture. *J Clin Endocrinol Metab*. 81:3428-3431.

Stahl, A., D.J. Hirsch, R.E. Gimeno, S. Punreddy, P. Ge, N. Watson, S. Patel, M. Kotler, A. Raimondi, L.A. Tartaglia, and H.F. Lodish. 1999. Identification of the major intestinal fatty acid transport protein. *Mol Cell*. 4:299-308.

Stamatovic, S.M., R.F. Keep, S.L. Kunkel, and A.V. Andjelkovic. 2003. Potential role of MCP-1 in endothelial cell tight junction `opening': signaling via Rho and Rho kinase. *Journal of Cell Science*. 116:4615.

Stan, M.N., J.A. Garrity, B.G. Carranza Leon, T. Prabin, E.A. Bradley, and R.S. Bahn. 2015. Randomized controlled trial of rituximab in patients with Graves' orbitopathy. *J Clin Endocrinol Metab*. 100:432-441.

Stan, M.N., and M. Salvi. 2017. MANAGEMENT OF ENDOCRINE DISEASE: Rituximab therapy for Graves' orbitopathy - lessons from randomized control trials. *Eur J Endocrinol*. 176:R101-r109.

Starkey, K.J., A. Janezic, G. Jones, N. Jordan, G. Baker, and M. Ludgate. 2003. Adipose thyrotrophin receptor expression is elevated in Graves' and thyroid eye diseases ex vivo and indicates adipogenesis in progress in vivo. *J Mol Endocrinol*. 30:369-380.

Stary, H.C. 2000. Lipid and macrophage accumulations in arteries of children and the development of atherosclerosis. *Am J Clin Nutr*. 72:1297S-1306S.

Steinhauser, M.L., S.L. Kunkel, C.M. Hogaboam, H. Evanoff, R.M. Strieter, and N.W. Lukacs. 1998. Macrophage/fibroblast coculture induces macrophage inflammatory protein-1alpha production mediated by intercellular adhesion molecule-1 and oxygen radicals. *Journal of leukocyte biology*. 64:636-641.

Straub, B.K., B. Gyoengyoesi, M. Koenig, M. Hashani, L.M. Pawella, E. Herpel, W. Mueller, S. Macher-Goeppinger, H. Heid, and P. Schirmacher. 2013. Adipophilin/perilipin-2 as a lipid droplet-specific marker for metabolically active cells and diseases associated with metabolic dysregulation. *Histopathology*. 62:617-631.

Straub, B.K., P. Stoeffel, H. Heid, R. Zimbelmann, and P. Schirmacher. 2008. Differential pattern of lipid droplet-associated proteins and de novo perilipin expression in hepatocyte steatogenesis. *Hepatology*. 47:1936-1946.

Stuhlmeier, K.M., and C. Pollaschek. 2004. Differential effect of transforming growth factor beta (TGF-beta) on the genes encoding hyaluronan synthases and utilization of the p38 MAPK pathway in TGF-beta-induced hyaluronan synthase 1 activation. *J Biol Chem*. 279:8753-8760.
Sztalryd, C., and D.L. Brasaemle. 2017. The perilipin family of lipid droplet proteins: Gatekeepers of intracellular lipolysis. *Biochimica et biophysica acta. Molecular and cell biology of lipids*. 1862:1221-1232.
Takahashi, I., G.H. Nuckolls, K. Takahashi, O. Tanaka, I. Semba, R. Dashner, L. Shum, and H.C. Slavkin. 1998. Compressive force promotes sox9, type II collagen and aggrecan and inhibits IL-1beta expression resulting in chondrogenesis in mouse embryonic limb bud mesenchymal cells. *J Cell Sci*. 111 (Pt 14):2067-2076.
Talele, N.P., J. Fradette, J.E. Davies, A. Kapus, and B. Hinz. 2015. Expression of alpha-Smooth Muscle Actin Determines the Fate of Mesenchymal Stromal Cells. *Stem cell reports*. 4:1016-1030.
Tan, J.T., S.V. McLennan, W.W. Song, L.W. Lo, J.G. Bonner, P.F. Williams, and S.M. Twigg. 2008. Connective tissue growth factor inhibits adipocyte differentiation. *Am J Physiol Cell Physiol*. 295:C740-751.
Tan, S., J.Y. Fang, Z. Yang, M.E. Nimni, and B. Han. 2014. The synergetic effect of hydrogel stiffness and growth factor on osteogenic differentiation. *Biomaterials*. 35:5294-5306.
Tao, W., R. Moore, E.R. Smith, and X.-X. Xu. 2016. Endocytosis and Physiology: Insights from Disabled-2 Deficient Mice. *Frontiers in cell and developmental biology*. 4:129-129.
Targett-Adams, P., M.J. McElwee, E. Ehrenborg, M.C. Gustafsson, C.N. Palmer, and J. McLauchlan. 2005. A PPAR response element regulates transcription of the gene for human adipose differentiation-related protein. *Biochim Biophys Acta*. 1728:95-104.
Thompson, B.R., S. Lobo, and D.A. Bernlohr. 2010. Fatty acid flux in adipocytes: the in's and out's of fat cell lipid trafficking. *Mol Cell Endocrinol*. 318:24-33.
Tomasek, J.J., G. Gabbiani, B. Hinz, C. Chaponnier, and R.A. Brown. 2002. Myofibroblasts and mechano-regulation of connective tissue remodelling. *Nat Rev Mol Cell Biol*. 3:349-363.
Tong, L., G.A. Prieto, and C.W. Cotman. 2018. IL-1β suppresses cLTP-induced surface expression of GluA1 and actin polymerization via ceramide-mediated Src activation. *Journal of neuroinflammation*. 15:127-127.
Tsai, C.C., S.B. Wu, H.C. Kau, and Y.H. Wei. 2018. Essential role of connective tissue growth factor (CTGF) in transforming growth factor-beta1 (TGF-beta1)-induced myofibroblast transdifferentiation from Graves' orbital fibroblasts. *Sci Rep*. 8:7276.
Tsou, P.S., A.J. Haak, D. Khanna, and R.R. Neubig. 2014. Cellular mechanisms of tissue fibrosis. 8. Current and future drug targets in fibrosis: focus on Rho GTPase-regulated gene transcription. *Am J Physiol Cell Physiol*. 307:C2-13.
Tsukahara, T., Y. Matsuda, and H. Haniu. 2017. Lysophospholipid-Related Diseases and PPARgamma Signaling Pathway. 18.
Tumanov, S., V. Bulusu, and J.J. Kamphorst. 2015. Analysis of Fatty Acid Metabolism Using Stable Isotope Tracers and Mass Spectrometry. *Methods Enzymol*. 561:197-217.
Tzach-Nahman, R., R. Nashef, O. Fleissig, A. Palmon, L. Shapira, A. Wilensky, and G. Nussbaum. 2017. Oral fibroblasts modulate the macrophage response to bacterial challenge. *Scientific Reports*. 7:11516.

Ueki, I., N. Abiru, M. Kobayashi, M. Nakahara, T. Ichikawa, K. Eguchi, and Y. Nagayama. 2011. B cell-targeted therapy with anti-CD20 monoclonal antibody in a mouse model of Graves' hyperthyroidism. *Clin Exp Immunol*. 163:309-317.

Umbarawan, Y., M. Syamsunarno, N. Koitabashi, H. Obinata, A. Yamaguchi, H. Hanaoka, T. Hishiki, N. Hayakawa, M. Sano, H. Sunaga, H. Matsui, Y. Tsushima, M. Suematsu, M. Kurabayashi, and T. Iso. 2018. Myocardial fatty acid uptake through CD36 is indispensable for sufficient bioenergetic metabolism to prevent progression of pressure overload-induced heart failure. *Sci Rep*. 8:12035.

Valyasevi, R.W., D.Z. Erickson, D.A. Harteneck, C.M. Dutton, A.E. Heufelder, S.C. Jyonouchi, and R.S. Bahn. 1999. Differentiation of human orbital preadipocyte fibroblasts induces expression of functional thyrotropin receptor. *J Clin Endocrinol Metab*. 84:2557-2562.

Valyasevi, R.W., D.A. Harteneck, C.M. Dutton, and R.S. Bahn. 2002. Stimulation of adipogenesis, peroxisome proliferator-activated receptor-gamma (PPARgamma), and thyrotropin receptor by PPARgamma agonist in human orbital preadipocyte fibroblasts. *J Clin Endocrinol Metab*. 87:2352-2358.

Van De Water, L., S. Varney, and J.J. Tomasek. 2013. Mechanoregulation of the Myofibroblast in Wound Contraction, Scarring, and Fibrosis: Opportunities for New Therapeutic Intervention. *Advances in wound care*. 2:122-141.

van Meer, G. 2001. Caveolin, cholesterol, and lipid droplets? *J Cell Biol*. 152:F29-34.

van Steensel, L., H. Hooijkaas, D. Paridaens, W.A. van den Bosch, R.W. Kuijpers, H.A. Drexhage, P.M. van Hagen, and W.A. Dik. 2012. PDGF enhances orbital fibroblast responses to TSHR stimulating autoantibodies in Graves' ophthalmopathy patients. *J Clin Endocrinol Metab*. 97:E944-953.

Vardouli, L., E. Vasilaki, E. Papadimitriou, D. Kardassis, and C. Stournaras. 2008. A novel mechanism of TGFbeta-induced actin reorganization mediated by Smad proteins and Rho GTPases. *The FEBS journal*. 275:4074-4087.

Vartiainen, M.K., S. Guettler, B. Larijani, and R. Treisman. 2007. Nuclear actin regulates dynamic subcellular localization and activity of the SRF cofactor MAL. *Science*. 316:1749-1752.

Velasquez, L.S., L.B. Sutherland, Z. Liu, F. Grinnell, K.E. Kamm, J.W. Schneider, E.N. Olson, and E.M. Small. 2013. Activation of MRTF-A-dependent gene expression with a small molecule promotes myofibroblast differentiation and wound healing. *Proc Natl Acad Sci U S A*. 110:16850-16855.

Vigetti, D., A. Genasetti, E. Karousou, M. Viola, P. Moretto, M. Clerici, S. Deleonibus, G. De Luca, V.C. Hascall, and A. Passi. 2010. Proinflammatory Cytokines Induce Hyaluronan Synthesis and Monocyte Adhesion in Human Endothelial Cells through Hyaluronan Synthase 2 (HAS2) and the Nuclear Factor-κB (NF-κB) Pathway. *Journal of Biological Chemistry*. 285:24639-24645.

Vining, K.H., and D.J. Mooney. 2017. Mechanical forces direct stem cell behaviour in development and regeneration. *Nat Rev Mol Cell Biol*. 18:728-742.

Visagie, M.H., T.V. Mqoco, L. Liebenberg, E.H. Mathews, G.E. Mathews, and A.M. Joubert. 2015. Influence of partial and complete glutamine-and

glucose deprivation of breast-and cervical tumorigenic cell lines. *Cell & bioscience*. 5:37.
Vroegrijk, I.O., J.B. van Klinken, J.A. van Diepen, S.A. van den Berg, M. Febbraio, L.K. Steinbusch, J.F. Glatz, L.M. Havekes, P.J. Voshol, P.C. Rensen, K.W. van Dijk, and V. van Harmelen. 2013. CD36 is important for adipocyte recruitment and affects lipolysis. *Obesity (Silver Spring)*. 21:2037-2045.
Walther, T.C., J. Chung, and R.V. Farese, Jr. 2017. Lipid Droplet Biogenesis. *Annu Rev Cell Dev Biol*. 33:491-510.
Wang, C., X. Zhu, W. Feng, Y. Yu, K. Jeong, W. Guo, Y. Lu, and G.B. Mills. 2016. Verteporfin inhibits YAP function through up-regulating 14-3-3sigma sequestering YAP in the cytoplasm. *American journal of cancer research*. 6:27-37.
Wang, H.S., W.H. Tung, K.T. Tang, Y.K. Wong, G.J. Huang, J.C. Wu, Y.J. Guo, and C.C. Chen. 2005. TGF-beta induced hyaluronan synthesis in orbital fibroblasts involves protein kinase C betaII activation in vitro. *J Cell Biochem*. 95:256-267.
Wang, W., L. Huang, Y. Huang, J.W. Yin, A.J. Berk, J.M. Friedman, and G. Wang. 2009. Mediator MED23 links insulin signaling to the adipogenesis transcription cascade. *Dev Cell*. 16:764-771.
Wang, X., T.J. Reape, X. Li, K. Rayner, C.L. Webb, K.G. Burnand, and P.G. Lysko. 1999. Induced expression of adipophilin mRNA in human macrophages stimulated with oxidized low-density lipoprotein and in atherosclerotic lesions. *FEBS Lett*. 462:145-150.
Weetman, A.P., S. Cohen, K.C. Gatter, P. Fells, and B. Shine. 1989. Immunohistochemical analysis of the retrobulbar tissues in Graves' ophthalmopathy. *Clin Exp Immunol*. 75:222-227.
Wei, J., S. Bhattacharyya, M. Jain, and J. Varga. 2012. Regulation of Matrix Remodeling by Peroxisome Proliferator-Activated Receptor-gamma: A Novel Link Between Metabolism and Fibrogenesis. *The open rheumatology journal*. 6:103-115.
Weisberg, S.P., D. McCann, M. Desai, M. Rosenbaum, R.L. Leibel, and A.W. Ferrante, Jr. 2003. Obesity is associated with macrophage accumulation in adipose tissue. *J Clin Invest*. 112:1796-1808.
Whitmarsh, A.J., P. Shore, A.D. Sharrocks, and R.J. Davis. 1995. Integration of MAP kinase signal transduction pathways at the serum response element. *Science*. 269:403-407.
Wiersinga, W.M., and G.J. Kahaly. 2007. Graves' orbitopathy - A Multidisciplinary Approach. Karger.
Wiersinga, W.M., T. Smit, R. van der Gaag, and L. Koornneef. 1988. Temporal relationship between onset of Graves' ophthalmopathy and onset of thyroidal Graves' disease. *J Endocrinol Invest*. 11:615-619.
Wiesweg, B., K.T. Johnson, A.K. Eckstein, and U. Berchner-Pfannschmidt. 2013. Current insights into animal models of Graves' disease and orbitopathy. *Horm Metab Res*. 45:549-555.
Witte, N., M. Muenzner, J. Rietscher, M. Knauer, S. Heidenreich, A.M. Nuotio-Antar, F.A. Graef, R. Fedders, A. Tolkachov, I. Goehring, and M. Schupp. 2015. The Glucose Sensor ChREBP Links De Novo Lipogenesis to PPARgamma Activity and Adipocyte Differentiation. *Endocrinology*. 156:4008-4019.
Wolins, N.E., B.K. Quaynor, J.R. Skinner, M.J. Schoenfish, A. Tzekov, and P.E. Bickel. 2005. S3-12, Adipophilin, and TIP47 package lipid in adipocytes. *J Biol Chem*. 280:19146-19155.

Wolins, N.E., J.R. Skinner, M.J. Schoenfish, A. Tzekov, K.G. Bensch, and P.E. Bickel. 2003. Adipocyte protein S3-12 coats nascent lipid droplets. *J Biol Chem*. 278:37713-37721.
Wynn, T.A. 2008. Cellular and molecular mechanisms of fibrosis. *J Pathol*. 214:199-210.
Wynn, T.A., and L. Barron. 2010. Macrophages: master regulators of inflammation and fibrosis. *Seminars in liver disease*. 30:245-257.
Xiong, Y., H. Tanaka, J.A. Richardson, S.C. Williams, C.A. Slaughter, M. Nakamura, J.L. Chen, and M. Yanagisawa. 2001. Endothelin-1 stimulates leptin production in adipocytes. *J Biol Chem*. 276:28471-28477.
Xu, G., C. Sztalryd, X. Lu, J.T. Tansey, J. Gan, H. Dorward, A.R. Kimmel, and C. Londos. 2005. Post-translational regulation of adipose differentiation-related protein by the ubiquitin/proteasome pathway. *J Biol Chem*. 280:42841-42847.
Yadav, H., C. Quijano, A.K. Kamaraju, O. Gavrilova, R. Malek, W. Chen, P. Zerfas, D. Zhigang, E.C. Wright, C. Stuelten, P. Sun, S. Lonning, M. Skarulis, A.E. Sumner, T. Finkel, and S.G. Rane. 2011. Protection from obesity and diabetes by blockade of TGF-beta/Smad3 signaling. *Cell Metab*. 14:67-79.
Yang, Y., Q. Qi, Y. Wang, Y. Shi, W. Yang, Y. Cen, E. Zhu, X. Li, D. Chen, and B. Wang. 2018. Cysteine-rich protein 61 regulates adipocyte differentiation from mesenchymal stem cells through mammalian target of rapamycin complex 1 and canonical Wnt signaling. *Faseb j.* 32:3096-3107.
Yoon, J.S., H.J. Lee, S.H. Choi, E.J. Chang, S.Y. Lee, and E.J. Lee. 2011. Quercetin inhibits IL-1beta-induced inflammation, hyaluronan production and adipogenesis in orbital fibroblasts from Graves' orbitopathy. *PLoS One*. 6:e26261.
Young, D.A., Y.S. Choi, A.J. Engler, and K.L. Christman. 2013. Stimulation of adipogenesis of adult adipose-derived stem cells using substrates that mimic the stiffness of adipose tissue. *Biomaterials*. 34:8581-8588.
Yu-Wai-Man, C., B. Spencer-Dene, R.M.H. Lee, K. Hutchings, E.M. Lisabeth, R. Treisman, and M. Bailly. 2017. Local delivery of novel MRTF/SRF inhibitors prevents scar tissue formation in a preclinical model of fibrosis. 7:518.
Yu, J.S., T.S. Ramasamy, N. Murphy, M.K. Holt, R. Czapiewski, S.K. Wei, and W. Cui. 2015. PI3K/mTORC2 regulates TGF-beta/Activin signalling by modulating Smad2/3 activity via linker phosphorylation. *Nat Commun*. 6:7212.
Yu, W., Z. Chen, J. Zhang, L. Zhang, H. Ke, L. Huang, Y. Peng, X. Zhang, S. Li, B.T. Lahn, and A.P. Xiang. 2008. Critical role of phosphoinositide 3-kinase cascade in adipogenesis of human mesenchymal stem cells. *Mol Cell Biochem*. 310:11-18.
Yuan, Y., W. Zhong, G. Ma, B. Zhang, and H. Tian. 2015. Yes-associated protein regulates the growth of human non-small cell lung cancer in response to matrix stiffness. *Molecular medicine reports*. 11:4267-4272.
Zechner, R., F. Madeo, and D. Kratky. 2017. Cytosolic lipolysis and lipophagy: two sides of the same coin. *Nat Rev Mol Cell Biol*. 18:671-684.
Zhang, L., G. Baker, D. Janus, C.A. Paddon, D. Fuhrer, and M. Ludgate. 2006. Biological effects of thyrotropin receptor activation on human orbital preadipocytes. *Invest Ophthalmol Vis Sci*. 47:5197-5203.

Zhang, L., F. Grennan-Jones, M.S. Draman, C. Lane, D. Morris, C.M. Dayan, A.R. Tee, and M. Ludgate. 2014. Possible targets for nonimmunosuppressive therapy of Graves' orbitopathy. *J Clin Endocrinol Metab*. 99:E1183-1190.

Zhang, L., F. Grennan-Jones, C. Lane, D.A. Rees, C.M. Dayan, and M. Ludgate. 2012. Adipose tissue depot-specific differences in the regulation of hyaluronan production of relevance to Graves' orbitopathy. *J Clin Endocrinol Metab*. 97:653-662.

Zhang, R., Y. Gao, X. Zhao, M. Gao, Y. Wu, Y. Han, Y. Qiao, Z. Luo, L. Yang, J. Chen, and G. Ge. 2018a. FSP1-positive fibroblasts are adipogenic niche and regulate adipose homeostasis. 16:e2001493.

Zhang, Y., Y. Xing, and J. Li. 2018b. Osteogenesis-Related Behavior of MC3T3-E1 Cells on Substrates with Tunable Stiffness. 2018:4025083.

Zhao, B., X. Ye, J. Yu, L. Li, W. Li, S. Li, J. Yu, J.D. Lin, C.-Y. Wang, A.M. Chinnaiyan, Z.-C. Lai, and K.-L. Guan. 2008. TEAD mediates YAP-dependent gene induction and growth control. *Genes & development*. 22:1962-1971.

Zhao, P., Y. Deng, P. Gu, Y. Wang, H. Zhou, Y. Hu, P. Chen, and X. Fan. 2013. Insulin-like growth factor 1 promotes the proliferation and adipogenesis of orbital adipose-derived stromal cells in thyroid-associated ophthalmopathy. *Exp Eye Res*. 107:65-73.

Zhao, X.H., C. Laschinger, P. Arora, K. Szaszi, A. Kapus, and C.A. McCulloch. 2007. Force activates smooth muscle alpha-actin promoter activity through the Rho signaling pathway. *J Cell Sci*. 120:1801-1809.